3D FINITE ELEMENT SIMULATION OF STEEL QUENCHING IN ORDER TO DETERMINE THE MICROSTRUCTURE AND RESIDUAL STRESSES

A THESIS SUBMITTED TO
THE GRADUATE SCHOOL OF NATURAL AND APPLIED SCIENCES
OF
MIDDLE EAST TECHNICAL UNIVERSITY

BY

CANER ŞİMŞİR

IN PARTIAL FULFILLMENT OF REQUIREMENT
THE DEGREE OF DOCTOR OF PHILOSOPHY
IN
METALLURGICAL AND MATERIALS ENGINEERING

FEBRUARY 2008

3D FINITE ELEMENT SIMULATION OF STEEL QUENCHING IN ORDER TO DETERMINE THE MICROSTRUCTURE AND RESIDUAL STRESSES

submitted by CANER ŞİMŞİR in partial fulfillment of the requirements for the degree of **Doctor of Philosophy in Metallurgical and Materials Engineering Department, Middle East Technical University** by,

Prof.Dr.Canan Özgen

Dean, **Graduate School of Natural and Applied Sciences** ____________________

Prof.Dr.Tayfur Öztürk

Head of the Department, **Metallurgical and Materials Eng.** ____________________

Assoc.Prof.Dr.C.Hakan Gür

Supervisor, **Metallurgical and Materials Engineering Dept., METU** ____________________

Examining Committee Members :

Prof.Dr.Tayfur Öztürk

Metallurgical and Materials Engineering Dept., METU ____________________

Assoc.Prof.C.Hakan Gür

Metallurgical and Materials Engineering Dept, METU ____________________

Prof.Dr.A.Erman Tekkaya

Institut für Umformtechnik und Leichtbau, University of Dortmund ____________________

Prof.Dr.Şakir Bor

Metallurgical and Materials Engineering Dept., METU ____________________

Assoc.Prof.Dr. Uğurhan Akyüz

Civil Engineering Dept., METU ____________________

Date :

I hereby declare that all information in this document has been obtained and presented in accordance with academic rules and ethical conduct. I also declare that, as required by these rules and conduct, I have fully cited and referenced all material and results that are not original to this work.

Caner ŞİMŞİR

ABSTRACT

3D FINITE ELEMENT SIMULATION OF STEEL QUENCHING IN ORDER TO DETERMINE THE MICROSTRUCTURE AND RESIDUAL STRESSES

Şimşir, Caner

Ph.D., Department of Metallurgical and Materials Engineering

Supervisor: Assoc.Prof.Dr.C.Hakan Gür

February 2008, 193 Pages

In the course of thermal treatments, materials are usually subjected to continuous heating and cooling cycles during which microstructural evolution and mechanical interactions occur simultaneously at different length and time scales. Modeling of these processes necessitates dealing with inherent complexities such as large material property variations, complex couplings and boundary conditions, coupled heat and mass transfer mechanisms and phase transformations. In this study, a mathematical framework based on finite element method (FEM) capable of predicting temperature history, evolution of phases and internal stresses during heat treatment of metals and alloys was developed. The model was integrated into the commercial FEA software MSC.Marc® by user subroutines. The accuracy of the model was verified by simulating the quenching of eccentrically drilled steel cylinders. Simulation results were justified via SEM observations and XRD residual stress measurements. According to the results, the model can effectively predict the trends in the distribution of microstructure and residual stresses with a remarkable accuracy.

Keywords: Heat Treatment, Modeling, Microstructure, Residual Stress, Quenching,

ÖZ

İÇYAPI VE KALINTI GERİLİMLERİN BELİRLENMESİ İÇİN ÇELİKLERE SU VERME İŞLEMİNİN 3 BOYUTLU SONLU ELEMANLAR YÖNTEMİ İLE BENZETİMİ

Şimşir, Caner

Doktora, Metalurji ve Malzeme Mühendisliği Bölümü

Tez Yöneticisi: Assoc.Prof.Dr.C.Hakan Gür

Şubat 2008, 193 Sayfa

Malzemeler, ısıl işlemler sırasında değişik ölçeklerde meydana gelen eşzamanlı içyapısal değişimler ve mekanik etkileşimlere neden olan ısınma ve soğuma süreçlerine maruz kalırlar. Bu işlemlerin modellenmesi, malzeme özelliklerindeki sert değişimler, faz dönüşümleri, karmaşık bağdaştırmalar ve sınır koşulları gibi güçlükleri ele almayı gerektirir. Bu çalışmada metal ve alaşımların ısıl işlemler sırasında maruz kaldığı sıcaklık geçmişi, iç yapı ve gerilimlerin oluşumu ve gelişimini öngörebilen, sonlu elemanlar yöntemi esaslı bir matematiksel çerçeve geliştirilmiştir. Bu çerçeve, ticari bir sonlu elemanlar yazılımı olan MSC.Marc® ’a kullanıcı altrutinleri vasıtasıyla entegre edilmiştir. Modelin doğruluğu eksentrik delik açılmış çelik silindirlere su verilmesi işleminin benzetimi ile teyit edilmiştir. Benzetimlerden elde edilen sonuçlar Tarama Elektron Mikroskobu (SEM) incelemeleri ve X Işınları Kırınımı (XRD) kalıntı gerilim ölçümleri vasıtasıyla doğrulanmıştır. Sonuçlar geliştirilen çerçevenin içyapı ve kalıntı gerilimi dağılımlarını güvenilir ve dikkate değer bir doğrulukla öngörebildiğini göstermektedir.

Anahtar Kelimeler: Isıl İşlem, Modelleme, İçyapı, Kalıntı Gerilim, Su Verme.

To Cennet and Fatih Şimşir,

ACKNOWLEDGEMENTS

The author wishes to express his deepest gratitude to his supervisor Assoc. Prof. Dr. C. Hakan Gür for his guidance, understanding and continuous support throughout the study.

The author would also like to thank to Prof.Dr.A.Erman Tekkaya for the supervision, support and introducing him with the concept of continuum mechanics and finite element method.

The author is also grateful to Prof.Dr.Ö.Tarık Oğurtanı for introduction in computational materials science and numerical methods.

The author also acknowledges to IUL at University of Dortmund and IWT at University of Bremen for the support and hospitality.

The author would also like to thank research assistant Kemal Davut and Semih Perdahcıoğlu for their friendship, support and inspiration throughout the study.

The author wishes to express his gratitude to his sister Muazzez Şimşir for continuous support and encouragement.

The author would also like to thank to Oğul Can Turgay, Gökhan Ertem, Mehmet Nalbantoğlu, Pınar Şerbetçioğlu, Özge Kutlu, Özlem Balcı, Selin Zaimoğlu, Özge Burç, Selen Gürbüz, Gül Çevik, Pınar Karpuz and to all those who will give him hard time for forgetting to mention them, for giving him the strength to have the degree by sharing the good and the bad times.

The author would like to thank to Burçak Demirok, Seçil Demşek and all of the women in his life for sharing the pleasure and the pain. He learned so much from them even though it was sometimes quite painful. Without them, his life would be bare and incomplete.

Finally, the author would like to express his deepest gratitude and love to Mine Kahveci for inspiration, love, support and for all the things beyond words. After many years of extreme highs and lows, he feels truly at home now.

TABLE OF CONTENTS

LIST OF TABLES

LIST OF FIGURES

LIST OF SYMBOLS AND ABBREVIATIONS

Abbreviations

CA	Cellular Automata
CFD	Computational Fluid Dynamics
FDM	Finite Difference Method
FEM	Finite Element Method
FEA	Finite Element Analysis
PFM	Phase Field Method
SEM	Scanning Electron Microscopy
TRIP	Transformation Induced Plasticity

Common Indices

p	number of microstructural constituents
$p-1$	microstructural constituents except the parent phase
P^k, P_k	property related to kth microstructural constituent
P	without a subscript k, stands for the overall property of the phase mixture.
P_a, P_b, P_m, P_p	Property of austenite, bainite, martensite and pearlite, respectively
P^m, P^j	value of P at the current (jth,mth) time step ,
$\overline{P}, \widehat{P}$	average value of P

$\tilde{P}$	approximate value of P
P^{eq}, P_{eq}	equilibrium value
$P^{\max}, P_{\max}$	maximum value
P^{o}, P_{o}	initial value of P

Operators

•	scalar product
˙	time derivative
¨	second time derivative
Δ	increment operator
∇	gradient operator
$\nabla \bullet$	divergence operator

Vectors and Tensors

α_{ij}	backstress tensor due to kinematic hardening
δ_{ij}	Kronecker's delta
D_{ijkl}	elastoplastic constitutive
S_{ijkl}	elastoplastic compliance tensor
ε_{ij}	total strain tensor
ε_{ij}^{e}	elastic strain tensor
ε_{ij}^{p}	plastic strain rate tensor
$\dot{\varepsilon}_{ij}^{th}$	thermal strain tensor

ε_{ij}^{pt}	phase transformation dilatational strain tensor
ε_{ij}^{tr}	transformation plasticity (TRIP) rate tensor
σ_{ij}	Cauchy stress tensor
S_{ij}	stress deviator

Matrices and Vectors

$\left[\mathrm{B}\right]$	matrix of spatial derivatives of shape functions
$\left[C\right]$	conductivity matrix
$\left[\mathrm{D_e}\right]$	elastic constitutive matrix
$\left[\mathrm{D_{ep}}\right]$	elastoplastic constitutive matrix
$\left[\mathrm{H}\right]$	heat capacity matrix
$\left[\mathrm{K}\right]$	stiffness matrix
$\left[\mathrm{M}\right]$	mass matrix
$\left[\mathrm{N}\right]$	matrix of shape functions
$\left[\mathrm{Q}\right]$	consistent tangent modular matrix based on radial return mapping
$\left[S\right]$	compliance matrix
$\left\{F\right\}$	force vector
$\left\{Q\right\}$	heat flux vector
$\left\{Q^I\right\}$	nodal heat flux vector due to deformation

$\left\{Q^F\right\}$	nodal heat flux vector due to friction
$\left\{R\right\}$	corrected load rate vector
$\left\{T\right\}$	nodal temperature vector
$\left\{\dot{T}\right\}$	nodal cooling rate vector
$\left\{T^*\right\}$	resultant temperature vector from the previous iteration
$\left\{u\right\}$	nodal displacement vector
$\left\{\dot{u}\right\}$	nodal velocity vector
$\left\{\ddot{u}\right\}$	nodal acceleration vector
$\left\{\omega\right\}$	stress correction vector for stress update algorithm

Latin Letters

b	time coefficient for JMAK equation
c	specific heat capacity
c^*	fictitious (modified) specific heat capacity
$d\varepsilon_{ij}^T$	strain increment due to change of material properties with temperature and phase transformations.
$\mathrm{d}\lambda$	plastic multiplier
$d\sigma_{ij}^T$	strain increment due to change of material properties with temperature
e^*	error norm
h	convective heat transfer coefficient
k_B	Stephan-Boltzmann constant

n	time exponent for JMAK equation
r	saturation parameter for generalized phase transformation kinetics function
t	time
$\mathrm{t_s}$	transformation start time
$\mathrm{t_f}$	transformation finish time
$\mathrm{A_{e3}}$	ferrite start temperature
$\mathrm{A_{e1}}$	eutectoid temperature
$\mathrm{A_{Fe_3C}}$	cementite start temperature
$\mathrm{A_{p1}}$	eutectoid temperature calculated using para-equilibrium approach
$\mathrm{A_{o1}}$	eutectoid temperature calculated using ortho-equilibrium approach
$\mathrm{B_s}$	bainite start temperature
C	kinematic hardening modulus or plastic strain localization factor
C^{tr}	backstress coefficient due to TRIP
D	parameter specifying the shift of the IT curves due to stress
E	elastic modulus
H	plastic hardening modulus
J_2	second invariant of stress deviator
K	TRIP constant
L	latent heat of transformation
M	Rule of mixture exponent.
$\mathrm{M_s}$	martensite start temperature
Q	internal heat source/sink term

$\bar{Q}$	integral average value of Q over a temperature increment
S	Scheil's Sum
T	temperature
T_{p1}	eutectoid temperature calculated using both ortho- and para-equilibrium approaches
T_s	surface temperature
T_∞	ambient/sink temperature
V	volume
V^e	volume of the element
w	weight function

Greek Letters

α	linear thermal expansion coefficient
$\bar{\varepsilon}^p$	equivalent plastic strain
κ	hardening parameter
λ	thermal conductivity
ν	Poisson's ratio
ρ	density
σ_{o}	yield strength
σ_{f}	flow stress
σ_{m}	mean stress
τ	fictitious isothermal time
τ_s	transformation start time

τ_{σ}^{IT}	the isothermal incubation period under the influence of stress
ζ	emmisivity
ξ_k	fraction of kth microstructural constituent
ξ_k^f	fraction of a microstructural constituent at the end of transformation
ξ_k^s	fraction of a microstructural constituent at the start of transformation
Δ	structural dilatation due to phase transformation
Φ	yield functional
Ω	Koistinen-Marburger constant
Ψ	heat flux density

CHAPTER 1

INTRODUCTION

1.1 GENERAL

“Quenching” in its most general meaning refers to rapid cooling. In polymer chemistry and materials science, quenching is used to prevent low-temperature processes such as phase transformations from occurring by only providing a narrow window of time in which the reaction is both thermodynamically favorable and kinetically accessible.

In metallurgy, it is most commonly used to control the microstructure of alloys. Most of the heat treatments performed on metallic alloys, from widely used steel to titanium and aluminum, involve a quenching stage. Quenching is used either to bypass certain phase transitions and to obtain a metastable structure or to control the amount and the morphology of microstructural constituents. Industrially, most common use of quenching is the hardening of steel by introducing a very strong and hard phase called “martensite”. Although, this chapter will provide general information on simulation of quenching of different metallic alloys, the content will be focused especially on quench hardening of steel components.

Quench hardening is a common manufacturing process to produce steel components with reliable service properties. A wide spectrum of mechanical properties can be obtained for steel components via manipulation of cooling rate. Besides the conventional through-hardening process, most of the surface and thermo-chemical heat treatment processes such as carburizing, nitriding involve a quenching stage. Moreover, thermal surface treatment processes such as induction, flame or laser hardening also involve a direct quenching stage via a quenchant or indirect quenching via heat conduction through the specimen.

Before a component is quenched, it is heated to a uniform temperature and rapidly cooled down by immersion into a liquid, spraying with a liquid or by blowing pressurized gas. Immersion quenching is today’s most widely used industrial quenching technique. Another popular technique is spray quenching, which provide a better control on heat transfer, distortion and residual stresses. Today, gas quenching is considered as a promising technique because of the environmental reasons and ease of control.

Although quench hardening is a vital part of production based on steel, it is also one of the major causes of rejected components, production losses and the components that need to be reworked. Distortion, cracking, achievement of desired distribution of microstructure and properties such as hardness were longtime considered to be the most important problems during quenching of steels. Later, the distribution of residual stresses was also considered to be primarily important in following manufacturing stages and service performance. For example, residual stress state on the surface is important in fatigue, wear and corrosion behavior and affects the service life of the component.

Residual stresses do not result only from quenching but also from the manufacturing history of the product such as metal working and machining. If the steel comes from different melt shops, rolling mills, forgers etc., quenching performance can vary. When a metal part has residual stresses before the heat treatment, distortion may occur during the heat treatment. Even if stress-free and microstructrally homogenous parts are quench hardened, distortion may occur due to non-homogeneous plastic flow and internal stresses. Because of those reasons, it may be hazardous to machine the part to the tolerances before quenching. On the other hand, machinability of the part is generally worse after hardening, and besides there is considerable danger of losing the hardness acquired (e.g., local heating effect of grinding on martensite).

Based on these facts, heat treatment industry needs computer simulation of the quenching processes in order to optimize the process parameters by taking the following issues into account:

- Avoidance of cracking
- Reduction of distortion
- Achievement of desired microstructure distribution
- Achievement of desired residual stress distribution
- Achievement of desired property distribution such as hardness, fatigue /creep / corrosion / wear resistance via controlling the microstructure and residual stress distribution.

All these reasons render the prediction and control of the as-quenched state of the component into a vital step in order to reduce production losses and achieve production goals.

Quenching is a multi-physics process involving a complicated pattern of couplings between different physical events such as heat transfer, phase transformations and stress evolution. Because of the complexity, coupled and non-linear nature of the problem, no analytical solution exists for the problem. The rigorous treatment of the problem requires a coupled total thermo-mechano-metallurgical theory. Such theories have been proposed by, for instance, Ziegler [1] for combined heat conduction – elastoplastic problem. However, a commonly accepted inclusion of the thermodynamics and kinetics of the phase transformation in such a coupled theory has not been made so far. However, many algorithms have been proposed for “staggered numerical solution” of this problem. Solution involves application of numerical methods like finite difference method (FDM), finite volume method (FVM) and finite element method (FEM). Because of its wide spectrum of applicability and ease of use, FEM may be the most popular and the most suitable method for this purpose. Because of this, the scope of this chapter will be confined on FEM.

From the scientific point of view, to study on the simulation of quenching is a good practice to gain and improve the knowledge on:

- Heat transfer
- Phase transformations
- Mechanics of materials
- Fluid dynamics
- Coupled multi-physics, multi-scale processes
- Numerical methods for computer implementation of problems.

1.2 PHENOMENA OCCURRING DURING QUENCHING

During quench-hardening heat transfer, phase transformation and mechanical interaction occurs simultaneously. Physical fields interact with each other either by sharing of state variables or by coupling interactions. Figure 1.1 summarizes the physical fields and couplings between them. Although quenching is a complex multi-physics problem, heat transfer is the driving physical event as it triggers the other processes. From the engineering point of view, heat transfer to the quenching medium may also be the sole event that an engineer may alter in many cases. Because of its vital importance, quenching techniques are usually nominated as immersion quenching (water, oil etc.), spray quenching or gas quenching, by referring to the type of the quenchant used and method of application of the quenchant.

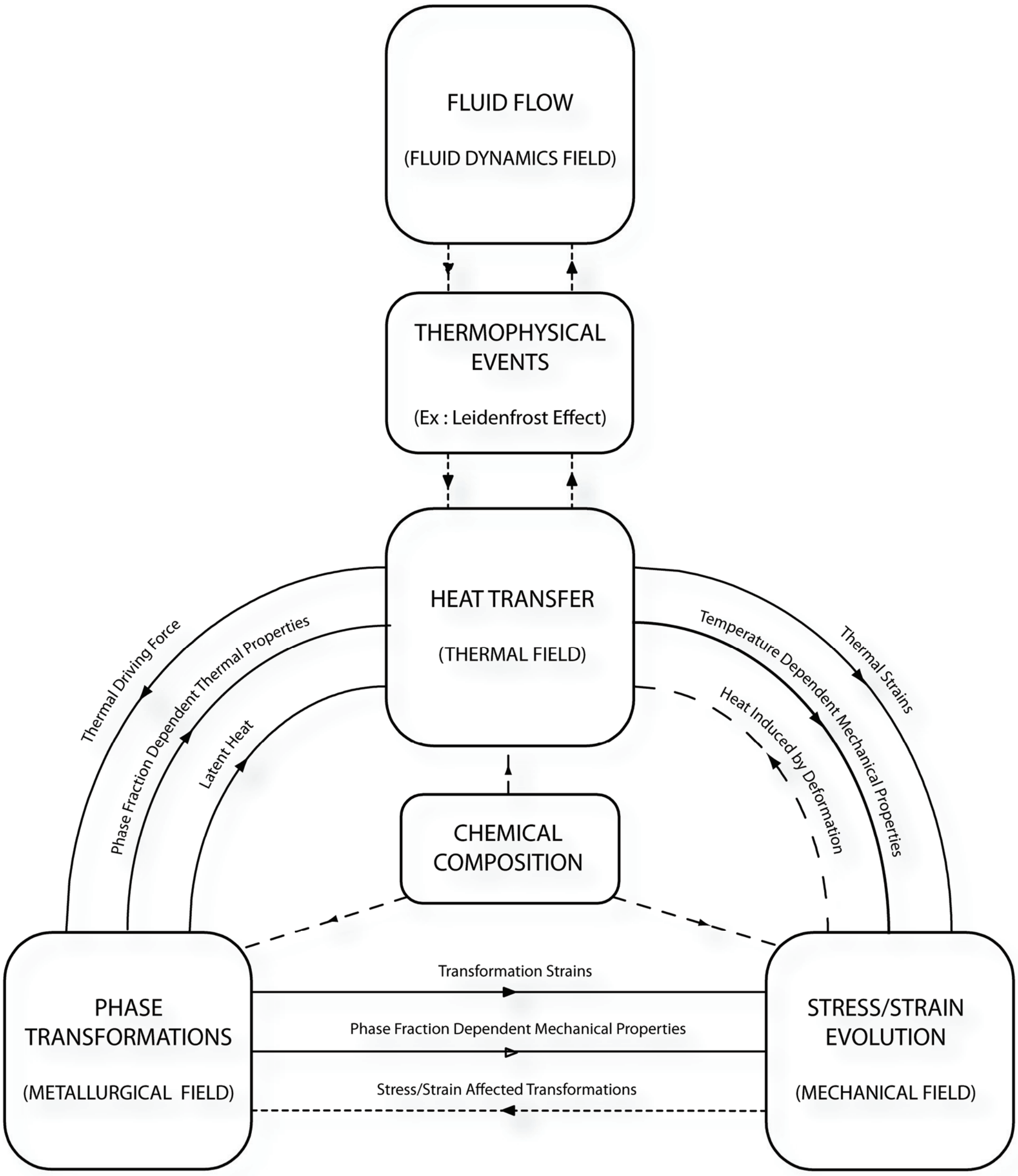

Figure 1.1 Physical fields and couplings between them during quenching.

Heat transfer from the surface is highly dependent on the fluid flow, thermo-physical and thermo-chemical processes occurring on the interface. For example, in the case of immersion quenching, quenching consists of three distinct stages of cooling, each characterized by different heat fluxes: vapor phase, nucleate boiling and the convective stage. Most of those physical and chemical processes can be explained by fundamental knowledge. However, a theory that can yield quantitative results for prediction of the onset of these events and the associated heat transfer coefficients is still not available despite the significant amount of research.

Variation of temperature in the component is the major driving force for the phase transformations. Upon cooling, thermodynamic stability of parent phase is altered, which results in the decomposition of austenite into transformation products. Transformation rate basically depends on the temperature and the cooling rate. On the other hand, there exists a heat interaction with surroundings during phase transformations. Phase transformations that occur during quenching are exothermic and they alter the thermal field by releasing latent heat of transformation. It has been shown that negligence of latent heat has a strong side effect on the accuracy of determination of temperature field [2].

Thermal stresses are generated in the quenched component due to large temperature gradients and the variation of mechanical properties with temperature. Varying cooling rates at different points lead to varying thermal contractions which must be balanced by an internal stress state. Those stresses may cause plastic flow or even cracking. Even tough, plastic deformation causes heat generation, the plastic deformations are relatively small (2-3%) in quenched part, thus, heat induced by deformation, almost without exception, is assumed to be negligible.

Interaction of the mechanical and metallurgical fields is one of the popular research areas for today’s structural mechanists, physicists and metallurgists. The ultimate objective is to develop a metallo-thermo-mechanical theory that can predict both the effect of mechanics on phase transformations and that of the phase transformations on deformation behavior. During decomposition of austenite into transformation products such as ferrite, pearlite, bainite and martensite, a volume increase is observed in the transforming region due to density difference between the parent and the product phases. Those strains are the primary source of fluctuating internal stress field, besides the thermal stresses and transformation induced plasticity (TRIP).

In addition, stress and plasticity affect the phase transformations by altering both the thermodynamics and the kinetics of the transformation. Most commonly observed effect of stress on transformation diagrams is the shift of critical temperatures and times. In some cases, transformations may be induced or totally inhibited by stress. This concept is generally referred as stress induced/inhibited phase transformation (SIPT). Similarly, it has been reported that prior plastic deformation of the parent phase affects subsequent phase transformations by changing the critical temperatures and transformation rates [3]. Detailed discussion of the effect of stress on phase transformations will be presented in Section 3.8.

During quenching, thermal and phase transformation strains co-operate and cause a continuously fluctuating internal stress field, which may even cause cracking in extreme cases. At any point in the quenched part, stress varies with time depending on the variation of thermo-mechanical properties with the temperature and the cooling rate. When the local yield strength is exceeded at some temperature at any point in the part, a non-uniform plastic flow occurs. This results in a residual stress state at the end of the quenching process, which may be beneficial or detrimental depending on the magnitude, sign and distribution of the stresses [4]. The stress state on the surface, at best, will end up as a compressive one. On the contrary, if the surface is in tension, for example, fatigue properties will be seriously impaired.

1.3 MATHEMATICAL FRAMEWORK

1.3.1 GENERAL

Modeling of thermal treatments is a complex multi-scale and multi-physics problem, during which parts are subjected to continuous heating and cooling cycles during with concomitant microstructural and mechanical evolutions. The rigorous treatment of the problem requires a totally coupled thermo-mechano-microstructural theory. However, a commonly accepted incorporation of the kinetics and irreversible thermodynamics of the phase transformations in such a coupled theory has not been made so far.

In this study, a “staggered numerical solution” of the problem is suggested. In the solution procedure, each field is treated independently by its governing equations, initial/ boundary conditions. Then, related couplings are generated and system is solved consecutively. This approach provides solution of quite complex multi-physics problem as long as proper time stepping procedure is used. However, it imposes a strong time stepping constraint since the solution requires at least the smallest of the time steps used for individual solution of governing equations. This might cause an efficiency problem, especially when one of the involved physics operates on a considerably different time scale.

Table 1.1 illustrates basic capabilities of the framework and currently implemented models for each physical fields and couplings. Those features can be accessed by using some flags in the subroutine source code. Many other models are also possible by minor modifications in the source code. In addition to the implemented ones, several features which are currently under the development are also mentioned.

Current framework consists of a modular system, in which each module deals with a certain physical field and related couplings. The computational features of the existing framework which are worth mentioning can be listed as follows:

- There are no particular restrictions on the forms of the governing equations of plasticity and microstructural evolution. Thus, although the model problem involves small strain total Lagrangian J_2 thermo-elastoplasticity coupled with Avrami kinetics, finite strain formulations with any other form of microstructural evolution kinetics is possible. This gives rise to a broad spectrum of possible applications from simulation of conventional heat treatments to state of art thermomechanical processing techniques, as long as a proper description of involved phenomena is supplied.
- Microstructural evolution calculation may involve application of a wide spectrum of numerical methods from conventional finite difference (FD) and finite element (FE) methods to multiscale treatment in representative volume element (RVE) using methods such as phase field (PF) and cellular automata (CA) method etc. Besides phase transformation kinetics, multi-scale treatment of transformation induced plasticity (TRIP) is possible by micromechanical calculations in a RVE. However, this type of treatment is quite new in the field and state of the art indicates that such kind of approaches are useful in understanding the physics of the process, but their implementations usually does not usually produce quantitatively reliable results .
- Thermo-physical events driving heat transfer (electrical induction, laser heating, fluid flow etc.) can be weakly coupled with the thermo-mechano-microstructural analysis. For example, a weak coupling of fluid flow field with is possible by importing mass flow rate of the fluid calculated in CFD program such as FLUENT®, CFX® as function of position and time and applying this data as thermal boundary condition.

The major drawbacks of the current framework mentioning can be listed as follows,

- Coupling of physical fields with chemical composition (diffusion) field is not yet available. After the implementation of this feature, thermochemical treatments such as carburizing and nitriding involving compositional changes may also be simulated.
- Currently, global remeshing is not supported due to problems in implementation in commercial FEA software. This drawback limits the finite strain applications of the framework.
- Adaptive time stepping and meshing procedures can significantly improve the accuracy and reduce run times by tracking the onset and transformation front. This feature is not currently available.
- Another drawback plaguing the finite strain applications of the framework is the lack of fundamental theories capable of yielding quantitative results for the involved phenomena. For example, a basic problem arising during simulation of

thermomechanical processing techniques is the interaction of large plastic strains with phase transformations, for which a commonly accepted theory which can produce reliable quantitative results is not yet available. Although the framework is finite strain capable. the predictions will not be reliable unless this gap is filled by fundamental research on materials physics.

Table 1.1 Some of the currently implemented capabilities of the framework

HEAT TRANSFER
Latent Heat: *Modified specific heat method.*
Convective Heat Transfer: *h(T), h(x,T), h(x,t)*
Conductivity Model : *Isotropic, Anisotropic**
Thermal Properties of the Phase Mixture : *Generalized rule of mixture*
PHASE TRANSFORMATIONS
Isothermal Kinetics :
JMAK, Austin-Rickett, Generalized JMAK, Koistinen-Marburger
Anisothermal Kinetics:
Scheil`s additivity principle, Direct-Integration of JMAK equation, Global Kinetics Model* *(Lusk* [11]*), Non-linear Additivity** *(Reti* [12]*)*
Stress Affected Martensitic Transformation:
Modified Koistinen-Marburger (Denis [13], *Inoue* [14], *Liu* [15]*), Modified Zener-Hillert** [16], *Modified Magee** [17]
Stress affected Diffusion Controlled Transformations:
Denis* [18] , *Inoue** [19]
MECHANICS
Formulation :
Small Strain , Large Strain Additive*
Plasticity : J_2 *Elastoplasticity*
Hardening Law:
Isotropic, Isotropic with plastic memory loss, Kinematic/Combined**
Mechanical Properties of the Phase Mixture : *Generalized rule of mixture*
Flow Stress of the Phase Mixture :
Generalized Rule of mixture with plastic memory loss, Reuss*, *Voigt** [20], *Geijsalers* [21], *Leblond** [22]
TRIP Models :
Abrassart [23], *Fischer* [8], *Leblond [24, 25], Sjostrom* [26], *Greenwood-Johnson* [6], *TRIP with back-stress*** [27, 28]
* *Not extensively tested* ** *Under development*

1.3.2 PHYSICAL FIELDS AND COUPLINGS

A brief representation of physical fields and couplings that has to be considered for simulation of heat treatments is illustrated on Figure 1.1. Solid lines represents the couplings which are currently implemented for simulation of quenching, whereas, the dashed line represents the neglected couplings. It should be noted that the current structure of the framework is capable of simulating all of those couplings except the mass transfer (diffusion), which is considered as a future study. Certain couplings are intentionally neglected due to their low significance or lack of accurate material data.

The most obvious couplings arise due to temperature and microstructure dependence of thermomechanical properties. In addition to those couplings, there exists other type of couplings which require the modification of the governing equations. The physical origin of those couplings will be discussed in the next section whereas; the implementation procedure will be presented in Chapter 2-4.

Thermo-mechanical Coupling

A continuously fluctuating thermal stress field is induced in the component due to variation of thermal contractions/expansions and thermomechanical properties as a function of position, temperature and time. On the other hand, it is well known that the plastic deformation of metals is accompanied by the heat generation. This means that the energy balance equation that governs the temperature evolution, should involve several terms arising from thermomechanical coupling. The first term relates the heat production to the recoverable deformations. A second term defines heating arising from the dissipation of mechanical work during breaking of internal bonds in crystal lattice. The third term describes the stored energy of cold work, which is motivated by the rearrangement of various defects in the structure during the plastic deformation. These effects are only important in some particular cases in the small strain regime and cannot be avoided in the most cases in finite strain regime In the modeling of quenching process, the heat generation due to mechanical energy dissipation is negligibly small compared to the heat transfer by cooling.

Thermo-microstructural Coupling

Variation of temperature at any point in the component is the driving force for phase transformations. Transformation rate basically depends on temperature, cooling/heating rate, concentration, stress and prior plastic deformation. On the other hand, there exists a heat interaction with surroundings during phase transformations due to the latent heat of transformation. It has been shown that neglection of this effect has a strong side effect in accuracy of determination of temperature field [2].

Mechano-microstructural Coupling

Phase transformations alter the mechanical field due to transformation strains. During a phase transformation, a transforming micro-region changes it volume and occasionally its shape, which results in dilatational and transformation induced plasticity (TRIP) strains. TRIP is the significantly increased plasticity during a phase change. Even for an externally applied load for which the corresponding equivalent stress is small compared to the normal yield stress of the material, plastic deformation occurs [5]. This phenomenon is explained by the existence of an irreversible strain resulting from phase transformations occurring under a stress field. TRIP is currently explained by the competition of Greenwood and Johnson [6] and Magee [7] mechanisms depending on thermomechanical loading conditions. The extensive review of the TRIP concept can be found elsewhere [8, 9].

On the other hand, both the driving forces for transformation and the kinetics of the process can be altered by mechanical interactions during phase transformations which occur under stress, prior or concomitant plasticity. The thermodynamics of phase transformations – i.e transformation temperatures, chemical composition of parent and product phases – is modified by the change of free energies of parent and product phases. Similarly, kinetics of transformation – i.e. transformation rates, path of transformation - may also be altered because of the change in the mobility of atoms due to elastic and plastic strains. Elastic strains effects the kinetics of transformation by changing the mobility of atoms by changing the free volume. Plasticity alters the transport processes by changing the point defect concentration, providing shortcuts for diffusion via dislocation cores or by providing a non-diffusive transport mechanism where the atoms are convected by moving dislocations. either geometrically, or via the drag effect due to dislocation/solute interaction [10].

1.4 STATE OF THE ART IN SIMULATION OF QUENCHING

First studies on prediction of microstructure and residual stress distribution in quenching by computer simulation originate from early 70's [29-36]. Some of those studies even neglected the effect of phase transformations. Most studies were performed for infinitely long solid and hollow cylinders due to lack of computational power. Results were commonly compared with X-ray diffraction residual stress measurements. Results indicated that this approach that considers only the thermo-mechanical behavior without the effect of phase transformations fails drastically in prediction of residual stress state after industrial quenching processes.

In early 80's, many studies have been conducted for implementation of phase transformation effects in previously developed models [37-43]. Similar to the studies that had been performed in the previous decade, those studies were mostly focused on simple 1D and 2D shapes such as infinitely long cylinders and cylinders of finite height. Moreover, the effect of transformation plasticity was usually neglected due to immature numerical models for transformation induced plasticity. Results were more reasonable, but neglecting transformation plasticity had a considerable impact on the accuracy of prediction of residual stresses and distortions.

In the second half of 80's, many research groups developed improved constitutive models for material behavior during quenching of steels. First mature models for the effect of stress on phase transformation and TRIP were developed [5, 13, 14, 22, 24-26, 44-52]. Previously neglected physical phenomena such as plastic memory loss during phase transformations, effect of stresses on transformation thermodynamics and kinetics, transformation plasticity were implemented in the simulations. Theory of heat transfer during quenching, selection of quenchant, and fundamentals of intensive quenching were presented [48, 53-55].

In 90's, improvements in computational power and the finite element software lead to an acceleration in research; especially the concepts of calculation TTT and CCT diagrams and TRIP become more mature [2, 8, 9, 11, 12, 15, 56-87]. Several commercial FEA software capable of simulating quenching process, such as DANTE®, HEARTS®, TRAST®, SYSWELD® and DEFORM-HT®, became available. Beside those specific purpose programs, some general commercial FEA packages, such as ABAQUS®, ANSYS®, MSC.MARC®, are improved by scientists via user subroutines in order to simulate heat treatments, allowing the scientists to concentrate on the research rather than developing efficient FE codes, pre-post processors. Table 1.2 presents a brief summary of currently used codes for simulation of quenching and their capabilities. Although some of these software are still improved, most of them originate from 90`s. From the viewpoint of heat transfer during quenching and quenching technologies, many studies and reviews are published for optimization of cooling conditions [56, 88-108]

In 2000`s, from the viewpoint of development of new technologies to control quenching, many articles and reviews have been published.[109-120]. Simulation of gas quenching and coupling quenching simulations with computational fluid dynamics (CFD) calculations became a major interest [120-124]. Currently, most of the research on the field is focused on single phase gas quenching. Although, CFD calculations still requires considerable amount of computational power, single phase calculations can be performed. This kind of simulations allows the engineers to optimize of gas quenching system to minimize the distortion and to obtain optimum residual stress and microstructure distribution. However, simulation of fluid flow during immersion quenching, which is the most common process in the industry, is not yet performed. Simulation of fluid flow for immersion quenching require two phase (liquid and gas) CFD calculations which is possible but which is also requires much more computational horsepower. The major drawback in this field is quantitative description of thermo-physical events occurring on the surface during quenching.

Simulation of quenching is a highly input sensitive process. Unfortunately, simulations require considerable amount of hard to acquire material and process data such mechanical, thermal, phase transformation data and thermal boundary conditions from the quench tank [125-131], which renders accurate acquisition of data and development of material databases into a vital task. Almost all of the currently developed models require input data as a function of temperature and chemical composition which makes the data acquisition a tedious and expensive process and increases the amount of input data drastically. A solution for this problem may be the development of a database for computer simulation of heat treatments by international collaboration [132]. An example for such an approach originated from Japan Society for Materials Science which constructed a materials database `MATEQ` for computer simulations in 2002[133]. Such a research is also ranked as a long term top priority task, in ASM VISION 2020 heat treating technology roadmap initiatives. According to this roadmap, development of continuous on-heating and on-cooling transformation data for a range of materials, including the effects of variation in steel mill processing, chemistry variation and non-homogeneous microstructures on transformation kinetics, construction of a database of thermal and mechanical properties from room temperature to heat treat temperature, development of low cost methods and industry standards for acquisition of data are vital steps for accurate predictions via simulation [134]. An alternative approach to solve material and process data bottleneck may be the development of models that require less and easily acquired data. Another alternative workaround may be the development of thermodynamic models or performing lower scale (atomistic, mesoscale) models to calculate the required data from fundamental physical properties. Unfortunately, most of the material properties required in simulation of quenching cannot be predicted by such kind of models or the accuracy of prediction is not good enough for quantitative evaluation.

Today, multiscale modeling is a major research interest which promotes multi-disciplinary studies in many research fields. This trend is also observed in simulation of quenching because of partial failure of continuum scale models in prediction of physical events such as effect of stress on phase transformations, transformation plasticity and mechanical behavior of phase mixtures [27, 125, 135-156]. Physical events that occur on lower scales such as phase transformations have been simulated on atomistic or mesoscopic scale by methods such as cellular automata, phase field, whereas macroscopic plasticity, heat conduction are modeled on continuum scale especially by FEM. Bridging between length scales have been performed using scale shifting methods or methods like representative volume element method (RVE). Unfortunately, even though those preliminary works are promising; they are still immature and have little industrial significance today. However, it is thought that fundamental solutions for the drawbacks in simulation of heat treatments lie in multiscale modeling concept.

To sum up, a lot of researches have been conducted in last three decades to develop numerical simulation tools for prediction of final state of the component after quenching. Nowadays, simulation of heat treatments may even be performed by engineers rather than scientist by use of commercial FEA software dedicated to simulation of heat treatments. However, there is still plenty of room for scientists to develop new methods or improve the currently available models. Current drawbacks and future improvements in simulation of quenching can be briefly summarized as follows:

From the industrial point of view:

- Development of models that require less experimental data
- Development of material databases and easy to perform, standard testing methods for acquisition of process data.

From the scientific point of view:

- Development of a fully coupled rigorous thermo-mechano-microstructural theory
- Incorporation of fundamentally based multiscale methods, especially for stress-phase transformation interactions.

Table 1.2 Some of the currently available software used in simulation of heat treatments

CODE	2D/3D	HASE TRANSFORMATION	MECHANICAL MODEL		COUPLING	SPECIAL APPLICATIONS		
			Elast-pl	Elasto-viscopl		Tempering	Induction Hardening	Carburizing
SYSWELD	√	√	√		T-S T-M S-M	√	√	√
HEARTS	√	√	√	√	T-S T-M	√	√	√
FORGE	√		√	√	T-S T-M S-M			
ANSYS	√		√	√	T-S			
ABAQUS	√		√	√	T-S			
MSC.MARC	√		√	√	T-S			
DANTE (ABAQUS)	√	√	√	√	T-S T-M S-M	√	√	√
DEFORM (HT)	√	√	√	√	T-S T-M S-M			

CHAPTER 2

MODELING THE HEAT TRANSFER

2.1 GENERAL

An often-ignored fact about quenching is that quenching is not only a metallurgical process but it also depends on the heat transfer characteristics of the component and the quenchant. Attaining required material properties is not possible unless the heat transfer is controlled and optimized. From the engineering point of view, heat transfer to the quenching medium may also be the sole event that an engineer may control in many cases. Because of its vital importance, quenching techniques are usually referred as immersion quenching (water, oil etc.), spray quenching or gas quenching, by referring to the type of the quenchant used and method of application of the quenchant.

Accurate prediction of thermal history of the quenched component is also vital for simulation purposes and this accuracy can only be achieved by deep understanding of heat transfer phenomenon. Accuracy of the thermal history prediction directly influences that of the phase transformation kinetics, thermal and phase transformation stress calculations. A poor heat transfer model or inaccurate heat transfer data will eventually result in considerable errors in the predicted microstructure and residual stresses even though phase transformation and mechanical modules are perfectly functioning.

In order to understand and model the heat transfer during quenching, heat transfer mechanisms and thermophysical events that control the heat transfer must be identified. Heat transfer during quenching occurs via all possible heat transfer mechanisms, i.e., conduction, convection and radiation. Basically, heat is removed from the surface of the specimen by convective heat transfer to the quenchant and by radiation, which results in thermal gradients driving the conduction inside the component.

Quenching can be defined as a transient heat conduction problem with convective and radiation boundary conditions with internal heat source and sink. The governing equation for this problem has been formulated by French physicist and mathematician Joseph Fourier in early 1800's. The essential point in modeling of quenching is an addition of an internal heat source term in this equation which originates from the latent heat released by phase transformations. It has been shown that accuracy cannot be achieved without incorporation of this term into heat conduction model. Many studies on alternative ways of coupling phase transformations and heat transfer and alternative numerical solution techniques have been carried out [2, 13, 74, 157]. Currently, those approaches are well settled in the community and there exist no controversy about the subject.

Heat transfer by radiation is another mechanism operating during quenching, which is usually dominant from the time in which component is removed from the furnace until it is immersed into quenchant. It also has a relatively significant effect during vapor blanket stage during which convection is very limited due to highly insulating vapor blanket. Radiation heat flux is also related with quench tank material and geometry. This type of treatment requires additional calculation of view factors, which is a computationally expensive task.

The effect of radiation may be introduced into Fourier equation by a 4th order Stephan-Boltzmann type of boundary condition. In many cases, heat flux due to this mechanism is not directly implemented into calculations, but its contribution is included in the general definition of surface temperature dependent convective heat transfer coefficient. Notice that the calculation of convective heat transfer coefficient is usually based on experimental temperature history measurements, which already include the effect of radiation. However, it should be noted that, heat flux due to radiation is highly dependent on quench system. So, determination of heat transfer coefficients has to be performed on actual quench system.

Convective heat transfer to the quenchant may be the most mind-boggling heat transfer mechanism during immersion quenching. In immersion quenching process, the surface heat transfer conditions between the steel part and the quenchant are the most important factors controlling the microstructural evolution, generation of stresses and distortion. The problem arise from very marked variation of the surface heat transfer coefficient during quenching and its sensitivity to small variations in the conditions of the quench bath and the state of the surface of the specimen. In order to deal with these variations, thermophysical and thermochemical events occurring on the component-quenchant interface must be understood.

As the component is immersed into the quenchant, the initial temperature of the component is generally well above the boiling point of the quenchant. Then , successive stages of heat transfer characterize the cooling process: vapor blanket stage, nucleate boiling and convective stage each associated with a distinct cooling regime [158] . There also exists a highly transient initial liquid contact stage. Those critical stages and associated changes in heat flux and heat transfer coefficient are illustrated on Figure 2.1.

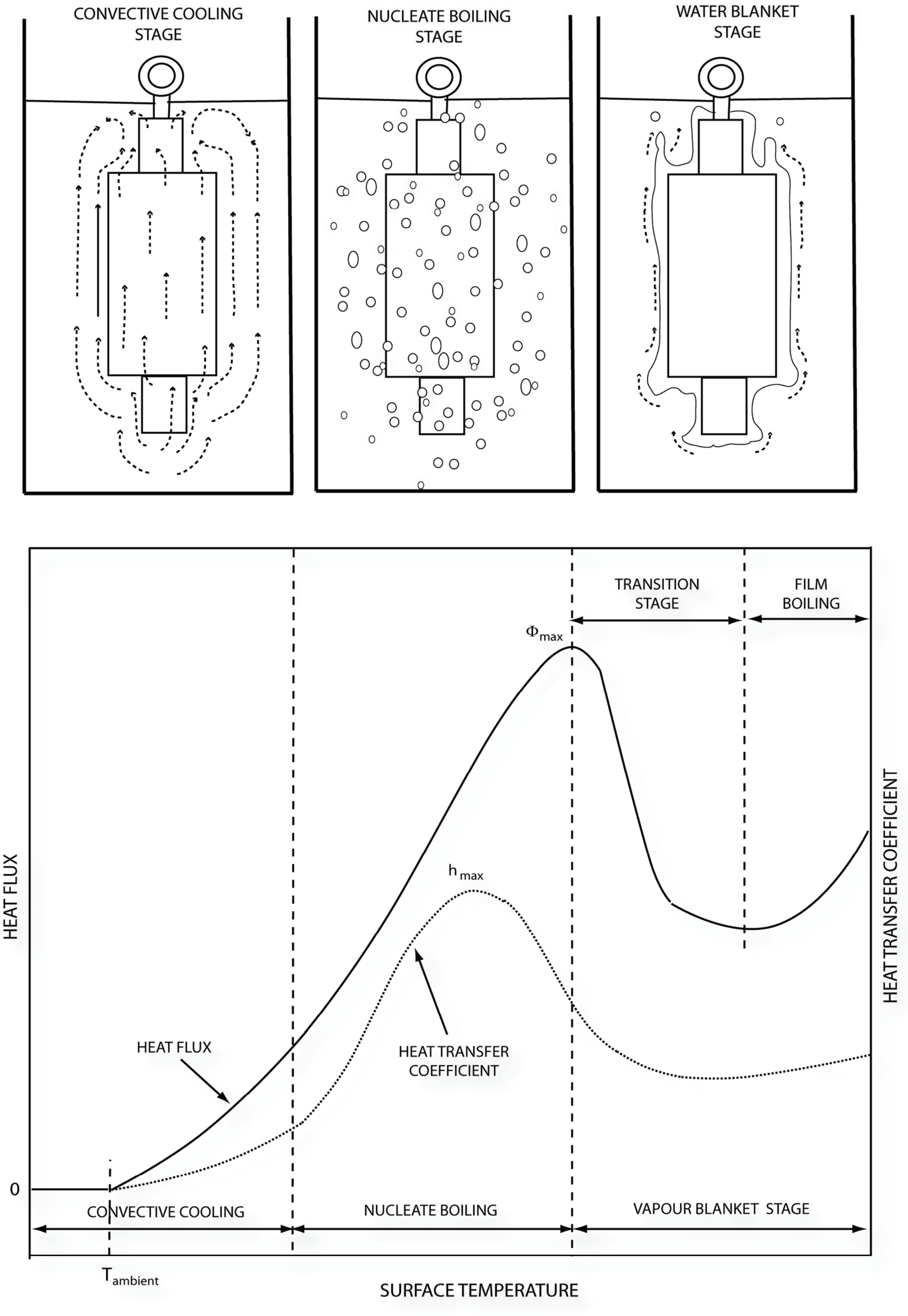

Figure 2.1 Cooling regimes and associated heat fluxes and heat transfer coefficient during immersion quenching.

During the initial transient boiling stage, liquid is in contact with the hot surface, causing intense boiling. This stage is rapidly terminated as soon as sufficient vapor has been generated to completely cover the whole surface. Rate of heat removal is very low in vapor blanket stage because of the low thermal conductivity of vapor layer. Contribution of radiation to overall heat transfer in this stage is remarkable. The temperature at which the stable film breaks down and the bubbles start to detach from the surface refers to Leidenfrost temperature. G. J. Leidenfrost described this wetting process in 1756. Leidenfrost temperature is influenced by a variety of factors, part of which cannot be precisely quantified even today [159, 160]. However, for a non-steady state process such as quenching of a large component, the surface temperature is not equal to the Leidenfrost temperature when the vapor blanket collapses and wetting begins by nucleate boiling because of the lateral heat conduction relative to the surface. Then, the heat flux increases and reaches to its maximum at the burnout point. Below the burnout point, the heat flux decreases until the surface temperature reaches the boiling point of the quenchant.

The change from the vapor blanket stage to nucleate boiling is not abrupt, a transition occurs when the surface heat transfer coefficient and the amount of liquid/solid contact increases as illustrated on Figure 2.2. This increase and decrease in the transition regions is achieved by the movement of “wetting front” that separates vapor blanket and nucleate boiling, on the surface of the immersion quenched component In most cases, wetting front ascends the cooling surface with a significant velocity during nucleate boiling, whereas it descends in the fluid direction during film boiling [159].

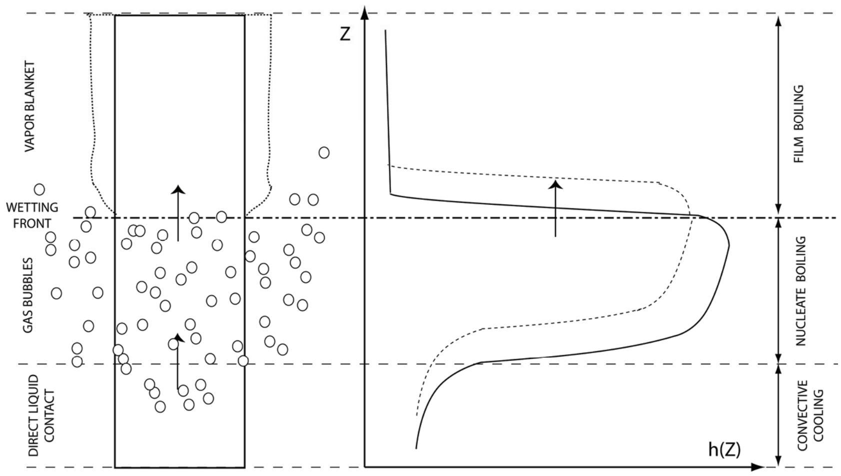

Figure 2.2 Motion of the wetting front and the variation of heat transfer coefficient as a function of position and time

A wetting process that occurs over a long time period is called non-Newtonian wetting, whereas a wetting process that occurs in a short time period or an explosion like wetting process is termed as Newtonian wetting. Type of the wetting process significantly affects cooling behavior of the quenchant. A Newtonian type of wetting usually promotes uniform heat transfer and minimizes the distortion and residual stress development. In the extreme cases of non-Newtonian wetting, because of large temperature differences, considerable variations in the microstructure, residual stresses are expected resulting in distortion and presence of soft spots. Thus, one can conclude that quench severity is not a sole function of the wetability (dihedral angle) but it is also a function of the kinetics of the wetting process.

Final stage of cooling of the quenched component is reached as the temperature of the component approaches to the boiling point of the liquid, the rate of vaporization decreases and the heat transfer is reduced rapidly to the value associated with convective flow. This stage is termed as convective cooling stage. Convective cooling rates are highly dependent on the fluid flow velocity, the viscosity and the heat capacity of the quenchant. Hence, agitation and use of a low viscosity quenchant is expected to increase the cooling rate. For example, convective cooling rate in water is high due to its low viscosity and high heat capacity. Thus, convective cooling stage makes a remarkable contribution to the overall cooling rate. On the other hand, convective cooling in oil is less intensive due to relatively high viscosity and lower heat capacity.

Quench oils are traditionally preferred quenchants when lower cooling rates are required. A variety of different quenching oils tend to show a prolonged first stage, a short second stage with a much lower cooling rate, and finally a prolonged convective cooling stage with a very modest cooling rate [161] . It may also be desirable to accelerate the cooling rate of a quench oil to reduce the duration of the vapor blanket formation and to increase the rate of nucleate heat transfer. In such cases, an additive may be introduced into the quench oil to improve the wetting characteristics since the composition of the quench oil significantly affects the wetting ability of the quenchant by altering the contact angle (dihedral angle) between the surface and the quenchant [159].

Some of the other factors that have to be taken into account during selection of quenchants may be the variation of thermophysical chemical properties with temperature and time (ageing behavior), the oxidative stability of the quenchant and the contamination.

Agitation exhibits one of the greatest and probably most controllable parameter that affects the cooling rate on all quenching stages. For example, fluid mass flow rate and turbulence may exhibit an enormous effect on quench severity. Increasing agitation rates would be expected to both decrease the interfacial film stability and sweep away the hotter quenchant faster, thus increasing the quench severity [100, 162].

Aqueous polymer solutions such as poly(alkylene glycol) (PAG) and poly(vinyl pyrolidone) (PVP) are other alternative quenchants. They differ from quench oils with their low wetting times leading to explosive like (Newtonian) wetting behavior which may improve the uniformity of the cooling. Theoretically, their cooling characteristics may be improved by additives similar to the quench oils. However, no such an additive is identified for aqueous polymer quenchants up today [97, 98].

Considering these concepts, one can clearly see the difficulty in quantitative description of the quenching performance of a quenchant. For this purpose, a commonly accepted early study was performed by Grossmann. He defined a “quench severity” factor, which is also referred as Grossman number, describing the ability of a quenchant to extract heat from the component [163]. This approach is a poor approach since it considers only the quenchant. However, quenching performance is not a sole property of the quenchant; it also depends on factors such as the quenching system, geometry and the material. In order to analyze a quenchant system adequately, it is necessary to model the heat transfer properties associated with both the quenchant and the system [163, 164]. Cooling curve analysis is commonly considered to be the best method of obtaining the required information. Several cooling curve interpretation methods have been proposed recently, including the use of rewetting times [53, 106, 165], an empirical hardening-power predictor [166-172] and a rigorous analysis of the cooling process [33, 119, 173, 174]. Another approach to the problem is the quench factor analysis which especially incorporates phase transformation kinetics into quenchant characterization [88, 90, 93, 116, 164]. An example study for such an approach was conducted by Bates and Totten[90]. In their study, they have evaluated a quench factor based on time-temperature-property (TTP) curves and Scheil’s additivity principle.

2.2 EQUATIONS GOVERNING HEAT TRANSFER DURING QUENCHING

The transient heat transfer within the component during quenching can mathematically be described by an appropriate form of Fourier’s heat conduction equation. Considering that the thermal field is altered by the latent heat of phase transformations, the equation can be expressed in its most general form as,

$$\rho c \dot{T} = \nabla \cdot (\nabla(\lambda T)) + Q \tag{2.1}$$

where ρ, c and λ are the density, specific heat and thermal conductivity of the phase mixture given as a function of temperature, respectively. Q is the internal heat source due the latent heat, which is a function of transformation rate and temperature.

Thermal properties of the phase mixture is approximated by a linear rule of mixture,

$$P(T,\xi_k) = \sum_1^N P_k \xi_k \tag{2.2}$$

where P represents an overall thermal property of the mixture, whereas, P_k is a thermal property of the k^{th} constituent of the phase mixture. ξ_k is the volume fraction of k^{th} constituent.

For the sake of simplicity, heat released due to phase transformation is almost always assumed as the change in the enthalpy per unit volume (ΔH_k)**.** Notice that, enthalpy change of a phase transformation is the heat response of the system under a constant pressure. Due to stress evolution during quenching, phase transformations does not occur under constant pressure. However, the effect of pressure on enthalpy is negligible for solids. Thus, latent heat release rate per unit volume can be expressed as:

$$\dot{Q} = \Delta H_k \dot{\xi}_k \tag{2.3}$$

where $\dot{\xi}_k$ is the phase transformation rate. Notice that, the energy change (i.e., the temperature drop) due to adiabatic expansion

$$\frac{E}{1-2\nu}\frac{\partial \varepsilon^{th}}{\partial T} T \dot{\varepsilon}_{mm} \tag{2.4}$$

and the energy due to the plastic flow $\sigma_{ij}\dot{\varepsilon}^p$ are usually neglected in simulation of the quenching process. Simple estimates show that their contribution to heat generation rate terms is less than 1% [26].

A common method for incorporation of latent heat into heat conduction equations is the definition of a fictitious specific heat in the form of

$$c^* = \sum_{k=1}^N c_k \xi_k + \Delta H_k \frac{d\xi_k}{dT} = c + \frac{\dot{\xi}_k}{\dot{T}} \Delta H_k \tag{2.5}$$

where c^* is the modified specific heat that includes both the changes in the specific heat and the latent heat of transformation. The basic principles underlying this derivation are illustrated on Figure 2.3.

Finally, initial and boundary conditions are set to complete the definition of the thermal problem. Initially all nodal temperatures are set to quenching temperature. Convective heat transfer boundary condition is set for the surfaces that are in contact with quenchant as,

$$\Psi(T_s,T_\infty) = h(T_s)(T_s - T_\infty) \tag{2.6}$$

where Ψ is the heat flux from the surface which is a function of the surface and the quenchant temperature. $h(T_s)$ is the surface temperature dependent heat transfer coefficient. Using a surface temperature dependent heat transfer coefficient provides a simple method to incorporate the effect of different cooling rates at different stages of quenching. However, this approach is not valid for complex geometries. Indeed, such geometries require the definition of the heat transfer at least as a function of the temperature and the position. Finally, surfaces which are not in contact with the quenchant and the symmetry surfaces are assumed to be insulated. Heat flux from those surfaces is set to 0 by

$$-\lambda \frac{\partial T}{\partial n} = 0 \tag{2.7}$$

where $\partial T / \partial n$ is the directional derivative of the temperature in the outer normal (n) direction.

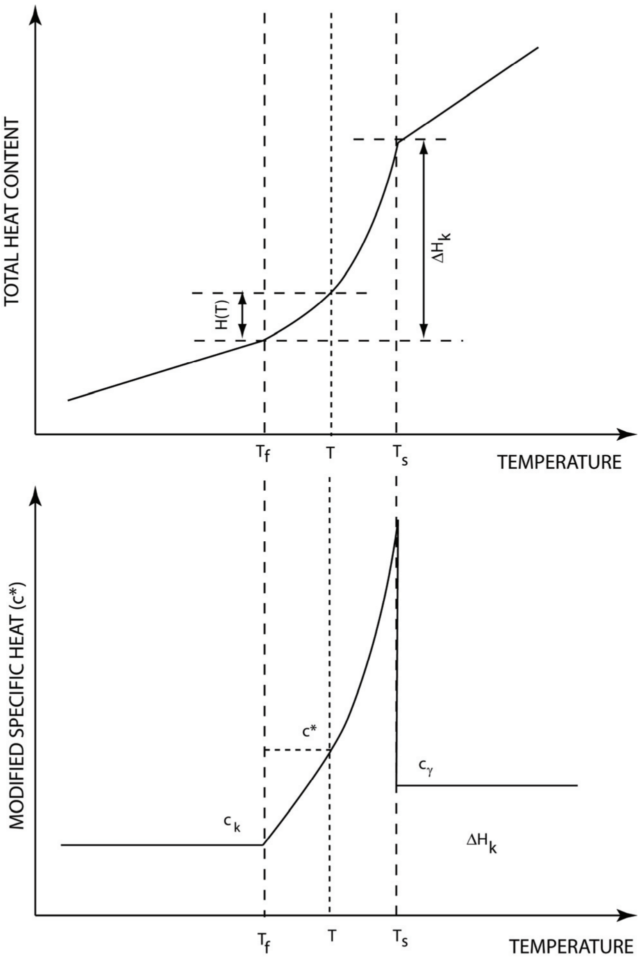

Figure 2.3 Calculation of modified specific heat for simulation of latent heat.

2.3 FINITE ELEMENT FORMULATION OF THE HEAT TRANSFER PROBLEM

The general form of heat conduction equation reduces to parabolic differential equation for a thermally isotropic body as

$$\lambda \nabla^2 T - \rho c \dot{T} + \dot{Q} = 0 \tag{2.8}$$

The governing partial differential equation of the heat transfer process in a quenched component will be satisfied when the weighted and integrated residua is minimized:

$$\iiint_V \omega \left(\lambda \nabla^2 T - \rho c \dot{T} + \dot{Q} \right) . dV \approx 0 \tag{2.9}$$

where ω is the weight function and R=$\left(\lambda \nabla^2 T - \rho c \dot{T} + \dot{Q} \right)$ is the residual.

Using the standard finite element approximation, nodal temperatures and temperature rates can be expressed by

$$T \approx \sum_i N_i T_i \tag{2.10}$$

where [N] is the matrix of shape functions.

After the substitution of discrete values for T and taking the weight functions same as the shape functions (Galerkin method), equation (2.9) takes the following form

$$\iiint_V \left(\lambda \nabla^2 \left(N_i T_i \right) - \rho c \left(N_i T_i \right) + \dot{Q}_i \right) N_j . dV \approx 0 \tag{2.11}$$

This expression can further be decomposed to element matrices and boundary terms by using the Gauss` divergence theorem.

2.3.1 CONSTRUCTION OF THE ELEMENT EQUATIONS

The finite element formulation of the governing equation for nonlinear transient heat transfer problem with internal heat source may be written in the incremental form as

$$\left[\frac{1}{\Delta t} [H] + [C] \right] \{ \Delta T_t \} = \frac{1}{\Delta t} \{ \Delta T_{t-\Delta t} \} + \{ Q \} \tag{2.12}$$

where [H] and [C] are the heat capacity and thermal conductivity matrices, respectively. Considering the effect of temperature dependent convective heat transfer coefficient and the latent heat of transformation on the conductivity matrix [C] and heat flux vector {Q}, this expression may be expanded in the following form :

$$\left[\frac{1}{\Delta t}[H] + ([C_c] + [C_h])\right]\{\Delta T_t\} = \frac{1}{\Delta t}\{\Delta T_{t-\Delta t}\} + \{Q_h\} + \{Q_l\} \tag{2.13}$$

where $\{Q_h\}$,$\{Q_l\}$ are the heat flux vectors due to h(T) and latent heat of transformation and $[C_h]$ is the change in the conductivity matrix due to h(T). $[C_c]$ is the conductivity matrix without the effect of h(T). Those vectors and matrices can be evaluated using equations following expressions :

$$[H] = \rho\iiint c[N]^T[N].dV \tag{2.14}$$

$$[C_c] = \iiint \lambda[B]^T[B].dV \tag{2.15}$$

$$[C_h] = \iint h[N]^T[N].dS \tag{2.16}$$

$$\{Q_l\} = \iiint \dot{Q}[N]^T.dV \tag{2.17}$$

$$\{Q_h\} = \iint hT_o[N]^T.dS \tag{2.18}$$

$$\{\Delta T_{t-\Delta t}\} = \{T_t\} - \{T_{t-\Delta t}\} \tag{2.19}$$

where [N], [B] are the matrices of shape functions and their spatial derivatives, respectively.

2.3.2 TIME DISCRETIZATION

Transient heat transfer during quenching is a highly non-linear problem consisting of

- Non-linearity in the equation due to the heat source term,
- Non-linearity in boundary conditions due to the temperature dependent convective heat transfer coefficient,
- Non-linearity due to temperature dependent thermal properties.

Hence, conductivity [H], heat capacity [C] matrices and thermal load vector {Q} are temperature dependent.

The technique of dealing with non-linearities in transient problems highly depends on the time stepping algorithm [175]. The time discretization scheme used for transient problems in FEM is quite equivalent to the ones used in finite difference methods. In this example, the general implicit method will be used for time marching.

In weighted residual approach for time discretization, the objective is to obtain an approximation for $\{T\}_{t+\Delta t}$ using the known values of $\{T\}_t$ and $\{Q\}_t$ acting in the finite interval of time Δt. In the interval, temperature is assumed to vary linearly,

$$T \approx \hat{T}(\tau) = T_t + \frac{\tau}{\Delta t}\left(T_{t+\Delta t} - T_t\right) \tag{2.20}$$

By translating in standard finite element expansion,

$$\hat{T}(\tau) = \sum N_i T = \left(1 - \frac{\tau}{\Delta t}\right)T_t + \left(\frac{\tau}{\Delta t}\right)T_{t+\Delta t} \tag{2.21}$$

where the unknown parameter is $T_{t+\Delta t}$. The equation by which this parameter is provided will be the weighted residual approximation of equation (2.22) i.e.,

$$\int_0^{\Delta t} w\left(\left[C\right]\left\{\dot{T}\right\} + \left[H\right]\left\{\hat{T}\right\} + \left\{Q\right\}\right).d\tau = 0 \tag{2.22}$$

The elemental equation can be expressed by introducing θ as a weighting parameter given by

$$\theta = \frac{1}{\Delta t \int_0^{\Delta t} w.d\tau} \int_0^{\Delta t} w\tau.d\tau \tag{2.23}$$

$$\left[C\right]\frac{\left(\left\{T\right\}_{t+\Delta t} - \left\{T\right\}_t\right)}{\Delta t} + \left[H\right]\left(\left\{T\right\}_t + \theta\left(\left\{T\right\}_{t+\Delta t} - \left\{T\right\}_t\right)\right) + \left\{\bar{Q}\right\} = 0 \tag{2.24}$$

where $\bar{Q}$ represents an integral average value of Q as,

$$\left\{\bar{Q}\right\} = \frac{\int_0^{\Delta t} \left\{Q\right\} w.d\tau}{\int_0^{\Delta t} w.d\tau} = \left\{\bar{Q}\right\}_t + \theta\left(\left\{\bar{Q}\right\}_{t+\Delta t} - \left\{\bar{Q}\right\}_t\right) \tag{2.25}$$

The solution of the equation for the unknown term yields

$$\left\{T\right\}_{t+\Delta t} = \frac{\left(\left[C\right] - \left[H\right](1-\theta).\Delta t\right)\left\{T\right\}_t - \left\{\bar{Q}\right\}.\Delta t}{\left[C\right] + \left[H\right]\theta.\Delta t} \tag{2.26}$$

θ is a factor between 0 and 1. If θ is equal to 0, the algorithm is termed “explicit” (Euler) else it is termed “implicit”. If θ is equal to ½ it is termed Crank-Nicolson scheme and it is called Galerkin scheme if it is equal to 2/3.

The selection of suitable time stepping procedure during quenching requires some trial and error approach because when thermal properties vary with temperature, the coefficients of the finite difference equations may vary from one time step to the next. Therefore, they have to be evaluated at a suitably chosen average temperature to achieve a reasonable accuracy. It should be noted that when explicit methods are used, the time step size is very limited and this limitation is highly dependent on the rate of variation of material properties. Too small time steps may result in considerable increase in computation time. On the other hand, certain considerations should be made before the selection of implicit methods in spite of the possibility of using larger time steps. For example, Hughes showed that many implicit algorithms used in transient heat conduction which are unconditionally stable for linear problems lose their property when applied to non-linear problems[176]. As a remedy, he suggested a family of one step methods which possess the same stability properties in both linear and non-linear problems [176-178]. Donea discussed different numerical integration schemes related with finite element solution of transient heat conduction problem. He concluded that the Galerkin time walk method provides a convenient scheme for the time integration of fast varying heat conduction problems. When the high frequency components become unimportant, the Crank-Nicholson scheme should be used to take advantage of its second order accuracy [179]. However, according to Wood and Lewis, Crank-Nicholson scheme with a simple averaging process yields solutions with minimum noise [180].

Efficiency of the numerical procedure is dependent on the first guess of the solution at each time step. The calculation is considered when the error, including all nodal values, falls below a critical value e^*,

$$\sqrt{\sum_{j=1}^{n}\left(\frac{T_i - T_{i-1}}{T_{i-1}}\right)^2} \le e^* \tag{2.27}$$

where i, n and e^* stands for iteration number, total number of nodes and the convergence limit.

An efficient time stepping is required to obtain a better accuracy, convergence and run time. If the time walk scheme is unconditionally stable, automatic time stepping procedures can effectively reduce the run time. By use of a self adaptive method, shorter time steps can be used when cooling rates are high (i.e., initial stages of quenching for example) whereas, large time steps can be used when the cooling rates are low (final stages of quenching). For this purpose, an error norm is calculated at the end of each time step, the time step is reduced by a factor and the step is repeated until the norm is acceptable.

CHAPTER 3

MODELING THE PHASE TRANSFORMATIONS

3.1 GENERAL

Phase transformations may be the most important phenomenon occurring during thermal treatments due to their complex and pronounced interactions with other physical fields. Basically, all physical fields are affected from phase transformations because of the microstructural dependence of material properties. Besides those, they exhibit complicated interactions with other physical fields, such as latent heat of transformation, transformation induced plasticity (TRIP), stress/strain-induced/assisted transformations. Most of these interactions are still active research fields and still require better explanations and quantitative theories.

During the course of thermal treatments, thermodynamic and thermokinetic stabilities of phases are intentionally altered to optimize the microstructure according to design needs. Thermochemical and mechanical driving forces are exploited in design of the new microstructure. In state of the art processing techniques, other driving forces such as magnetism and electricity may also be exploited to achieve the desired microstructure.

Production of optimized and new materials is a challenging task both from the scientific and engineering viewpoints. First, the process requires a deep understanding of the involved physics and their interactions. Then, it necessitates quantitative theories, models and simulation tools since prediction of the results of a coupled multi-physics process are not easy to predict without performing simulations. Finally, the process involves design of the engineering systems to control the “forces of nature” according to the design needs determined by numerical simulations

Modeling and simulation of heat treatments is a very good research subject in understanding of the “irreversible thermodynamics” of materials which will lead to optimization of current processing systems and development of new processes. Deep understanding of the all of the involved phenomena and the prediction of the final state of the component after a thermal treatment has not been achieved to the full yet, even though their long history starting from the early ages of humans. This may be owed to the lack of basic knowledge on materials physics, accurate quantitative models and powerful simulation tools.

Phase transformations occurring in the course of steel quenching may be considered as a material system under thermochemical and mechanical driving forces. Variation of the temperature is major driving force (thermochemical) for phase transformations. Upon fast cooling, thermochemical stability of austenite is significantly altered due to changes in temperature (Figure 3.1). This results in the decomposition of austenite into new phases and phase mixtures. Transformation rate, in its most basic sense, depends on the temperature and the cooling rate. Besides thermochemical driving forces, mechanical driving forces such as elastic strains may alter both the thermodynamics and the kinetics of the transformation. Similar to elastic strains, prior or concomitant plastic strains, which cannot be directly considered as driving forces, may also substantially alter the phase transformation behavior. These concepts are reviewed in detail in Section 3.8 while the consequences of the phase transformations such as TRIP are discussed in Section 4.4.

In this chapter, a model for computation microstructural evolution coupled with transient thermal and mechanical fields, which can yield the microstructure at any location of a component as a function of time, temperature and stress, is presented with a detailed review of other possible approaches. The outputs of the microstructural field will be used in evaluations of the thermal and mechanical response of the system according to the procedures given in Chapter 2 and 4.

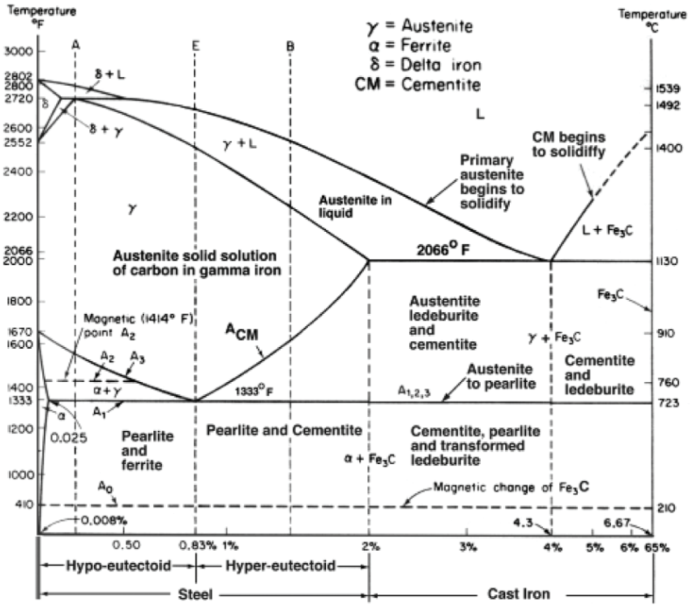

Figure 3.1 Fe-C phase diagram [181]

3.2 PHASE TRANSFORMATION MECHANISMS

In its most general sense, phase transformations that occur during quenching of steels can be categorized in two major categories according to their mechanism:

3.2.1 RECONSTRUCTIVE PHASE TRANSFORMATIONS

Reconstructive transformations are the phase transformations that require re-arrangement of the lattice via diffusional mechanisms (Figure 3.2). Formations of pearlite, allotriomorphic and idiomorphic ferrite in steels are examples for this kind of phase transformations (Figure 3.3). Both single and polycrystals experience only isotropic volume change as a consequence of reconstructive transformations.

Kinetics of reconstructive transformations is mainly determined by temperature and cooling rate. Their thermodynamics and kinetics may also be altered due to elastic or plastic strains. However, the effect of the mechanical driving forces is less significant with respect to displacive phase transformation. The main effect of elastic strains is because of the change of the free volume and the modification of the diffusion coefficient. Those concepts and possible modeling approaches are discussed in detail in Sections 3.8.2 and 3.8.3.

3.2.2 DISPLACIVE PHASE TRANSFORMATIONS

Displacive Phase Transformations are transformations that occur via a special deformation causing change of the lattice (Figure 3.2). Martensitic, bainitic, Widmanstatten ferritic phase transformations are transformations of that kind (Figure 3.4). Martensitic transformation is the sole transformation that occurs just by displacive mechanism. Bainite and Widmanstatten ferrite also transforms by displacive mechanism, however the growth of bainite and Widmanstatten ferrite requires the partitioning of the interstitial carbon. Because of this reason, their growth is controlled by diffusion although the transformation from FCC to BCC crystal structure is via displacive mechanism

Displacive transformation from FCC to BCC (and BCT) crystal structure occurs with 24 possible variants, each characterized by a distinct lattice orientation relationship. Special deformation which results in formation of variants is characterized by a transformation strain involving a dilatational (δ) component perpendicular to the habit plane and a shear component (γ) on the habit plane. In general, only the preferred variants are nucleated upon thermomechanical loading depending on the stress state.

Displacive transformations results in both volume and shape change for single crystals whereas, they may lead to isotropic volume change or anisotropic shape change in polycrystals. The anisotropic irreversible strain observed on polycrystals also referred as transformation plasticity and it may be due to transformation under a stress field or prior texture in the parent phase.

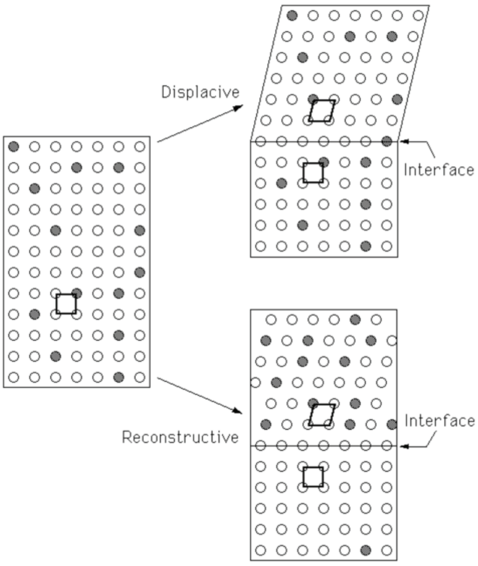

Figure 3.2 Displacive and reconstructive phase transformation mechanisms [3]

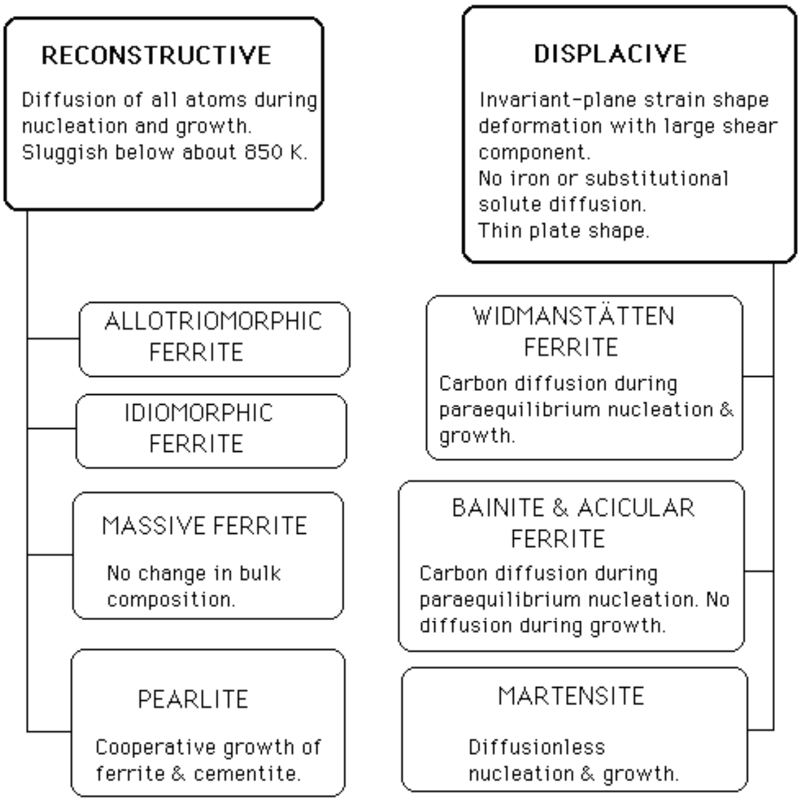

RECONSTRUCTIVE: Diffusion of all atoms during nucleation and growth. Sluggish below about 850 K.

DISPLACIVE: Invariant-plane strain shape deformation with large shear component. No iron or substitutional solute diffusion. Thin plate shape.

MASSIVE FERRITE: No change in bulk composition.

PEARLITE: Cooperative growth of ferrite & cementite.

WIDMANSTÄTTEN FERRITE: Carbon diffusion during paraequilibrium nucleation & growth.

BAINITE & ACICULAR FERRITE: Carbon diffusion during paraequilibrium nucleation. No diffusion during growth.

MARTENSITE: Diffusionless nucleation & growth.

Figure 3.3 Categorization of phase transformations during quenching of steels [3].

3.3 PHASE TRANSFORMATIONS DURING STEEL QUENCHING

Calling attention to steel quenching, if the initial temperature of the component is high enough to have an austenitic microstructure, depending on the cooling rate, austenite may transform to product phases such as ferrite, pearlite, bainite or martensite.

Martensite forms by a time independent displacive transformation at temperatures below M_s. Martensite is simply a supersaturated solid solution of carbon in α-Fe since the cooling rate is such that majority of carbon atoms in γ phase remain in α phase. Physically, the transformation occurs by nucleation and growth, however; the growth rate is so high that the rate of transformation is almost entirely controlled by the nucleation stage. In fact, austenite/martensite interface reaches almost the speed of the sound inside the solid. M_s temperature is associated with a certain driving force for the diffusionless transformation of austenite into martensite. In low carbon steels, M_s is about 500^oC, but increasing alloying element content cause progressive decrease. Interstitial alloying elements such as carbon and boron are more effective in decreasing the M_s temperature than substitutional elements. Beside the chemical composition, M_s temperature also depends on the stress state and prior plastic deformation.

Ferritic transformation occurs by nucleation at the austenite grain boundaries and then by growth into the austenite grains. Volume fraction of the ferrite is a function of the nucleation rate, the area and the velocity of the ferrite/austenite interface. The nucleation rate is primarily a function of the undercooling below A_{e3} line and the austenite grains size [182].

Pearlite consists of a lamellar structure with an interlamellar spacing which depends on the temperature of transformation. The effect of temperature on interlamellar spacing is due to the changes in the diffusivity of the carbon and alloying elements. Coupled nucleation of the ferrite and cementite at austenite grain boundaries leads to formation of pearlite colonies. Coupled growth of ferrite and cementite occur by diffusion along the interface between the eutectoid structure and the matrix.

The bainitic transformation displays characteristics of both martensitic and diffusional transformations. Bainite covers a range of different ferrite plus carbide structures in which nucleation involves formation of ferrite by a displacive mechanism. However, subsequent growth of the phase mixture occurs by a diffusion-controlled process.

The most straight forward approach for calculating microstructural evolution during a continuous cooling process would simply be to introduce CCT diagrams into the computer program. A CCT diagram is only valid for the exact temperature histories used to draw it, and those cooling curves are normally plotted on the diagram. However, during quenching, cooling rate at a point is generally not constant and hence, it does not follow one of those curves; therefore, the CCT diagram is no longer valid. Moreover, two different thermal histories exhibiting same cooling rate would yield the same transformation amount, which is an unsatisfactory result [45]. As a workaround, Scheil`s additivity principle is commonly employed to relate a TTT diagram to the transformation behavior for an arbitrary continous cooling path [182-184]. Thus, the cooling curve can be treated as a series of small isothermal time steps connected by instantaneous temperature jumps following constant volume fraction lines. The transformed volume fractions are then calculated isothermally during each time step.

3.4 DETERMINATION OF CRITICAL TEMPERATURES

The first step in simulation of phase transformation during quenching is the determination of temperature ranges in which different phase transformations occur. These ranges are bounded by the critical temperatures. These temperatures can directly be extracted from TTT and equilibrium phase diagrams or calculated using analytical expressions. The use of TTT and phase diagrams is straight forward. In literature, there are several proposals for determination of the critical temperatures as a function of chemical composition. Some of them are based on thermodynamic calculations, whereas, the others are purely phenomenological expressions based on regression analysis.

The A_{e3} temperature can be calculated using an ortho-equilibrium approach which assumes full partitioning of alloying elements [185]. This assumption is physically reasonable since the ferrite transformation usually occurs at high temperatures at which substitutional and interstitial elements can quickly diffuse and become partitioned[85].

On the other hand, Lusk et al. [11] derived a purely empirical formula based on regression analysis of approximately 4000 steel grades.

$$\begin{aligned} \mathrm{A_{c3}}(^{\circ}\mathrm{C}) = {} & 883.49 - 275.89\ \mathrm{C} + 90.91\ \mathrm{C}^2 - 12.26\ \mathrm{Cr} + 16.45\ \mathrm{C\ Cr} \\ & - 29.96\ \mathrm{C\ Mn} + 8.49\ \mathrm{Mo} - 10.80\ \mathrm{C\ Mo} - 25.56\ \mathrm{Ni} \\ & + 1.45\ \mathrm{Mn\ Ni} + 0.76\ \mathrm{Ni}^2 + 13.53\ \mathrm{Si} - 3.47\ \mathrm{Mn\ Si} \end{aligned} \tag{3.1}$$

Kirkaldy and Barganis [186] proposed a similar type of expression which also includes several alloying elements (W, As, Ti, Al. Cu) which is not included in the previous expression as:

$$\begin{aligned} \mathrm{A_{e3}}(^{\circ}\mathrm{C}) = {} & 912 - 203\ \mathrm{C}^{0.5} + 15.2\ \mathrm{Ni} + 44.7\ \mathrm{Si} - 104\ \mathrm{V} + 31.5\ \mathrm{Mo} + 13.1\ \mathrm{W} \\ & - 30\ \mathrm{Mn} - 11\ \mathrm{Cr} - 20\ \mathrm{Cu} + 700\ \mathrm{P} + 400\ \mathrm{Al} + 120\mathrm{As} + 400\ \mathrm{Ti} \end{aligned} \tag{3.2}$$

Lust et al. [11] obtained the following expression by a similar para-equilibrium treatment by regressing 2000 $\mathrm{A_{Fe_3C}}$ temperatures for 20.000 steel grades

$$\begin{aligned} A_{Fe_3C}(^\circ C) = {} & 217.50 + 977.65\ C - 417.57\ C^2 - 35.29\ Cr + 21.36\ C\ Cr \\ & - 1.50\ Cr^2 - 0.95\ Mn - 1.37\ C\ Mn - 2.76\ Mo - 3.77\ C\ Ni \\ & + 30.36\ Si - 8.10\ C\ Si + 2.58\ Cr\ Si \end{aligned} \tag{3.3}$$

The predictions of A_{e1} by orthoequilibrium approach are not satisfactory because substitutional elements are not fully partitioned during eutectoid transformation. As a remedy to this problem, paraequilibrium thermodynamic models, assuming a uniform carbon chemical potential and a continuous substitutional element-to-iron mole fraction ratio at the transforming interface are employed [42, 50, 63, 64, 76, 77, 85, 126, 185, 186]. A_{e1} temperatures calculated under this assumption are denoted by A_{p1}.However, most of experimental A_{e1} temperatures are located between A_{o1} and A_{p1}. Kirkaldy and Venugopalan [187] proposed the following intermediate model to predict the A_{e1} temperatures of low alloy steels that have arbitrary chemical compositions:

$$T_{pl} = A_{p1} + (A_{o1} - A_{pl})\ \frac{Cr}{Ni + Cr + Mo} \tag{3.4}$$

Although this expression improves the prediction of A_{e1}, it only implies full partitioning of Cr but does not consider the partitioning of a very common alloying element Mn. Lusk et al. [85] improved this model to take into account Mn partitioning as follows :

$$T_{p1} = A_{p1} + (A_{o1} - A_{p1})\ \frac{P_{Mn}^{(avg)}(13.4\ Mn) + 24.4\ Cr}{13.4\ Mn + 13.4\ Si + 5.0\ Ni + 24.4\ Cr + 4.4\ Mo} \tag{3.5}$$

However, this expression still requires calculation of A_{o1} and A_{p1} by ortho and para-equilibrium models. To obtain a simpler expression, three different equations are derived based on different P_{Mn} values [11].

$$T_{p1}(^\circ C) = \begin{cases} 726.16 + 17.27\ Cr - 0.39\ C\ Cr - 1.97\ Cr^2 \\ - 11.79\ Mn + 3.95\ Cr\ Mn + 3.76\ Si \\ - 7.46\ Cr\ Si - 4.64\ Mn\ Si + 18.61\ Si^2 & ;\ Ni=Mo=0 \\ \\ 729.00 - 15.67\ Mn + 1.33\ C\ Mn - 1.46\ Mn^2 \\ - 18.56\ Ni - 2.13\ Mn\ Ni + 1.65 Ni^2 + 9.15\ Si \\ - 1.85\ Mn\ Si + 6.63\ Si^2 & ;\ Cr=Mo=0 \\ \\ 727.37 + 13.40\ Cr - 1.03\ C\ Cr - 16.72\ Mn \\ + 0.91\ C\ Mn + 6.18\ Cr\ Mn - 0.64\ Mn^2 \\ + 3.14\ Mo + 1.86\ Cr\ Mo - 0.73\ Mn\ Mo \\ - 13.66\ Ni + 0.53\ C\ Ni + 1.11\ Cr\ Ni & ;\ Mn \neq 0 \\ - 2.28\ Mn\ Ni - 0.24\ Ni^2\ 6.34\ Si - 8.88\ Cr\ Si \\ - 2.34\ Mn\ Si + 11.98\ Si^2 \end{cases} \tag{3.6}$$

B_s can be calculated using the equation proposed Steven and Haynes [188],

$$\mathrm{B_s}(^{\circ}\mathrm{C}) = 656 - 58\ \mathrm{C} - 35\ \mathrm{Mn} - 75\ \mathrm{Si} - 15\ \mathrm{Ni} - 34\ \mathrm{Cr} - 41\ \mathrm{Mo} \tag{3.7}$$

Andrews [189] proposed the following equation for prediction of M_s temperature as a function of chemical composition.

$$\mathrm{M_s}(^{\circ}\mathrm{C}) = 561 - 474\ \mathrm{C} - 33\ \mathrm{Mn} - 17\ \mathrm{Ni} - 17\ \mathrm{Cr} - 21\ \mathrm{Mo} \tag{3.8}$$

Kirkaldy and Venugoplan[187] derived an alternative as,

$$\begin{aligned}\mathrm{M_s}(^{\circ}\mathrm{C}) = 512 &- 453\ \mathrm{C} - 16.9\ \mathrm{Ni} + 15\ \mathrm{Cr} - 9.5\ \mathrm{Mo} + 217\ \mathrm{C}^2 \\ &- 71.5\ \mathrm{C\ Mn} - 67.6\ \mathrm{C\ Cr}\end{aligned} \tag{3.9}$$

3.5 KINETICS OF DIFFUSION CONTROLLED TRANSFORMATIONS

During quenching of steels, thermodynamic stability and hence the solubility of carbon in austenite decreases as the temperature decreases, which requires removal of excess carbon and alloying elements. Removed alloying elements will aggregate as different phases and phase mixtures. The transformation occurs via nucleation and growth. The kinetics of transformation generally has three distinct stages: Initial nucleation, growth of initial nuclei with steady nucleation and finally site saturation and impingement of grains [190-194].

3.5.1 ISOTHERMAL TRANSFORMATION MODELS

Several mathematical models have been proposed for mathematical description of isothermal transformation kinetics of solid state transformations, most of which are based on same principles with minor modifications. In these models, initial transformed amount is expressed by:

$$\xi_k = b_k . t^{n_k} \tag{3.10}$$

where b and n are the temperature dependent time coefficient and the time exponent. n depends on the ratio of nucleation and growth rate whereas b depends on the absolute values of the nucleation and the growth rate. The values of b and n can be either be extracted from TTT, CCT diagrams or determined by experiments. The method of extraction will be discussed in Section 3.7.

As transformation proceeds, the available volume for nucleation becomes exhausted and later, growing phase boundaries impinge each other, both leading to a decrease in transformation rate. This situation leads to a more general equation in the form of

$$\dot{\xi}_k = (1 - \xi_k)^{r_k} n_k b_k (b_k t)^{n_k - 1} \tag{3.11}$$

where r is the saturation parameter depending on the growth mode and the temperature. Different choices of r result in different kinetic equations. For example, the equation obtained is the Avrami equation when r=1 and Austin-Rickett equation when r=2 [190]. Other choices are also possible. Integration of this rate equation yields,

$$\xi_k = \begin{cases} 1\text{-}\exp\left(\text{-}b_k t^{n_k}\right) & ;\ r=1\ \text{(Avrami)} \\ 1\text{-}\left(1+b_k t^{n_k}\right)^{-1} & ;\ r=2\ \text{(Austin-Rickett)} \\ 1\text{-}\left(1+\left(r_k\text{-}1\right)b_k t\right)^{\left(\frac{r_k-1}{n_k}\right)} & ;\ r \neq 1 \end{cases} \tag{3.12}$$

This expression may be corrected to account for phase transformations that start from a phase mixture and do not saturate to 100% as:

$$\xi_k(t) = \xi_k^o + \left(\xi_k^{\max} - \xi_k^o\right)\left(1 - \exp\left(b_k t^{n_k}\right)\right) \tag{3.13}$$

where ξ^o and ξ^{eq} are the initial and the equilibrium concentrations.

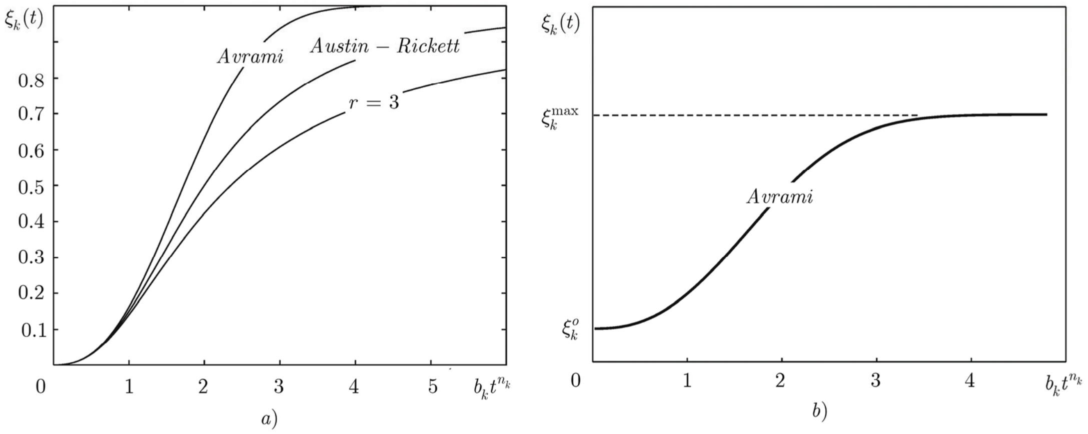

Figure 3.4 a) Different isothermal kinetic functions b) Modification of the Avrami kinetics

3.5.2 ANISOTHERMAL EXTENSIONS OF ISOTHERMAL TRANSFORMATION MODELS

Simulation of phase transformations during quenching, in which each point in the specimen has a distinct thermal history, requires mathematical models for anisothermal transformations. For thermally activated transformations, the thermal history of the specimen determines the state of transformation. Consider the three different thermal paths on Figure 3.4. Each path will result in different amount of the product phase although the paths start and end at the same temperature and time.

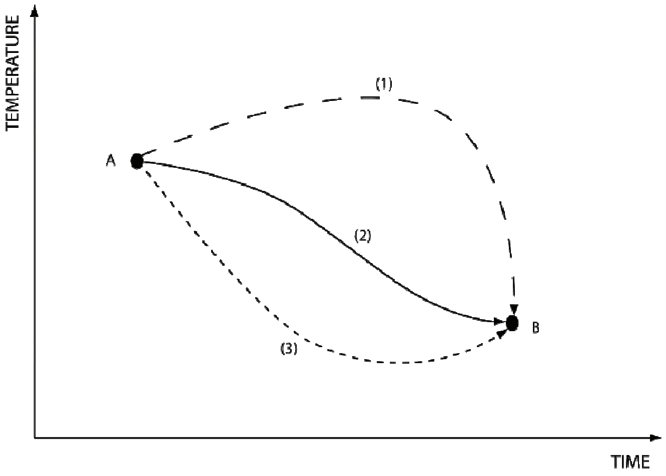

Figure 3.5 Three different thermal paths starting and ending at the same time and temperature, resulting in different amount of transformation.

Thus, both T and t cannot be used as state variables. Thus, a new state variable (β), depending on the thermal path, has to be defined for anisothermal processes. Then, an unspecified kinetic function F(β), which relates the transformed fraction to the thermal path, is defined

$$\xi_k = F_k(\beta) \tag{3.14}$$

F(β) can be in the form of any of the isothermal kinetic equations presented previously. If the transformation mechanism is invariable for the region of interest, then, the new state variable may be considered to be proportional to the number of atomic jumps. Temperature determines the atomic mobility and time defines the duration of the process [195].

$$\beta = \int_0^t c_k(T).dt \tag{3.15}$$

where c(T) is the temperature dependent rate constant. The temperature dependence of c(T) may be expressed in the form of an Arrhenius-type equation as,

$$c_k(T) = c_k^o.\exp\left(-\frac{E_k}{RT}\right) \tag{3.16}$$

where $\mathrm{c_k^o}$ is the pre-exponential factor, E is the activation energy and R is the gas constant.

Using these concepts, the transformation rate in terms of the new state variable (β) can be described by the time derivative of ξ as,

$$\dot{\xi}_k = \frac{dF}{d\beta}\frac{d\beta}{dt} = c(T)\frac{dF}{d\beta} \tag{3.17}$$

Hence, β, ξ and T are the state variables for the transformation rate. This realization introduces the notion of "additivity", which has first been proposed by Scheil [184]. This concept has later been extended to solid state phase transformation by Cahn [183] and generalized by Christian [182].

Additivity principle has long been discussed, reviewed and adopted by many authors [2, 12, 77, 78, 84, 116, 127, 196-203]. General conclusion that can be drawn from these studies is that conventional Scheil-Cahn-Christian additivity principle is not quite accurate in calculation of anisothermal kinetics from isothermal kinetic data. Some of the cited works improved the additivity principle to achieve a better fit with experimental data, however; most of these methods require additional experiments to be performed. As an alternative, Lusk et al. [11] developed a global non-additive kinetic model, which is also incorporated in DANTE(R) software.

Henceforth, scope of the rest of this text will confine on Johnson-Mehl-Avrami-Kolmogorov (JMAK) kinetic equation and classical "additivity" principle, regardless of their applicability. The treatment can also be extended to different kinetic equations and improved additivity rules by considering similar principles.

According to Scheil`s additivity rule, if $\tau(\xi_k, T)$ is the isothermal time required to reach certain transformed amount $\xi_k$, the same transformation amount will be reached under anisothermal conditions when the following Scheil`s sum (S) equals to unity [204]:

$$S = \int_0^t \frac{dt}{\tau(\xi_k, T)} = 1 \tag{3.18}$$

For computational purposes, this sum can be expressed in incremental form :

$$S = \sum_{i=1}^{n} \frac{\Delta t_i}{\tau_i(\xi_k, T_i)} \approx 1 \tag{3.19}$$

where Δt_i , τ_i are the time step size and isothermal time to reach ξ_k at the current time step.

Calculation of Anisothermal Incubation Time

Scheil`s additivity principle can be exploited in calculation of both the incubation times and the anisothermal kinetics of transformations, by incorporating with one of the isothermal kinetic functions defined in the previous section.

The calculation of incubation time, which is summarized on Figure 3.6, is straight forward, replacing $\tau_i(\xi_k, T_i)$ with isothermal incubation time ($\tau_s(T_i)$) results in

$$S = \sum_{i=1}^{n} \frac{\Delta t_i}{\tau_s(T_i)} \approx 1 \tag{3.20}$$

when S equals to nearly to unity, the incubation is considered to be completed under anisothermal conditions.

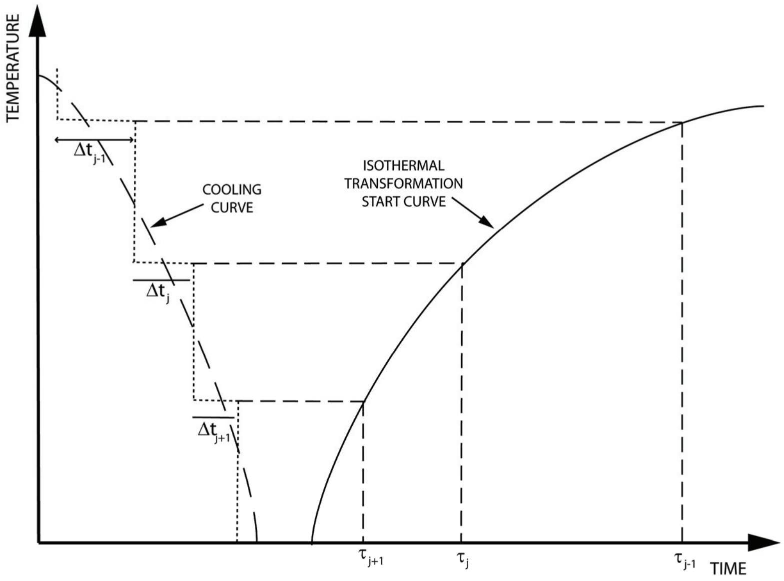

Figure 3.6 Calculation of anisothermal incubation time from IT diagrams using the principle of additivity.

Calculation of Anisothermal Growth Kinetics

After the completion of incubation time, growth kinetics needs to be calculated. Considering the Avrami kinetic equation, a fictitious time τ, which is dependent on the fraction transformed up to the end of the previous time step, is calculated:

$$\tau = \left(-\frac{\ln\left(1 - \xi_k(t)\right)}{b_k} \right)^{\frac{1}{n_k}} \tag{3.21}$$

Next, the fictitious time is incremented by time step size (Δt) in order to calculate a new fictitious transformed fraction. Then, the fictitious transformed fraction is further corrected to take into account the amount of austenite available for the transformation and reactions that does not saturate to full completion. Figure 3.7 summarizes this procedure which yields the following equation

$$\xi_k^{t+\Delta t} = \xi_k^{\max}\left(\xi_\gamma^t - \xi_k^t\right)\left(1-\exp\left(b_k\left(\tau+\Delta t\right)^{n_k}\right)\right) \tag{3.22}$$

where $\xi_k^{\max}$ is the maximum fraction of the product phase. For pearlitic or bainitic transformation, it is the fraction of austenite at the beginning of the transformation ($\xi_p^{\max} = \xi_b^{\max} = \xi_\gamma^t$). If the quenching process starts with 100% homogenous austenite, it can be assumed that $\xi_p^{\max} = \xi_b^{\max} = \xi_\gamma^t = 1$. In the case of proeutectoid transformations, $\xi_p^{\max}$ can be calculated using lever rule on equilibrium phase diagram.

Alternative Approach: Direct Integration of JMAK Kinetic Equation

An alternative way of calculating microstructural evolution during quenching relies on derivation of a rate equation which is inherently additive. Assuming that additivity principle holds, a kinetic function which relates the transformation rate to the instantaneous state can be defined in the form of:

$$\dot{\xi}_k = \dot{\xi}_k(\xi_k, T) \tag{3.23}$$

After elimination of time from isothermal kinetic equations, following rate equations are obtained :

$$\dot{\xi}_\mathrm{k} = \begin{cases} \mathrm{bn}(1\text{-}\xi_\mathrm{k})\left(\ln\left(\dfrac{1}{1\text{-}\xi_\mathrm{k}}\right)\right)^{\left(1\text{-}\frac{1}{\mathrm{n}}\right)} & ;\ \mathrm{r}=1\ \text{(Avrami)} \\ \\ \mathrm{bn}(1\text{-}\xi_\mathrm{k})^{\left(1+\frac{\mathrm{r-1}}{\mathrm{n}}\right)}\left(\dfrac{1\text{-}\left(1\text{-}\xi_\mathrm{k}\right)^{(\mathrm{r-1})}}{\mathrm{r-1}}\right)^{\left(1\text{-}\frac{1}{\mathrm{n}}\right)} & ;\ \mathrm{r} \neq 1 \end{cases} \tag{3.24}$$

Then, following approximate rate equation is derived by applying a Taylor expansion to the last factor of these equations and making the appropriate corrections for transformation having non-zero initial fractions and saturating to an equilibrium fraction [80]:

$$\dot{\xi}_k \approx bn\left(\frac{\xi_k^{eq} - \xi_k}{\xi_k^{eq} - \xi_k^o}\right)^{\left(1+\frac{r-1}{n}\right)}\left(\frac{\xi_k - \xi_k^o}{\xi_k^{eq} - \xi_k^o}\right)^{\left(1-\frac{1}{n}\right)} \tag{3.25}$$

Incremental form of this rate equation can directly be used in phase transformation subroutine rather than the conventional additivity procedure due to its additive nature.

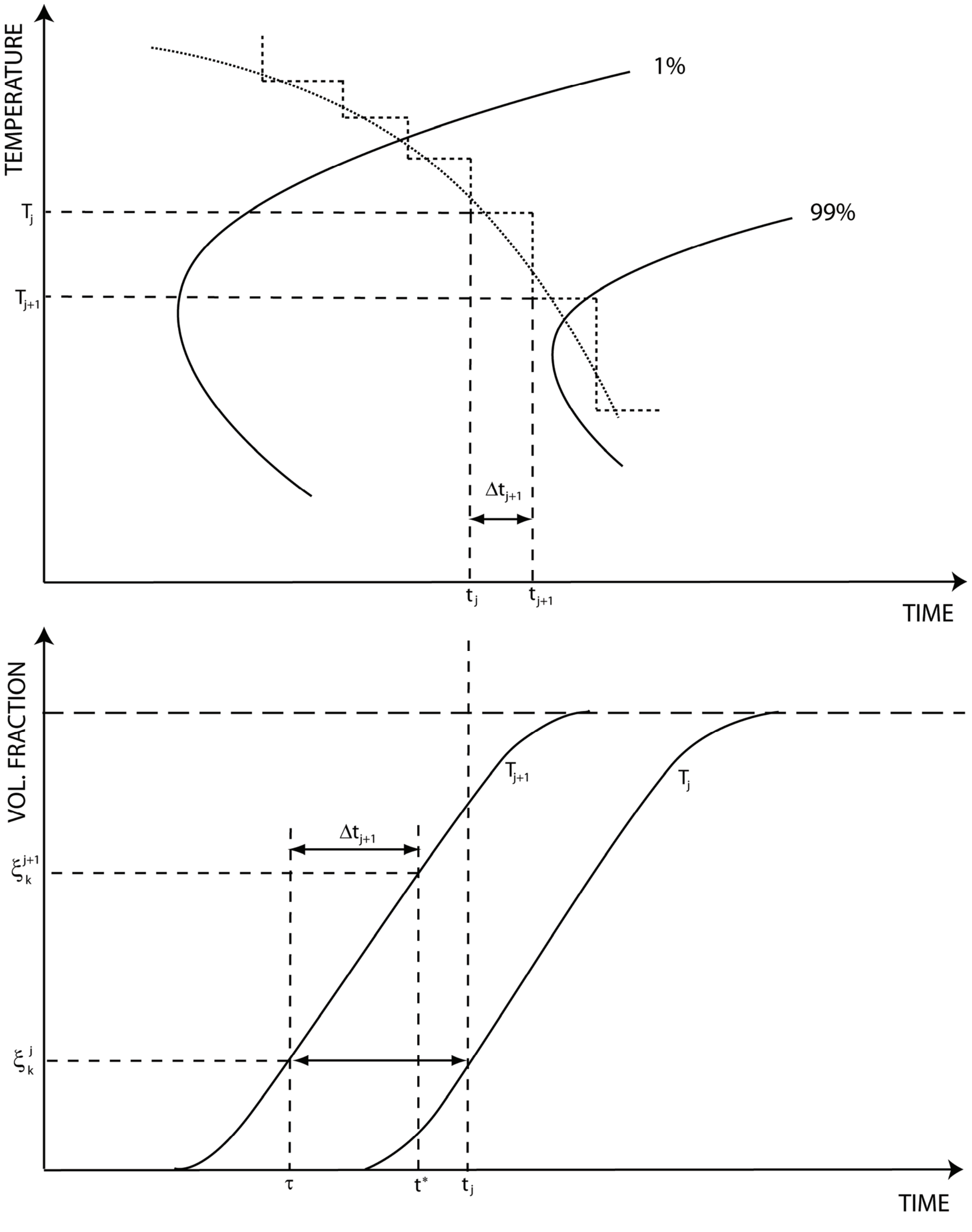

Figure 3.7 Calculation of anisothermal growth kinetics using the principle of additivity.

3.6 MODELING THE MARTENSITIC TRANSFORMATION

Martensite is commonly considered to form by a time independent transformation below M_s temperature. Physically, there exists a nucleation and growth stage, but the growth rate is so high that the rate of volume transformation is almost entirely controlled by nucleation. In fact, austenite/martensite interface moves almost at the speed of sound in the solid. Therefore, its kinetics is essentially not influenced by the cooling rate.

M_s temperature is dependent on the stress state, prior plastic deformation and diffusional phase transformations. The effect of stress and prior plastic deformation on M_s is discussed in detail and possible modeling approaches are presented in Section 3.8.1. In addition to the stress and plasticity, prior diffusional transformations also affect the M_s temperature due to carbon enrichment of austenite during transformations. However, this affect is not incorporated in any of the current quenching models.

Kinetics of martensitic transformation cannot be described by Avrami type of kinetic equations. The amount of martensite formed is often calculated as a function of temperature using the law established by Koistinen and Marburger[205],

$$\xi_m = \xi_\gamma \left(1 - \exp\left(-\Omega\left(M_s - T\right)\right)\right) \tag{3.26}$$

where Ω is constant for many steels, whose value is 0.011 regardless of the chemical composition.

Although Koistinen and Marburger proposed this equation from solely phenomenological point of view, later, Magee [7] had shown that such kind of a relationship may also be derived from first principles by assuming that the increase in martensite plates for an infinitesimal temperature decrease below M_s is proportional to increase in the driving force for austenite-martensite transformation as :

$$\frac{dN_m}{dT} = -c_1 \frac{d\left(\Delta G^{a-m}\right)}{dT} \tag{3.27}$$

where c_1 is a positive proportionality constant expressing increase in density of activated nucleation sites due to increase in activation energy. The increase of the volume fraction of martensite for an infinitesimal temperature increment dT is then given by:

$$\frac{d\xi_m}{dT} = \zeta\left(1 - \xi_m\right)\frac{dN_m}{dT} = -c_1\zeta\left(1 - \xi_m\right)\frac{d\left(\Delta G^{a-m}\right)}{dT} \tag{3.28}$$

where ζ is the average volume for martensite crystal. Assuming that all the terms except ξ_m is independent of temperature over the transformation range and integrating equation (3.28) from $\xi_m = 0$, $T = M_s$ to actual volume fraction at a given temperature and rearranging, following expression which is similar to Koistinen-Marburger is obtained as,

$$\xi_m = 1 - \exp\left(c_1 \zeta \frac{d(\Delta G^{a-m})}{dT} \left(M_s - T \right) \right) \tag{3.29}$$

Finally, Lusk et al. [11], in their Global Kinetics Model (GMK), used an alternative approach to evaluate the amount of martensite formed by describing the kinetics by an equation having an explicit dependence on the cooling rate.

$$\frac{d\xi_m}{dT} = \xi_a v_m \left(\xi_m + \xi_m^* \right)^{c_1} \left(1 - \xi_m \right)^{(c_2 - 1)} \tag{3.30}$$

where v_m is the mobility of the martensite interface as a function of carbon content and ξ_m^* is the enhanced nucleation of martensite due to presence of other phases. c_1 and c_2 are exponents which should be fitted from a combination of isothermal and continuous cooling dilatometry data.

Effect of Austenite Grain Size

The prior austenite grains size affects martensitic transformation. The effect of prior austenite grains size may be incorporated into martensite kinetics by using a modified Zener-Hillert [16] equation by:

$$\frac{d\xi_m}{dT} = \frac{2^{(c_1 G)}}{c_2} \left(\xi_m \right)^{(c_3 + c_4 G)} \left(1 - \xi_m \right)^{(c_5 + c_6 G)} \tag{3.31}$$

where G is the ASTM grain size number and c_1-c_6 are constants that must be fitted from the experiments.

3.7 DETERMINATION OF KINETIC PARAMETERS

Kinetic parameters for presented models can be extracted either TTT,CCT diagrams or can be determined experimentally by measuring any property which is sensitive to phase transformations (such as volume, heat response, conductivity, magnetic permeability change etc.). In this section, extraction of kinetic parameters from TTT and CCT diagrams will be presented.

3.7.1 EXTRACTION OF KINETIC PARAMETERS FROM TTT DIAGRAMS

Transformation start and finish curves on a TTT diagram are represented by C shape curves. To define the C-shaped curve for the entire interval between the upper and the lower temperature limits, pearlite start and finish curves are extrapolated towards A_{e1}, while the finish curve of bainite is extrapolated towards the upper limit of bainitic transformation. Extraction of isothermal kinetics parameters can be performed directly by using the start and finish times. Taking ξ^s=0.01, ξ^f=0.99 and considering the Avrami kinetics, this treatment yields :

$$n_k = \frac{\log\left(\dfrac{\ln(1-\xi_k^f)}{\ln(1-\xi_k^s)}\right)}{\log\left(\dfrac{t_s}{t_f}\right)} \approx \frac{2.661}{\log(t_f) - \log(t_s)} \tag{3.32}$$

$$b_k = -\frac{\ln(1-\xi_k^s)}{\left(t_s\right)^{n_k}} \approx \frac{0.01}{\left(t_s\right)^{n_k}} \tag{3.33}$$

After calculation of b and k for a series of temperatures, a curve fitting algorithm can be used to determine the temperature dependence of b and k. For example, Tzitzelkov [206] suggested a 3rd order polynomial fit for this purpose as,

$$n_k(T) = n_k^1 T + n_k^2 T^2 + n_k^3 T^3 \tag{3.34}$$

$$\log b_k(T) = b_k^1 T + b_k^2 T^2 + b_k^3 T^3 \tag{3.35}$$

Other fitting alternatives are also possible as long as they accurately represent the transformation curve.

In plain carbon steels, there is a significant overlap between the pearlitic and bainitic transformation. For the temperature range in which both transformations occur at the same time, b and n values cannot be determined. As a solution to this problem, it is commonly assumed that the pearlite growth degenerates to bainite transformation when B_s is reached. If pearlite exists when B_s is crossed, then it is assumed that the existing pearlite/austenite interface continues to transform, but now yielding bainite [207] .

3.7.2 EXTRACTION OF KINETIC PARAMETERS FROM CCT DIAGRAMS

As opposed to generation of CCT diagrams from TTT diagrams, TTT diagrams can be generated from CCT diagrams by an inverse use of additivity principle. Although it may appear strange to extract isothermal kinetic constants from continuous cooling transformation (CCT) diagrams, this method has certain advantages in simulation of quenching. First advantage of this approach is improved accuracy for simulations. Microstructural evolution subroutines in most of the quenching simulations are based on the additivity principle. Indeed, the isothermal parameters extracted from CCT diagrams by an inverse additivity procedure will perform better than the ones extracted from TTT diagrams.

Second advantage of this method arises from the fact that CCT diagrams are less sensitive to overlapping transformations. Thus, a better representation of transformation behavior can be achieved.

Geijsalers [21] suggested following expressions for extraction of isothermal times from CCT diagrams as,:

$$t_{\alpha}^{1} = \frac{dT_1}{d\left(\dot{T}_c \dfrac{t_{\alpha}^{1}}{t_{\alpha}^{2}} \right)} \tag{3.36}$$

$$t_{p}^{2} = \frac{dT_2}{d\dot{T}_c + \dfrac{1}{\xi_{\alpha}^{eq}} \displaystyle\int_{T_{\alpha}^{e}}^{T_{A_1}} \frac{d\xi_{\alpha}}{t_{p}^{2}} .dT} \tag{3.37}$$

where $\dot{T}_c$ is a constant cooling rate; t_{α}^{1} , t_{p}^{2} are the isothermal times for the start and the end of transformations. which can later be used to calculate n. It should also be noted that calculation of t_{p}^{2} requires an iterative procedure. For detailed derivation and procedure, please refer to the original paper [21].

3.8 EFFECT OF THE STRESS AND PLASTICITY ON PHASE TRANSFORMATIONS

During heat treatment of engineering components, many parts are subjected to continuous heating and cooling cycles during which phase transformations occurs. Another important aspect of industrial heat treatment processes is the generation of a fluctuating internal stress field. Internal stresses are generated in the component due to thermal gradients and phase transformations. Typically, a material undergoing a heat treatment is subjected to a fluctuating triaxial stress and small plastic strains (up to 2-3%). During the process, mechanical field and phase transformations interact with each other. For example, stresses (internal or external) may alter transformation temperatures (such as A_{e3}, A_{e1}, M_s, B_s) or accelerate/decelerate the kinetics of austenite decomposition. They may even induce martensitic transformation or may stabilize austenite against martensitic transformation. On the other hand, phase transformations alters the stress field by dilatational and transformation plasticity, which will be discussed in detail in Section 4.

Phase transformations which occur under stress and with prior or concomitant plasticity can be considered as examples of `materials systems under driving forces` in which both the driving forces for transition and the kinetics of the process can be altered by mechanical interactions. In order to understand the effect of mechanical field on phase transformations , the mechanisms of mechanical energy storage in materials should be investigated[10].

Mechanical energy in a material is stored in the form of elastic strains in the lattice and epitaxial defects, plastic strains in dislocations and interfaces such as phase and grain boundaries. An important aspect of sequential deformation and phase transformation is the change of the scale produced by deformation, for instance the reduction of distance in a diffusion controlled process [208]. The interaction of mechanical driving forces and phase transformations depends both on the alloy and loading conditions.

Thermodynamics of phase transformations – i.e transformation temperatures, chemical composition of parent and product phases – is changed by the change of free energies of parent and product phases. Similarly, kinetics of transformation – i.e. transformation rates, path of transformation - may also be altered because of the change in the mobility of atoms due to elastic and plastic strains. Elastic strains effects the kinetics of transformation by changing the mobility of atoms via modification of the free volume. Plasticity alters the transport processes by changing the point defect concentration, providing shortcuts for diffusion via dislocation cores or by providing a non-diffusive transport mechanism where the atoms are convected by moving dislocations either geometrically or via the drag effect due to dislocation/solute interaction [10].

In correlation with simulation of quenching studies, these effects have been reviewed by several authors for different phase transformations as regards to the mechanisms involved, experimental determination and the modeling [18, 46, 51, 209, 210].

The effect of stress and plasticity on martensitic transformation, which is primarily important in quench hardening, has been investigated by many authors [8, 27, 51, 73, 81, 87, 136, 139, 147, 148, 151, 153, 197, 211-218]. The overall effect of elastic strains on M_s temperature is summarized on Figure 3.8. Martensitic transformation, which is accompanied by a dilatation, is expected to be shifted to lower temperatures by hydrostatic pressure, which opposes the volumetric expansion. In fact, there is a general agreement, based on both experimental, theoretical and simulation studies, on the fact that the application of hydrostatic pressure causes a decrease in M_s. However, it has been observed that a uniaxial stress that only causes elastic deformation in parent austenite irrespective to the sign of the stress, leads to an increase in M_s. This phenomena can be explained by interaction of shear components of global stress state with displacive transformation strains.

In contrast to elastic strain, prior plastic strain in austenite leads to a decrease in the M_s. This effect may be related with strain hardening of austenite. This retardation of transformation by plastic deformation is referred as “mechanical stabilization” and can be explained in terms of the structure of the transformation interface. Displacive transformations occur by the advance of glissile interfaces which can be rendered sessile when they encounter dislocation debris. Thus, whereas an appropriate stress can stimulate displacive transformation in the same way that it enables normal deformation, mechanical stabilization actually retards the decomposition of the austenite.

In regards to the effect of stress on diffusional transformations in steels (ferritic, pearlitic etc.), there is a general agreement that the application of hydrostatic pressure causes retardation of the diffusive phase transformations. The effect of hydrostatic pressure on the IT and CCT diagrams is the shift of transformation curves for ferrite, pearlite and bainite towards longer times (Figure 3.8). In fact, all transformations, which are accompanied by a reduction in density, are expected to be retarded by hydrostatic pressure, which opposes a volume expansion. The effect of hydrostatic pressure is twofold: it reduces the diffusion coefficients by decreasing the available free volume and it influences the free energy change for transformation [219]. On the other hand, it is observed that the kinetics of diffusional transformations is accelerated due to an increase in the free volume and the nucleation rate under uniaxial stress. A similar behavior is observed for ferritic and pearlitic transformations when a prior plastic strain exists. It is also observed that a tensile stress accelerates diffusive phase transformations more than a compressive stress. This phenomenon is generally owed to both the increase in mobility due to increase in the free volume and defect concentration.

Bainitic transformation is a hybrid type of transformation which involves a displacive nucleation stage and diffusion controlled growth stage [220-223]. Therefore, it is highly expected that both the thermodynamics and kinetics of transformation is affected by applied stress and prior plastic deformation. This expectation is justified by several authors [15, 46, 68, 75, 112, 224-226]. First, observation from the results is the decrease in B_s temperature as the hydrostatic stress increases. This fact can easily be explained considering the facts discussed previously in this chapter. Similar to the martensitic transformation, a uniaxial stress results in an increase in B_s. Another observation is the acceleration of both the onset and the kinetics of transformation up to a threshold stress after which the transformation is decelerated. Although experimental results are commonly in agreement, the explanation of the involved mechanisms is not yet clear. The effect of stress on incubation time is commonly explained by selection of nucleation sites which comply with stress [196, 227, 228]. However, another mechanism is required for explanation of the large increase in transformation rate [228]. This phenomenon may occur due to an autocatalytic or self-promoting nucleation or transformation [3, 196, 227-229].

The effect of prior plasticity on bainitic transformation is more complicated and harder to describe quantitatively. Figure 3.9 illustrates the effect of ausforming (plastic deformation in the austenitic phase). From this figure, it is observed that both the formation of high temperature (upper) and low temperature (lower) bainite transformation kinetics is highly affected from prior deformation. Although the incubation time is decreased in both cases, the incubation time of lower bainite is affected more significantly. This may be owed to increase in the nucleation rate because of the increase in the number of nucleation sites due lattice defects introduced by plastic deformation. This might have a more pronounced effect in lower bainite which already has a higher driving force for transformation but limited mobility.

Bainite growth kinetics is also highly influenced from prior plasticity besides the incubation time. It is clear that growth kinetics are pronouncedly accelerated at the initial stages and transformation reaches to saturation significantly earlier It is also observed that lower bainite transformation does not reach to completion due to mechanical stabilization. Refinement of the structure and reduction of bainite amount due to mechanical stabilization may be observed in Figure 3.10. Based on the observations from Figure 3.9 and Figure 3.10, the author dares to suggest a new kinetic equation in the form of equation (3.12) with a plastic strain dependent saturation limit and exponent(r) besides JMAK equation which may better represent transformation behavior with prior plasticity.

From the modeling side, several models have been developed for quantitative description of the effects discussed in this section [46, 230, 231]. Most of those models are based on modification of critical temperatures and governing kinetic equations. For example, Koistinen-Marburger law, Johnson-Mehl-Avrami-Kolmogorov (JMAK) equation and Scheil`s additivity principle have been modified to incorporate the effect of stress on phase evolution. However, those equations are not quite mature and usually require hard to acquire experimental data. They usually have a phenomenological nature and their physical basis may usually be arguable.

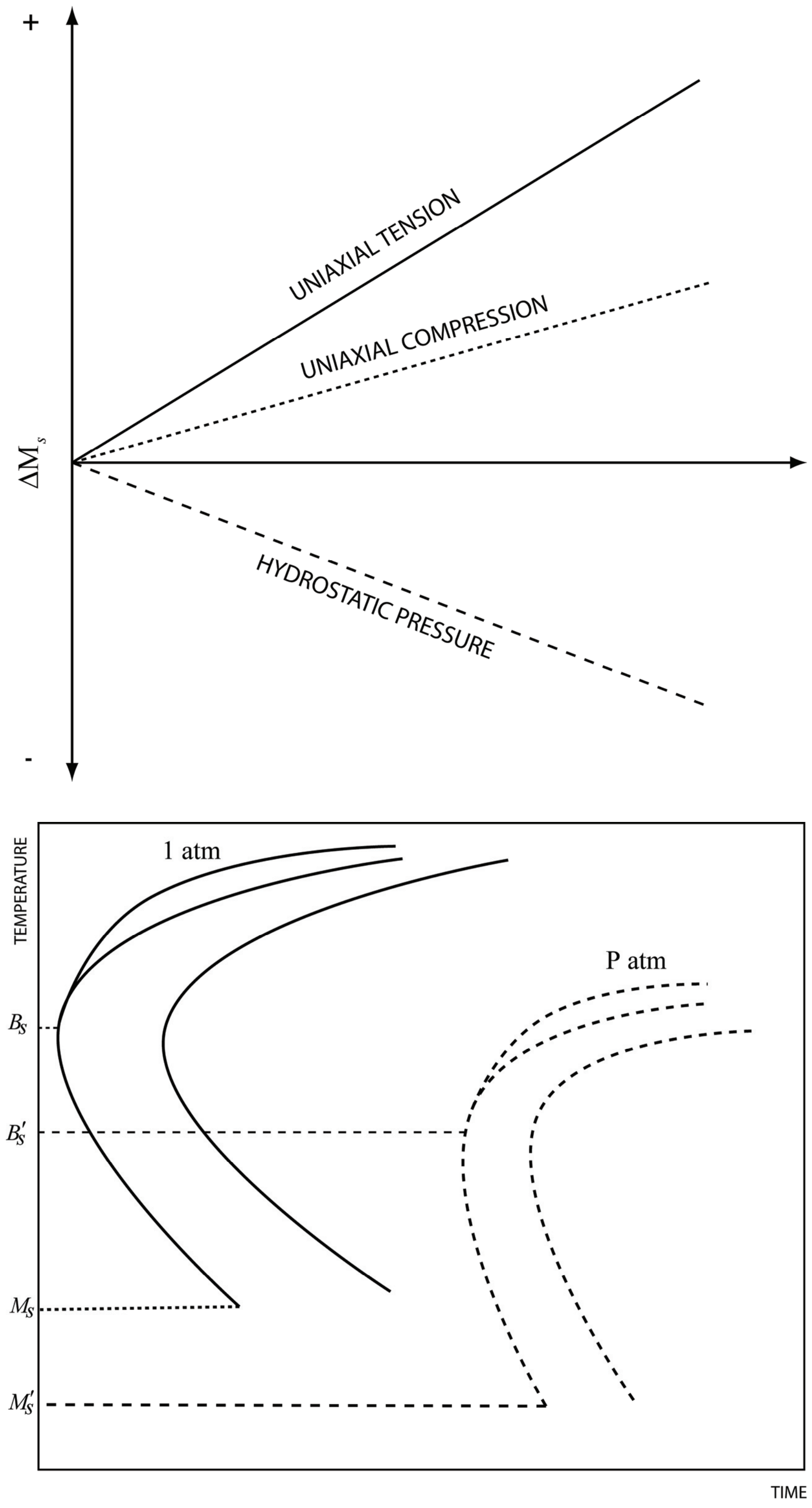

Figure 3.8 The effect of uniaxial stress and hydrostatic pressure on M_s temperature.

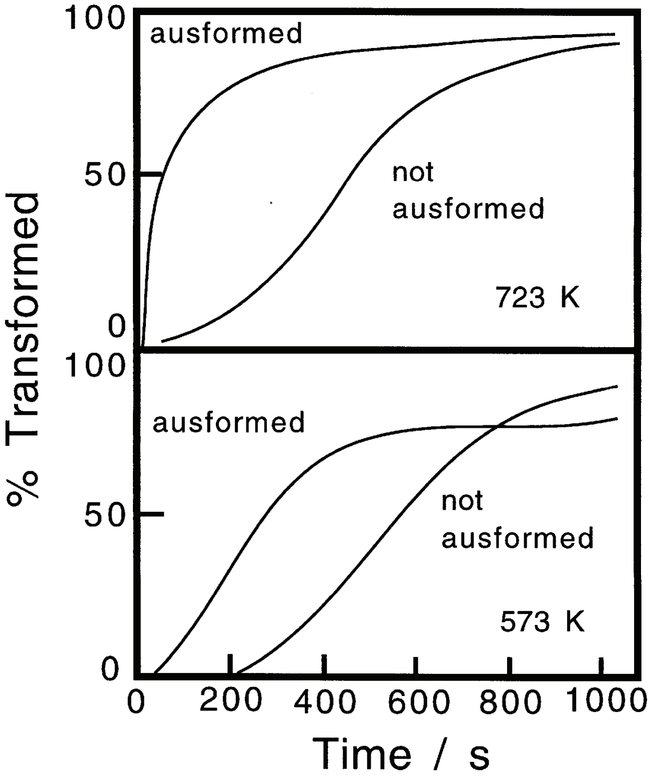

Figure 3.9 The effect of ausforming on the kinetics of bainitic transformation on the Fe-0.59C-2.01Si-1.02Mn alloy [3]

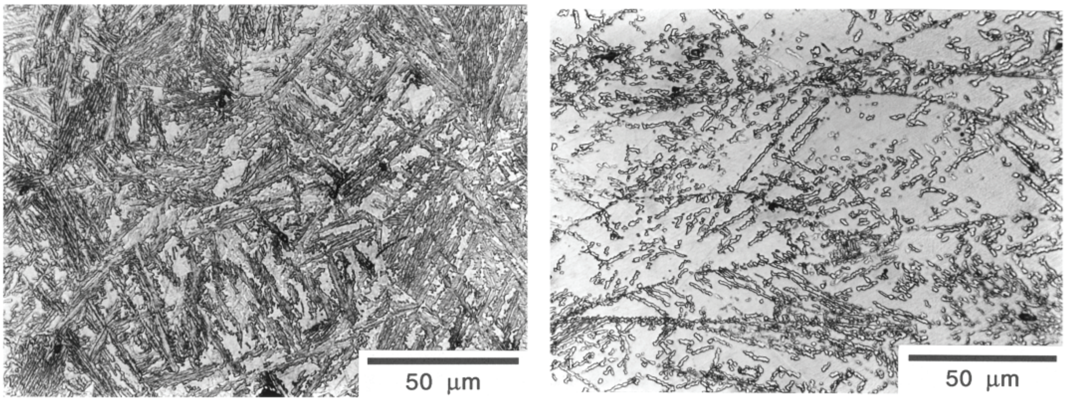

Figure 3.10 Optical micrographs illustrating the effect of mechanical stabilization on refining the microstructure and in reducing the amount of bainite : transformation from a) undeformed b) deformed austenite [67]

3.8.1 MODELING THE EFFECT OF STRESS ON MARTENSITIC TRANSFORMATION

First observations and modeling studies in the field are focused on the effect of stress and plastic strain on martensitic transformations, especially on the change of M_s temperature under stress. The progress of martensitic transformation during quenching is generally described by Koistinen-Marburger law. It has commonly been assumed that the only parameter in that law that is dependent on the state of stress/plastic strain is the M_s temperature. For example, Inoue [14] proposed a model in which the change in M_s (ΔM_s) as a function of mean stress (σ_m) and the second invariant of deviatoric stress tensor (J_2). According to his model, the change in the M_s is described as,

$$\Delta M_s = A\sigma_m + BJ_2^{1/2} \tag{3.38}$$

where A, B material are dependent constants which can be determined experimentally.

Denis [13] defined a similar type of relationship for the shift of martensite start temperature as function of mean stress (σ_m) and effective stress ($\bar{\sigma}$) as,

$$\Delta M_s = A\sigma_m + B\bar{\sigma} \tag{3.39}$$

However, both of those approaches neglect the effect of stress on the evolution of phase transformation during the whole transformation process by considering Ω of Koistinen-Marburger Equation as a constant. Owing the change in M_s to stress only takes into account the effect of stress on the starting point of transformation and neglects the effect of stress during the transformation, which is more important in determination of residual stresses [15].Based on uniaxial dilatometer tests, Liu et al. incorporated this effect into Koistinen-Marburger equation by considering Ω as a linear function of effective stress as,

$$\Omega = \Omega_0 + \Omega_1\bar{\sigma} \tag{3.40}$$

By using a purely heuristic approach, Ju et al. [17] proposed a generalized Koistinen-Marburger equation that includes the effect of stress and carbon concentration as,

$$\xi_m = 1 - exp\left(c_1T + c_2\left(C - C_o\right) + c_{31}\sigma_{ij} + c_{32}J_2^{1/2} + c_4\right) \tag{3.41}$$

where c_1-c_4 are constants that should be fitted from the experiments.

The author would like to propose an approach in which overall transformation amount is computed by using a method similar to Magee`s where the mechanical driving force is included in the calculations. Since the mechanical driving force under a stress field is different for each variant, the calculation transformation amount is performed per variant and the overall kinetics is calculated by summing over the variants.

3.8.2 MODELING THE EFFECT OF STRESS ON FERRITIC, PEARLITIC TRANSFORMATIONS

Since 1950's, several researches have been conducted on modeling the effect of stress on diffusional (ferrite, pearlite) and diffusion controlled (bainite) phase transformation [232-237].Most of the approaches in this field is based on modification JMA equation and Scheil's additivity hypothesis to incorporate the effect of stress and strain.

Concerning the shift of IT curves in time scale, the general assumption to model the phenomena is the modification of the additivity rule. Assuming that the effect of plastic strain (at least for small deformations in the case of quenching is less significant) and the mean stress (at least for quenching of mid-size components) is negligible [13], the onset of transformation can be expressed by

$$D_k = g_k(\overline{\sigma}) \tag{3.42}$$

$$\tau_{\sigma}^{IT} = \tau^{IT}\left(1 + D_k\right) \tag{3.43}$$

where τ_{σ}^{IT} is the isothermal incubation period under the influence of stress. D_k is the shift of the IT curves; g_k is function which should be derived experimentally.

On the other hand, Inoue [19] proposed a different model for the shift of IT curves as a function of mean stress.

In regards to the effect of stress on growth kinetics, most of the studies focus on modification JMA equation. For example, Inoue [19] described pearlitic transformation under normal stress level by a modified JMA equation as,

$$\xi_p = \xi_\gamma \cdot \left(1 - \exp(-\int_0^t f(T,\sigma)(t-\tau)^3 . d\tau\right) \tag{3.44}$$

$$f(T,\sigma) = \exp(C\sigma_m).f(T) \tag{3.45}$$

Denis [18] modified the coefficient of the JMA to incorporate the effect of stress on phase transformations and presented an equation in the form of

$$\xi_k = \xi_\gamma(1 - \exp(\frac{b_k}{(1 - C\overline{\sigma})^n}\tau^{n_k})) \tag{3.46}$$

Another Denis et al.'s model [46] assumes the reaction order as a function of effective stress. Just another model by Denis et al. [13] assumes that the TTT curves for the onset of pearlite transformation as well as for 10% and 90% pearlite formed are shifted with the same relative amount. However, this assumption may not always be reasonable since it is observed that both the incubation time and growth kinetics are affect by stress and plastic strain.

Recently, Hsu performed a review of additivity hypothesis and then developed several thermodynamic and kinetic models for phase transformation under stress [196]. Besides proposing methods for prediction of Ae_3, M_s and B_s temperatures; he also proposed a modified JMAK equation in which both the coefficient (b) and the exponent (n) of kinetic equation are functions of stress as

$$\xi_p = \xi_\gamma \cdot \left(1 - \exp\left(-b(\bar{\sigma}) t^{n(\sigma)}\right)\right) \tag{3.47}$$

$$b(\bar{\sigma}) = b(0)(1 + A\bar{\sigma}^B) \tag{3.48}$$

$$n(\bar{\sigma}) = n(0) \tag{3.49}$$

where parameter A and B can only be determined by regression of experimental data and are dependent on the material and phase transformation type. b(0) and n(0) can be calculated from TTT data.

3.8.3 MODELING THE EFFECT PLASTICITY ON DIFFUSION CONTROLLED TRANSFORMATIONS

Studies on development of models describing the kinetics of phase transformations from deformed austenite are popular since early 1990`s [224, 238-251]. However, those predictions are often inconsistent with experiments, especially in case of severe plastic deformation of austenite[240]. Hsu et al. [196] calculated incubation period of ferrite and pearlite by using the additivity hypothesis as:

$$\frac{1}{v^b} \int_0^{t_x} \frac{dt}{\tau_x\left(T\right)} = 1 \tag{3.50}$$

In this equation, the determination of v^b requires at least two continuous cooling tests with different cooling rates. Although calculated results are in agreement with experimental data, this model may not be widely used since the hypothesis of additivity is not always applicable.

There exists no commonly accepted model in regards to the effect of stress and plasticity on bainitic transformation due to the lack of knowledge on involved mechanisms [67, 68, 196, 211, 224, 225, 227-229, 252-258]. The effect of stress and plasticity on bainitic transformation kinetics during quenching is commonly described by models which are mainly derived for ferritic and pearlitic transformations. Similarly the effect of stress on B_s temperature is often described by expressions similar to the ones used in martensitic transformation. Those approaches introduce some error in residual stress predictions.

CHAPTER 4

MODELING THE MECHANICAL INTERACTIONS

4.1 GENERAL

Although there exist a large number of quantitative results available for the prediction of residual stresses after quenching [4, 14, 18, 26, 34, 35, 37, 44, 140, 259-266], the mechanism governing their formation is still unclear [87, 218]. The most common explanation for the mechanism of generation of residual stresses during quenching given is as follows: When a steel component is quenched, at the initial stage of quenching, austenite cools down without phase transformations. The surface of the component cools down faster than the core due to large thermal gradients. Hence, surface contracts faster than the core, leading to generation of tensile type of stresses on the surface. On the other hand, the core loads in compression to balance the stress state on the surface. Thermal stresses build in this stage may even cause non uniform plastic flow in soft austenite. Second stage of quenching commences as soon as the martensitic transformation starts on the surface. Dilatational phase transformation strains and transformation plasticity causes a fast unloading and reverse loading on the surface. Untransformed core reacts to balance those stresses. Large compressive stresses are built on the surface in this stage. The third stage in the quenching starts as soon as the phase transformations start at the core. In this stage, the surface is completely transformed and it cools down.

Despite the widespread view, plastic yielding is neither necessary nor sufficient for the existence of residual stresses after quenching. By using a physical model consisting of a simple system of two bars, Todinov [218] has shown that this definition is not completely true. According to his study, quenching does not result in residual stresses only if for all elemental volumes of the quenched body, the amount of plastic strain created by the odd strain shifts equals that created by the even strain shifts. Non-uniform plastic yielding is neither necessary nor sufficient for the existence of residual stresses.

4.2 CONSTITUTIVE MODELS

Material models that have been proposed for the simulation of quenching up today can be classified into three major categories:

- Elastoplastic constitutive models
- Elasto-viscoplastic constitutive models
- Unified plasticity models

Almost all of the formulation of constitutive equations for simulation of quenching is based on the additive decomposition of the strain tensor. A multiplicative decomposition of the strain rates is also possible. The assumption of additive decomposition is discussed in Belytschko et al. [267] whereas; the multiplicative decomposition is discussed in Simo et al. [268].

In almost all of the simulation of quenching studies, it is assumed that the total strain rate is the sum of the strain rates from different physical events, namely, temperature variation and phase transformations as

$$\dot{\varepsilon}_{ij} = \dot{\varepsilon}_{ij}^{e} + \dot{\varepsilon}_{ij}^{p} + \dot{\varepsilon}_{ij}^{th} + \dot{\varepsilon}_{ij}^{pt} + \dot{\varepsilon}_{ij}^{tr} \tag{4.1}$$

where $\dot{\varepsilon}_{ij}$, $\dot{\varepsilon}_{ij}^{e}$, $\dot{\varepsilon}_{ij}^{p}$, $\dot{\varepsilon}_{ij}^{th}$, $\dot{\varepsilon}_{ij}^{pt}$,$\dot{\varepsilon}_{ij}^{tr}$ are the total, elastic, plastic, thermal, phase transformation and transformation plasticity strain rates, respectively. Then, a hypo-elastic constitutive relationship may be employed to relate stress and strain rates:

$$\dot{\sigma}_{ij} = D_{ijkl}\dot{\varepsilon}_{kl}^{e} = D_{ijkl}\left(\dot{\varepsilon}_{kl} - \dot{\varepsilon}_{kl}^{p} - \dot{\varepsilon}_{kl}^{th} - \dot{\varepsilon}_{kl}^{pt} - \dot{\varepsilon}_{kl}^{tr}\right) \tag{4.2}$$

Assuming that the material isotropic, this expression is reduced to:

$$\dot{\sigma}_{ij} = B\left(\dot{\varepsilon}_{ij} - \dot{\varepsilon}_{ij}^{th} - \dot{\varepsilon}_{ij}^{pt}\right)\delta_{ij} + G\left(\varepsilon_{ij}' - \dot{\varepsilon}_{ij}^{tr}\right) \tag{4.3}$$

where ε_{ij}' is the deviator of strain tensor and B ,G are bulk and shear modulus, respectively.

4.2.1 ELASTOPLASTIC MATERIAL MODELS

Rate independent elastoplastic models are the most frequently used material models employed in simulation of quenching. Three fundamental rules must be specified for definition of an elastoplastic problem:

- Yield function
- Flow rule
- Hardening rule

Yield criterion determines when the plastic flow occurs, the flow rule determines how the flow occurs and the hardening rule determines the evolution of yield surface.

During plastic flow, stress state can never lie outside the yield surface. A stress state inside the yield surface implies an elastic process. On the other hand, a stress state on the yield surface implies the plastic flow.

Most of the studies in the field use von Mises type of yield surfaces in which the plastic flow occurs when the effective stress ($\bar{\sigma}$), given in the form of equation (4.4), reaches the yield surface.

$$\bar{\sigma} = \sqrt{\frac{3}{2}\left(S_{ij} - \alpha_{ij}\right)\left(S_{ij} - \alpha_{ij}\right)} \tag{4.4}$$

where S_{ij} is the stress deviator given by equation (4.5) and α_{ij} is the back stress tensor due to kinematic hardening.

$$S_{ij} = \sigma_{ij} - \frac{1}{3}\delta_{ij}\sigma_{mm} \tag{4.5}$$

Although there is a strong agreement in implementation of Von Mises yield surface and Prandtl-Reuss flow rule for the simulation of quenching, the selection of hardening rule is still questionable due to complex material behavior resulting from phase transformations.

In general, the hardening behavior of a material has isotropic and kinematic components. In case of purely isotropic hardening, the yield surface expands in stress space proportional to its original position and geometry in the case of purely isotropic hardening, whereas, in the case of purely kinematic hardening, it translates in stress space without changing its dimensions. In combined hardening, both effects are observed. Isotropic and kinematic hardening rules can be expressed respectively by,

$$\sigma_f = \sigma_0 + H.\bar{\varepsilon}^p \tag{4.6}$$

$$\alpha_{ij} = C\varepsilon_{ij}^p \tag{4.7}$$

where σ_0, H and C are material parameters depending on the temperature and the fraction of the microstructural constituents.

In literature, purely isotropic hardening rule are commonly used for simulation of quenching. However, presence of kinematic hardening may have a considerable impact on simulation results due to loading, unloading and reverse loading, which is common during quenching. There exist several studies reporting that kinematic hardening rule produces better results in the case of surface treatments such as induction and laser hardening or quenching after thermochemical treatments such as carburizing, nitriding during which phase transformations occur only in a part of the component while a large proportion of the component remains unaffected[41, 269-273]. Such a case is also reported for the simulation of quenching of large components where the time difference between the start of phase transformations at the surface and the core is large. However, most of these reports are based on comparison of experimental and simulation results and none of them includes a strong discussion of the microstructural origin of the kinematic hardening. Ordinarily, Bauschinger effect does not have a strong effect in low alloy steels. If such an effect exists during quenching, it may be related to phase transformations and plastic history loss due to reconstructive transformations.

4.2.2 ELASTO-VISCOPLASTIC MODELS

Viscoplasticity or the rate independent plasticity has many similarities with elastoplasticity. However, the main difference between viscoplasticity (rate dependent plasticity) and the rate independent elastoplasticity arises from the influence of the strain rate. For a viscoplastic material, an increase in strain rate at the same strain will give an increase in the stress. Moreover, the concept of yield limit is no longer strictly applicable. For example, creep may be considered as a special case of viscoplastic material behavior without elastic domain.

In elasto-viscoplasticity, an elastic potential surface similar to yield surface in elastoplasticity is defined as a reference. A stress state inside the elastic potential surface produces a reversible deformation. On the other hand, a stress state outside the elastic potential surface is termed as the plastic flow surface. The plastic strain rate is a function of the distance between the elastic potential and the current stress state.

In literature, there exist several studies implementing or discussing the applicability of the viscoplastic models for simulation of heat treatments [274-277].However, those models are proposed especially for heat treatments involving slow cooling rather than quenching. Air cooling of several industrial products such as hot rolled sheets, rails may be considered as an example case for the application of viscoplastic models. Such an approach may also be applicable for the prediction of distortion in quenching of tool, die steels. Essentially, viscoplastic models may be advisable for any high temperature heat treatment with slow cooling rate. Viscoplastic effects will become more pronounced with long times at high temperatures due to increased atomic mobility and longer diffusion time.

4.2.3 UNIFIED PLASTICITY MODELS

Since early 1970`s, progress has been made in constitutive models capable of predicting the non-elastic deformation under general conditions. This approach has lead to the development of models that combines plasticity and viscoplasticity into a single set of constitutive law. As an example for such kind of models, models proposed by Bodner and Partom [49], Chaboche [278] and Miller et al. [49] may be cited. A common problem with these kinds of constitutive relationships is the large number of independent parameters that has to be specified. Another drawback of such models is that they may sometimes require certain material data which is not a basic physical property requiring specific experimentation to be extracted. Details of such models are left out of the scope of this chapter for the sake of brevity.

4.2.4 PREDICTION OF MECHANICAL PROPERTIES OF THE PHASE MIXTURE

During quenching of steels, microstructure at any time, at any point of the component evolves until all the phase transformations complete. The dynamic changes in the microstructure lead to changes in the mechanical properties of the phase mixture. Then, the prediction of overall mechanical properties such as the flow stress of the phase mixtures becomes a major problem.

In literature, common method of calculation of yield stress of the phase mixture is the use of a linear rule of mixture [13, 26, 35, 41, 142]. The rule of mixture, in a general form, may be written as,

$$P(\xi_k, T) = \left(\sum_{k=0}^{p} \xi_k \left(P_k \right)^M \right)^{1/M} \tag{4.8}$$

where P_k and P are a property of a constituent and the mixture, while, m defines the type of the rule of mixture. The mixture rule is referred as linear (arithmetic) when M=1, geometric when M=0 and harmonic when M=-1. Geometric rule of mixture (M=0) cannot be used in equation (4.8) due to singularity. However, this equation can be mathematically modified to deal with this problem, so, the equation becomes:

$$P(\xi_k, T) = \exp\left(\sum_{k=0}^{p} \xi_k \ln\left(P_k \right) \right) \tag{4.9}$$

Moreover, partial derivatives with respect to temperature and phase fractions are required to calculate the time rate of change of a property during a thermal treatment, which can be computed by,

$$\frac{\partial P}{\partial T} = \begin{cases} P\left(\dfrac{\xi_k}{P_k} \dfrac{dP_k}{dT} \right) & , \ M \ = \ 0 \\ \dfrac{P^{1-m}}{m} \left(\displaystyle\sum_{k}^{p} \xi_k \left(P_k \right)^{1-m} \dfrac{dP_k}{dT} \right) & , \ M \neq 0 \end{cases} \tag{4.10}$$

$$\frac{\partial P}{\partial \xi_k} = \begin{cases} P \ln\left(\dfrac{P_k}{P_a} \right) & , \ M \ = \ 0 \\ \dfrac{P^{1-m}}{m} \left(\left(P_k \right)^m - \left(P_a \right)^m \right) & , \ M \neq 0 \end{cases} \tag{4.11}$$

where P_a is a property of parent phase (austenite).

The overall behavior of the mixture material is greatly influenced by the local distribution of the phases. If the distribution is regular, a micro-region may apparently have an orthotropic or anisotropic behavior since the material properties such as elastic modulus are different in different directions. On the other hand, some other material properties such as heat capacity and density are direction independent properties even though the distribution of phases is regular. Several composite models have been proposed to deal with variation of material properties due to distribution of phases. For example .an alternative is the Reuss model. Reuss [279] proposed a uniform stress assumption. The stress in each phase is the same as the total average stress based on the consideration that the real stress field is not homogeneous when a macroscopically homogeneous stress σ_{ij} is imposed due to the microscopically heterogeneous structure**.** This assumption leads to following constitutive relation,

$$d\sigma_{ij} = D_{ijkl}\left(d\varepsilon_{kl} + d\varepsilon_{kl}^{T}\right) \tag{4.12}$$

where D_{ijkl} and $d\varepsilon_{ij}^{T}$ are the 4th order elastoplastic constitutive tensor and the strain increment due to variation of material properties with temperature and phase transformations, defined by equations (4.13)-(4.16).

$$S_{ijkl} = \sum_{m} \xi_m S_{ijkl}^{m} \tag{4.13}$$

$$d\varepsilon_{ij}^{T} = \sum_{m} \xi_m S_{ijkl}^{m} d\sigma_{kl}^{Tm} \tag{4.14}$$

$$D_{ijkl}^{ep} = \left(S_{ijkl}\right)^{-1} \tag{4.15}$$

$$d\varepsilon_{ij} = S_{ijkl} d\sigma_{kl} - d\varepsilon_{ij}^{T} \tag{4.16}$$

Another alternative is the model proposed by Voigt. Analogous to iso-stress model, Voigt proposed a model in which the strain is the same in each phase and it is equal to total average strain [20]. His assumptions resulted in following constitutive relations:

$$d\sigma_{ij} = D_{ijkl} d\varepsilon_{kl} + d\bar{\sigma}_{ij}^{T} \tag{4.17}$$

where,

$$D_{ijkl} = \sum_{m} \xi_m D_{ijkl} \tag{4.18}$$

$$d\sigma_{ij}^{T} = \sum_{m} \xi_m d\sigma_{ij}^{Tm} \tag{4.19}$$

However, all these approaches are accurate enough as long as all of the coexisting phases have comparable hardness [21]. Unfortunately, the transformation which dominates the final stress distribution after quenching is the transformation of the soft austenite to the hard martensite. It is obvious that a linear rule of mixture which postulates an iso-strain or iso-stress condition is not valid for such a mixture. In reality, plastic strains will tend to concentrate in the softer phase resulting in a softer mixture than predicted by the rule of mixture. Thus, the validity of average property model becomes questionable. For this case, Leblond et al. stated that as long as the fraction of the hard phase is small, the deviatoric components of stress in all phases are equal [22]. A detailed investigation of this has been performed by Stringfellow and Parks [57]. Similarly, Geijsalers estimated overall mechanical properties of the phase mixture based on a set of simple assumptions of soft matrix with periodically distributed small hard inclusions [21]. An approximation for the compound yield stress is given as:

$$\sigma_f = \sum_{k=1}^{p} f(\xi_k)\sigma_f^k \tag{4.20}$$

where,

$$\mathrm{f}(\xi_{\mathrm{k}}) = \begin{cases} \xi_{\mathrm{m}}\left(\mathrm{C}+2\left(1\text{-C}\right)\xi_{\mathrm{m}}\text{-}\left(1\text{-C}\right)\left(\xi_{\mathrm{m}}\right)^2\right) & ;\ \text{for martensite} \\ \xi_{\mathrm{k}} & ;\ \text{for all other phases} \end{cases} \tag{4.21}$$

and C is the plastic strain localization factor defined as :

$$C = 1.383\frac{\sigma_f^{\gamma}}{\sigma_f^{m}} \tag{4.22}$$

The results obtained by this equation are almost identical to the results reported by Leblond et al. However, this equation is only applicable when the difference between the hardness of martensite and the austenite is large. Its application to a mixture of two phases with equal yield stress will produce incorrect results.

4.2.5 PLASTIC MEMORY LOSS DUE TO PHASE TRANSFORMATIONS

The definition of plastic history for a deformation process with phase transformations is not straight forward, causing problems in calculation of actual flow stress. Phase transformations (especially reconstructive ones) cause a plastic memory loss since the newly nucleated phase is assumed to be strain free. Remember that the memory of plastic deformation is stored in the steel by certain arrangement of dislocation pile-ups and entanglements. During continuous phase transformations, the plastic deformation accumulated in the austenitic phase will be lost partially or totally.

A workaround for incorporation of this effect in flow stress calculations may be defining a new hardening parameter κ instead of the effective plastic strain ($\bar{\varepsilon}^p$) to determine the amount of actual strain hardening.

$$\dot{\kappa}_k \approx \left(\dot{\bar{\varepsilon}}^p - \frac{\dot{\xi}_k}{\xi_k} \kappa_k \right).dt \tag{4.23}$$

Notice that, κ must equal to effective plastic strain since austenite phase exists from the very first moment of quenching. However, for other phases transformed from austenite, it might be calculated and updated using the following expression.

$$\dot{\kappa}_{k_{(t+\Delta t)}} = \int_{tsk}^{t} \left(\dot{\bar{\varepsilon}}^p - \frac{\dot{\xi}_k}{\xi_k} \kappa_{k_{(t)}} \right).dt \tag{4.24}$$

Making use of the new state variable and a linear rule of mixture, the definition of flow stress becomes:

$$\sigma_f = \sum_{k=1}^{p} \xi_k \sigma_k^o + \sum_{k=1}^{p} \xi_k \kappa_k H_k = \sigma_0 + \sum_{k=1}^{p} \xi_k \kappa_k H_k \tag{4.25}$$

If a harmonic rule of mixture of is used considering the localization of plasticity on the soft phase, the definition of the new flow stress becomes:

$$\sigma_f = \left(\sum_{k=1}^{p} \left(\frac{\xi_k}{\sigma_k^o + \xi_k \kappa_k H_k} \right) \right)^{-1} \tag{4.26}$$

Finally, if a geometric rule of mixture, which yields a flow stress between the upper and lower bounds , the new definition of flow stress is :

$$\sigma_f = \exp\left(\sum_{k=1}^{p} \xi_k \ln\left(\sigma_k^o + \xi_k \kappa_k H_k \right) \right) \tag{4.27}$$

4.3 EQUATIONS GOVERNING MECHANICAL BEHAVIOR

In any continuum model, one needs to determine the displacement field u_i, the strain field ε_{ij} and the stress field σ_{ij} in a given domain V with a boundary A which represents the physical body in real world. If the quenching process is considered as a quasi-static problem with the transient temperature field, the forces must satisfy the following equations of equilibrium,

$$\sigma_{ji,j} + F_i = 0 \text{ in V} \tag{4.28}$$

$$\sigma_{ji} n_j = T_i \text{ on A} \tag{4.29}$$

where F_i and T_i represents prescribed body forces in the interior and traction forces on each point of the boundary. If the displacements are small, strains and displacement are related by

$$\varepsilon_{ij} = \frac{1}{2}\left(u_{i,j} + u_{j,i}\right) \text{ in V} \tag{4.30}$$

$$u_i = U_i \text{ on A} \tag{4.31}$$

where u_i and U_i are the nodal displacements and the prescribed boundary displacements, respectively.

After these considerations and assumptions, one must specify constitutive equations relating the stress and the strain fields. A treatment of non-isothermal response of structures experiencing simultaneous changes in both the load and temperature requires substantial modification of isothermal procedures. The treatment of thermoplasticity requires constitutive equations to account for TRIP and the influence of temperature on dynamically changing thermomechanical properties of the material.

4.3.1 FORMULATION OF PURELY ELASTIC BEHAVIOR

If the material is assumed to be linearly elastic, the elastic strain increment is related to stress increment by Hooke's law:

$$\varepsilon_{ij}^{e} = \frac{1}{E}\left[\left(1+\nu\right)\sigma_{ij} - \delta_{ij}\nu\sigma_{mm}\right] \tag{4.32}$$

where elastic modulus (E) and Poisson's ratio (υ) are dependent on temperature and fraction of phases. Dependence of E and υ can be described by an appropriate rule of mixture. In this study, a linear rule of mixture is employed for this purpose.

Then, the elastic strain rate is defined by

$$\dot{\varepsilon}_{ij}^{e} = \frac{1}{E}\left[-\left(\frac{\left(1+\nu\right)\sigma_{ij} - \delta_{ij}\nu\sigma_{mm}}{E}\right)\dot{E} + \left(\sigma_{ij} - \delta_{ij}\nu\sigma_{mm}\right)\dot{\upsilon} + \left(1+\nu\right)\dot{\sigma}_{ij} - \delta_{ij}\nu\dot{\sigma}_{mm}\right] \quad (4.33)$$

4.3.2 FORMULATION OF THERMAL STRAINS

Thermal strain increment due to thermal expansion is defined as

$$\varepsilon_{ij}^{th} = \sum_{k=1}^{p} \xi_k \int_0^T \alpha_k . dT \quad (4.34)$$

where α_k is the temperature dependent thermal expansion coefficient for the phase k. If the thermal strain is assumed to be zero for austenite at 0^0C, then the rate form is given by

$$\dot{\varepsilon}_{ij}^{th} = \sum_{k=1}^{p} \left[\dot{\xi}_k \int_0^T \alpha_k . dT + \xi_k \alpha_k \dot{T}\right] \quad (4.35)$$

4.3.3 FORMULATION OF DILATATIONAL PHASE TRANSFORMATION STRAINS

Volumetric strain due to a phase transformation can be formulated by

$$\varepsilon_{ij}^{pt} = \sum_{k=1}^{p} \frac{1}{3} \delta_{ij} \Delta_k \xi_k \quad (4.36)$$

where Δ_k represents the structural dilation due to decomposition of austenite to the k^{th} phase. By differentiating the equation with respect to time, the rate form is found as

$$\dot{\varepsilon}_{ij}^{pt} = \sum_{k=1}^{p-1} \frac{1}{3} \delta_{ij} \Delta_k \dot{\xi}_k \quad (4.37)$$

4.3.4 FORMULATION OF TRANSFORMATION PLASTICITY

Transformation plasticity strain rate, in its mostly used form, can be represented by:

$$\dot{\varepsilon}_{ij}^{tr} = \frac{3}{2} K_k \dot{\xi}_k (1 - \xi_k) S_{ij} \quad (4.38)$$

Many other alternatives are also possible. Please refer to Section 4.4 for the details of TRIP concept and proposed models.

4.3.5 FORMULATION OF PLASTIC BEHAVIOR DURING QUENCHING

At any given state with a specified history, it is assumed that there exist a yield functional Φ, which depends explicitly on the stress state F(σ_{ij}) and a variable flow stress σ_f. For the quenching problem, a yield functional is defined in the form of

$$\Phi = F(\sigma_{ij}) - (\sigma_f(T, \xi_k, \bar{\varepsilon}^p))^2 \tag{4.39}$$

where variable flow stress is a function of the temperature, the constitution of the microstructure and the plastic history.

As mentioned in Section 4.2.5, phase transformations cause a plastic memory loss and $\bar{\varepsilon}^p$ cannot be used as a state variable. However, the problem will be formulated similarly to the conventional thermo-elastoplasticity problem and then required modifications will be performed to account for this effect.

The stresses must remain on the yield surface as the plastic deformation to occur. Plastic consistency equation is obtained by differentiation of the yield functional.

$$\frac{d\Phi}{dt} = \frac{\partial F}{\partial \sigma_{ij}} \dot{\sigma}_{ij} - 2\left[\frac{\partial \sigma_f}{\partial T}\dot{T} + \sum_{k=1}^{p}\left(\frac{\partial \sigma_f}{\partial \xi_k}\dot{\xi}_k\right) + \frac{\partial \sigma_f}{\partial \bar{\varepsilon}^p}\dot{\bar{\varepsilon}}^p\right] = 0 \tag{4.40}$$

Next step in defining the elasto-plastic problem is the definition of the flow rule. The concept of plastic potential is used in determination of flow rule. It is assumed that there exists a scalar function of stress, F(σ_{ij}), from which the components of the plastic strain increments are proportional to $\frac{\partial F}{\partial \sigma_{ij}}$. If the von Mises' yield criterion is assumed to derive elasto-plastic constitutive relationship, then the function equals to

$$F(\sigma_{ij}) = \frac{3}{2} S_{ij} S_{ij} \tag{4.41}$$

This assumption represents a result of the Drucker's postulate. According to this postulate, during a complete cycle of loading and unloading which causes plastic work, the net work done by external forces has to be greater than zero. The plastic dissipation work is the recoverable part of the total work and it can be expressed as

$$d\varepsilon_{ij}^p d\sigma_{ij} \geq 0 \tag{4.42}$$

During the plastic flow the following equation holds true

$$\frac{\partial \Phi}{\partial \sigma_{ij}} d\sigma_{ij} \geq 0 \tag{4.43}$$

The plastic flow theory that is used for simulation of quenching in this section is characterized by two major considerations. First, plastic strain rate is assumed to be in the direction of outward normal to the plastic potential functional, which yields a Prandtl-Reuss flow rule. Secondly, plastic potential is assumed to be in the same form as the yield surface, resulting in associated linear flow theory. Then, the following equation is derived from the normality principle,

$$\dot{\varepsilon}_{ij}^{p} = d\lambda \frac{\partial F}{\partial \sigma_{ij}} = d\lambda \frac{\partial F}{\partial S_{ij}} \tag{4.44}$$

where dλ is the plastic multiplier.

Effective plastic strain is determined by the plastic history. Equivalent plastic strain rate consistent with von Mises' yield surface and Prandtl-Reuss relations is given by

$$\dot{\varepsilon}^{p} = d\lambda \left(\frac{2}{3} \frac{\partial F}{\partial \sigma_{ij}} \frac{\partial F}{\partial \sigma_{ij}} \right)^{1/2} \tag{4.45}$$

The final stage of the definition of the elasto-plastic problem is the definition of a hardening rule. In solid mechanics, there exist 3 major types of hardening termed as isotropic, kinematic and combined hardening. In literature, both isotropic and kinematic hardening rules are used for the simulation of quenching. However, the scope of this chapter will focus on isotropic linear hardening rule.

In isotropic hardening, the yield surface is allowed to grow in size proportionally to its original position and shape. This implies that an increase in tensile yield strength also causes an increase in compressive yield strength. A variable flow stress for linear isotropic hardening can be defined as

$$\sigma_{f} = \sigma_{0} + H\bar{\varepsilon}^{p} \tag{4.46}$$

where σ_o and H represents the yield strength and the plastic hardening modulus respectively.

For the simulation of quenching, the effect of phase transformations and temperature changes on plastic material properties is assumed to be performed only into the calculations of σ_0 and H. After substitution of the derivative of the flow function, plastic consistency equation becomes,

$$\frac{\partial F}{\partial \sigma_{ij}}\dot{\sigma}_{ij} - 2\sigma_f\left[\frac{\partial \sigma_f}{\partial T}\dot{T} + \sum_{k=1}^{p}\frac{\partial \sigma_f}{\partial \xi_k}\dot{\xi}_k - H\dot{\bar{\varepsilon}}^p\right] = 0 \tag{4.47}$$

Notice that, the stresses associated with the same plastic strain are different at different temperatures due to temperature dependence of σ_0 and H. This condition must be considered in calculations.

A new state variable (κ) is defined instead of $\bar{\varepsilon}^p$ to take plastic memory loss into account, the yield functional is updated accordingly as

$$\Phi = F(\sigma_{ij}) - (\sigma_f(T, \xi_k, \kappa_k))^2 \tag{4.48}$$

Thus, the plastic consistency condition becomes,

$$\frac{\partial F}{\partial \sigma_{ij}}\dot{\sigma}_{ij} - 2\sigma_f\left[\frac{\partial \sigma_f}{\partial T}\dot{T} + \sum_{k=1}^{p}\frac{\partial \sigma_f}{\partial \xi_k}\dot{\xi}_k + \sum_{k=1}^{p-1}\frac{\partial \sigma_f}{\partial \kappa_k}\dot{\kappa}_k\right] = 0 \tag{4.49}$$

where the summation is over all the constituent phases except austenite. Next, the corresponding derivatives of the the flow stress are introduced in the equation

$$\frac{\partial F}{\partial \sigma_{ij}}\dot{\sigma}_{ij} - 2\sigma_f\left[\frac{\partial \sigma_f}{\partial T}\dot{T} + \sum_{k=1}^{p}\frac{\partial \sigma_f}{\partial \xi_k}\dot{\xi}_k + \sum_{k=1}^{p-1}\frac{\partial \sigma_f}{\partial \kappa_k}\dot{\kappa}_k\right] = 0 \tag{4.50}$$

After some modifications, the equation can be rewritten as

$$\frac{\partial F}{\partial \sigma_{ij}}\dot{\sigma}_{ij} - 2\sigma_f\left(\frac{\partial \sigma_f}{\partial T}\dot{T} + H_\gamma \kappa_\gamma \dot{\xi}_\gamma\right) = 2\sigma_f\sum_{k=1}^{p}\left(\xi_k H_k d\lambda\left(\frac{2}{3}\frac{\partial F}{\partial \sigma_{ij}}\frac{\partial F}{\partial \sigma_{ij}}\right)^{1/2}\right) \tag{4.51}$$

After rearrangement of the terms, the equation (4.51) becomes,

$$\frac{\partial F}{\partial \sigma_{ij}}\dot{\sigma}_{ij} + C_1 - C_2 d\lambda = 0 \tag{4.52}$$

where C_1 and C_2 are constants given by:

$$C_1 = -2\sigma_f\left[H_\gamma \kappa_\gamma \dot{\xi}_\gamma + \sum_{k=1}^{p}\left((\dot{\sigma}_o)_k + \kappa_k \dot{H}_k\right)\right] \tag{4.53}$$

$$C_2 = 2\sigma_f \sum \xi_k H_k\left(\frac{2}{3}\frac{\partial F}{\partial \sigma_{ij}}\frac{\partial F}{\partial \sigma_{ij}}\right)^{1/2} \tag{4.54}$$

4.3.6 THERMO-ELASTO-PLASTIC FORMULATION OF QUENCHING

The material within the element boundaries is subjected to initial strain increments {dε^o/dt} due to the temperature change and the phase transformations. Then, the stress increment will be caused by the difference between the increments of actual and initial strains. By using Hooke's law and the equations (4.32) and (4.44), the following relation is derived:

$$\dot{\sigma}_{ij} = \left[D_{ep}\right]\left(\left\{\dot{\varepsilon}\right\} - \left\{\dot{\varepsilon}^o\right\}\right) \tag{4.55}$$

where [D_e] is the elastic constitutive matrix. For axisymmetric case, [D_e] can be calculated using, Plastic increment of the strain will occur only if the elastic stress tends to put the stress on the yield surface. On the other hand, if this change is such that unloading occurs then no plastic strains will develop. The stress rate can be calculated by rearranging the equation (4.55),

$$\left\{\dot{\sigma}\right\} = \left[D_e\right]\left(\left\{\dot{\varepsilon}\right\} - \left\{\dot{\varepsilon}^o\right\} - d\lambda\left\{\frac{\partial F}{\partial \sigma}\right\}\right) \tag{4.56}$$

The elasto-plastic matrix [D_{ep}] is substituted into the equation by combining the terms,

$$\left\{\dot{\sigma}\right\} = \left[D_{ep}\right]\left(\left\{\dot{\varepsilon}\right\} - \left\{\dot{\varepsilon}^o\right\}\right) \tag{4.57}$$

If the instantaneous dλ is negative, it is set to zero and the correct stress rate is given by the elastic part only. This procedure allows the detection of plastic unloading.

Derivation of Tangent Modular Matrices

The use of consistent elastoplastic tangent moduli instead of the standard ones improves the convergence rate and allows the use of large time steps. For finite values of the time increment, use of the classical elastoplastic moduli [D_{ep}] leads to loss of the asymptotic rate of quadratic convergence characteristics of Newton's methods. In this section, the derivation of both the consistent and the standard moduli will be presented.

The standard tangent moduli can be derived by multiplying the equation (4.52) by $\left[D_{ep}\right]\frac{dF}{d\sigma_{ij}}$, subtracting from the equation(4.57), and solving for dλ :

$$d\lambda = \frac{\left(\left\{\dot{\varepsilon}\right\} - \left\{\dot{\varepsilon}^o\right\}\right)\left[D_e\right]\left\{\frac{\partial F}{\partial \sigma}\right\} + C_1}{\left\{\frac{\partial F}{\partial \sigma}\right\}^T \left[D_e\right]\left\{\frac{\partial F}{\partial \sigma}\right\} + C_2} \tag{4.58}$$

By rearranging the equations, the standard tangent modular matrix is obtained as,

$$\left[S_{ep}\right] = \left[D_e\right] + \frac{1}{C_2}\left\{\frac{\partial F}{\partial \sigma}\right\}\left\{\frac{\partial F}{\partial \sigma}\right\}^T \tag{4.59}$$

And the elasto-plastic constitutive matrix [D_{ep}] is obtained by inversion of the compliance matrix by,

$$\left[D_{ep}\right] = \left[S_{ep}\right]^{-1} \tag{4.60}$$

A general form of the consistent tangent modular matrix can be derived from,

$$\left\{\sigma\right\} = \left\{\sigma^B\right\}\Delta\lambda\left[D_e\right]\left\{\frac{\partial F}{\partial \sigma}\right\} \tag{4.61}$$

where σ^B denotes the elastic trial stresses. Differentiation with respect to the time yields,

$$\left\{\dot{\sigma}\right\} = \left[D_e\right]\left(\left\{\dot{\varepsilon}\right\} - \left\{\dot{\varepsilon}^o\right\} - d\lambda\left\{\frac{\partial F}{\partial \sigma}\right\} - \Delta\lambda\left\{\frac{\partial^2 F}{\partial \sigma^2}\right\}\right) \tag{4.62}$$

After some modifications, equation becomes similar to equation (4.57) ,

$$\left\{\dot{\sigma}\right\} = \left[Q\right]\left(\left\{\dot{\varepsilon}\right\} - \left\{\dot{\varepsilon}^o\right\} - d\lambda\left\{\frac{\partial F}{\partial \sigma}\right\}\right) \tag{4.63}$$

where [Q] is the consistent tangent modular matrix based on the radial return mapping given by

$$\left[Q\right] = \left[D_e\right]\left[1 + \Delta\lambda\left[D_e\right]\left\{\frac{\partial^2 F}{\partial \sigma^2}\right\}\right]^{-1} \tag{4.64}$$

Solution Algorithm

If the known strain rates due to thermal gradients and phase transformations are assumed constant throughout each time interval then the equation (4.55) defines an initial value problem in which the stresses, hardening parameter, temperature, volume fraction of phases are known at the initial time increment. The most obvious way of solving this initial value problem is a forward-Euler integration scheme in which the load history is divided into incremental load steps. At each step, the forces caused by thermal gradients and phase transformations are applied and the displacement of each node is determined by global stiffness equations. Then, the strains are evaluated at integration points using strain-displacement rate relations. Similarly, stresses are computed at integration points by using elastoplastic constitutive law. If the plastic yielding occurs, elastic and plastic strain increments can be determined by decomposition of total strain tensor. The solution to the non-linear behavior due to plastic flow is obtained by an iterative sequence of linear solutions. However, an uncorrected forward-Euler integration scheme would lead to an unsafe drift from the yield surface due to error accumulation unless the stresses are brought back to the yield surface. To overcome this problem, the following procedures may be employed:

- Adding a return to the yield surface to the forward-Euler scheme,
- Using sub-increments,
- Using some form of backward or mid-point Euler scheme.

In each case, the aim is to update the stresses at Gauss points given the old stresses, strains. First step is to use elastic relationship to update the stresses for all procedures. If the updated stress state lies in the yield surface, the material remained elastic or elastically unloaded from yield surface. In this case, there is no need to integrate the rate equations. Nevertheless, if the stress state lies outside of the yield surface an integration procedure should be adopted.

An effective procedure for numerical integration of plasticity rate equations is the use of return mapping algorithms. For an arbitrary convex yield functional, the integration problem may be reduced to the standard minimization problem of finding the minimum distance of a point to a convex set [280, 281]. A return mapping algorithm can be conveniently defined based on the elastic-plastic split by first integrating the elastic equations to obtain an elastic predictor, which is taken as an initial condition for the plastic equations. These define a plastic predictor whereby the elastically predicted stresses are relaxed onto a suitably updated yield surface. This procedure is referred as “radial return mapping” in the particular case of the von Mises’ yield condition with associative flow rule and isotropic hardening. This algorithm is usually employed with standard tangent modulus matrix. However, the use of the consistent tangent modular matrix can significantly improve the convergence behavior [282].

A generalized trapezoidal rule developed by Ortiz and Popov [283] for integration of strain rates states that

$$\sigma_D = \sigma_A + \left[D_e\right]\left(\Delta\varepsilon - \Delta\varepsilon^P\right) = \sigma_B - \left[D_e\right]\Delta\varepsilon^P \tag{4.65}$$

$$\Delta\varepsilon^P = \Delta\lambda\left[\left(1-\eta\right)\frac{\partial\Phi_A}{\partial\sigma} + \eta\frac{\partial\Phi_D}{\partial\sigma}\right] \tag{4.66}$$

$$\Delta\varepsilon^P = \Delta\lambda\left\{\frac{\partial\Phi}{\partial\sigma}\left[\left(1-\eta\right)\sigma_A + \eta\sigma_B\right]\right\} \tag{4.67}$$

where A is the starting point and D is the final point on the yield surface (Figure 4.1).The trial stress vector is returned to the updated yield surface, partially along the initial and final plastic flow directions.

Three common procedures depending on the value of η can be employed for integration of the plasticity rate equations in the case of von Mises' yield surface, associated flow rule and isotropic hardening. The value of η determines the stability and the accuracy of the integration. When η is equal to 0, the method is termed explicit forward-Euler method. When η is greater than zero, integration schemes are referred implicit. For example, integration scheme is called implicit mean normal method when η equals to 0.5 and it is called backward-Euler (elastic predictor-radial return) method in the case of η=1. For the Von Mises' yield surface, the integration procedure is unconditionally stable only for the values greater than or equal to 0.5 [281].

For the Von Mises' yield condition, Prandtl-Reuss flow rule and isotropic strain hardening, when η=0, the generalized trapezoidal rule is termed as tangent stiffness-radial corrector method. The direction of the plastic flow is parallel to the yield surface normal at the contact point (σ_n). The integration may be written in the matrix form as,

$$\left\{\sigma\right\}_{n+1} = \left\{\sigma\right\}_n + \left[D_{ep}\right]\left\{\Delta\varepsilon\right\} \tag{4.68}$$

This corresponds to one-step, forward Euler method. The method is exact if the strain increment vector is parallel to the deviatoric component of the contact stress (radial loading). For other orientations of strain increment vector, errors are introduced in both the orientation of the updated stress vector and the radius of the yield surface.

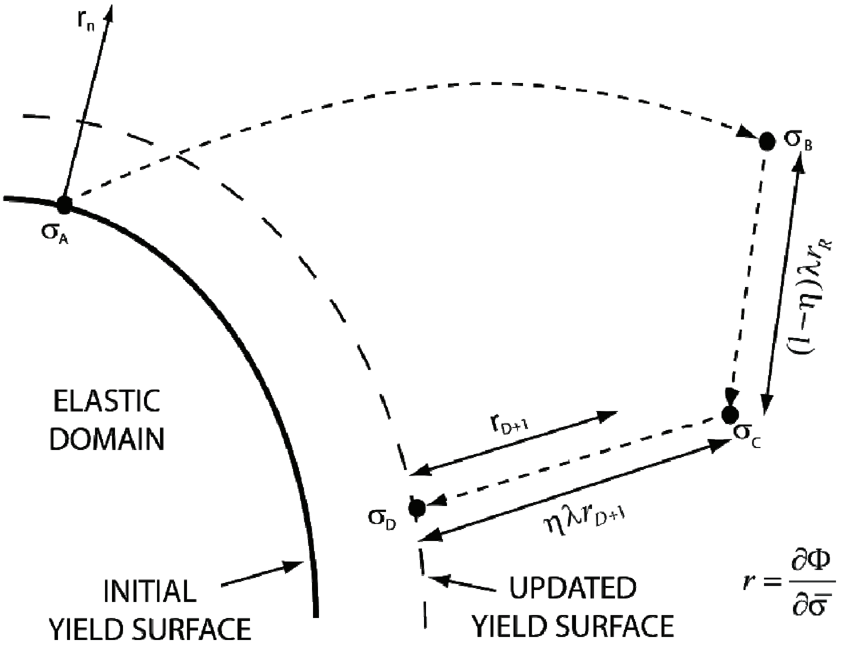

Figure 4.1 Return mapping procedure.

The integration scheme can be summarized as follows:

1. At the outset all stress and strain values are zero, and the constitutive matrix [D] equals to the elastic one $[D_e]$ for all sampling points. These values prevail in the first computational cycle. Then, apply the first incremental load $\{\Delta f_0\}_1$, which is calculated from the temperature gradient and the amount of phase transformations for the given time increment.
2. $[D]_{i-1}=[D_e]_{i-1}$ for sampling points that yet to yield ($\Phi<0$ for the current $\{\sigma\}_{i-1}$ or are unloading ($d\Phi<0$ for the most recent changes in $\{\sigma\}$). Otherwise, there is plastic deformation, and evaluate elasto-plastic tangent modulus matrix $[D_{ep}]_{i-1}$ for each Gauss point which is deformed plastically.
3. Evaluate elemental stiffness matrices. The overall tangent stiffness matrix is formed by the usual assembly, $[K]_{i-1}$.
4. Solve for structural displacement rates, and calculate increment of displacements $\{\Delta a\}_{i-1}$ and strain increments $\{\Delta \varepsilon\}_{i-1}$ at the Gauss points.
5. Calculate the stress increments assuming a complete elastic deformation.

$$\left\{\Delta\sigma\right\}_i = \left[D_e\right]\left(\left\{\Delta\varepsilon\right\}_i - \left\{\Delta\varepsilon^o\right\}_i\right) \tag{4.69}$$

Then, add this value to the existing stress values and calculate the effective stress value. Next, check whether the effective stress is greater than the yield stress at each integration point. For Gauss points in elastic range simply go to step 9.

6. For the Gauss points in the plastic regime, the proportion of the stress greater than the yield limit must be reduced to the yield surface. To satisfy the yield criterion and to prevent artificial hardening, the stress points cannot move outside the yield surface. Consequently, the stress point only transverse the surface until both equilibrium conditions and the constitutive relations are satisfied [284].

$$\left\{\Delta\sigma\right\}_D = \left\{\Delta\sigma\right\}_B - \Delta\lambda\left[D_e\right]\left\{\frac{\partial F}{\partial\sigma}\right\} \tag{4.70}$$

   There is a complication that has to be taken into account in the computations. For Gauss points that make elastic-to-plastic transition (i.e., initially yielded), the contact stress must be found to permit division of the stress increment vector into purely elastic (1-ω) and elasto-plastic (ω) parts. On loading from point A in the elastic regime, the stress point moves elastically until the yield surface is met. Elastic behavior beyond this point would result in a final stress state defined by point B (Figure 4.2).

7. Update the solution.

$$\left\{u\right\}_i = \left\{u\right\}_{i-1} + \left\{\Delta u\right\}_i \tag{4.71}$$

$$\left\{\sigma\right\}_i = \left\{\sigma\right\}_{i-1} + \left\{\Delta\sigma\right\}_i \tag{4.72}$$

8. Corrective loads are introduced to prevent progressive drift. Then, the load correction in the next iteration $\{f_0\}_i$-$\{g\}_i$ where

$$\left\{g\right\}_i = \int\left[B\right]^T\left\{\sigma\right\}_i .dV \tag{4.73}$$

   in the absence of external loads in cycle i. The summation spans all the elements of the structure and expresses the loads that elements apply to nodes because they have stresses $\{\sigma\}_i$, which are the updated values.

9. Update the displacements using the equation(4.67), apply the next load increment and return to step 2.

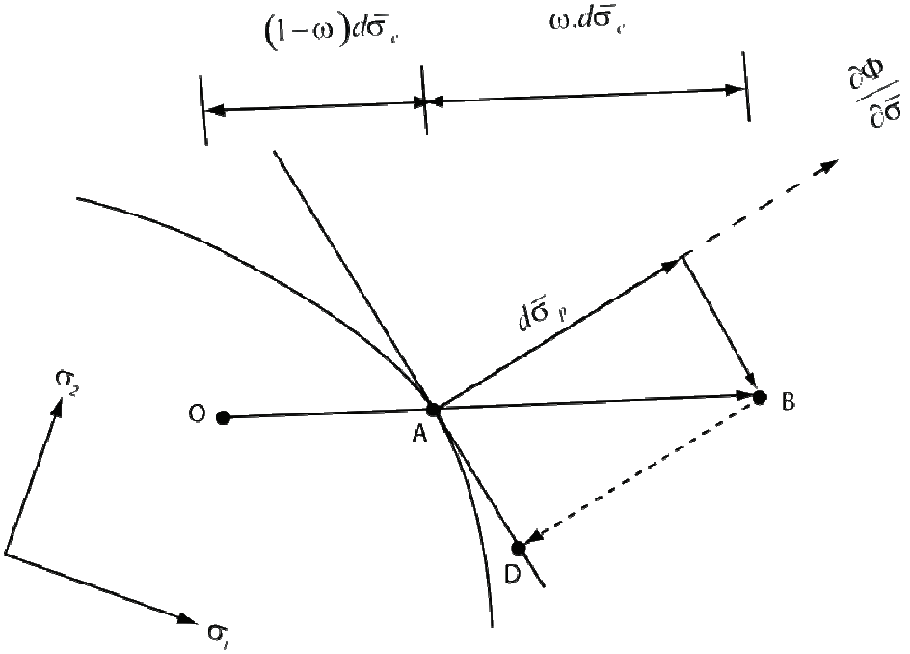

Figure 4.2 Stress state at initial yielding.

4.4 MODELING THE TRANSFORMATION INDUCED PLASTICITY (TRIP)

Prediction of residual stress state after quenching requires development of quantitative models for transformation induced plasticity. As a consequence, modeling of TRIP have been a popular research field since 1980`s. In the literature, there exist several models based on either Greenwood-Johnson or Magee mechanisms. For the sake of brevity, only a short review of the models applicable in quenching of steels will be presented in this section. A detailed review of `classical` approaches in modeling TRIP can be found elsewhere [9].

4.4.1 GENERAL

During decomposition of austenite into phase transformation products such as ferrite, pearlite, bainite and martensite, a volume increase is observed in the transforming region due to density difference between the parent and the product phase. Those strains are the primary source of fluctuating internal stress field, beside the thermal stresses and transformation induced plasticity (TRIP). TRIP affects the stress evolution, residual stress state and distortion after quenching process.

In its classical definition, TRIP is the significantly increased plasticity during a phase change. Even for an externally applied load for which the corresponding equivalent stress is small compared to the normal yield stress of the material, plastic deformation occur [5].

This phenomenon is explained by the existence of an irreversible strain resulting from phase transformation under stress. This softening has its origin in the fact that during a phase transformation a microregion may change its volume and shape. To achieve compatibility, the misfit must be compensated (or accommodated) by an eigenstress state which may vary from grain to grain or within a grain of a polycrystalline material [8]

In many cases, such as the case of steel quenching, the misfit leads at least to a plastification of the neighborhood material of the microregions, or sometimes even to a plastification of the microregions. It may easily be thought that this eigenstress state is influenced by the applied stress. The superposition of these stressing or straining mechanisms may initiate plastification. Therefore, a macroscopic plastic deformation of the specimen can be observed. This mechanical effect associated with phase transformations has originally been considered as TRIP. Even in the case of only elastic accommodation of the strain-incompatibility, a global deformation of the specimen may remain in addition to the global volume change. This may happen, if the transformed microregions are arranged spatially in such a way that their shape changes add up to a non-zero overall strain. In the case of stress-induced thermoelastic martensitic transformation the applied stress has a strong effect on the orientation of the microregions. In this case, too, the term TRIP has been adopted for the non-elastic deformation of a specimen even though this deformation is generally reversible during the reverse transformation from the product to the parent phase [27].

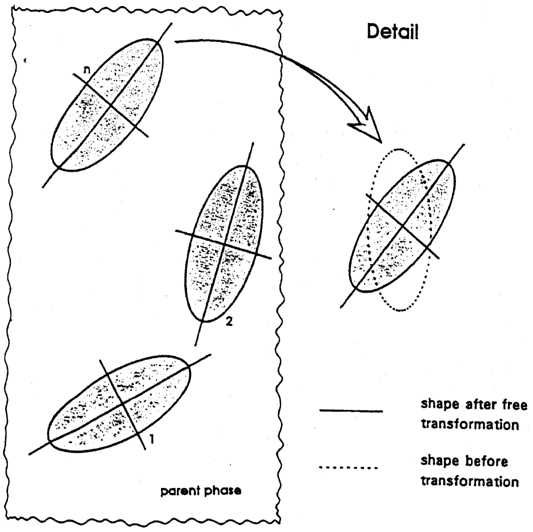

Figure 4.3 Transforming micro-regions in a parent phase [8]

More specifically, TRIP is currently explained by the competition of two mechanisms:

- *Plastic Accommodation (Greenwood-Johnson) Mechanism:* During phase transformations under a stress field, the interaction of the load stress and the geometrically necessary stress to accommodate the transformation eigenstrain results in an irreversible strain. This pioneering explanation of TRIP was given by Greenwood and Johnson [6]. This mechanism is operational for both displacive (martensitic) and reconstructive (diffusional) phase transformations. This concept have later been revised by various authors such as Abrassart [23] **,** Leblond [24, 25], Denis [75, 112, 140, 213] , Fischer [8, 9, 27] etc.
- *Variant Selection (Magee) Mechanism:* Martensitic transformation from FCC to BCC (and BCT) crystal structure occurs with 24 possible variants, each characterized by a distinct lattice orientation relationship. At the mesoscopic scale, each variant is defined by a transformation strain involving a dilatational (δ) component perpendicular to the habit plane and a shear component (γ) on the habit plane. In general, only the preferred variants are nucleated upon thermo-mechanical loading depending on the stress state. The earliest observation of this mechanism based on variant selection belongs to the works of Patel and Cohen [285]. Later, this mechanism is called "Magee" mechanism due to his famous study on the importance of formation of preferred variants in iron based alloys [7]. This concept have later been reviewed and adopted by many authors such as Cherkaoui, Fischer**,** Jacques, Taleb and Turteltaub [8, 69, 70, 82, 125, 135-139, 143, 146, 147, 150-153, 156, 286-292].

The competition between these mechanisms depends on the progress of transformation, which depends principally on thermomechanical loading conditions [135]. The interaction between two mechanisms can be determined quantitatively by cooling tests under various applied stress. Transformation plasticity strain of a fully transformed specimen is usually referred as `the extent of the transformation plasticity`. A linear relationship is commonly observed between the extent of transformation plasticity and TRIP strain (ε^{tr}), as long as the applied stresses are lower than the yield strength of austenite. Moreover, the variation of transformation plasticity with the progress of transformation has been found linear for ferritic and pearlitic transformations [47, 293]. However, for martensitic transformation, it is generally observed that TRIP strain increases rapidly at the start of phase transformation and then TRIP strain rate decreases as the transformation proceeds. This phenomenon is related to variation of contribution of each mechanism during the progress of transformation. The orientation (Magee) mechanism is dominant at the beginning of the transformation. In this stage, only martensitic variants which are favorably oriented with respect to the applied stress are nucleated. This leads to an anisotropic deformation which attains its maximum in the direction of the applied stress. TRIP strain due to orientation of variants reaches to its maximum as the applied stress approaches the yield strength of austenite. One can conclude that a relaxation process occurs by plastic deformation of the austenite and both of the mechanisms are active in such a manner that the first mechanism favors the second. As the transformation progress, variants are selected by the internal stress state rather than the applied stress. This results in a decrease in ε^{tr} in the direction of the applied stress which is primarily due to Greenwood-Johnson mechanism.

A phenomenological approach has generally been used to derive expressions for the evolution of TRIP. Under uniaxial stress, transformation plasticity strain can be written in a general form as:

$$\varepsilon^{tr} = K.\sigma.\phi(\xi) \tag{4.74}$$

where σ is the applied stress; K is the transformation plasticity parameter and $\phi(\xi)$ is a function describing the progress of transformation plasticity. $\phi(0)$ is equal to 0 and $\phi(1)$ is equal to 1 by definition. Both K and $\phi(\xi)$ can be determined either experimentally or by calculation.

In case of triaxial stress state, it is generally assumed that the same relations hold for classical plasticity and transformation induced plasticity. For example, the transformation plasticity strain rate is assumed to be proportional to stress deviator as a consequence of von Mises associated flow rule [39, 294]. However, TRIP lacks a yield criterion because it even occurs under very small stresses.

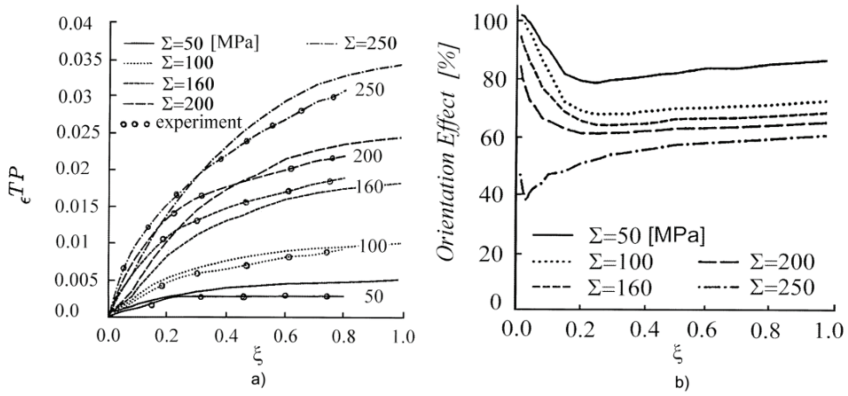

Figure 4.4 a) TRIP strain as a function of martensite fraction due to experiment [51] and modeling [295, 296], b) Fraction of “Greenwood-Johnson” and “Magee” effects

4.4.2 PARAMETER DETERMINATION FOR TRIP MODELS

Experimental determination procedure of K (for diffusional transformations) involves isothermal stressed dilatometry tests under various applied loads. The slope of the regression line of σ vs ε^{tr} gives the TRIP parameter K as :

$$K = \lim_{\sigma \to 0} \frac{\partial \varepsilon^{tr}}{\partial \sigma}\bigg|_{T=const} \tag{4.75}$$

Beside experimental methods, several methods have been proposed for calculation of K using physical properties of the material. Greenwood and Johnson [6, 297] made the earliest approach to calculate transformation plasticity parameter as,

$$K = \frac{5}{6}\frac{\Delta_k}{\sigma_y^a} \tag{4.76}$$

where Δ_k , σ_y^a are structural dilation due to transformation and the yield strength of parent austenite, respectively. Δ_k may also be approximated by using the densities of the parent and the product phases :

$$\Delta_k = \frac{\rho_a - \rho_k}{\rho_a} \tag{4.77}$$

Later, Abrassart [23] proposed a similar model with a different constant,

$$K = \frac{1}{4}\frac{\Delta_k}{\sigma_y^a} \tag{4.78}$$

Finally, Leblond [24, 25] postulated a similar relationship again with a different constant,

$$K = \frac{2}{3}\frac{\Delta_k}{\sigma_y^a} \tag{4.79}$$

Both of those models consider basically the dilation due to phase transformation and the yield strength of the austenite. The major difference lies in selection of constants. Thus, K can be described in its most general as

$$K = k\frac{\Delta_k}{\sigma_y^a} \tag{4.80}$$

where k is a constant between 0.25 and 0.83.

Fischer et al. [8] proposed a different model for displacive transformations including the effect of crystallography and distribution of variants and the yield strength of parent and product phases (σ_y^*) as

$$K = \frac{5}{6}\frac{\sqrt{\delta^2 + \frac{3}{4}\bar{\gamma}^2}}{\sigma_y^*} \tag{4.81}$$

$$\sigma_y^* = \sigma_y^k \left(\frac{1 - \left(\sigma_y^a \,/\, \sigma_y^k\right)}{\ln\left(\sigma_y^k \,/\, \sigma_y^a\right)} \right) \tag{4.82}$$

where $\bar{\gamma}$ stands for an average transformation shear depending on the distribution of variants and including some self accommodation.

Similar to the calculation of K, there exist several proposals ((4.83)-(4.87)) for the evolution of transformation plasticity ($\phi(\xi)$), partially based on experiments and partially derived from theoretical considerations.

Abrassart [23] proposed an approximation of $\phi(\xi)$ for martensitic transformation as,

$$\phi(\xi) = \xi\left(3 - 2\sqrt{\xi}\right) \tag{4.83}$$

Dasalos [298] proposed a model applicable to both diffusive and martensitic transformation. In this model, $\phi(\xi)$ is approximated by a second order polynomial:

$$\phi(\xi) = \xi\left(3 - 2\sqrt{\xi}\right) \tag{4.84}$$

Sjöström [26] proposed a model in which $\phi(\xi)$ is approximated by a α^{th} order polynomial:

$$\phi(\xi) = \frac{\xi}{\alpha - 1}\left(\alpha - \xi^{\alpha - 1}\right) \tag{4.85}$$

where α is a fitting parameter. It should be noticed that the formulation of Sjöström reduces to Abrassart's model when k=1.5 and to Desalos model when k=2.

Leblond [299] used a logarithmic approximation in his mostly referred study,

$$\phi(\xi) = \xi\left(1 - \ln(\xi)\right) \tag{4.86}$$

Fischer suggested a similar logarithmic approximation for diffusional phase transformations,

$$\phi(\xi) = 2\ln\left(1 + \frac{\xi}{\alpha}\right) \tag{4.87}$$

where α is a fitting parameter.

4.4.3 INCORPORATION OF TRIP IN CONSTITUTIVE EQUATIONS

In regards to practical applications such as simulation of quenching, the total strain rate tensor is decomposed into elastic, plastic, thermal, dilatational and TRIP strain rate tensors additively as shown on equation (4.1).Considering the expressions proposed in the previous section, the TRIP strain rate tensor $\left(\dot{\varepsilon}^{tr}\right)$ is formulated in its most general form as:

$$\dot{\varepsilon}^{tr} = f(\Delta_k, \sigma_y^a).g(\xi, \dot{\xi}).h(S_{ij}, \sigma_y^k) \tag{4.88}$$

where f is a function of structural dilation and the yield strength of austenite; g is a function of transformed amount and transformation rate and h is a function of stress deviator and yield strength of product phase [135].

For practical purposes, this equation is usually implemented in the well-known Leblond incremental form,

$$\dot{\varepsilon}_{ij}^{tr} = \frac{3}{2}K\frac{d\phi}{d\xi}S_{ij}\dot{\xi} \tag{4.89}$$

where S_{ij} stands for the stress deviator [9, 27, 112, 129, 211, 299-302].

Although, this expression has been implemented in many quenching simulations, it has several drawbacks. First, the relation is derived by assuming a constant stress deviator [27]. However, in the case of simulation of quenching internal stress state fluctuates with time. In addition, this expression stems from a derivation where no \`orientation\` effect has been considered. However, this effect may be of the same order of magnitude as the accommodation effect [27]. Moreover, assuming the evolution of TRIP (ϕ) solely a function of volume fraction of transformation product (ξ) is purely heuristic. There is clear evidence that ϕ must depend on S_{ij}. The origin of this admittedly weak coupling can be found in the transformation kinetics due to the dependence of ξ also on the stress state [8, 51].

Finally, the equation (4.89) predicts a constant TRIP strain for an unloading. However, it is observed that TRIP strain changes in a steel specimen after unloading and continuation of the transformation by cooling [8]. This effect is due to variant selection mechanisms by which the variants are selected by internal stress state after sudden removal of the load [8]. Omitting this effect may lead to considerable errors in simulation of quenching where loading-unloading cycles are characteristic. As a remedy to this problem, several authors introduced a backstress term [27, 28].

$$\dot{\varepsilon}^{tr}(x,t) = \frac{3}{2}\tilde{K}(T(x,t))(S_{ij}(x,t) - \alpha_{ij}^{tr}(x,t))\frac{d}{dt}\tilde{\phi}(\xi(x,t)) \qquad (4.90)$$

where α_{ij}^{tr} is the backstress tensor due to TRIP itself. $\tilde{K}$ and $\tilde{\phi}$ are represented in this form since their corresponding values differ from K and ϕ. It is easily noted that equation (4.90) reduces to equation (4.89) in the case of constant stress deviator. Fischer et al. suggested further decomposition of backstress tensor into backstress due to plastic accommodation, (α_{ij}^{tr}) and variant selection mechanisms (β_{ij}^{tr}) [9].

The simplest proposal for X_{ij}^{tr} involves assuming the backstress proportional to the TRIP strain [130] :

$$\alpha_{ij}^{tr} = C^{tr}\varepsilon_{ij}^{tr} \qquad (4.91)$$

where C^{tr} is positive material parameter. Substitution of equation (4.91) into (4.90) and solution of the initial value problem corresponding to initial condition $\varepsilon^{tr}(x,0) = 0$ yields transformation plasticity strain as,

$$\varepsilon_{ij}^{tr}(x,t) = \frac{3}{2}\int_0^t \left[\left(\tilde{K}S_{ij}\frac{d}{dt}\tilde{\phi}\left(\xi\left(x,\tau_1\right)\right) \right).\exp\left(-\frac{3}{2}\int_{\tau_1}^{\tau_2} C^{tr}\tilde{K}\frac{d}{dt}\tilde{\phi}\left(\xi\left(x,\tau_1\right)\right).d\tau_2 \right) \right].d\tau_1 \qquad (4.92)$$

It should be noted that use of this model requires additional material parameters ($\tilde{K}$, $\tilde{\phi}$, C^{tr}) to be determined experimentally. Wolff et al. suggested such a method based on uniaxial tension-compression tests with stepwise loading [130]. Their method can also be adapted to other simple experiments like torsion and torsion-tension tests.

CHAPTER 5

IMPLEMENTATION OF THE MODEL

5.1 GENERAL

Simulation of quenching by using Msc.Marc involves modification of a coupled thermo-mechanical analysis to incorporate phase transformation effects. There exist many ways to implement phase transformation effects, each having certain pros and cons. In this section, two alternative ways of implementation proposed by the other will be presented and discussed in detail; other possibilities will be mentioned briefly.

Figure 5.1 illustrates the basic algorithm and list of user subroutines for incorporation of phase transformation effects and couplings into Msc.Marc. At the beginning of the analysis, all the material and process data such as thermo-mechanical material properties of each phase, isothermal phase transformation kinetic data are stored in a common block via USDATA subroutine which can accessed by any other user subroutine. Then, the temperature distribution in the component is calculated at each time step. During the thermal analysis ANKOND, USPCHT subroutines are invoked to incorporate the effect of phase transformations. After the thermal pass, microstructural evolution is calculated in UBGITR subroutine between the thermal and mechanical calculations. The UBGITR user subroutine is called at the beginning of each iteration in the solution of the nonlinear problem. It can be used to define or modify data variables stored in common blocks.

This can also be performed alternatively by UBGINC, UBGPASS, UEDINC or UEPASS subroutines with minor differences. After the thermal pass, fraction of each phase is determined by using isothermal kinetic data and Scheil`s additivity principle. Fraction of each phase is stored in the common blocks and post file using PLOTV subroutine. Thus, transformation strains and latent heat can be calculated and incorporated in the model by use of constitutive subroutines. Finally, the control is given back to Msc.Marc for mechanical calculations. During the mechanical pass ANEXP, HOOKLW, WKSLP subroutines are invoked to create thermo-metallo-mechanical couplings. This procedure is repeated at each time step

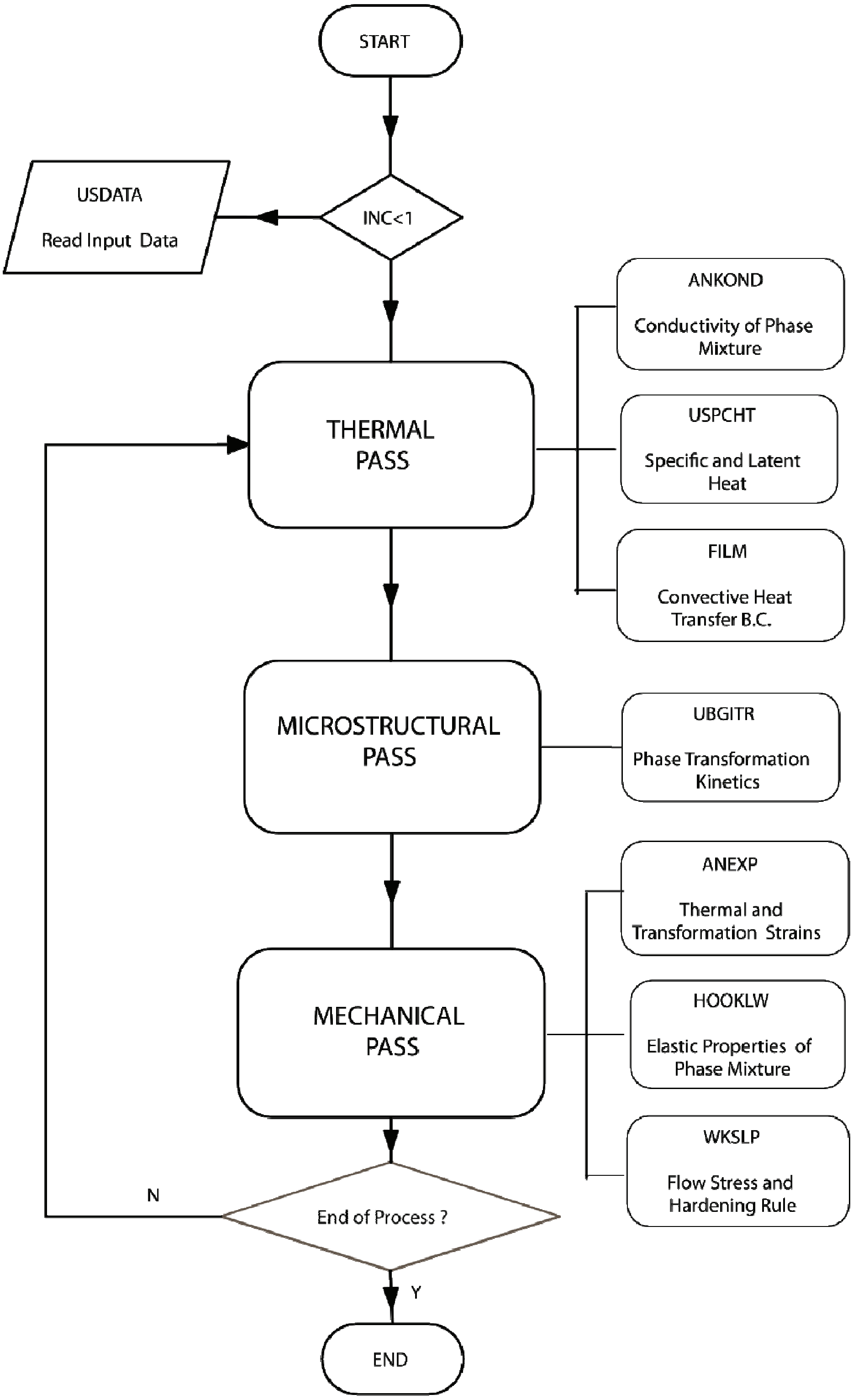

Figure 5.1 Basic algorithm and list of subroutines for implementation of model in commercial FEA software MSC.Marc®

5.1.1 THERMAL ANALYSIS PROCEDURE

MSC.Marc® uses a similar solution procedure for nonlinear transient heat conduction problem given in Section 2.3. Finite element formulation of the governing equation for nonlinear transient heat transfer problem with internal heat source may be written in the form of:

$$\left[H\right]\left\{\dot{T}\right\}+\left[C\right]\left\{T\right\}=\left\{Q\right\} \tag{5.1}$$

where [C] and [K] are temperature dependent heat capacity and thermal conductivity matrices,{T} is the nodal temperature vector, $\left\{\dot{T}\right\}$ is the nodal cooling rate vector and {Q} is the heat flux vector.

Using the backward difference scheme, same expression can be expressed in incremental form as:

$$\left[\frac{1}{\Delta t}\left[H\right]+\left[C\right]\right]\left\{\Delta T_j\right\}=\left\{Q_j\right\}+\frac{1}{\Delta t}\left[C\right]\left\{\Delta T_{j-1}\right\} \tag{5.2}$$

For the evaluation of temperature-dependent matrices, the temperatures at two steps before provide a linear (extrapolated) temperature description over the desired interval

$$\left\{T(\tau)\right\}=\left\{T(t-\Delta t)\right\}+\frac{\tau}{\Delta t}\left(\left\{T\left(t-\Delta t\right)\right\}-\left\{T\left(t-2\Delta t\right)\right\}\right) \tag{5.3}$$

This temperature is then used to obtain an average property of the material over the interval to be used in equation(5.2), such that

$$\tilde{P}=\frac{1}{\Delta t}\int_{t-\Delta t}^{t}P\left(T\left(\tau\right)\right).d\tau \tag{5.4}$$

During iteration, the average property is obtained based on the results of the previous iteration:

$$\left\{T(\tau)\right\}=\left\{T(t-\Delta t)\right\}+\frac{\tau}{\Delta t}\left(\left\{T^{*}\left(t\right)\right\}-\left\{T\left(t-\Delta t\right)\right\}\right) \tag{5.5}$$

where {T*} are the resulting temperature vector from the previous iteration.

The variation of thermal conductivity of the phase mixture is modeled using ANKOND subroutine. This subroutine allows the definition of an anisotropic conductivity matrix. Although, the heat transfer during phase transformations is assumed to be isotropic, this routine is invoked since there are no subroutines to define an isotropic conductivity matrix in

MSC.Marc. In fact, the matrix that will be calculated using equation in ANKOND subroutine will be isotropic anyway.

Latent heat may be simulated by defining a fictitious specific heat, which includes the effect of the variation of specific heat with temperature-microstructure and the latent heat of transformation. Such kind of specific heat may be defined using equation (2.5) in USPCHT subroutine, which is called at each increment for every element in the mesh, hence, allowing the user to specify a nonlinear relationship.

In heat transfer analysis for the simulation of quenching, it is necessary to include nonuniform film coefficients and sink temperatures for the calculation of convection or radiation boundary conditions. The surface temperature dependent convective heat transfer coefficient and sink temperature can be specified using subroutine FILM. A smooth curve fitting to heat transfer coefficient and providing the derivative of the heat transfer coefficient with respect to temperature improve the accuracy and convergence significantly. So, the use of piecewise linear approximation of h(T) data should better be avoided.

5.1.2 MICROSTRUCTURAL EVOLUTION ANALYSIS PROCEDURE

In MSC.Marc, it is convenient to perform phase transformation calculations between the thermal and mechanical analysis. Thus, the temperature history calculated in the thermal pass can be used in microstructural evolution calculations. Then the microstructural constitution can be used to calculate coupling terms and update material properties for subsequent thermal and mechanical passes. In MSC.Marc®, there exist many “dummy” subroutines that allow running special code before and end of passes of thermo-mechanical analysis. UBGITR, UBGINC, UEDINC, UBGPASS are such kind of subroutines. These subroutines are referred as “dummy subroutines” since they are compiled unconditionally and perform nothing without user modification. They can be used to modify the data stored in common blocks.

In this thesis, UBGITR subroutine that can be set to run in iteration loop in any pass of coupled analysis was used. UEDINC, UBGPASS, UBINC subroutines can also be used with minor revisions. It should be noted that use of UBGITR is safer but has higher computational costs. Basic flow chart for coupled calculation of microstructure and heat transfer is illustrated on Figure 5.2. First, possibility of martensitic transformation is controlled in each increment by comparing nodal temperature with martensite start temperature. If martensitic transformation occurs, the fraction of martensite is calculated by using Koistinen-Marburger equation. If there is no martensitic transformation, the possibility of a diffusional transformation is checked by using the Scheil`s sum. If the incubation is complete (S=1), then transformed amounts are calculated using JMAK equation and the principle of additivity. Calculated phase fractions are stored in common blocks and written in the post file.

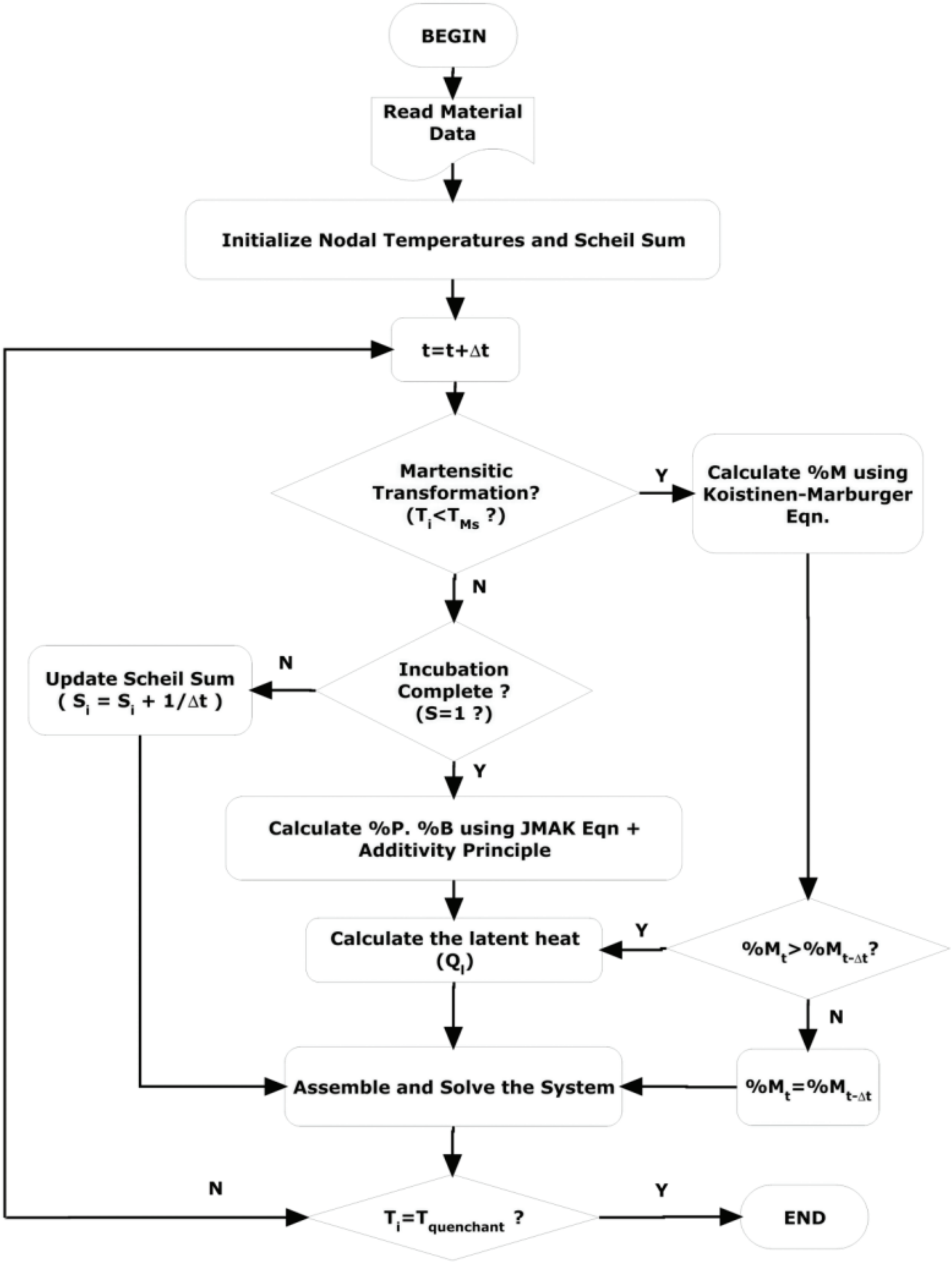

Figure 5.2 Flowchart for calculation of microstructural evolution coupled with heat transfer.

5.1.3 MECHANICAL ANALYSIS PROCEDURE

The mechanical pass is immediately performed after the microstructural analysis. Coupling terms are created using the imported thermal and microstructural analysis results. The general governing equations for finite element thermo-mechanical analysis in MSC.Marc based can be written in the form of:

$$[M]\{\ddot{u}\}+[D]\{\dot{u}\}+[K]\{u\}=\{F\} \tag{5.6}$$

$$[H]\{\dot{T}\}+[C]\{T\}=\{Q\}+\{Q^{I}\}+\{Q^{F}\} \tag{5.7}$$

where $\{Q^I\}$is the vector of heat generation due to deformation and $\{Q^F\}$is the heat generated due to friction, which can be safely neglected for the simulation of quenching. All the matrices are temperature dependent except [M].

A common constitutive model for strain increment decomposition for the simulation of quenching was presented in equation(4.1). This expression can further be rearranged so that the total strain increment is decomposed to thermal and mechanical strain increments:

$$d\varepsilon_{ij}=d\varepsilon_{ij}^{thermal}+d\varepsilon_{ij}^{mechanical} \tag{5.8}$$

where the thermal strain increment defined using ANEXP subroutine and it consists of thermal and phase transformation strain increments :

$$d\varepsilon_{ij}^{thermal}=d\varepsilon_{ij}^{th}+d\varepsilon_{ij}^{pt}+d\varepsilon_{ij}^{tp} \tag{5.9}$$

On the other hand, mechanical strain increment is composed of elastic and plastic strain increments

$$d\varepsilon_{ij}^{mechanical}=d\varepsilon_{ij}^{e}+d\varepsilon_{ij}^{p} \tag{5.10}$$

Thermal strain increment is defined in user subroutine ANEXP, while the mechanical strain increment is implemented using HOOKLW and WKSLP subroutines, respectively.

Calculation mechanical strain increment requires the modification of elastic and plastic constitutive laws. Elastic strain constitutive law can be defined by use of HOOKLW subroutine. ANELAS subroutine may also be used with some revisions. In the HOOKLW subroutine, the elastic stress-strain law is supplied by the user. A maximum of 21 terms are necessary for a three-dimensional body. This law is given in terms of the coordinate system defined in the ORIENTATION option. The user should insure that the stress-strain law is symmetric. Note that this user subroutine is called for each integration point of those elements that have anisotropic properties. The user can define either the stress-strain relation or the compliance strain-stress relation. The returned value of argument IMOD must be set accordingly. For example, if IMOD=1, the stress-strain law is given and the user returns to the array 6x6 [B] matrix such that:

$$\{\sigma\} = [B]\{\varepsilon\} \tag{5.11}$$

It should be noted that for temperature dependent properties, this user subroutine is called twice for each integration point. The first time to evaluate the stress-strain law at the beginning of the increment; the second time at the end of the increment.

WKSLP subroutine is invoked to specify temperature, phase fractions and plastic history dependent flow stress. YIEL subroutine may also be an alternative. As mentioned earlier in this chapter, during continuous phase transformations, the plastic deformation accumulated in the austenitic phase will be lost partially or totally. As a workaround, a new hardening parameter κ has been defined and updated using equations (5.12) and (5.13) instead of effective plastic strain ($\bar{\varepsilon}^p$) to determine the amount of actual strain hardening.

$$\dot{\kappa}_k \approx \left(\dot{\bar{\varepsilon}}^p - \frac{1}{\xi_k} \dot{\xi}_k \kappa_k \right) dt \tag{5.12}$$

$$\dot{\kappa}_{k_{(t+\Delta t)}} = \int_{tsk}^{t} \left(\dot{\bar{\varepsilon}}^p - \frac{1}{\xi_k} \dot{\xi}_k \kappa_{k_{(t)}} \right) dt \tag{5.13}$$

Using this new state variable, the definition of flow stress becomes:

$$\sigma_f = \sum_{k=1}^{p} \xi_k \sigma_o^k + \sum_{k=1}^{p} \xi_k \kappa_k H_k = \sigma_o + \sum_{k=1}^{p} \xi_k \kappa_k H_k \tag{5.14}$$

which can be implemented in Msc.Marc® via WKSLP subroutine.

For thermomechanical calculations, HYPELA2 subroutine may also be employed as an alternative instead of using HOOKLW and WKSLP subroutines.

5.2 ALTERNATIVE IMPLEMENTATION METHOD

The governing equation for small strain elastic-plastic analysis becomes non-linear when a nonlinear relationship exists between stress and strain. Solution of such problems is generally performed by iterative methods. Load, displacement, stress and strain vectors can be written in incremental form as:

$$\{F\}^{m+1} = \{F\}^{m} + \{\Delta F\}^{m+1} \tag{5.15}$$

$$\left\{U\right\}^{m+1} = \left\{U\right\}^{m} + \left\{\Delta U\right\}^{m+1} \tag{5.16}$$

$$\left\{\sigma\right\}^{m+1} = \left\{\sigma\right\}^{m} + \left\{\Delta\sigma\right\}^{m+1} \tag{5.17}$$

$$\left\{\varepsilon\right\}^{m+1} = \left\{\varepsilon\right\}^{m} + \left\{\Delta\varepsilon\right\}^{m+1} \tag{5.18}$$

Similarly, the governing equation can also be written in the incremental form as:

$$\iiint \left[B\right]^{T} \left\{\Delta\sigma\right\}.dV = \left\{F\right\}^{m+1} - \iiint \left(\left[B\right]^{T}\right)^{m} \left\{\sigma\right\}.dV = \left[K\right]\left\{\Delta U\right\} \tag{5.19}$$

MSC.Marc uses an algorithm that determines the stress increment {Δσ} for a given strain increment {Δε}. MSC.Marc can only handle the well-known stress-strain relations without user subroutines. However, simulation of quenching enforces the use of multi-phase constitutive laws in which the phase transformation effects are incorporated. Fortunately, those effects can be implemented using ANEXP and HYPELA2 subroutines. ANEXP subroutine allows the user to define a custom thermal expansion behavior, whereas; HYPELA2 allows the definition of a custom hypo-elastic stress-strain relation in the form of

$$\dot{\sigma}_{ij} = D_{ijkl}\dot{\varepsilon}^{e}_{kl} = D_{ijkl}\left(\dot{\varepsilon}_{ij} - \dot{\varepsilon}^{p}_{ij} - \dot{\varepsilon}^{th}_{ij} - \dot{\varepsilon}^{pt}_{ij} - \dot{\varepsilon}^{tr}_{ij}\right) \tag{5.20}$$

Msc.Marc supplies the user with the total displacement, incremental displacement, total mechanical strain (mechanical strain = total strain – thermal strain), the increment of mechanical strain, and other information. Stress, total strain, and state variable arrays at the beginning of the increment are passed to HYPELA2. The user is expected to calculate stresses, tangent stiffness, and state variables that correspond to the current strain at the end of the increment. As can be seen, this type of implementation is more complex since the user must deal with plasticity and perform many calculations in the subroutine.

During quenching of steels, a commonly used constitutive model for strain increment decomposition is given in equation(4.1). Starting from this expression, the total strain increment can be subdivided into thermal and mechanical strain increments as,

$$d\varepsilon_{ij} = d\varepsilon^{thermal}_{ij} + d\varepsilon^{mechanical}_{ij} \tag{5.21}$$

where the thermal strain increment consists of thermal, dilatational and phase transformation strain increments and is defined in user subroutine ANEXP by,

$$d\varepsilon^{thermal}_{ij} = d\varepsilon^{th}_{ij} + d\varepsilon^{pt}_{ij} + d\varepsilon^{tp}_{ij} \tag{5.22}$$

Thermal strain increment can easily be calculated by using temperature and microstructure history In ANEXP subroutine, thermal expansion coefficient (α) of the mixture is calculated using a linear rule of mixture:

$$\alpha(T,\xi_k) = \sum_1^N \alpha_k \xi_k \tag{5.23}$$

where α is the thermal property of the mixture and α_k is the thermal expansion coefficient of k^th constituent.

On the other hand, mechanical strain increment is composed of elastic and plastic strain increments,

$$d\varepsilon_{ij}^{mechanical} = d\varepsilon_{ij}^{e} + d\varepsilon_{ij}^{p} \tag{5.24}$$

It`s value is calculated by subtracting the thermal strain increment from total strain increment and used in calculation of stress increment in HYPELA2 subroutine. The stress calculation procedure is presented in Figure 5.3.

Algorithm consists of following steps:

- Compute the strain increment using equation (5.19) and strain displacement relation.

$$\left\{\Delta\varepsilon\right\} = \left[B\right]\left\{\Delta U\right\} \tag{5.25}$$

- Compute the trial stress increment {Δσ} by assuming only solely elastic behavior.

$$\left\{\Delta\sigma^e\right\} = \left[D\right]\left\{\Delta\varepsilon\right\} \tag{5.26}$$

- Determine the scaling factor φ: A material which is in elastic state at the end of previous step may lead into a elastoplastic stress state after the addition of trial stress state. According to theory of plasticity, a stress state must not lie outside the yield surface. This can be checked by using the yield functional after the addition of trial stress to current stress state. If $F\left(\left(\left\{\sigma\right\}^m + \left\{\Delta\sigma^e\right\}\right), \sigma_f\right) > 0$, then the stress state is outside the yield surface and should be returned to the yield surface. A common method for this is to calculate a scaling factor (φ) which brings the stress state ($\left\{\sigma\right\} = \left\{\sigma\right\}^m + \varphi\left\{\Delta\sigma^e\right\}$) exactly on the yield surface where ,

$$\phi = \frac{\sqrt{S_{ij}^{m} \Delta S_{ij} - \left(S_{ij}^{m}\right)^{2} \left[\left(\Delta S_{ij}\right)^{2} - \frac{2}{3}\left(\sigma_{f}\right)^{2}\right]} - S_{ij}^{m} \Delta S_{ij}}{\left(S_{ij}^{m}\right)^{2}} \tag{5.27}$$

Calculate the stress increment and plastic strain increment by

$$\Delta\varepsilon_{ij}^{p} = \Delta\varepsilon_{ij} - \Delta\varepsilon_{ij}^{e} = \Delta\varepsilon_{ij} - S_{ijkl}\left(\Delta\sigma_{kl}^{e} - \Delta\sigma_{kl}^{T}\right) \tag{5.28}$$

where $\Delta\sigma_{ij}^{T}$ and S_{ijkl} are the stress increment due to variation of material properties with temperature and elastoplastic compliance tensor, respectively.

- Force the subsequent stress state to be on the yield surface. According to theory of plasticity, the consistency condition (dF=0) must hold. This enforces the subsequent stress to lie on the yield surface. Unfortunately, this condition may not hold due to computational errors in numerical solutions. As a remedy. a correction vector (ω) can be defined as :

$$\omega = \frac{1}{3}\left(\frac{\sigma_{f}}{\overline{\sigma}_{e}} - 1\right) \tag{5.29}$$

Then, the stress and yield surface center is finally updated as:

$$\left\{\sigma\right\} = \left\{\sigma\right\} + 3\omega\left\{\Delta S\right\} \tag{5.30}$$

$$\left\{\omega\right\} = \left\{\omega\right\} + \left\{\Delta\omega\right\} \tag{5.31}$$

- Update the stress state and elastic-plastic constitutive tensor (D_{ijkl}).

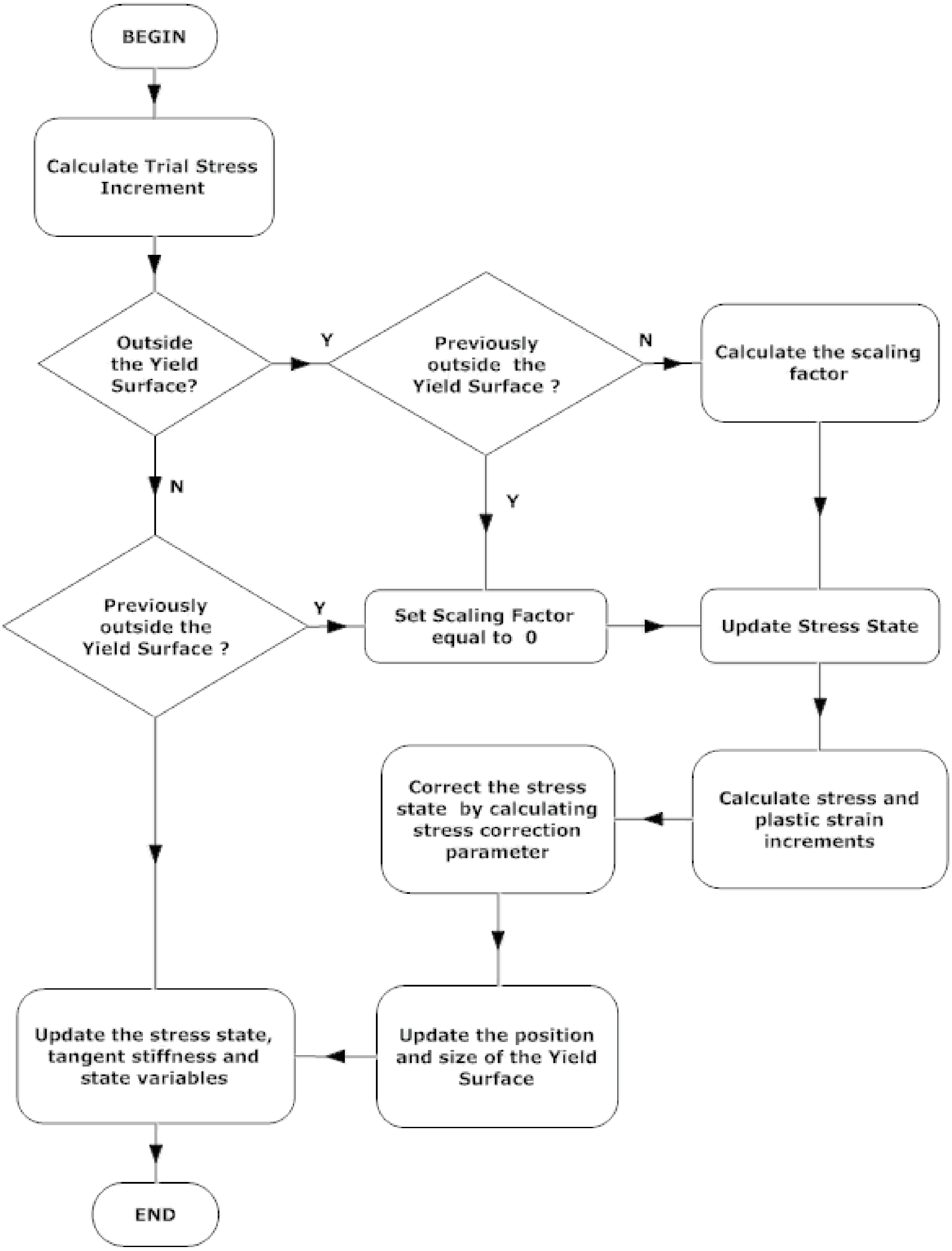

Figure 5.3 Basic flowchart for HYPELA2 subroutine.

CHAPTER 6

SUBROUTINE INFORMATION

This chapter is designed to provide detailed information on subroutines used for implementation of the model into commercial FEA software MSC.Marc®, which was not provided on Chapter 5. Implementation procedures, alternate strategies, hints and important points will also be highlighted.

6.1 HEAT TRANSFER SUBROUTINES

Simulation of thermal processing techniques requires simulation of dynamically changing conductivity, specific heat and latent heat as a function of temperature, composition and microstructure. Moreover, it is usually necessary to include nonuniform film coefficients and sink temperatures for the calculation of convection or radiation boundary conditions. That effect can be implemented into MSC.Marc® using the following subroutines. However, it should be noted that the subroutines and methods of implementation given in this chapter are not unique and many alternatives are possible.

6.1.1 ANKOND – USER DEFINED ANISOTHERMAL CONDUCTIVITY

This subroutine is used for simulation of dynamically changing heat conductivity of the phase mixture, which is crucial in simulation of thermal processing techniques with concomitant microstructural evolution. For anisotropic heat transfer analysis, this user subroutine allows the user to define an anisotropic conductivity matrix (λ_{ij}) at each integration point in each element defined as :

$$q_i = \lambda_{ij} \frac{\partial T}{\partial x_j} \tag{6.1}$$

where the q_i is the heat flux vector due to conduction.

It should be noted that this subroutine may also be used for definition of a isotropic although it is designed for definition of anisotropic conductivity matrix. Indeed, the thermal conductivity matrix that is defined in this subroutine for this thesis is assumed to be isotropic as,

$$\lambda_{ij} = \lambda\delta_{ij}$$

where λ is the overall heat conductivity of the phase mixture calculated by the rule of mixture.

The anisotropic conductivity matrix is defined with respect to the preferred orientation specified in the ORIENTATION option, which is taken the same as the global coordinates.

Interface

User subroutine ANKOND is written with the following headers:

```
SUBROUTINE ANKOND

(COND,CANISO,N,NN,KCUS,MATUS,ID,T,DT,TIME,

* DELTME,JOULHT)

IMPLICIT REAL *8 (A-H, O-Z)

DIMENSION COND(ID,ID),CANISO(3),MATUS(2),KCUS(2)

        user coding

RETURN

END
```

Input

`CANISO`	:	anisotropic conductivities $\lambda_{ij}(T)$ established by the user via data blocks.
`N`	:	element number.
`NN`	:	integration point number.
`KCUS(1)`	:	layer number (always 1 for continuum elements).
`KCUS(2)`	:	internal layer number (always 1 for continuum element).
`MATUS(1)`	:	user material identifier.
`MATUS(2)`	:	internal material identifier.
`ID`	:	size of the `COND` matrix; that is, the number of derivatives $\partial T / \partial x_j$
`T`	:	temperature at the beginning of the time increment.
`DT`	:	estimated temperature increment.
`TIME`	:	transient time at the beginning of the increment.
`DELTME`	:	increment of time.
`JOULHT`	= 0	return thermal conductivity.

= 1 return electrical conductivity.

Output:

The conductivity matrix λ_{ij} (COND) has to be-redefined by the user. Undefined terms of the conductivity matrix will remain unmodified.

USPCHT – USER DEFINED SPECIFIC HEAT AND LATENT HEAT

During thermal processing of materials, specific heat of the phase mixture may substantially change due to changes in temperature, composition, microstructure and electronic structure. Latent heat is another important thermal effect which should be taken into account for processing techniques involving phase transformations. This user subroutine allows the user to define a fictitious specific heat (c^*) which includes the effects of the variation of enthalpy of phase mixture due to both the change of state variables (T,C, ξ_k) and the latent heat. For a thermo-microstructural coupled analysis, c^* can be calculated by:

$$c^* = \sum_{k=1}^{p} c_k \xi_k + \Delta L_k \frac{d\xi_k}{dT} = c + \frac{\dot{\xi}_k}{\dot{T}} \Delta L_k \tag{6.2}$$

This user subroutine is called at each increment for every element in the mesh.

Interface

User subroutine USPCHT is written with the following headers:

```
SUBROUTINE USPCHT (SPHEAT,M,NN,KCUS,INC,NCYCLE,MATUS,
+NSTATS,DT,DTDL,CPTIM,TIMINC)
IMPLICIT REAL *8 (A-H, O-Z)
DIMENSION M(2),MATUS(2),KCUS(2)
        user coding
RETURN
END
```

Input

M(1) : user element number.

M(2) : internal element number.

NN : integration point number.

KCUS(1) : layer number (always 1 for continuum elements).

KCUS(2) : internal layer number (always 1 for continuum element).

INC : increment number.

NCYCLE : cycle number.

MATUS(1) : user material identifier.

MATUS(2) : internal material identifier.

NSTATS : number of state variables.

DT : temperature at the start of the increment.

DTDL : estimated increment of temperature.

CPTIM : time at the beginning of the increment.

TIMINC : increment of time.

Output

SPHEAT is the specific heat per unit mass. This is to be defined by the user.

6.1.2 FILM – USER DEFINED CONVECTIVE HEAT TRANSFER COEFFICIENT

In heat transfer analysis, it is often necessary to include nonuniform film coefficients and sink temperatures for the calculation of convection or radiation boundary condition as in the case of simulation of immersion quenching in which the variation of heat transfer coefficient is pronounce due to significantly different cooling regimes. The simplest way of simulating this effect is to define a surface temperature dependent heat transfer coefficient as,

$$\Psi(T_s, T_\infty) = h(T_s)(T_s - T_\infty) \tag{6.3}$$

where Ψ is the heat flux from the surface which is a function of the surface and the sink temperature.

However, this approach is not valid for complex geometries. Indeed, such geometries require the definition of the heat transfer at least as a function of the temperature and the position.

This subroutine allows definition of heat transfer coefficient and sink temperature as a function of surface temperature, position, time or any other parameter. It is called for integration point on each element surface given in the FILMS model definition set, and allows the user to modify the film coefficient and sink temperature. A smooth curve fitting to heat transfer coefficient and providing the derivative of the heat transfer coefficient with respect to temperature improve the accuracy and rate of convergence significantly. So, the use of piecewise linear approximation of h(T) data should better be avoided.

This subroutine may also be exploited in simulation of gas quenching. The mass flow rates which are exported as a function of position and time may be converted to heat transfer coefficients and applied as a boundary condition.

Interface

User subroutine FILM is written with the following headers:

```
SUBROUTINE FILM (H,TINF,TS,N,TIME)

IMPLICIT REAL *8 (A-H, O-Z)

DIMENSION H(2), N(7),TS(6)

        user coding

RETURN

END
```

Input

TS(1) : estimated surface temperature at the end of the increment.

TS(2) : is the surface temperature at the beginning of the increment.

TS(3) : not used.

TS(4) : integration point 1st coordinate.

TS(5) : integration point 2nd coordinate.

TS(6) : integration point 3rd coordinate.

N(1) : element number.

N(2) : IBODY code.

N(3) : integration point number.

N(4) : film index.

N(5) : sink temperature index.

N(6) : not used.

N(7) : internal element number.

TIME : current time.

Output

H(1) is the ratio of the desired film coefficient to that given on the FILMS data set for this element to be defined by the user (preset to 1).

H(2) is the derivative of the ratio of the film coefficient to that given on the FILMS data set; this can be defined optionally and may improve the convergence behavior in a nonlinear heat transfer analysis.

TINF is the ratio of the desired sink temperature to that given on the FILMS data set for this element to be defined by the user (preset to 1).

Note that since H and TINF are defined as ratios, if the user does not re-define them in this user subroutine, the data set values are used. If the user wishes to give absolute values here, the corresponding values on the FILMS data set can be conveniently set to 1.

6.2 MECHANICAL ANALYSIS SUBROUTINES

During thermal processing of materials, mechanical properties may substantially change due to changes in temperature, composition and microstructure. Transformation plasticity is another important mechano-microstructural effect which should be taken into account for processes techniques involving phase transformation, which results in considerable volume and shape change in the transforming region.

In the current developed framework, there exist no particular restrictions on the forms of the governing equations of plasticity and microstructural evolution. Thus, although this thesis involves small strain total Lagrangian J2 thermo-elastoplasticity, finite strain formulations with any other form of mechanical constitutive law such as visco-elastoplasticity is possible. This gives rise to a broad spectrum of possible applications from simulation of conventional heat treatments to state of art thermomechanical processing techniques, as long as a proper description of involved phenomena is supplied. However, application of the most of the subroutines discussed in this section is limited to additive decomposition of deformation gradient and multiplicative decomposition is not possible using this set of subroutines.

For the sake of brevity, only the subroutines related to small strain thermo-elastoplasticity coupled with microstructural evolution will be discussed henceforth. Those subroutines allow the definition of both the elastic and plastic properties of the phase mixture and constitutive behavior of the material. Although, two alternative methods of implementation will be presented in this section, many other implementation methods are also possible. First approach involves the modification of elastic constitutive law (Hooke`s law) and plastic hardening law by HOOKLW and WKSLP user subroutines, respectively. Second approach is based on definition of a hypo-elastic constitutive relationship in the form of strain rates. Although this approach is more formal and flexible, it is considerably harder to implement since the user must deal with plasticity (detection of yielding, return mapping, stress update etc.) by updating the stress state and state variables. The user must also supply a tangent modulus,

6.2.1 HOOKLW – USER DEFINED ELASTIC CONSTITUTIVE LAW

Elastic properties of a thermally processed material may change pronouncedly due to the changes in temperature, composition and microstructure, in the processing temperature interval. For processes with concomitant microstructural evolution, elastic properties may be approximated considering the evolution of individual elastic properties as a function of primary state variables such as temperature and composition by a convenient rule of mixture or micromechanical analysis. Since the elastic properties of the phase mixture is related to the distribution of phases, a proper method of homogenization is necessary. For a phase mixture with random arrangement, geometric rule of mixture for elastic modulus is an acceptable approximation, since it lies between upper (linear) and lower (harmonic) bounds.

HOOKLW user subroutine allows definition of an elastic stress-strain law in the form of:

$$\{\sigma\} = [D_e]\{\varepsilon\} \tag{6.4}$$

This user subroutine is called for each integration point of those elements that have anisotropic properties. The user can define either the stress-strain relation or the compliance strain-stress relation. The returned value of argument IMOD must be set accordingly. For example, if IMOD=1, the stress-strain law is given and the user returns to the array B such that:

$$\begin{Bmatrix} \sigma_{11} \\ \sigma_{22} \\ \sigma_{33} \\ \tau_{12} \\ \tau_{23} \\ \tau_{31} \end{Bmatrix} = \begin{bmatrix} D_{11} & D_{12} & D_{13} & D_{14} & D_{15} & D_{16} \\ D_{21} & D_{22} & D_{23} & D_{24} & D_{25} & D_{26} \\ D_{31} & D_{32} & D_{33} & D_{34} & D_{35} & D_{36} \\ D_{41} & D_{32} & D_{43} & D_{44} & D_{45} & D_{46} \\ D_{51} & D_{35} & D_{53} & D_{54} & D_{55} & D_{56} \\ D_{61} & D_{36} & D_{63} & D_{64} & D_{65} & D_{66} \end{bmatrix} \begin{Bmatrix} \varepsilon_{11} \\ \varepsilon_{22} \\ \varepsilon_{33} \\ \gamma_{12} \\ \gamma_{23} \\ \gamma_{31} \end{Bmatrix} \tag{6.5}$$

A maximum of 21 terms are necessary for an isotropic three-dimensional body. This law is given in terms of the coordinate system defined in the ORIENTATION option, which is taken as the global coordinate axes for the application problem. The user should insure that the stress-strain law is symmetric. This user subroutine is called twice for each integration point for temperature dependent properties during which it evaluates the constitutive law at the beginning at the end of the increment..

Interface

User subroutine HOOKLW is written with the following headers:

```
  SUBROUTINE HOOKLW(M,NN,KCUS,B,NGENS,DT,DTDL,E,PR,NDI,
+NSHEAR,IMOD,RPROPS,IPROPS)
  IMPLICIT REAL *8 (A-H, O-Z)
  DIMENSION B(NGENS,NGENS),DT(1),DTDL(1),RPROPS(1),IPROPS(1),
+M(2),KCUS(2)
              user coding
 RETURN
 END
```

Input

M(1)	: user element number.
M(2)	: internal element number.
NN	: integration point number.
KCUS(1)	: layer number (always 1 for continuum elements).
KCUS(2)	: internal layer number (always 1 for continuum element).
NGENS	: number of stresses and strain components.
DT	: state variables at the beginning of the increment (temperature first).
DTDL	: increment of state variables.
E	: Young's modulus including temperature effects.
PR	: Poisson's ratio including temperature effects.
NDI	: number of direct components of stress.
NSHEAR	: number of shear components of stress.
RPROPS	: array of real properties.
IPROPS	: array of integer properties.

Output

B is the user-defined stress-strain law if IMOD=1; or the user-defined compliance relation if IMOD=2 to be defined here.

6.2.2 WKSLP – USER DEFINED HARDENING LAW

Simulation of processes involving phase transformations requires computation of dynamically changing flow stress of the phase mixture. This user subroutine makes it possible for the user to program the yield stress and the corresponding work-hardening as a function of deformation history and temperature.

It should be noted that it is not convenient to use effective plastic strain ($\bar{\varepsilon}^p$) as a hardening parameter since the plastic deformation accumulated in the parent phase will be lost totally or partially during phase transformations .In the application problem, a special linear isotropic hardening rule which takes the effect of phase transformations on plastic flow is proposed, in which a new hardening parameter (κ_k) that tracks the history of the plastic deformation for each phase is introduced as

$$\kappa_k(\tau+\Delta\tau)=\int_{\tau=0}^{\tau}\left(\dot{\bar{\varepsilon}}^p-\frac{\dot{\xi}_k}{\xi_k}\kappa_k(\tau)\right).d\tau \tag{6.6}$$

where κ_k is the related strain hardening parameter for kth constituent.

Then, a new variable flow stress for the phase mixture is defined using κ as the state variable:

$$\sigma_f=\sum_{k=1}^{p}\xi_k\sigma_k^0+\sum_{k=1}^{p}\xi_k H_k\kappa_k=\sigma_0+\sum_{k=1}^{p}\xi_k H_k\kappa_k \tag{6.7}$$

where σ_k^o and H$_k$ are the yield stress and hardening modulus for kth microstructural constituent.

If the problem is based on concentration of plastic strains on the considerably softer phase (case of austenite with respect to austenite). A harmonic mean for flow stress may produce better results.

In the subroutine, the user needs to define the value of work hardening slope ,

$$Slope=\frac{d\bar{\sigma}}{d\kappa}+\frac{\bar{\sigma}\left(\kappa,\dot{\kappa}\right)-\bar{\sigma}\left(\kappa,0\right)}{\dot{\kappa}\Delta t} \tag{6.8}$$

must be specified. The second term in the SLOPE expression allows the user to include strain-rate effect if desired..

The current yield stress can optionally be defined. If the value of the current yield is not given here, MSC.Marc® calculates it from the initial yield value and the work-hardening slopes defined in this user subroutine.

The user subroutine is called as required by Marc during the elastic-plastic calculations. The number of times it is called per increment depends on the number of points going plastic, on the nonlinearity of the work-hardening curve, and on temperature dependence.

Interface

User subroutine WKSLP is written with the following headers:

```
SUBROUTINE WKSLP(M,NN,KCUS,MATUS,SLOPE,EBARP,ERAT,STRYT,DT,IFIRST)

IMPLICIT REAL *8 (A-H, O-Z)

 DIMENSION MATUS(2),KCUS(2)

                user coding

RETURN

END
```

Input

`M` is the current user element number.

`NN` is the integration point number.

`KCUS(1)`	: layer number (always 1 for continuum elements).
`KCUS(2)`	: internal layer number (always 1 for continuum element).
`MATUS(1)`	: user material id.
`MATUS(2)`	: internal material identifier.
EBARP	: current total equivalent plastic strain,
ERAT	: equivalent plastic strain rate,
DT	: current total temperature.

Output

SLOPE	: work-hardening slope, H
STRYT	: current flow stress, $\bar{\sigma}$.

6.2.3 ANEXP – THERMAL & PHASE TRANSFORMATION STRAINS

Simulation of thermomechanical behavior of materials undergoing phase transformations during anisothermal processes requires computation of thermal and phase transformation strains. Thermal, dilatational phase transformation and TRIP strains have the same nature and can be simulated by defining a fictitious thermal strain increment including all of those effects:

$$d\varepsilon_{ij}^{thermal} = d\varepsilon_{ij}^{th} + d\varepsilon_{ij}^{pt} + d\varepsilon_{ij}^{tp} \tag{6.9}$$

where, thermal , dilatational and TRIP strains are given respectively by,

$$d\varepsilon_{ij}^{th} = \sum_{k=1}^{p}\left[\dot{\xi}_k \int_{0}^{T} \alpha_k .dT + \xi_k \alpha_k \dot{T}\right] \tag{6.10}$$

$$\dot{\varepsilon}_{ij}^{pt} = \sum_{k=1}^{p-1}\frac{1}{3}\delta_{ij}\Delta_k\dot{\xi}_k \tag{6.11}$$

$$\dot{\varepsilon}_{ij}^{tr} = \frac{3}{2}K_k\dot{\xi}_k(1-\xi_k)S_{ij} \tag{6.12}$$

If only the thermal and dilatational phase transformations are considered resulting thermal strain would be isotropic type. However, implementation of TRIP requires definition of an anisothermal strain increment due to deviatoric nature of TRIP strains.

The ANEXP user subroutine can be used to specify anisotropic thermal strain increments, in which the temperature at the beginning of the increment, the temperature increment, and the base value of the thermal expansion coefficients are supplied and the user must supply the incremental thermal strain vector as an output Any components of the incremental thermal strain vector not defined in the user subroutine assume their default program calculated values.

The ANEXP user subroutine is called for all elements at all integration points if the temperature is nonzero for all material models. If the HYPELA2 user subroutine is used, it necessary to enter 1 to activate ANEXP in the second field of the third data block of the HYPOELASTIC model definition option.

Format

User subroutine ANEXP is written with the following headers:

```
SUBROUTINE ANEXP (N,NN,KCUS,T,TINC,COED,NDI,NSHEAR,EQEXP)

IMPLICIT REAL *8 (A-H, O-Z)

DIMENSION EQEXP(1),TINC(1),T(1),COED(NDI),N(2),KCUS(2)

          user coding

RETURN

END
```

Input

N(1) : user element number.

N(2) : the internal element number.

NN : integration point number.

KCUS(1) : layer number (always 1 for continuum elements).

KCUS(2) : internal layer number (always 1 for continuum element).

T(1) : total temperature at the beginning of the increment.

T(2 : total values of other state variables at the beginning of the increment.

TINC(1) : temperature increment.

TINC(2) : increments of other state variables.

COED(I) : the base value of the Ith coefficient of thermal expansion as given through the input data. There are NDI coefficients for each element.

NDI is the number of direct components of strain at this point.

NSHEAR is the number of shear components of strain at this point.

Output

EQEXP is the thermal strain increment vector, to be defined by the user in this user subroutine

6.2.4 HYPELA2 – USER DEFINED USER HYPOELASTIC CONSTITUTIVE LAW

This user subroutine gives the user the ability to implement arbitrary material models in MSC.Marc® using hypo-elastic material model. In conjunction to simulation of thermal processing of materials, a generalized constitutive relationship in the following form may be set up using HYPELA2 :

$$\dot{\sigma}_{ij} = D_{ijkl}\dot{\varepsilon}^{e}_{kl} = D_{ijkl}\left(\dot{\varepsilon}_{kl} - \dot{\varepsilon}^{p}_{kl} - \dot{\varepsilon}^{th}_{kl} - \dot{\varepsilon}^{pt}_{kl} - \dot{\varepsilon}^{tr}_{kl}\right) \tag{6.13}$$

In this subroutine, MSC.Marc® supplies the user with the total displacement, incremental displacement, total mechanical strain (mechanical strain = total strain – thermal strain), the increment of mechanical strain, and other information. In order to incorporate phase transformation strains, thermal strain should be modified as the sum of thermal and phase transformation strains using ANEXP subroutine.

Stress, total strain, and state variable arrays at the beginning of the increment are passed to HYPELA2. The user is expected to calculate stresses **S**, tangent stiffness **D**, and state variables that correspond to the current strain at the end of the increment.

Before using this user subroutine, it is highly recommended to justify the subroutine with one-element problems under displacement and load control boundary conditions, where the displacement controlled boundary condition is used to justify the accuracy of the stress update procedure while the load controlled problem checks the accuracy of the tangent stiffness.

Stresses and Strains

It should be noted that the stress and strains which are passed to the subroutine depends on the formulation. For example, engineering strains and stress are passed for small displacement-small strain problem, whereas, Green-Lagrange strains and 2nd Piola-Kirchhoff stresses are passed for a small strain – large displacement formulation. Similarly, logarithmic strains and Cauchy stresses are passed for an updated Lagrangian formulation.

For simulation of quenching, for which small strain-small displacement formulation is used in this thesis, stresses and strains that are passed are engineering stresses and strains. However, care must be taken for other formulations. For example, quenching of a long shaft, or a long profile may require the use of small strain-large displacement formulation which eventually yield Green-Lagrangian strain and 2nd Piola-Kirchhoff stress.

Coordinate System

It is crucial to note that strain and stress components are rotated by Marc to account for rigid body motion before HYPELA2 is called for large strain inelasticity. So, the stress integration for the co-rotational part is performed in HYPELA2 based on rotation free values. The user is required to pass back the updated rotation free stress based on the co-rotational system. If the ORIENTATION model definition option is used, the stress and strain components are stored in the local orientation axis. The basis vectors rotate with the material by rotation tensor (R) and, so the stress and strain are already stored in the rotated orientation axis before HYPELA2 is called.

For the application problem in the thesis, consideration of the coordinate system is not a problem since it involves small strain-small displacement formulation.

Updating the Stress State

The user must provide updated stress at the end of the increment based on stress at the beginning of the increment by :

$$\left\{\sigma\right\}^{m+1} = \left\{\sigma\right\}^{m} + \left\{\Delta\sigma\right\}^{m+1} \tag{6.14}$$

In order to update the stress state for an elastoplastic problem, the user must detect yielding and use perform return mapping if yielding occurred. The algorithm and flow chart for such kind of procedure can be found in Section 5.2 and Figure 5.2 .

Updating Tangent Stiffness

The user needs to provide the tangent stiffness D based on the updated stress.

$$D_{ij} = \frac{\partial\left(\Delta\sigma_i\right)}{\partial\left(\Delta\varepsilon_j\right)} \tag{6.15}$$

The rate of convergence or a nonlinear problem depends critically on the user supplied tangent stiffness. A fully consistent exact tangent stiffness provides quadratic convergence of the displacement or residual norm.

For the application problem, a tangent stiffness consistent to the return mapping scheme implemented has been used. The details of formulation can be found in Section 4.3.6. Use of this tangent resulted in a weak and stable convergence behavior. So, an alternative must be derived. Use of a numerically calculated tangent stiffness may be an alternative solution, which is more time consuming but more flexible. However, such an approach has not been tested yet.

Thermal and Phase Transformation Stresses

For thermal and phase transformation stress problems, the change in stress (**G**) due to temperature and microstructure dependent material properties must be provided by,

$$G_i = \Delta D_{ij} \Delta\varepsilon_j \tag{6.16}$$

where ΔD_{ij} and $\Delta\varepsilon_j$ are the variation of tangent stiffness due to material property changes and $\Delta\varepsilon_j$ is strain increment which is passed to HYPELA2.

Updating the State Variables

The state variables other than temperature should also be updated in this subroutine. The increments of the state variables should be calculated and returned as the array DT ( ). For simulation of quenching, those state variables are plastic deformation memory (κ_k) and fraction of phases (ξ_k) which can also be calculated in HYPELA2 subroutine without the need of using UBGITR subroutine.

$$\Delta\kappa_k = \kappa_k^{m+1} - \kappa_k^m$$

$$\Delta\xi_k = \xi_k^{m+1} - \xi_k^m$$

It is crucial to notice that any vectorial or tensorial state variables require to be rotated by using the rotation tensor (R) if the problem involves a large strain formulation.

Interface

User subroutine HYPELA2 is written with the following headers

```
SUBROUTINE HYPELA2(D,G,E,DE,S,T,DT,NGENS,N,NN,KCUS,MATUS,
2 NDI,NSHEAR,DISP,DISPT,COORD,FFN,FROTN,STRECHN,EIGVN,FFN1,
3 FROTN1,STRECHN1,EIGVN1,NCRD,ITEL,NDEG,NDM,NNODE,
4 JTYPE,LCLASS,IFR,IFU)
IMPLICIT REAL *8 (A-H, O-Z)
DIMENSION E(1),DE(1),T(1),DT(1),G(1),D(NGENS,NGENS),S(1)
DIMENSION N(2),COORD(NCRD,NNODE),DISP(NDEG,NNODE),
2 DISPT(NDEG,NNODE),FFN(ITEL,ITEL),FROTN(ITEL,ITEL)
3 STRECHN(ITEL),EIGVN(ITEL,ITEL),FFN1(ITEL,ITEL)
4 FROTN1(ITEL,ITEL),STRECHN1(ITEL),EIGVN1(ITEL,ITEL)
DIMENSION MATUS(2),KCUS(2),LCLASS(2)
        user coding
RETURN
END
```

Input

E : total elastic mechanical strain.

DE : increment of mechanical strain.

T : state variables (comes in at t = m; must be updated to have state variables at t = m +1).

DT : increment of state variables.

NGENS : size of the stress-strain law.

N : element number.

NN : integration point number.

KCUS(1) : layer number (always 1 for continuum elements).

KCUS(2) : internal layer number (always 1 for continuum element).

MATUS(1) : user material identifier.

MATUS(2) : internal material identifier.

NDI : number of direct components.

NSHEAR : number of shear components.

DISP : incremental displacements.

DISPT : displacements at t = m (at assembly lovl = 4) and the displacements at t = m +1 (at stress recovery lovl = 6).

COORD : coordinates.

NCRD : number of coordinates.

NDEG : number of degrees of freedom.

ITEL : the dimension of F and R; 2 for plane-stress and 3 for the rest of the cases.

NNODE number of nodes per element.

JTYPE : element type.

LCLASS(1) :element class.

LCLASS(2) 0 for displacement element.

1 for lower-order Herrmann element.

2 for higher-order Herrmann element.

IFR : 1 if R has been calculated.

IFU : if STRECH has been calculated.

At t = m (the beginning of the increment):

FFN : deformation gradient.

FROTN : rotation tensor.

STRECHN : square of principal stretch ratios, lambda (i).

EIGVN (I,J) : I principal direction components for J eigenvalues.

At t = m+1 (the current time step):

FFN1 : deformation gradient.

FROTN1 : rotation tensor.

STRECHN1 : square of principal stretch ratios

EIGVN1(I,J) : I principal direction components for J eigenvalues.

Output

D : the stress strain law to be formed.

G : change in stress due to temperature effects.

S : stress to be updated.

6.3 INPUT/OUTPUT AND MODIFICATION OF USER DATA

A major requirement of the developed framework is the material data for each phase as a function of temperature, which cannot be supplied to user subroutines via MSC.Mentat® interface. These data must be stored in the user subroutine file. For ease of access by all the subroutines used for implementation, the data is read from a data file at the first increment at the beginning of the analysis and stored in common blocks which can be accessed by all constitutive subroutines via USDATA subroutine.

A vital part of the developed framework is the use of new state variables. Current architecture involves 11 additional state variables which are the fraction of phases (austenite, pearlite, ferrite, bainite, martensite), hardening parameters associated to those phases and Scheil`s sum. Those state variables are initialized and updated using INITSV and NEWSV subroutines. The use of NEWSV is optional in certain cases (such as in HYPELA2 subroutine) in which the subroutine already requires the update of state variables as an output.

Another requirement of the framework is the output of required quantities such as fraction of phases, coupling terms like TRIP strain etc. into the output file, which will be used in the post-processing. PLOTV subroutine is invoked for this purpose.

6.3.1 USDATA - USER INPUT DATA

This user subroutine is a mechanism to allow the user to read data into a user-defined common block. This common block is stored on the restart file, and available in subsequent increments. The common block USDACM must be given the correct length in this user subroutine. This common block can also be used in any other user subroutine. Note that the maximum length of USDACM should be defined here. It should agree in length in real *4 words as with that given on the USDATA model definition option.

Interface

User subroutine USDATA is written with the following headers:

```
SUBROUTINE USDATA(KIN,KOU,IC)

COMMON/USDACM/MYDATA

IMPLICIT REAL *8 (A-H, O-Z)

        user coding

RETURN

END
```

Input

`KIN` is the unit number for input, usually 5.

`IC` is the reader flag.

= 1 pre-reader.

= 2 real reader.

Output

`KOU` is unit number for output, usually 6.

6.3.2 INITSV – INITIALIZATION OF STATE VARIABLES

This allows the user to define initial values of state variables such as fraction of phases, associated hardening parameters including the effect of plastic memory loss due to diffusional phase transformations and the Scheil`s sum. When not using the table driven input format, it is called in a loop over all the elements in the mesh when the INITIAL STATE option appears in the model definition options with a 2 in the second field of the second data block of that option. When using the table driven input, it is called for those elements specified in the INITIAL STATE model definition option if a 7 is given in the second field of the second data block and the initial condition is activated by the LOADCASE model definition option.

Interface

User subroutine INITSV is written with the following headers:

```
SUBROUTINE INITSV(SV,LAYERS,INTPTS,M,ID)

IMPLICIT REAL *8 (A-H, O-Z)

DIMENSION SV(LAYERS,INTPTS)

        user coding

RETURN

END
```

Input

LAYERS	: is the number of layers through the thickness if this is a shell element, or the number of points in the cross-section if this is a beam element. It is 1 for a continuum element.
INTPTS	:the number of integration points in this element if the ALL POINTS parameter is used. If the CENTROID parameter is used, INTPTS = 1.

M : user element number.

ID : the state variable number

Output

SV : array of values of this state variable; to be defined here for this element.

6.3.3 NEWSV – NEW VALUES FOR STATE VARIABLES

This user subroutine allows the new values of any state variable to be defined at the end of the current step. By using this subroutine, the fraction of phases and associated hardening parameters are updated. It should be noted that this subroutine is not required using HYPELA2 subroutine since it already requires updating of state variables as an output.

When not using the table driven input format, it is called in a loop over all the elements in the mesh when the CHANGE STATE option appears in the model definition or the history definition set with a 2 in the second field of the second data block of that option. When using the table driven input, it is called for those elements specified in the CHANGE STATE model definition option, if a 7 is given in the second field of the second data block and the boundary condition is activated by the LOADCASE option.

Interface

User subroutine NEWSV is written with the following headers:

```
SUBROUTINE NEWSV(SV,LAYERS,INTPTS,M,ID)

IMPLICIT REAL *8 (A-H, O-Z)

DIMENSION SV(LAYERS,INTPTS)

        user coding

RETURN

END
```

Input

LAYERS : number of layers through the thickness if this is a shell element, of the number of points in the cross-section if this is a beam element. It is 1 for a continuum element.

INTPTS: is the number of integration points in this element if the ALL POINTS parameter is used. If the CENTROID parameter is used, INTPTS=1.

M : user element number.

ID : state variable number

Output

SV : array of new values of this state variable; to be defined here for this element by the user.

CPTIM : the total time at the end of the last step.

TIMINC : time increment at the current step.

6.3.4 PLOTV – OUTPUT OF USER QUANTITIES

The PLOTV user subroutine is used in conjunction with either element code 19 or a negative code entered in the POST option. This allows the user to define an element variable to be written to the post file. In the current framework, it is used to output fraction of phases, thermal and phase transformation stresses and Scheil`s sum at each increment.

Format

User subroutine PLOTV is written with the following headers:

```
 SUBROUTINE PLOTV(V,S,SP,ETOT,EPLAS,ECREEP,T,M,NN,KCUS,NDI,
+ NSHEAR,JPLTCD)
 IMPLICIT REAL*8 (A-H, O-Z)
 DIMENSION S(*),SP(*),ETOT(*),EPLAS(*),ECREEP(*),T(*),
+ M(2),KCUS(2)
        user coding
RETURN
END
```

Input

S : the array of stresses at this integration point.

SP : array of stresses in the preferred direction if ORIENTATION is used.

ETOT : total strain (generalized) at this integration point.

EPLAS : total plastic strain at this integration point.

ECREEP : total creep strain at this integration point.

T : array of state variables at this integration point (temperature first).

M(1) : user element number.

M(2) : internal element number.

NN : integration point number.

KCUS(1) : internal layer number (always 1 for continuum elements).

KCUS(2) : internal layer number (always 1 for continuum elements).

NDI : number of direct stresses.

NSHEAR : number of shear stresses.

JPLTCD : absolute value of the user’s entered code.

Output

V is the variable to be plotted or put onto the post file, to be defined in this routine.

6.4 MICROSTRUCTURAL EVOLUTION SUBROUTINES

In the current framework, phase transformation calculations are performed between thermal and mechanical passes. In the alternative implementation method using HYPELA2, they might also be performed with mechanical pass without the need of using additional subroutines. There exist many possibilities to perform the microstructural analysis using the “dummy” subroutines (i.e., UBGITR, UBGINC, UEDINC, UBGPASS and UEDPASS) that run at the beginning or the end of thermal and mechanical passes of the termomechanically coupled analysis. The computations maybe performed at the end of the pass or the iteration loop during the solution of the nonlinear problem. The latter is less effective but safer. That`s why UBGITR subroutine has been used in this study.

6.4.1 UBGITR

This subroutine is used to compute microstructural evolution kinetics for a modified thermomechanical analysis. In the alternative implementation method using HYPELA2, use of this subroutine may not be necessary since the microstructural evolution may be calculated in the mechanical pass prior to solution.

The microstructural evolution calculation used in this thesis relies on Scheil`s additivity principle and the details of computation is given in Section 3.5.2. However, the framework has a flexible architecture and any kind of microstructural evolution calculation method is possible. Even the multi-scale / multi-grid methods are possible in a representative volume element (RVE).

The UBGITR user subroutine is called at the beginning of each iteration in the solution of the nonlinear problem. It can be used to define or modify data variables stored in common blocks. No special flag is required in the input file.

Interface

User subroutine UBGITR is written with the following headers:

```
SUBROUTINE UBGITR(INC,INCSUB,NCYCLE)
IMPLICIT REAL *8 (A-H, O-Z)
        user coding
RETURN
END
```

Input

INC	: increment number.
INCSUB	: sub-increment number.
NCYCLE	: iteration number (the first is labeled zero).

CHAPTER 7

EXPERIMENTAL AND NUMERICAL ANALYSIS PROCEDURE

7.1 EXPERIMENTAL PROCEDURE

Experimental procedure consists of specimen preparation, heat treat treatment, XRD residual stress measurement and SEM inspection. Details of the each step are presented in the next sections.

7.1.1 SPECIMEN PREPARATION

First, C60 steel (0.6%C, 0.25%Si, 0.75%Mn) bars of 30 mm diameter are cut down into cylinders having length of 30 mm. Then, holes of various diameters and degree of eccentricity (S2/S1) are drilled on those specimens as illustrated on Figure 7.1.

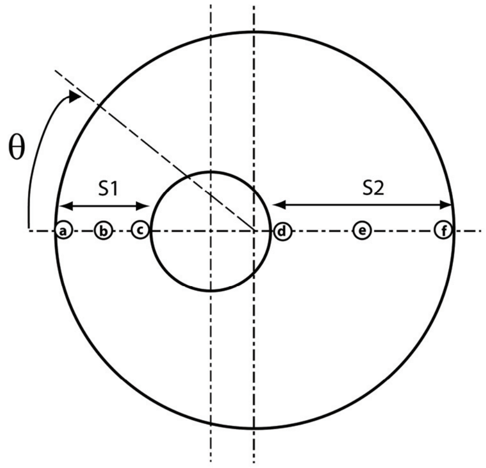

Figure 7.1 Specimen geometry and residual stress measurement direction and microstructural investigation points

The specimens are labeled as shown on Table 7.1. Holes on the specimens were closed before heat treatment in order to avoid contact with the quenchant on the inner surface. This will minimize the heat loss from inner surface and eliminate hard to predict turbulent fluid flow.

Table 7.1 Set of specimens used.

Eccentricity (S2/S1)	**Specimen** ***Φ = 30 mm , L = 60 mm***				
1	A1	B1	C1	D1	E1
2	A2	B2	C2	D2	E2
4	A3	B3	C3	D3	E3
Hole Diameter	6 mm	9 mm	12 mm	15 mm	18 mm

7.1.2 HEAT TREATMENT

During heat treatment, in order to minimize the danger of distortion and cracking, all specimens were preheated at 200°C for 20 min. Then, they were soaked for 30 min at heat treating temperature in a salt bath to prevent decarburization and to ensure uniformity of the temperature and microstructure throughout the entire volume. After austenization stage, the specimens were immediately quenched into water at 20°C. It should be noted that decarburization may drastically alter the residual stress state on the surface [218].

7.1.3 XRD RESIDUAL STRESS MEASUREMENT

X-ray measurements were carried out on a Ψ diffractometer using Cr-Kα radiation on set of crystallographic planes. Since the peak shift due to lattice strains at high diffraction angles is considerably higher, peak having high indices and intensity is preferred for measurements. The intensity and angular position data for analysis is provided by scintillation detector and scaler. Counting has undertaken for a fixed time of 2 s at 2θ angles between 152^0 to 160^0 by 0.1^0 steps.

Parabola method was used for the determination of the peak maximum and position. Then, corresponding values for interplanar spacing and strains are calculated. Finally, the stress was determined by linear regression analysis by determining the slope of the regression line of lattice strain versus $\sin^2\psi$ plot and multiplying it with elastic modulus of the material. Elastic modulus used in the calculations was the one that had been obtained by mechanical tests. To minimize the instrumental error, adjustment of the measurement system and effect of specimen curvature on the results were checked by several tests measuring the residual stress on iron powder. To control the reliability and reproducibility of the results, residual stresses were measured repeatedly at the same points on a selected specimen.

7.1.4 METALLOGRAPHIC PREPARATION AND SEM INSPECTION

For microstructural characterization, cylindrical samples were taken from heat treated C60 specimens. The samples were mounted, finely ground and polished. In order to enhance contrast between ferrite, pearlite, bainite and martensite; the specimens were etched with picral. Some of the D-coded specimens were etched by 2% Nital in order to reveal fine martensitic structure. The prepared cross sections of heat treated cylinders were examined under scanning electron microscope (SEM). For quantitative analysis of microstructure the SEM micrographs were analyzed using Clemex Image analysis software.

7.2 FINITE ELEMENT ANALYSIS PROCEDURE

Finite element analyses were performed using the developed framework which involves total Lagrangian small strain J_2 thermoelastoplasticity coupled with anisothermal JMAK transformation kinetics. The framework has been first tested for single element solutions and small systems. Then, it has been justified both experimentally and by using the numerical results from the literature. The framework has been first tested on quenching of 1D, 2D and 3D geometries without phase transformation effects. Then, the model is extended to the case of quenching of 1D, 2D and 3D geometries with phase transformations. In each case, the model is verified by both experiments (residual stress measurements, SEM investigations) and available literature.

7.2.1 MESHING AND TIME STEPPING

Using the symmetry, only ¼ of the cylinders are modeled to improve the efficiency and the stability of the solution. A convergence and mesh independence analysis was carried out to ensure the quality of the results at minimum cost. According to the results, it has been observed that the tangential residual stress state becomes insensitive to number of elements and time step for N>3600 and Δt<0.01 within an error norm of 10 MPa. Thus, a FE mesh, which is refined near the outer surface, was created using 3600 8-noded hexahedral elements.

7.2.2 INITIAL AND BOUNDARY CONDITIONS

Initially, the temperature is set to 830^{0}C for all nodes and all of the elements were assumed to be made up of 100% homogeneous austenite. Non-linear convective heat transfer boundary condition was set on outer surface beside the thermal and mechanical symmetry boundary conditions. Convective heat transfer coefficient data as a function of surface temperature, as illustrated on Figure 7.2, is presented by :

$$\begin{aligned} h(T_s) = 10^{-9}T_s^5 \ - \ 3.10^{-6}T_s^4 \ + \ 0.0014T_s^3 \ - \ 0.2883T_s^2 \\ + \ 39.088T_s \ + \ 4354.6 \end{aligned} \tag{7.1}$$

7.2.3 MATERIAL DATA

Thermo-mechanical data used in simulations for C60, Ck45 and St50 steels are presented on Tables 7.2-7.4 and they are obtained from the studies of Gür [4, 262, 263], Geijsalers [21], Schroeder [303], Yu [304, 305]. Those data are also illustrated graphically as a function of temperature on Figures 7.7-7.9. For the sake of brevity, Material properties which are considered independent of the temperature are not plotted on those figures.

In regards to phase transformation data for C60 steel, kinetic constants of the JMAK equation are extracted from CCT (Figure 7.4) diagram using the inverse additivity algorithm proposed by Geijsalers [21]. As opposed to generation of CCT diagrams from ITT (Figure 7.3) diagrams, ITT diagrams can also be generated from CCT diagrams by an inverse use of additivity principle. Although it may appear strange to extract isothermal kinetic constants from continuous cooling transformation (CCT) diagrams, this method has certain advantages. First advantage of this approach is improved accuracy for simulations. The isothermal parameters extracted from CCT diagrams by an inverse additivity procedure will perform better than the ones extracted from ITT diagrams under anisothermal conditions. Second advantage of this method arises from the fact that CCT diagrams are less sensitive to overlapping transformations. Thus, a better representation of transformation behavior can be achieved.

Figure 7.5 illustrates the accuracy of computation of the CCT diagram by extraction of isothermal kinetic constants both from the TTT and CCT diagrams. It can clearly seen that the CCT diagram calculated using TTT data is not an accurate representation of the actual CCT data and involves considerable errors. On the other hand, the CCT curve which has been generated by extraction of isothermal constants from CCT data using the procedure discussed in the previous section, yields almost the exact CCT curve.

After the extraction of b and k for a series of cooling curves, a 3rd order polynomial fit, as shown on equations (7.2) and (7.3), is used to determine the temperature dependence of b and k. Similarly, a second order curve fit is applied to extracted isothermal incubation times as shown on equation (7.4).

$$n(T) = n_0 + n_1 T + n_2 T^2 + n_3 T^3 \tag{7.2}$$

$$\log b(T) = b_0 + b_1 T + b_2 T^2 + b_3 T^3 \tag{7.3}$$

$$\log \tau_s(T) = \tau_0 + \tau_1 T + \tau_2 T^2 \tag{7.4}$$

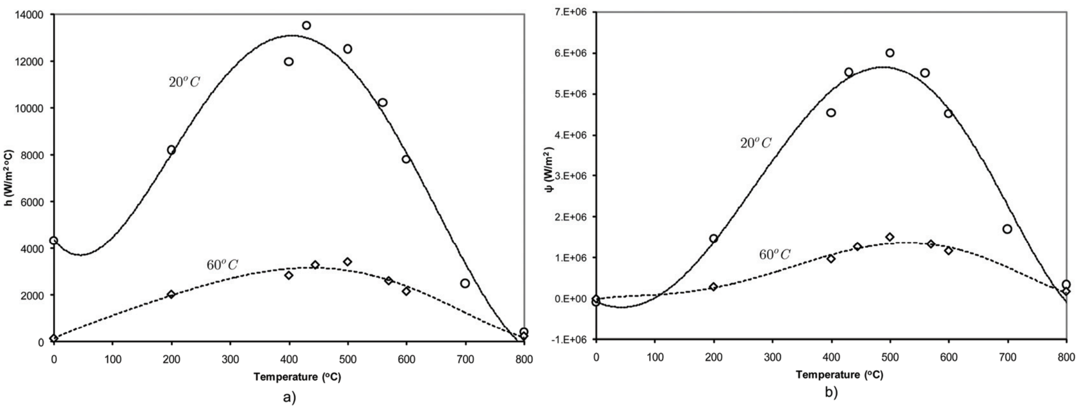

Figure 7.2 Variation of a) Convective heat transfer coefficient (h), b) Heat flux (ψ) as function of surface temperature

Table 7.2 Thermomechanical data for C60 steel [4].

T (°C)	E (GPa)	ν	σ_Y (MPa)	H (MPa)	α (μ/°C)	λ (J/ms °C)	c (MJ/m^3 °C)
				Austenite			
0	200	0.29	220	1000	21.7	15.0	4.15
300	175	0.31	130	16000	21.7	18.0	4.40
600	150	0.33	35	10000	21.7	21.7	4.67
900	124	0.35	35	500	21.7	25.1	4.90
				Ferrite , Pearlite , Bainite			
0	210	0.28	450	1000	15.3	49.0	3.78
300	193	0.30	230	16000	15.3	41.7	4.46
600	165	0.31	140	10000	15.3	34.3	5.09
900	120	0.33	30	500	15.3	27.0	5.74
				Martensite			
0	200	0.28	1750	1000	13.0	43.1	3.76
300	185	0.30	1550	16000	13.0	36.7	4.45
600	168	0.31	1350	10000	13.0	30.1	5

Table 7.3 Thermomechanical data for St50 steel [304].

T (°C)	**E (GPa)**	ν	σ_Y **(MPa)**	**H (MPa)**	α **(μ/°C)**	λ **(J/ms °C)**	**c (MJ/m^3 °C)**
0	206	0.3	349	1000	14.1	43.6	4.52
200	206	0.3	294	16000	14.1	43.6	4.52
600	206	0.3	58	10000	14.1	43.6	4.52

Table 7.4 Thermomechanical data for Ck45 steel [303]

T (°C)	**E (GPa)**	ν	σ_Y **(MPa)**	**H (MPa)**	α **(μ/°C)**	λ **(J/ms °C)**	**c (MJ/m^3 °C)**
				Austenite			
0	210	0.28	360	1000	14.0	49.0	3.78
300	193	0.30	230	16000	14.0	41.7	4.46
600	165	0.31	140	10000	14.0	34.3	5.09
900	120	0.33	30	500	14.0	27.0	5.74

Table 7.5 Phase transformation kinetics data for C60 steel.

	b_0	b_1	b_2	b_3
Bainite	-4.617	0.096	0.0003	3.10^{-7}
Pearlite	404.2	-1.939	-0.031	$-2,10^{-6}$
Ferrite	-16314	73.35	-0.1907	5.10^{-5}
	n_0	n_1	n_2	n_3
Bainite	-5.8923	0.0622	-0.0002	1.10^{-7}
Pearlite	-237.67	1.0332	-0.0014	7.10^{-7}
Ferrite	32336	-145.21	0.217	-1.10^{-4}
	τ_0	τ_1	τ_2	
Bainite	6.397	-0.0217	2.10^{-5}	
Pearlite	45.13	-0.1635	1.10^{-4}	
Ferrite	25.67	-0.0944	9.10^{-5}	
A_{e1} = 750 °C	**A_{e3} = 720 °C**	**B_s = 540 °C**	**M_s = 300 °C**	

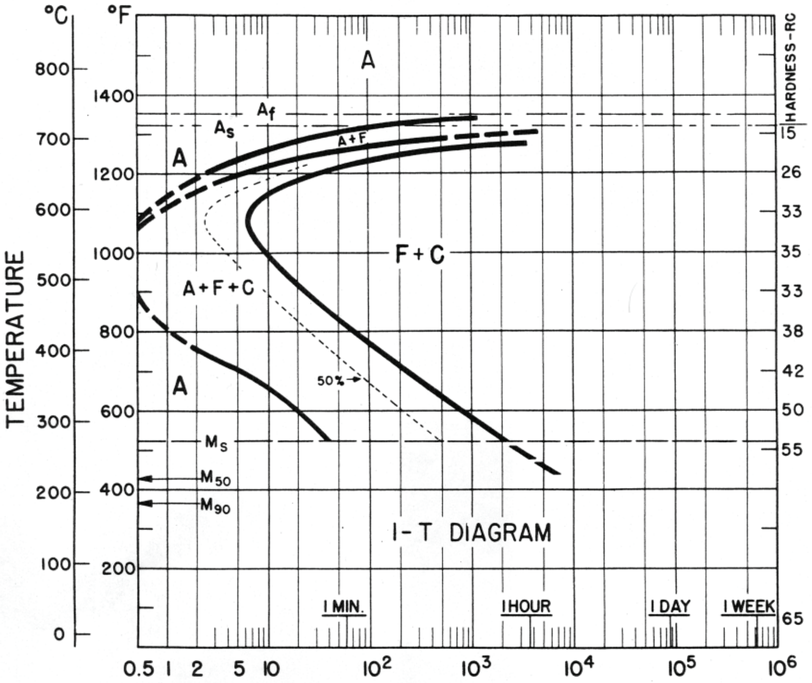

Figure 7.3 TTT diagram for C60 steel [306]

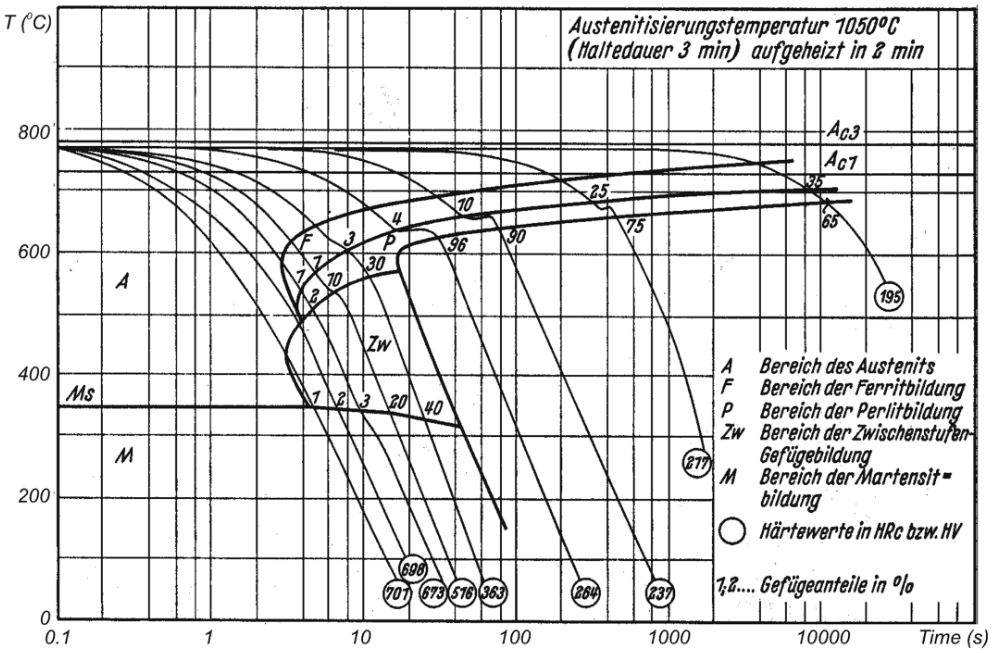

Figure 7.4 CCT diagram for C60 steel [306]

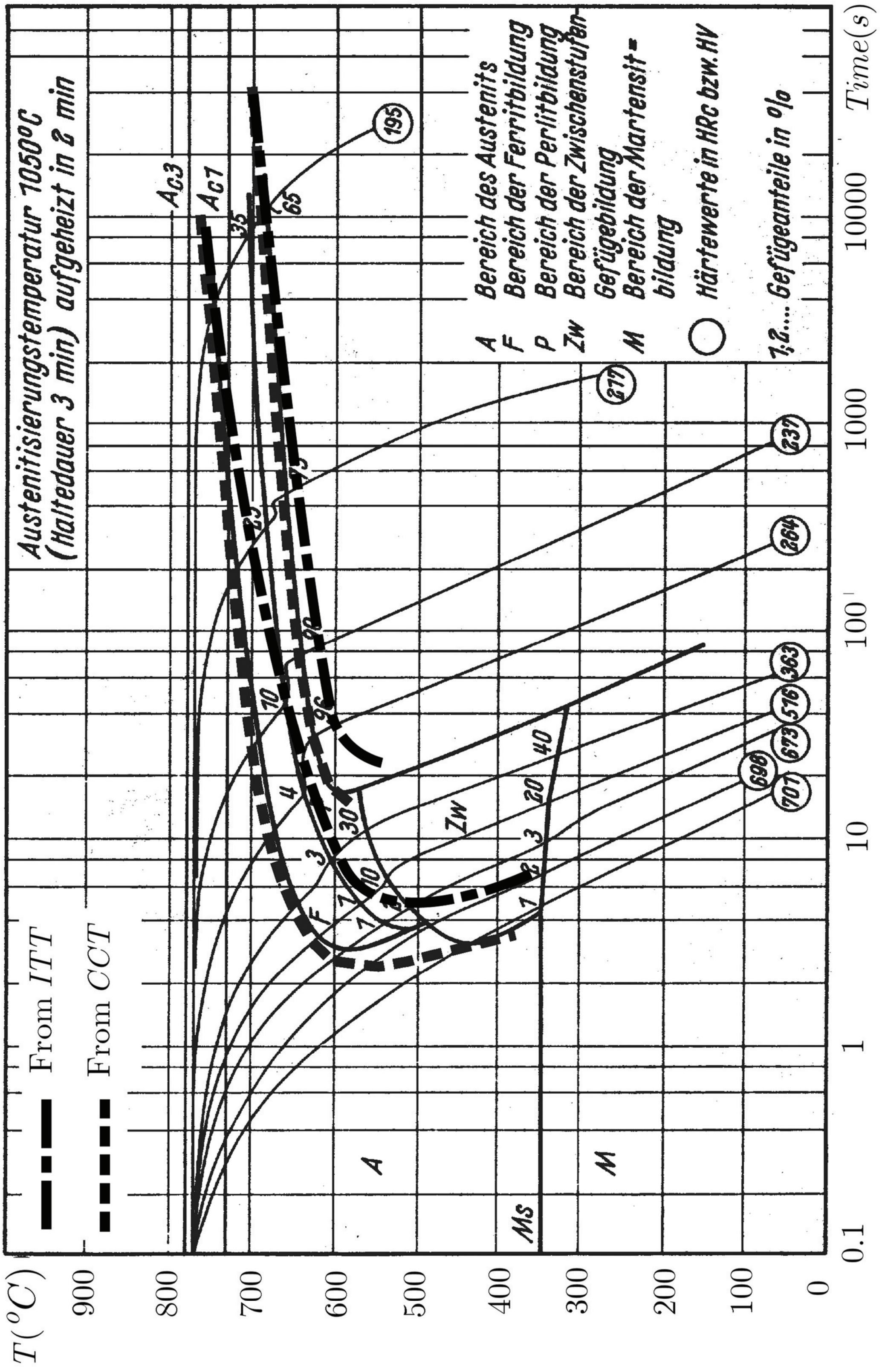

Figure 7.5 Comparison of CCT diagrams generated using the additivity principle by extraction of IT kinetic data from ITT and CCT diagrams

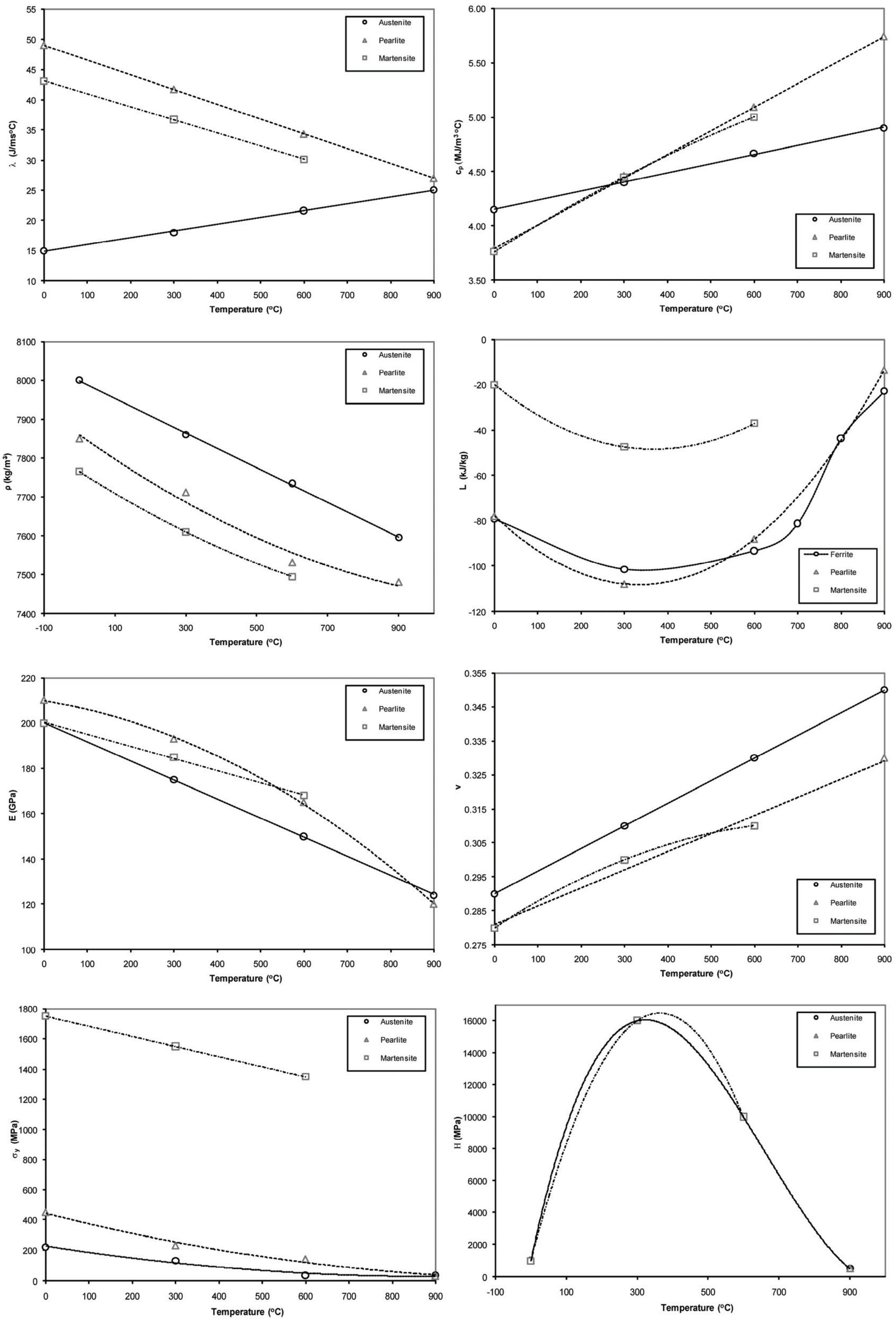

Figure 7.6 Graphical representation of the material data used for C60 steel.

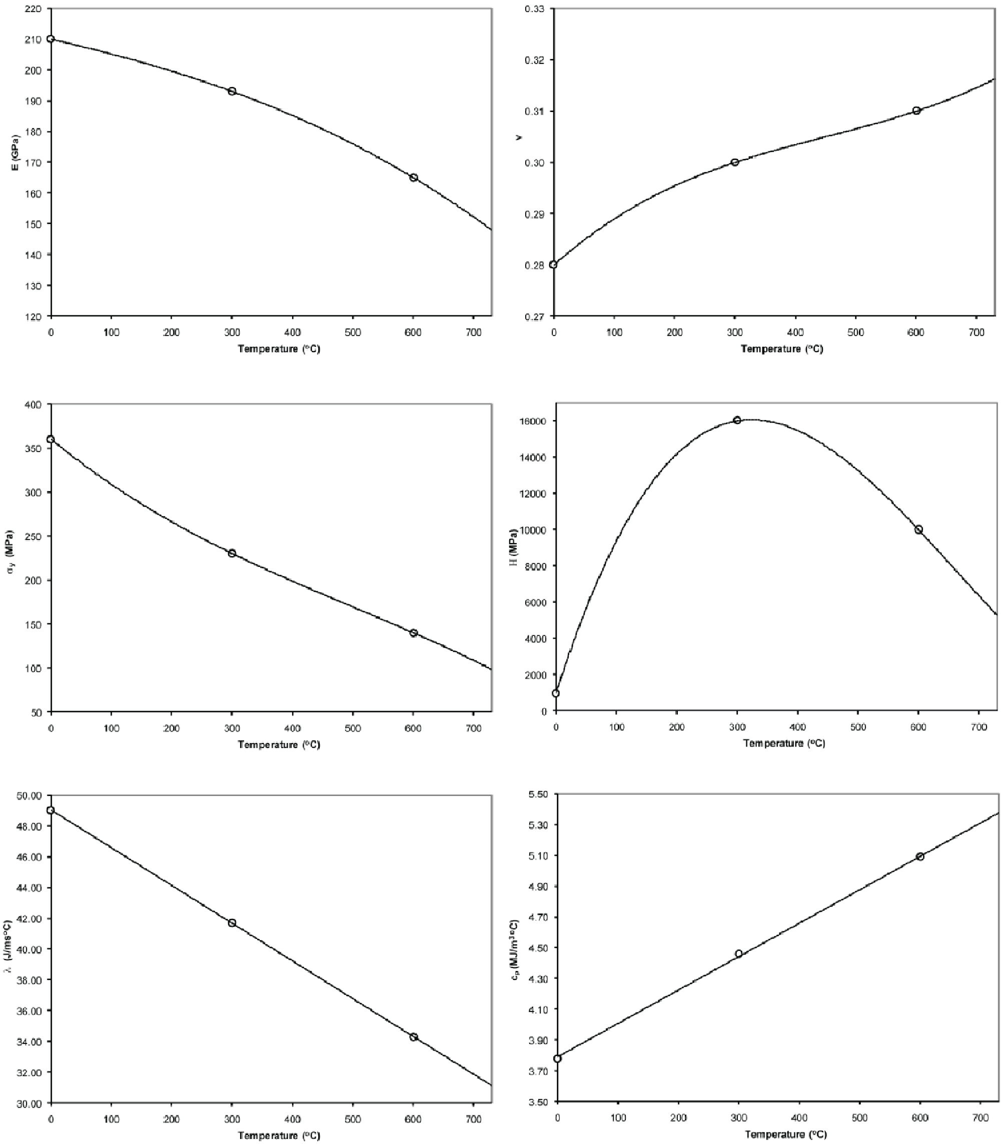

Figure 7.7 Graphical representation of material data for Ck45 steel.

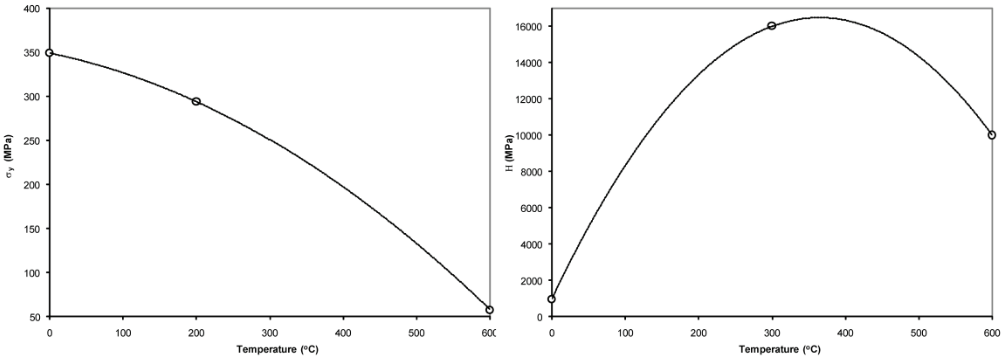

Figure 7.8 Graphical representation of material data for St50 steel

CHAPTER 8

RESULTS AND DISCUSSION

8.1 GENERAL

The major aim of this thesis was the development of a flexible framework on which a variety of thermal processing techniques can be simulated. As an application problem, simulation of through hardening process was performed to verify the accuracy and physical consistency of the framework. Structure of the current chapter is consisted of two major categories: 1) Simulation of quenching without phase transformations 2) Simulation of quenching with phase transformations. Each subsection starts with the verification of the proposed model and followed by a parametric study in which the effect of important intrinsic and extrinsic parameters on the evolution of residual stresses and microstructure is investigated.

First, simulation of quenching without phase transformation was performed in order to verify the basic capabilities of the framework and to investigate the evolution of thermal stresses during quenching, even though practical applications of quenching usually involve phase transformations, the verification of this sub-section was carried out by using results from several numerical simulations in the literature and a series of experiments. Then, a parametric study was conducted to investigate the phenomena occurring and to determine important parameters affecting quench performance. In the next sub-section, all possible effects of phase transformation were integrated in the framework. Then, the simulation of quenching with phase transformations was performed on the same set of geometries (1D-2D) used in the previous section. The capability of the framework to deal with phase transformation related couplings is justified using both literature and experiments. Then, the effect of several important parameters such as the geometrical features of the specimen and phase transformation related couplings are investigated and discussed in the parametric study part. Finally, all of the capabilities and improvements of the framework related to quenching was demonstrated by simulating the quenching of eccentrically drilled cylinders which may be used as a reference specimen to comprehend the problems associated with quenching of components having complex 3D geometries. The accuracy of the prediction of the microstructure was justified via tedious SEM inspections. Then, the accuracy of the prediction of residual stress state was performed by making use of XRD measurement of first kind of residual stresses.

8.2 QUENCHING WITHOUT PHASE TRANSFORMATIONS

In many cases of quenching, plastic deformation occurs in the soft austenite phase due to thermal stress before the start of the phase transformations. Large stresses and large amount of distortion may occur in the austenitic phase even without phase transformation stresses. Moreover, thermal stresses and prior plasticity that develop in the early stages of quenching may significantly affect both the thermodynamics and kinetics of phase transformations. These reasons render the prediction of evolution of thermal stresses and distortion during quenching without phase transformations.

Simulation of quenching without phase transformations may also reveal the underlying physics of development of thermal stresses and distortion, which may be quite complicated if a model involving all the physics is used. Moreover, it is also a step to justify the basic capabilities of the framework.

8.2.1 QUENCHING OF INFINITELY LONG CYLINDERS (1D)

Quenching of infinitely long cylinders was carried as a preliminary stage in order to verify the model and investigate several concepts in quenching process due to significant reduction in computation time owing to generalized plain strain assumption. Parameters and concepts investigated for this case may be extended for 2D and 3D cases. The investigated parameters are effect of temperature dependant convective heat transfer coefficient, quench bath temperature, diameter of the specimen. Finally, the physics and underlying mechanisms of fluctuating internal stress field concept was investigated.

For simulations, a fully coupled thermomechanical analysis was performed using MSC.Marc®. Total quenching time was selected as 120s for all specimens in order to guarantee that the final stress distribution is the residual stress distribution. Because of the severe non-linearity of the problem due to temperature dependence of material properties and convective heat transfer coefficient, a tight convergence ratio (0.001) based on the residuals was imposed. An adaptive time stepping procedure with an initial time step of 0.001 s was invoked. The time step was increased up to 20% after a sufficiently convergent increment. This procedure provided an efficient analysis without sacrificing so much from the accuracy of the solution since the solution of the problem is more time step dependent on the early stages of quenching due to large temperature gradients. As the quenching proceeds with smoother thermal gradients, considerably larger time steps (in the order of seconds) may efficiently be used.

Finally, a surface temperature dependent convective heat transfer coefficient was used as a non-linear boundary condition. FILM subroutine, which runs for all integration points of all elements with convective heat transfer boundary condition, was used for this purpose.

Verification of the Model

The model was verified on infinitely long cylinders by repeating the studies of Gür [263], Yu [304, 305] and Schröder [307]. Then, solid (1D-2D), hollow (1D-2D) and eccentrically drilled (3D) cylinders were used for parametric study. For 3D simulations, cylinders with different hole-diameter and different degree of eccentricity as illustrated on Table 7.1 were used.

Verification of prediction of transient temperature field was performed first since it is vital for accurate prediction of thermal stresses. Without the accurate prediction of thermal field, prediction of stress field will not be accurate even though all the procedures and mechanical data are accurate. Verification of is carried out by re-performing numerical experiments carried out by Yu and Gür with the same material and process data ,on infinitely long St50 steel cylinders quenched from 600^{o}C into water at 0^{o}C. Comparison of cooling curves for surface and core of the specimen are presented on Figure 8.1. It is clear that the results obtained in this study are in agreement with previous results especially in determination of cooling history of the core. The discrepancies may be due to different time walk schemes used and implementation of the finite element codes. However, the results obtained in this study for the surface are probably the most realistic results due to very small time steps used at the critical initial stage of quenching. This also explains the good agreement of the cooling history of the core, even though totally different time walk schemes and FE implementations were used.

Secondly, verification of the predicted stress field was performed on the same specimens. Figure 8.2 presents the distribution of the axial, radial and tangential residual stresses as a function of the normalized distance from the core. From this figure, it can be observed that the all of the components of the residual stresses predicted by different models are quite close to each other. The minor discrepancies may especially be due to discrepancies associated with the prediction of transient thermal field, which is discussed in the previous paragraph. The effect of FE code and adaptive time stepping on mechanical calculations may be the other sources of discrepancies.Finally, the results was justified experimentally using simulation and neutron diffraction measurements by Schröder for Ck45 steel quenched from 680^{o}C into oil at 20^{o}C. Also numerical simulation results obtained by Schröder and Gür are presented on Figure 8.3. It can be seen that the results are in excellent agreement with simulation results and very good agreement with experimental measurements. To sum up, it can be concluded that the model and the simulation scheme used in this study is consistent both with other numerical simulations and experimental results.

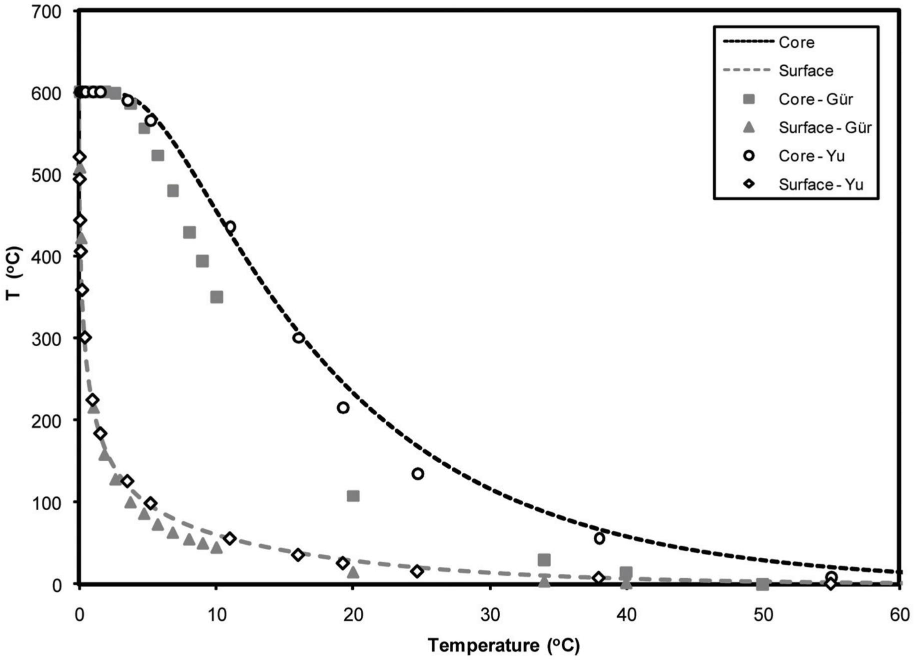

Figure 8.1 Cooling curves for the surface and the core of infinitely long St50 Steel cylinders (Φ = 50 mm) quenched from 600°C in to water at 0°C

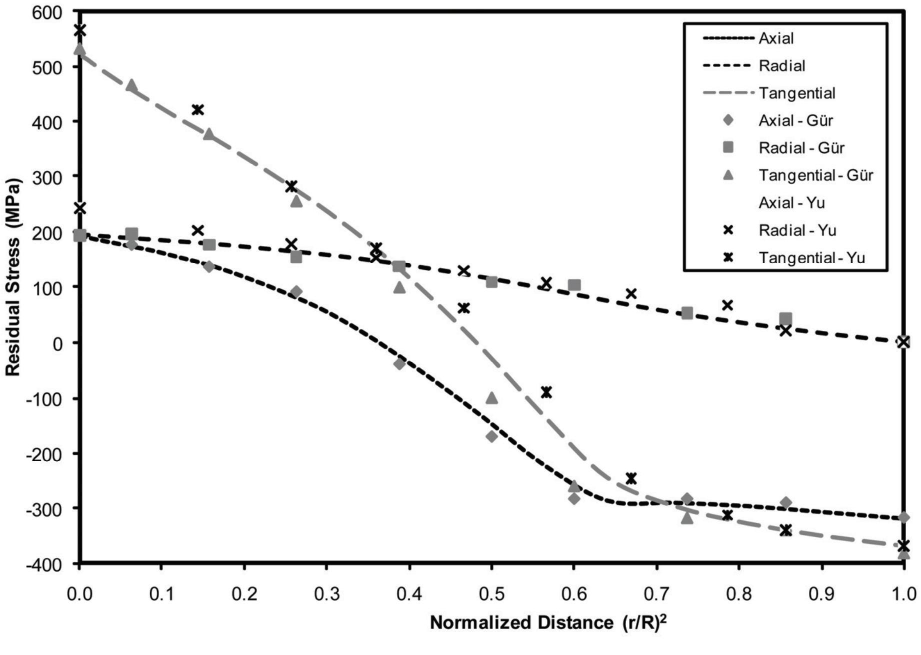

Figure 8.2 Comparison of residual stress distribution along the radius of infinitely long St50 steel cylinders (Φ = 50 mm) quenched from 600°C into water at 0°C

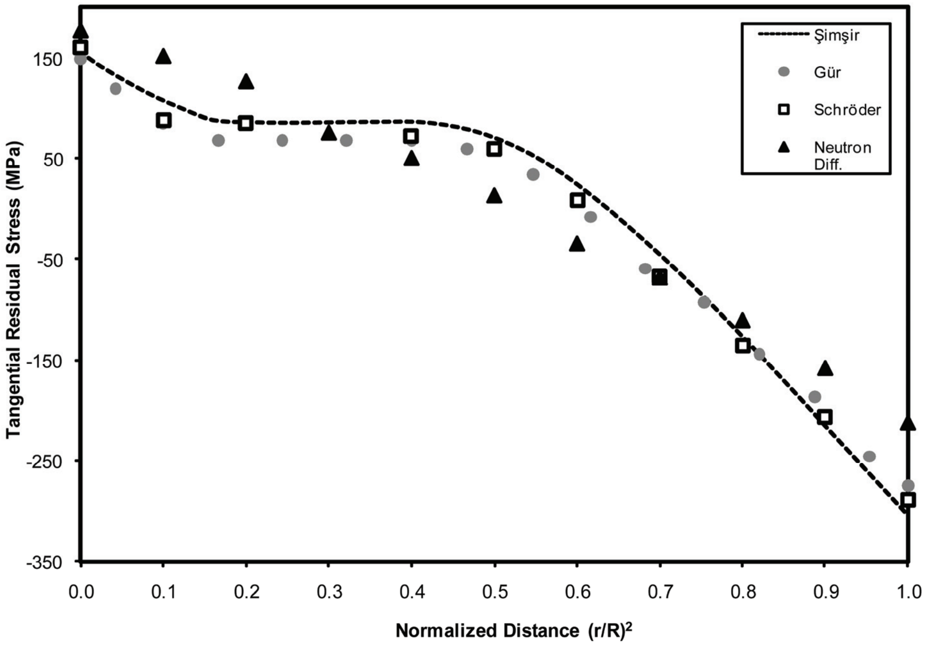

Figure 8.3 Comparison of tangential residual stress distribution along the radius of infinitely long Ck45 steel cylinders (Φ = 30 mm) quenched from 680°C into oil at 20°C.

Effect of Constant and Variable Convective Heat Transfer Coefficient

Convective heat transfer to the quenchant may be the most mind-boggling heat transfer mechanism during immersion quenching. In immersion quenching process, the surface heat transfer conditions between the steel part and the quenchant are the most important factors controlling the microstructural evolution, generation of internal stresses and distortion. The problem arise from very marked variation of the surface heat transfer coefficient during quenching and its sensitivity to small variations in the conditions of the quench bath and the state of the surface of the specimen. In order to deal with these variations, thermophysical and thermochemical events occurring on the component-quenchant interface must be understood.

As the component is immersed into the quenchant, the initial temperature of the component is generally well above the boiling point of the quenchant. Then , successive stages of heat transfer characterize the cooling process: vapor blanket stage, nucleate boiling and convective stage each associated with a distinct cooling regime [158] . There also exists a highly transient initial liquid contact stage. Those critical stages and associated changes in heat flux and heat transfer coefficient are illustrated on Figure 2.1.

An indirect way to deal with Leidenfrost effect in numerical simulations is to use a temperature dependant heat transfer coefficient. In reality, surface heat transfer problem is far more complex while using a liquid quenchant. For complex geometries, heat transfer coefficient should also be a function position and time. From the material point of view, concepts of blanket formation, nucleation of bubbles is also a function of dihedral angle and the surface condition of the specimen. For more accurate results, time consuming multi-phase CFD simulations coupled with quenching models should be carried out. Moreover, this is not currently possible due to lack of quantitative theories on the determination of the onset of critical stages of quenching On the other hand; use of a temperature dependant heat transfer coefficient is an efficient way to fix this problem for fairly simple geometries. Figure 7.2 illustrates temperature dependant convective heat transfer coefficient and corresponding surface heat fluxes used in this study. In order to incorporate this effect, user subroutine FILM is used in MSC.Marc® to impose a nonlinear boundary condition.

Numerical simulation results for infinitely long C60 steel cylinder quenched from 720°C into water at 20°C, with constant (average) and temperature dependant heat transfer coefficients are presented on Figure 8.4. It is observed that both axial and tangential components of residual stress are underestimated on the surface and the core. This effect should be much more evident in 2D and 3D simulations in which there is a variation of heat transfer coefficient on the entire surface. It can be concluded that usage of an average value of heat transfer coefficient leads large errors in residual stress prediction, even in fairly simple geometries.

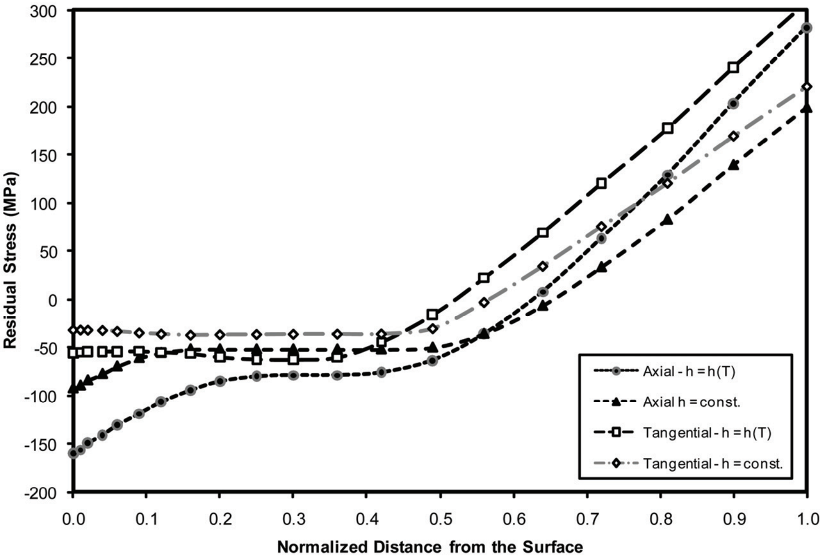

Figure 8.4 Distribution of axial and tangential residual stresses using constant and variable heat transfer coefficients for C60 steel cylinders (Φ = 30 mm) quenched from 720°C into water at 20°C and 60°C

Effect of Quench Bath Temperature

An easy method of optimizing the quenching process is selecting a suitable temperature for quench bath. Usually selecting a higher quench bath temperature decreases both the temperature dependant heat transfer coefficient and also the thermal gradient at the surface, resulting in slower cooling rates. Slower cooling rates allow obtaining of more uniform residual stresses by allowing the conduction to produce smoother thermal gradients throughout quenched specimen.

The effect of quench bath temperature was illustrated by numerical simulations in Figure 8.5 on which the residual stress distribution for C60 steel cylinders quenched from 720^{o}C into water at 20^{o}C and 60^{o}C was presented. It can be seen that both the magnitude and the variation of axial, radial and tangential components are decreased along the radius when a higher temperature is selected for quench bath. This eventually leads to a decrease in effective stress distribution.

On the other hand, modification of quench bath temperate for a quenching process without phase transformations has little practical significance. If the cracking and distortion is not a problem, using a lower temperature quenchant is even better since it generates larger compressive stresses on the surface.

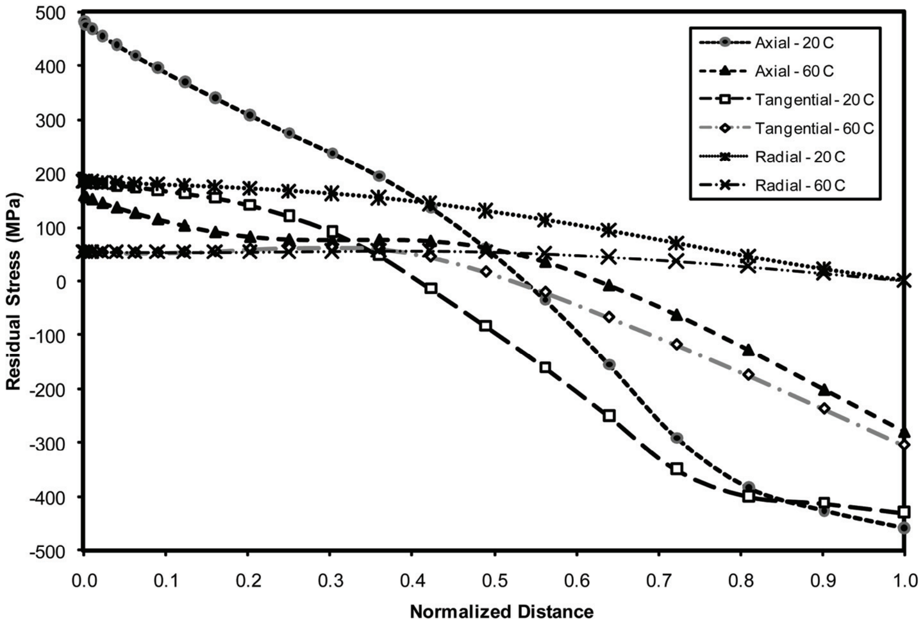

Figure 8.5 Variation of axial, tangential and radial residual stresses for an infinitely long C60 steel cylinders (Φ = 30 mm) quenched from 720^{o}C into water at 20^{o}C and 60^{o}C

Evolution of Internal Stress Field

During quenching without phase transformations, a fluctuating internal stress field is developed inside the component due to temperature gradients and variation thermal contractions and thermomechanical properties as a function of time and position. The magnitude of this stress field is dependent on the severity of the spatial variation of thermomechanical properties with time.

Figure 8.6 demonstrates axial and tangential components of internal stress field at different times during quenching. According to this figure, 3 distinct stages of quenching can be defined as follows:

Stage 1: At the beginning of the quenching, surface of the component cools and hence contracts faster than the core of the component (t=1 s). As a result of the compatibility constraint, an eigenstress field is generated inside the component. Surface is loaded on tension in axial and tangential direction to oppose the contraction of the surface, whereas the core is loaded on compression to balance this situation.

Stage 2: As the quenching proceeds (t=10s), the thermal gradients tend to become smoother on the surface and the temperature difference between the surface and core starts to vanish. As a result, the surface starts to unload and this leads to a decrease in axial and tangential components of the internal stress field. Similarly, the magnitude of compressive stresses on radial direction also starts to decrease. In order to equilibrate surface, the core starts to unload from compression, but at a slower rate which depends on the diameter of the specimen. The rate of unloading of the core is inversely proportional to the diameter of the specimen.

Stage 3: At later stages of quenching (t=30 s), the regions close to the surface is almost cooled down to quenchant temperature. On the other hand, the core still cools down and experience significantly high thermal contractions with respect to the core. Consequently, the core, which has started to unload in Stage 2, starts to load in the reverse direction. Then, the surface equilibrates this stress state by unloading and loading into compression. This results in a compressive stress state in axial and tangential directions on the surface and the core responds by getting into tension, radial component of the stress state is tensile type.

At the end of quenching.(t=120), when the thermal equilibrium is almost reached, the surface is on compression in regards to axial and tangential components. The core is on tension accordingly. Radial component of stress state is on tension on the core, whereas, it is tensile type on the surface. When all the thermal gradients are eliminated, equilibrium is reached both thermally and mechanically. Final stress state of the component remains as the residual stress state of the component.

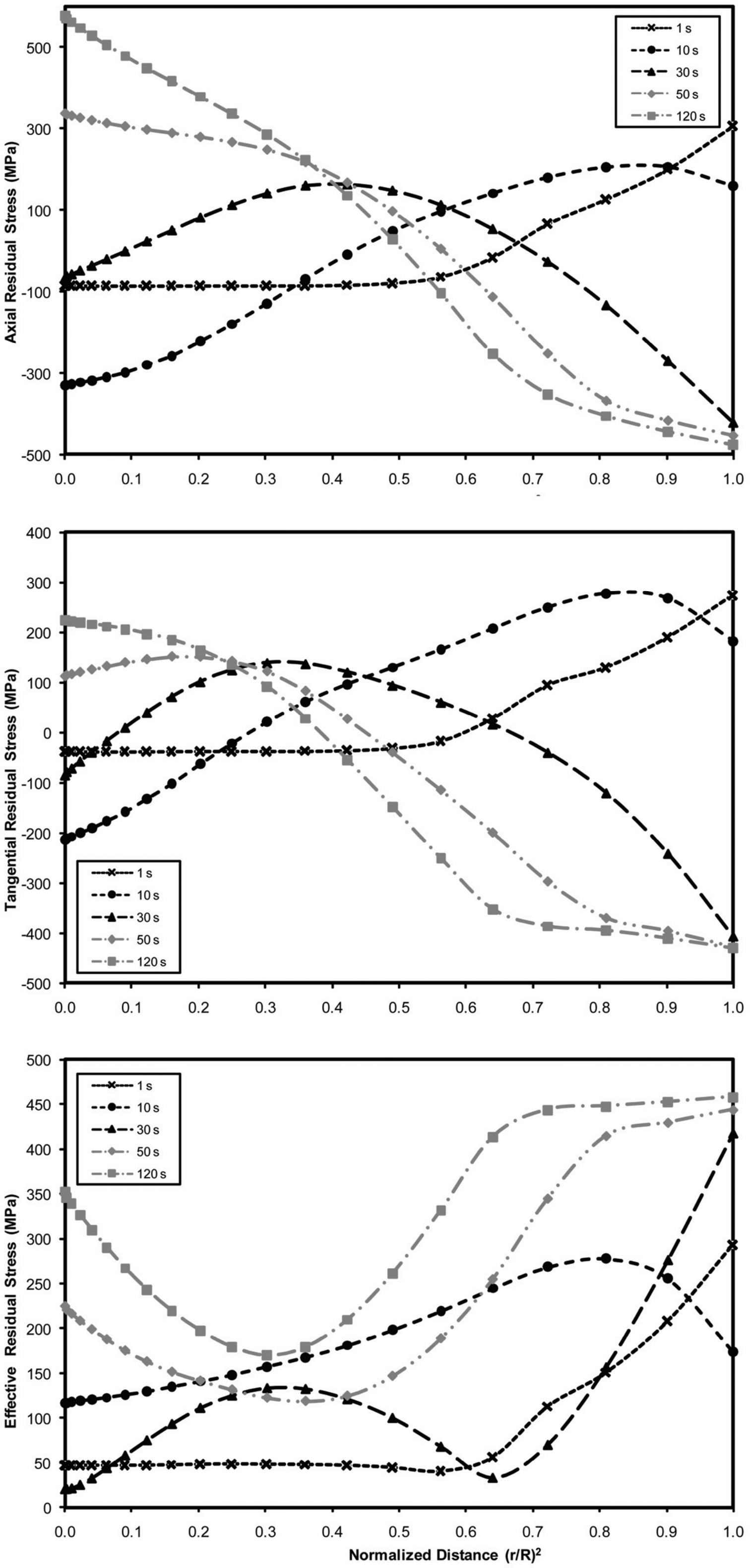

Figure 8.6 Comparison of residual stress distribution along the radius of infinitely long Ck45 steel cylinders (Φ = 30 mm) quenched from 680°C into water at 20°C.

Effect of Cylinder Diameter

Component geometry and dimensions have strong influence on evolution of internal stresses and microstructure, which also result in an impact at final distribution of the microstructure and residual stresses. Although specimen geometry is usually not a design criterion and it is usually possible to perform only minor modifications in the geometry, it should be considered with the material selection and heat treatment procedure.

Even during quenching without phase transformations, residual stress state and distortion behavior is highly affected from specimen geometry and dimensions. In this specific case, the main effect of the geometry is on the solution of the thermal field which affects internal stress evolution and hence residual stress state. Therefore, the problem of residual stress development should be considered coupled with the heat transfer problem.

In order to establish a common relationship, the effect of component dimensions was investigated in the simple case of quenching of infinitely long cylinders for which the only dimension is the diameter. Figure 8.7 illustrates the distribution of components of residual stress state for C60 steel cylinders with various diameters (Φ=15 mm, 30 mm, 60 mm) quenched from 720^{o}C into water at 20^{o}C. It is seen that residual stress distribution is highly affected by changes in diameter and the magnitude of the maximum tensile stress at the core of the cylinder is a monotonously increasing function of the diameter of the specimen. It may also be observed that the effect of increasing diameter is decreasing while moving away from the core to the surface. As a consequence of the increase in the stresses induced at the core, the stress state on the surface becomes less compressive.

This can be explained by the retardation of the cooling of the specimen resulting in higher differences in cooling rates of the surface and the core. Naturally, large thermal gradients induce large gradients in thermal strains which should be balanced by a larger eigenstress state, which results in a residual stress distribution with a larger amplitude. As a rule of thumb, it can be suggested that the higher the difference between the temperature of the core and the surface is, the higher the resulting internal stresses are during quenching without phase transformations.

If the effect of the diameter, heat conduction and quenching conditions are considered, a more general rule may be setup. It can be seen that the amplitude of the resulting residual stress distribution is proportional to the Biot number defined as:

$$Bi = \frac{\bar{h}D}{\bar{\alpha}} \tag{8.1}$$

where $\bar{h}$ and $\bar{\alpha}$ are mean heat transfer coefficient and conductivity.

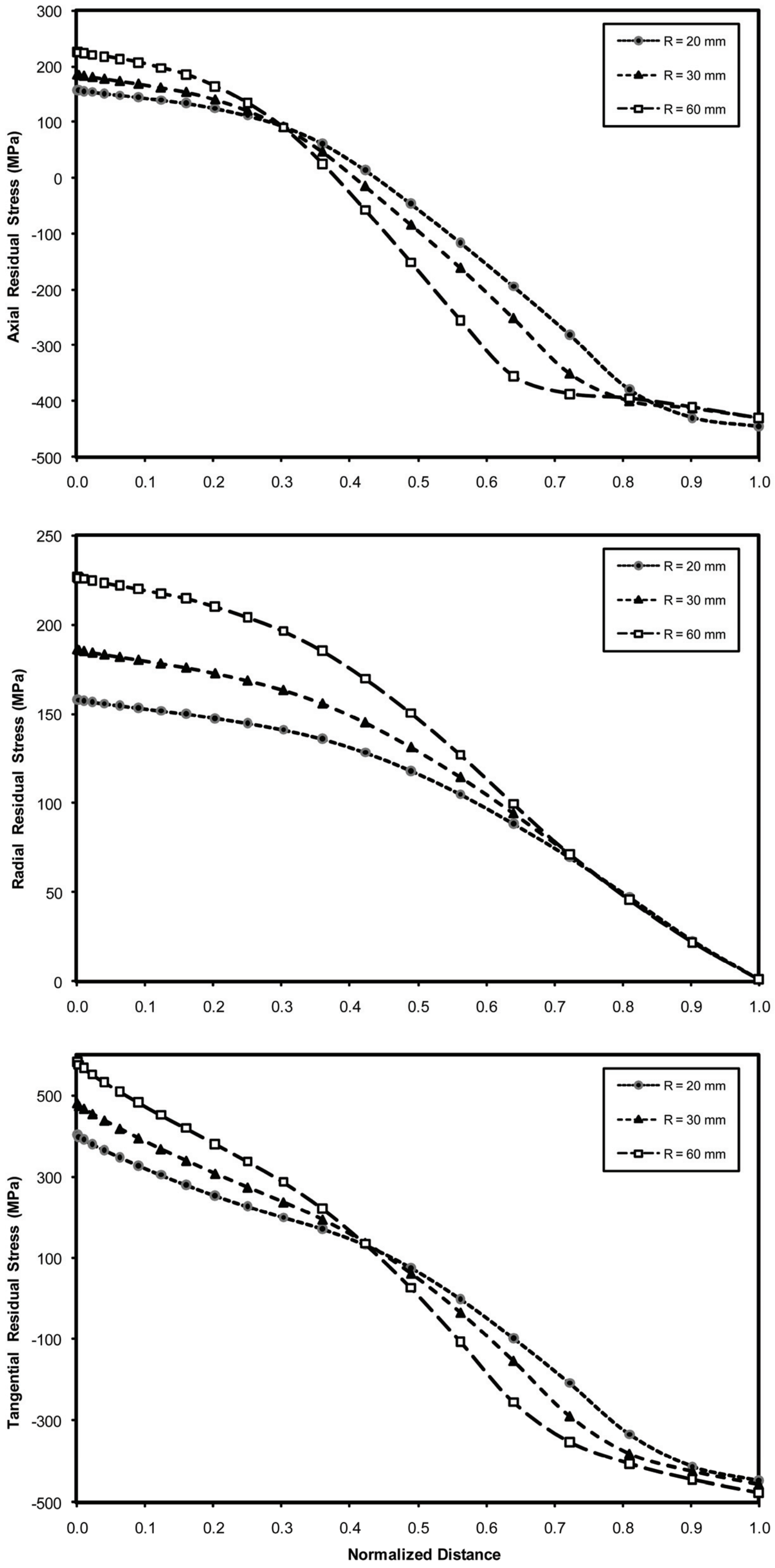

Figure 8.7 Distribution of axial, radial and tangential residual stresses for C60 steel cylinders (Φ=15 mm, 30 mm, 60 mm) quenched from 720^{o}C into water at 20^{o}C.

8.2.2 QUENCHING OF CYLINDERS WITH FINITE HEIGHT (2D)

Many engineering components that are quench-hardened such as shafts, transmission rods etc. have axisymmetric geometries with finite heights. This section allows investigation of problems which are better representations of the real world. The main difference of the 2D problem lies in the geometry and boundary conditions. For a cylinder of finite height, there exist axial displacement and heat conduction and additional heat loss at the end of the cylinder. This “side cooling” effect makes the problem more geometry dependant both in terms of heat transfer and internal stress evolution.

Effect of Cylinder Height

Heat transfer coefficients for different 2D geometries such as cylinders and plates are fundamentally different and they should be measured on the actual quenching system. In many cases, the heat transfer coefficient at side surface and top/bottom surfaces of the cylinders are also significantly different due to complex thermophysical events and fluid flow. However, those are taken the same function of temperature in this study for the sake of simplicity.

On the other hand, infinitely long cylinder assumption may also be a very good assumption for cylindrical rods having H/D ratio larger than a critical value, which is found as 3 for the case investigated in the next section. But, it should be noted that this critical H/D ratio is not a rule of thumb and is only valid for the investigated set of material and process parameters. Actually, critical H/D ratio is a function of thermomechanical properties and heat transfer coefficient. And it has been observed that the thermal conductivity and the heat transfer coefficient have more pronounced effect then the mechanical properties.

The effect of side cooling is twofold both affecting the internal stress evolution and residual stress state. Figure 8.8 and 8.9 illustrate contour plots for axial and tangential components of C60 steel cylinders (H=15mm, 30mm, 60mm, Φ=30 mm) quenched from 720^{o}C into water at 20^{o}C at different times (t=1s, 10s, 100s). From this figure, it can observed that side cooling has a strong effect for cylinders with H/D < 1 and its effect is decreased as the H/D ratio increases. Moreover, it can be noticed that the effect of side cooling is more pronounced at the earlier stages of quenching during which large temperature gradients are present.

Figure 8.10 illustrates the distribution of axial, radial and tangential residual stresses along the normalized distance from the core for the same set of specimens with an addition of infinitely long cylinder. It can be seen that cylinders with H/D<1 exhibit a completely distinct behavior, whereas, cylinders with increasing H/D ratios behaves closer to the infinitely long cylinder. This behavior is owed to decreasing effect of side cooling as the H/D ratio increases.

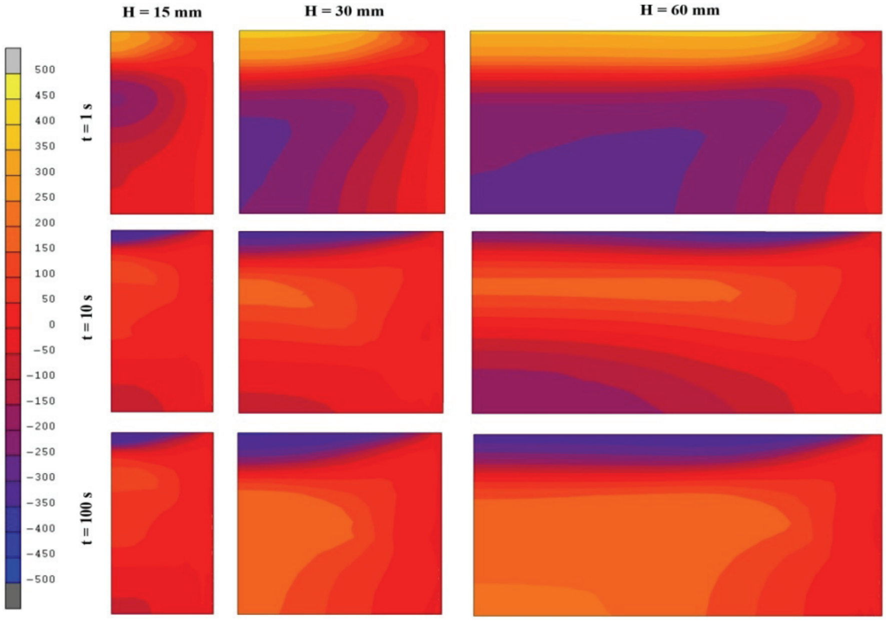

Figure 8.8 Variation of axial stress for C60 steel cylinders (H=20mm, 30mm, 60mm, Φ=30 mm) quenched from 720°C into water at 20°C at different times (t=1s, 10s, 100s).

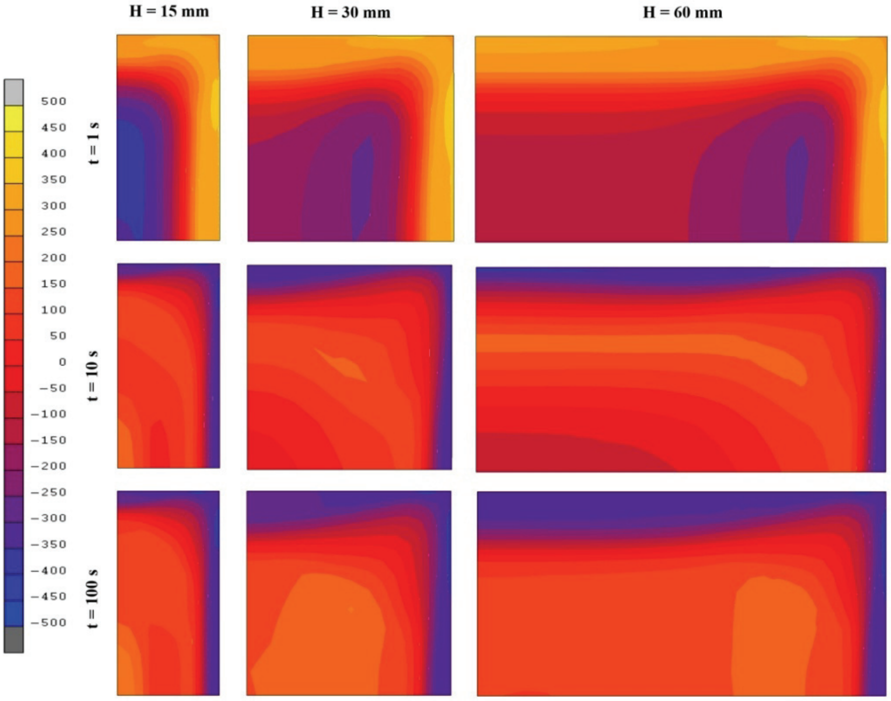

Figure 8.9 Variation of tangential stress for C60 steel cylinders (H=15 mm, 30 mm, 60 mm, Φ=30 mm) quenched from 720°C into water at 20°C at different times (t=1s,10s,100s).

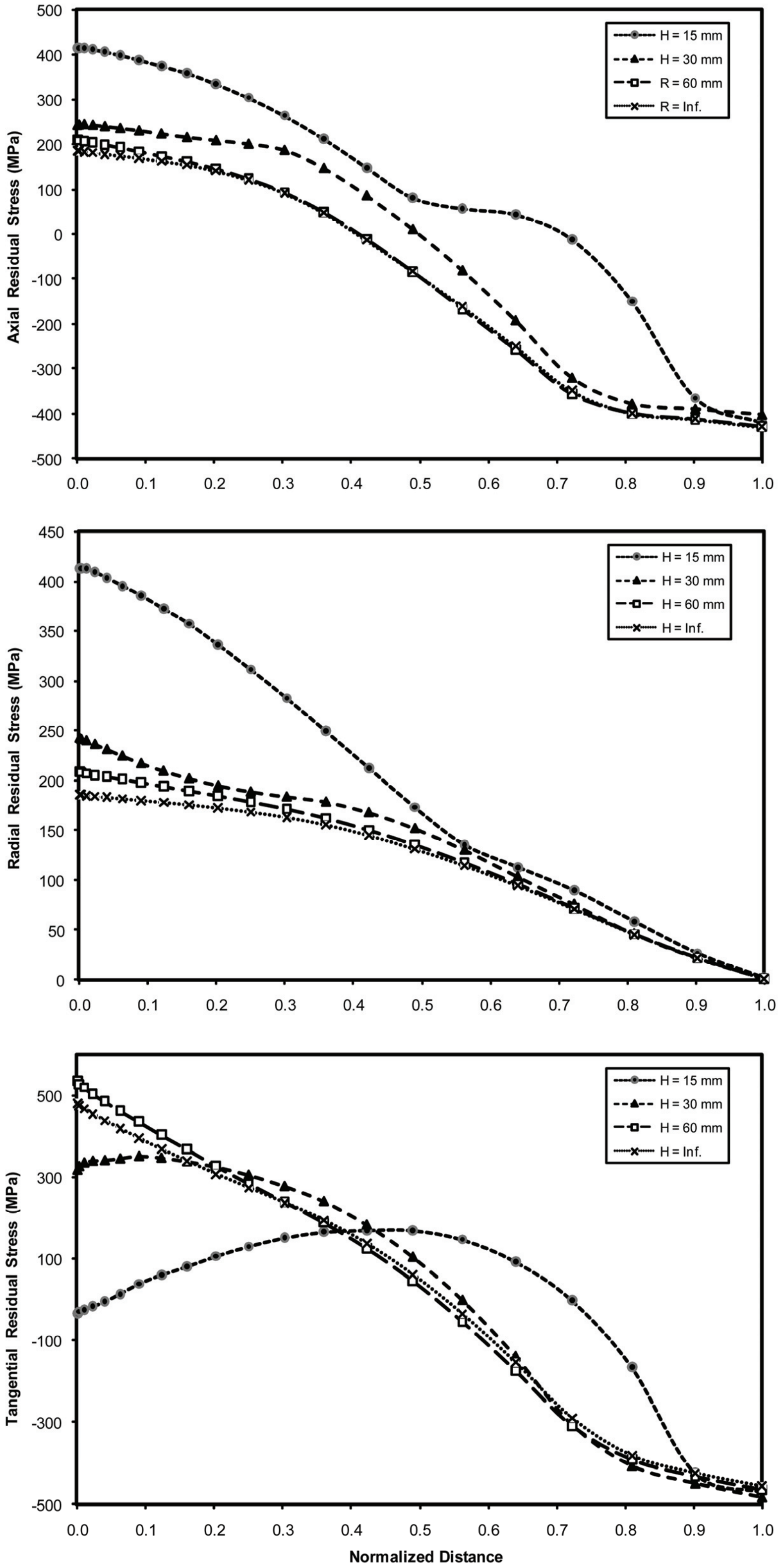

Figure 8.10 Variation residual stress state along the radius for an C60 steel cylinders (H=15mm, 30mm, 60mm, Φ=30 mm) quenched from 720°C into water at 20°C

8.2.3 QUENCHING OF ECCENTRICALLY DRILLED CYLINDERS (3D)

Components with complex 3D asymmetric geometries are most problematic components for a heat treatment engineer. Distortion, cracking and uneven residual stress and microstructure distribution are common problems for quench hardened complex 3D shaped components. Although, development of residual stresses and distortion may usually be qualitatively described by simple rules, the behavior of such kind of components cannot be easily predicted even qualitatively. Geometrical complexity of a component for a heat treatment process is a function of asymmetry, number of sections and the ratio of the thinnest section to the overall dimension of the part. In many cases, the sole tool for prediction of distortion and residual stress development is numerical methods such as FEM.

Eccentrically drilled cylinders having finite height with varying eccentricity ratios (S2/S1) and hole diameters are used to evaluate 3D capabilities of the framework and to establish some common rules on the effect of hole diameter and eccentricity on distortion and residual stress development. Although, this geometry seems to be a fairly simple 3D geometry, it is surely not. According to the definition of the “complexity” given in the previous paragraph, this geometry is a quite complex geometry since it involves asymmetry and many different cross sections.

Total quantitative expression of the distortion and final residual stress distribution of a 3D component is a cumbersome process since it requires the use of charts of nodal displacements and 3 components of residual stress state through many cross-sections. It is also difficult to visualize those data in 3D space. For the purpose of brevity and comprehensibility, instead of full quantitative results of the analyses, qualitative results in the form of figures and contour maps will be presented in the next section. It should also be emphasized that both figures and contour maps are adjusted to the same scale to make comparison process easy.

Effect of Hole Diameter

Changes in the hole diameter at fixed eccentricity significantly affects final geometry and residual stress distribution. For investigation of this effect, two sets of specimens with the same eccentricity (2 and 4), but varying diameters (6mm -18 mm) were used. All the specimens made out of C60 steel were quenched from 720^{o}C into water at 20^{o}C.

Distortion was investigated on center plane along longitudinal direction for specimens with the same eccentricity by drawing initial and deformed states on the same figure (Figure 8.11). Dark lines represent initial shape, whereas, light grey lines are for distorted shape. Deformations are multiplied by a factor of 10 for all figures to make them more visible.

From Figure 8.11, it is hard to express the effect of hole diameter on distortion behaviour of quenched specimens by a simple rule of thumb. An obvious observation is the increase of contraction on both outer cylindrical surface and on the inner hole. However, relative contraction ratio (R_{final}- $R_{initial}$)/ $R_{initial}$ along both X and Y directions seems to be quite constant. Nevertheless, those ratios are not a full measure of distortion, complete shape of outer cylinder and inner hole must be known in order to describe the curvature change. Another observation is the non-uniform behavior of distortion of outer surface and inner hole along longitudinal (Z) direction. From 6 mm diameter to 15 mm, it was observed that both outer surface and inner hole was twisted on X-Y plane. This twisting behavior was not observed for specimens with holes of 18 mm diameter. However, this effect is fairly negligible with respect to distortion of drilled hole.

Residual stress state of outer surface and inner hole is important for further machining and fatigue life of such components. To determine the dominant stress state without presenting stress state on three global coordinate, the magnitude of the major principle stress is plotted on contour maps (Figure 8.12). For the specimens with eccentricity ratio 2, the outer surface is on compression whereas the inner hole is on tension. This is an expected behavior for quenching of hollow steel cylinders without phase transformation, as long as the hole diameter is too large. At first stage of quenching, outer surface cools very rapidly whereas the inner surface cools slowly. This leads to contraction of surface while the core is nearly unaffected. This phenomenon results in a tensile stress state on surface and a compressive state on inner hole. However, at later stages of quenching, the surface is already cooled down, whereas the core is still cooling. This leads in a reverse stress state, i.e., compression on the surface and tension on the hole.

When the eccentricity ratio is 4, the behavior describe above changes especially for the specimens with large diameters such as E4. In that case, existence of too thin sections causes extension of inner tension zone to the outer surface in some places, whereas, compressive zone on outer surface extends to left-hand side of the eccentrically drilled hole on some other places. Another observation that can be made is the extension of compressive zone on surface and tensile zone on the inner hole as the diameter increases from 6 mm to 12 mm (A3, B3 and C3). Then, this behavior is reversed while diameter increases from 12 mm to 18 mm (D3, E3) since some sections get too thin

To sum up, it is hard to establish a quite general rule since the coupling of temperature and strain fields on non-symmetric bodies is quite complex with both material, geometric and boundary condition non-linearity even without phase transformations. Complete computer simulations involving calculation and tracing of temperature and strain fields at each stage of quenching are currently the sole tools for prediction of distortion and residual stress distribution.

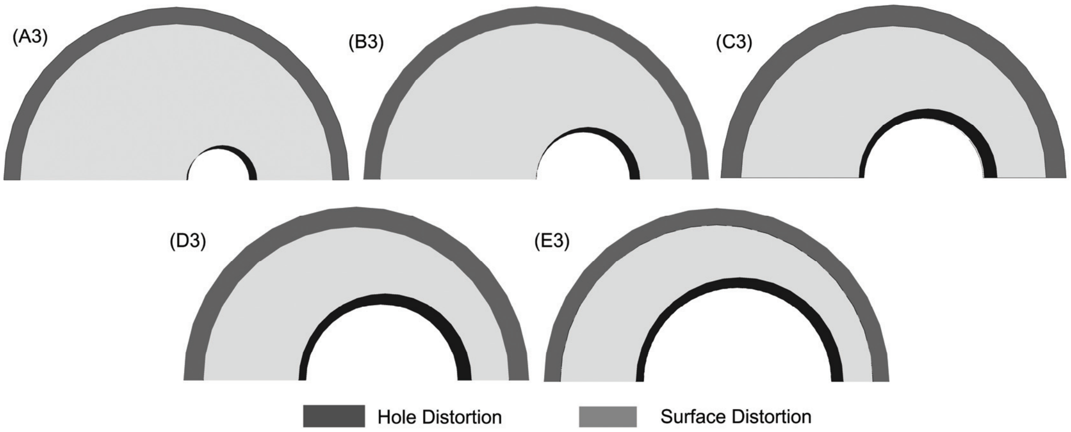

Figure 8.11 Initial and distorted geometries of central cross-sections of C60 steels quenched from 720ºC into water at 20ºC. (Eccentricity ratio = 2; deformations x 10)

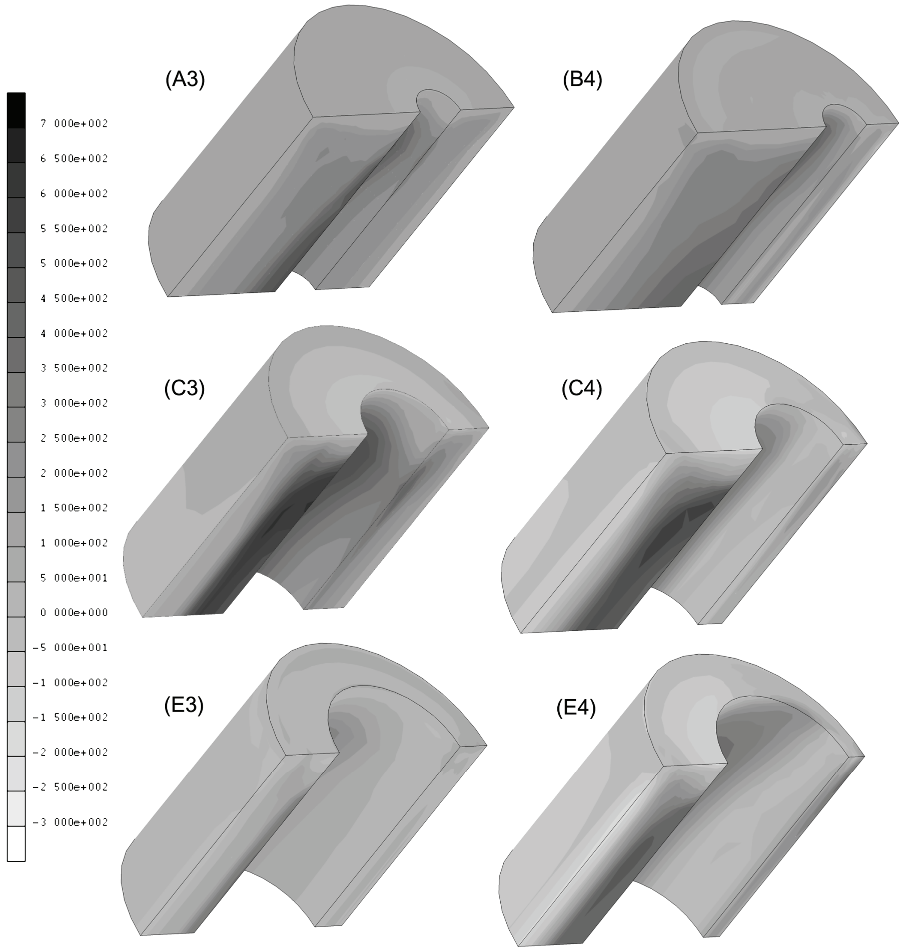

Figure 8.12 Residual stress distributions (major principle stress) for eccentrically drilled C60 steel cylinders (Eccentricity ratio = 2) quenched from 720^{o}C into water at 20^{o}C

Effect of Eccentricity

Although the effect of varying hole diameter at constant eccentricity on distortion is not too clear, the effect of eccentricity is easier to comprehend qualitatively. The definition of distortion involves both dimensional changes and more pronouncedly shape changes.. Asymmetric heat flow and variation of thermomechanical properties cause more asymmetric deformations for specimens with higher eccentricity ratio, as the eccentricity ratio defines the degree of deviation from symmetry. Asymmetric deformations will eventually result in shape changes which are more important with respect to the dimensional changes.

The effect of eccentricity on distortion is illustrated on Figure 8.13. From the figure, it can be observed that specimens with eccentricity ratio 4 are more distorted with respect to the ones with eccentricity ratio 2. It can also be seen that the distortion is more evident as the shape change of the inner hole. Moreover, it can be stated that distortion becomes more pronounced with larger hole diameters.

On the other hand, degree of eccentricity also affects the final stress distribution significantly (Figure 8.14). From this figure, it can seen that tensile zone on the right-hand side of inner hole was enlarged both in terms of magnitude and area as the eccentricity ratio increased from 2 to 4. Similarly, compressive zone on right-hand side of outer surface was enlarged in terms of both magnitude and area. Secondly, it is observed that compressive zone on left-hand side of outer surface and the tensile zone on left-hand side of inner hole start to interact for highly eccentric specimens with large inner diameters (E4). This results in some tensile zones on outer surfaces and some compressive zones on inner hole.

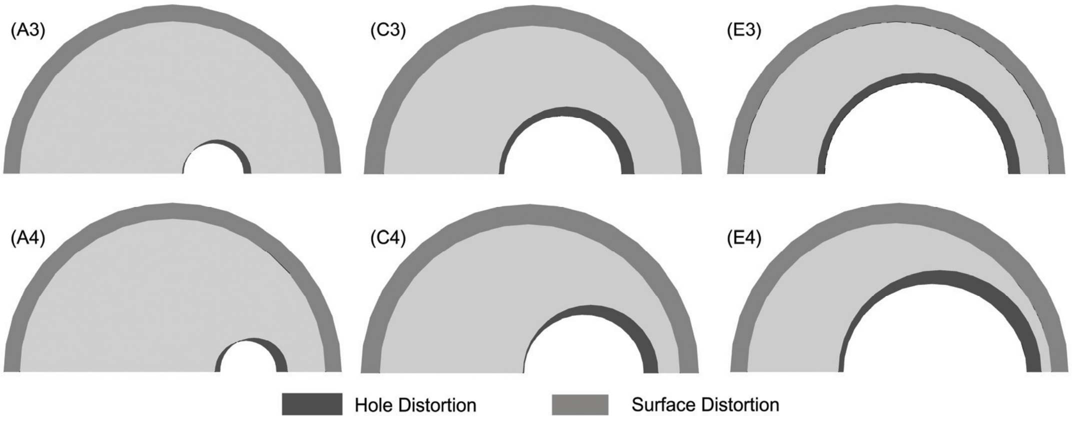

Figure 8.13 Initial and distorted geometries of central cross-sections of C60 steels quenched from 720°C into water at 20°C. (Eccentricity ratio = 2; Deformations x 10)

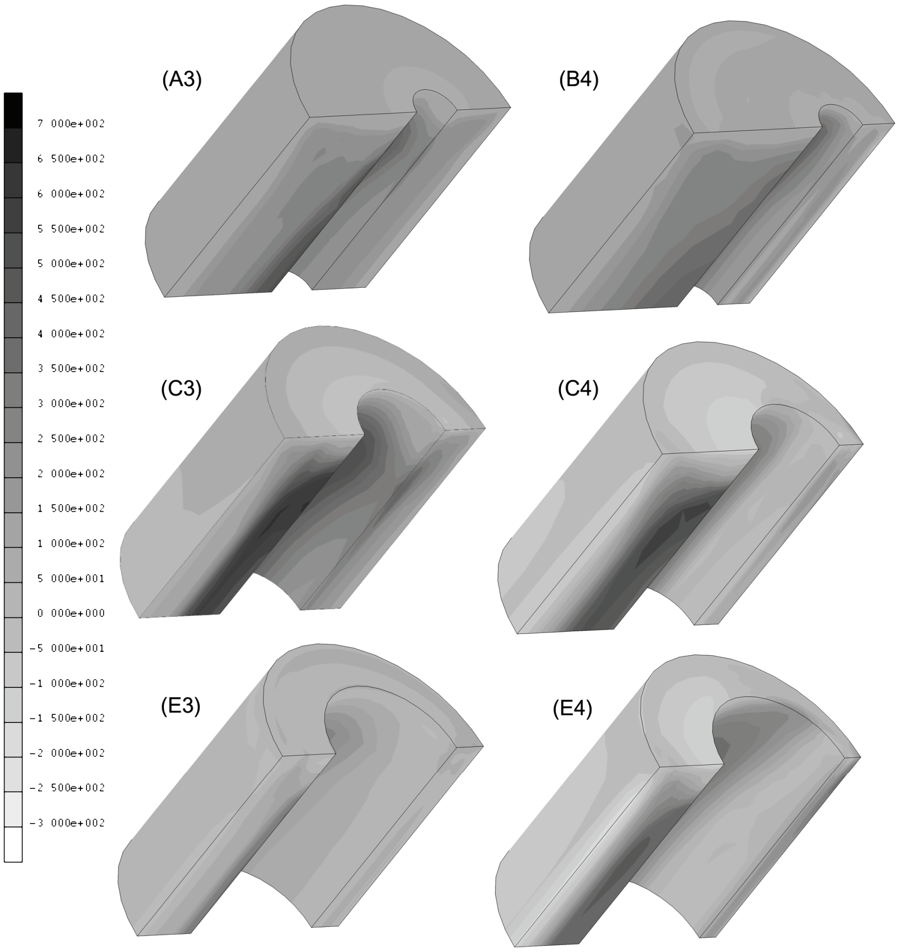

Figure 8.14 Residual stress distributions (major principle stress) for C60 steels quenched from 720°C into water at 20°C

8.3 QUENCHING WITH PHASE TRANSFORMATIONS

In the previous section, quenching simulations without the effects of phase transformations have been performed to understand the development of thermal stresses and to test the framework. However, most important industrial uses of quenching are in through-hardening, carburizing and induction hardening processes involving the introduction of hard martensite into the microstructure. Hence, almost all of the practical problems occurring during quenching are associated with quenching of components with phase transformations. For this purpose, a flexible framework capable of dealing with phase transformations and related couplings was developed and implemented into commercial FEA software according to the concepts discussed in Chapters 2-7. The framework is capable to simulate all the possible couplings but not all of them are used in each run in order to understand their significance. Certain couplings such as the effect of prior plasticity and stress on phase transformations were neglected due to instability of the proposed models and lack of material data.

First stage of verification of the framework has been performed on simulation of quenching of infinitely long cylinders and comparison of the results with numerical results by Gür [262]. For a meaningful comparison, same material/process data are and implemented couplings were used. Then, a parametric study has been performed using cylinders of finite height to investigate the effect of phase transformations, evolution of stress field, effect of quench bath temperature and effect of TRIP. Finally, experimental verification of the all of the quench hardening related capabilities of the framework was performed on quenching of eccentrically drilled cylinders. Experimental verification is based on SEM investigation and XRD residual stress measurements. In this case, all the possible couplings and improvements are invoked in the simulations to test the “real” capabilities of the framework.

8.3.1 QUENCHING OF INFINITELY LONG CYLINDERS (1D)

Verification of the developed model is performed by repeating numerical simulations carried out by Gür in which quenching of infinitely long C60 steel cylinders are quenched from 830^{o}C into water at 20^{o}C and 60^{o}C. Since the residual stress distribution is highly dependent on solution of thermal history and the phase evolution, firstly, the final distribution of the phases along the radius are compared. Figure 8.15 illustrates the distribution of martensite phase and axial/tangential components of the residual stresses along the normalized radius of the quenched C60 steel cylinder. Since both heat transfer model and the phase transformation kinetics model is used similar to Gür’s study, it is highly expected that final distribution of the martensite will be almost the same. Results show good agreement with this argument. Secondly, the distribution of residual stresses is verified on the same specimens. Again from Figure 8.15, it can be clearly seen that, both results are in good agreement with a maximum deviation of nearly +-50 MPa. Minor differences may be because of the numerical solution procedure, meshing etc.

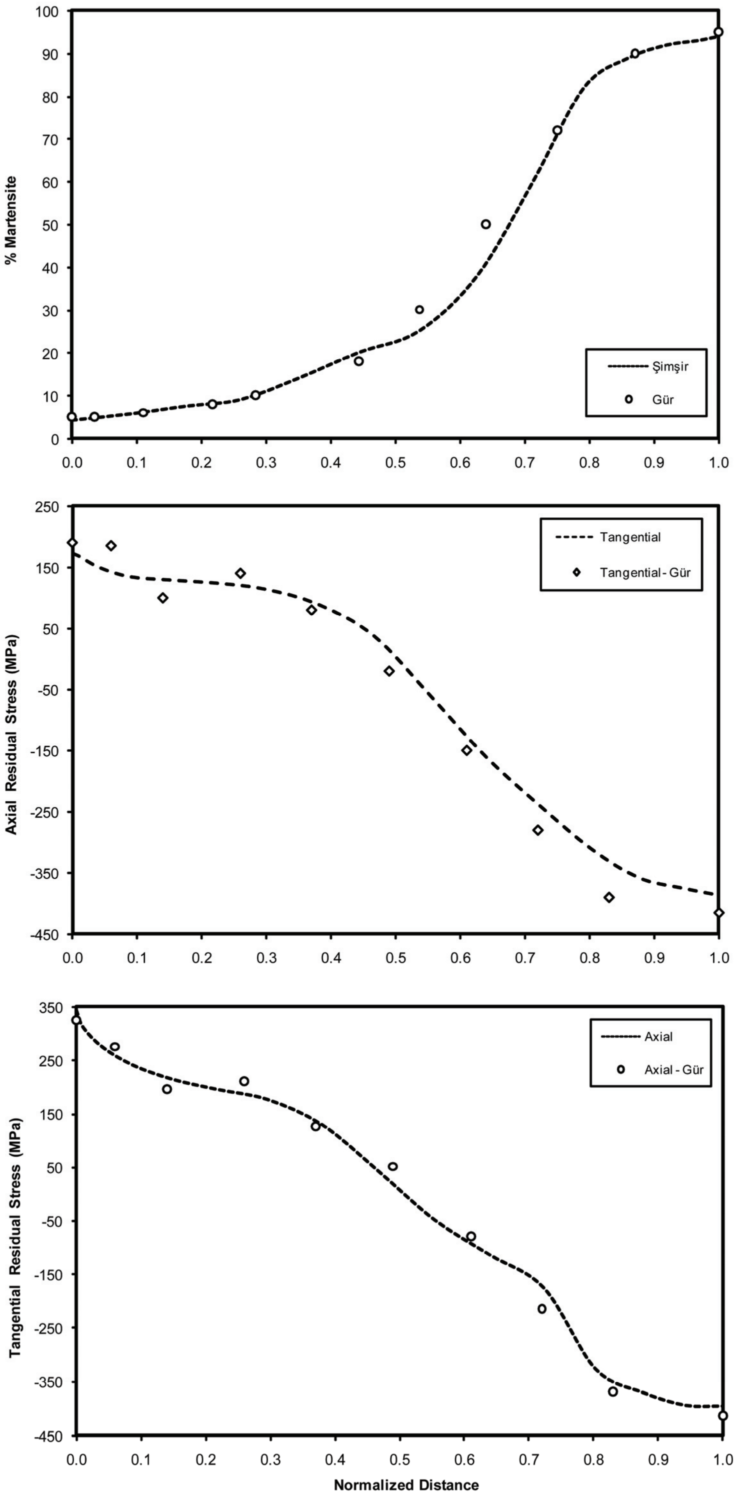

Figure 8.15 Variation of axial/tangential components of residual stress and %martensite along the radius for an infinitely long C60 steel cylinder (Φ = 30 mm) quenched from 830^{o}C into water at 20^{o}C

8.3.2 QUENCHING OF CYLINDERS WITH FINITE HEIGHT (2D)

Effect of Phase Transformations

Phase transformations that occur during quenching drastically alter all the involved physical fields. Thermal field is modified due to latent heat of transformation and continuously evolving thermal properties due to phase transformations. Mechanical field is the most affected field due to phase transformations. Both the phase transformation strains (dilatational and TRIP) and significant variation of mechanical properties due to transformations results in a completely different evolution scheme and residual stress distribution than quenching without phase transformations.

Figure 3.4 demonstrates the distribution of tangential residual stresses at the initial and the final stage of quenching for the cases with/without phase transformation. It is clear that the phase transformation effects have a strong impact and they even reverse the predicted stress state during whole course of quenching. For example, at the beginning of quenching, it is observed that stress state of the core and the surface are reversed in the cases of with/without phase transformation effects. This dramatic effect is mainly due to dilatational and TRIP strains due to phase transformations. Those stresses are usually larger than thermal contraction strains, which results in domination of the stress field by phase transformation stresses rather than thermal stresses. On the other hand, a steel cylinder quenched without phase transformation exhibits compressive axial and tangential residual stresses on the surface, whereas, a through hardened steel cylinder usually has tensile axial and tangential residual stresses.

In order to understand and predict the thermal and mechanical fields with concomitant transformations, it is necessary to model the evolution of microstructure as a function of thermal and mechanical paths followed. This requires the coupling of microstructural evolution with thermal and mechanical fields. In this study, the effect of anisothermal path is included in microstructural evolution calculations using JMAK kinetics and Scheil`s additivity principle. The effect of stress may also be coupled by modifying the critical temperatures and use of modified isothermal constants as a function of effective and mean stress. However, the effect of stress and prior plasticity on phase transformations is neglected due lack of accurate models and material data. Figure 8.17 and 8.18 illustrate sample results of this thermo-microstructrally coupled model, on which predicted distribution of temperature and microstructure at different times, for specimens A1 and C1 quenched from 830^{o}C into water at 20^{o}C are presented. It is clear that microstructural evolution is a function of current temperature, cooling rate and the thermal path followed. It may also be noticed that both thermal and microstructural evolution problem is highly dependent on the inner hole diameter.

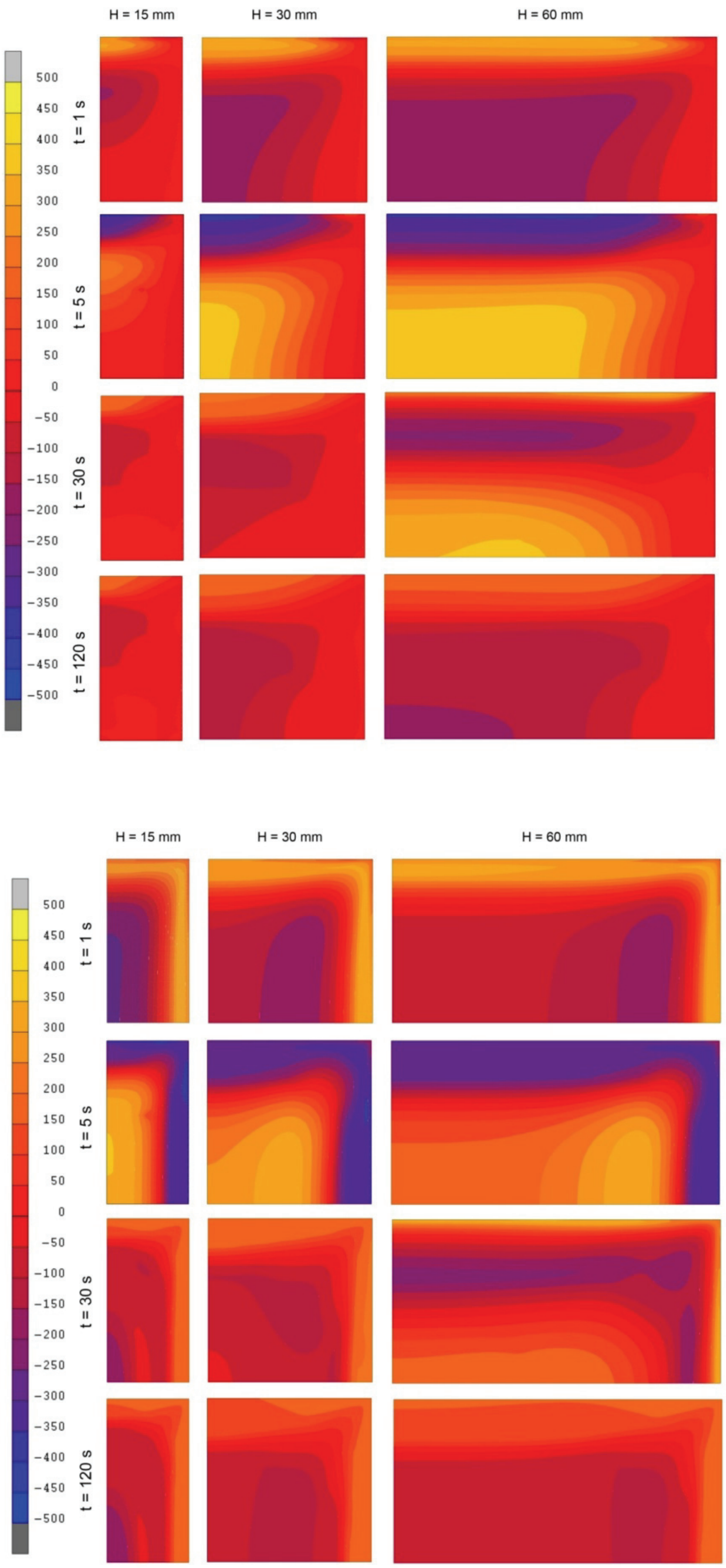

Figure 8.16 Distribution of a) axial., b) tangential component of stress for a C60 steel cylinder (Φ = 30 mm, H = 15mm, 30mm, 60mm) quenched from 830°C into water at 20°C.

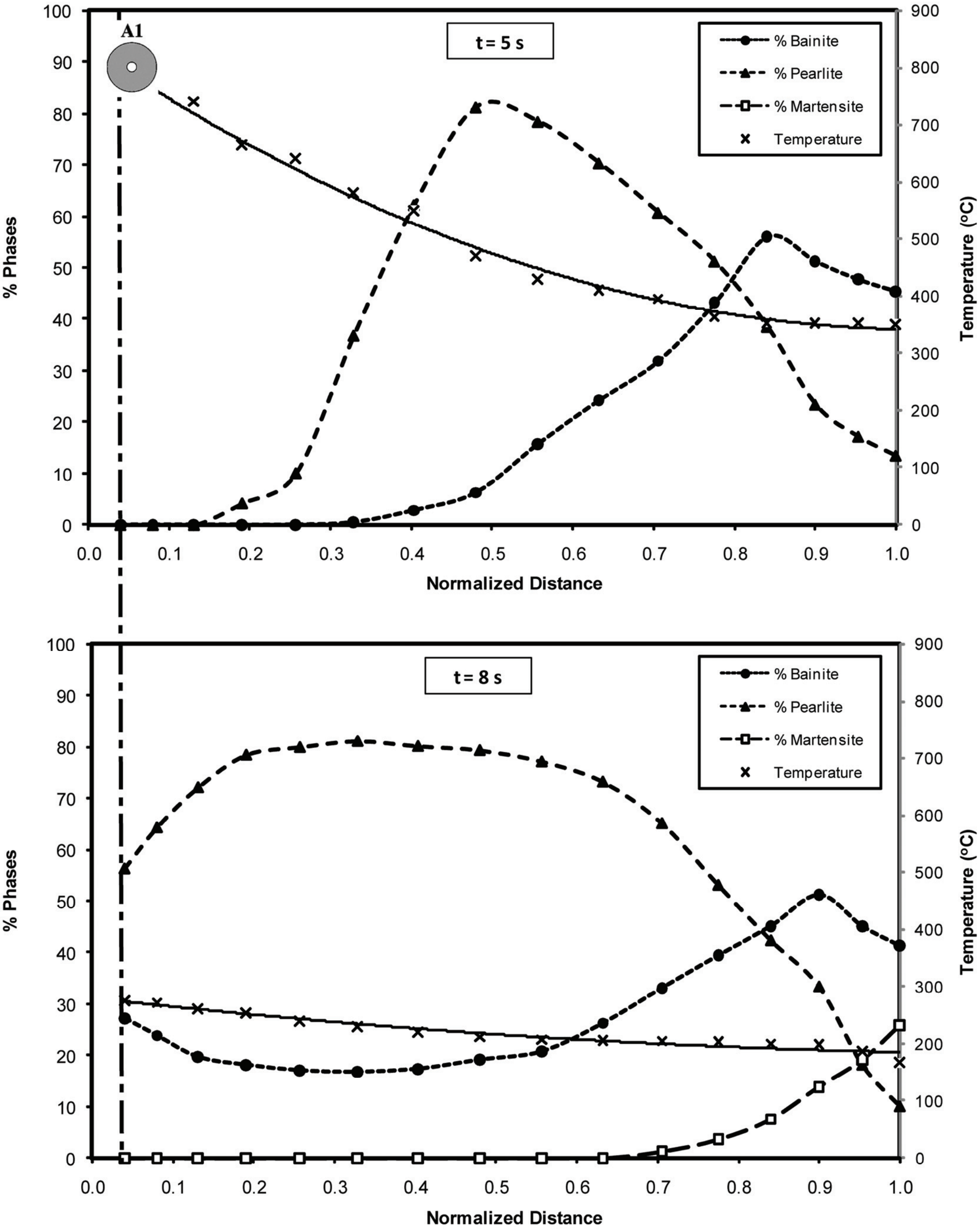

Figure 8.17 Variation of the microstructure and temperature as a function of time during quenching of specimen A1 from 830°C into water at 20°C.

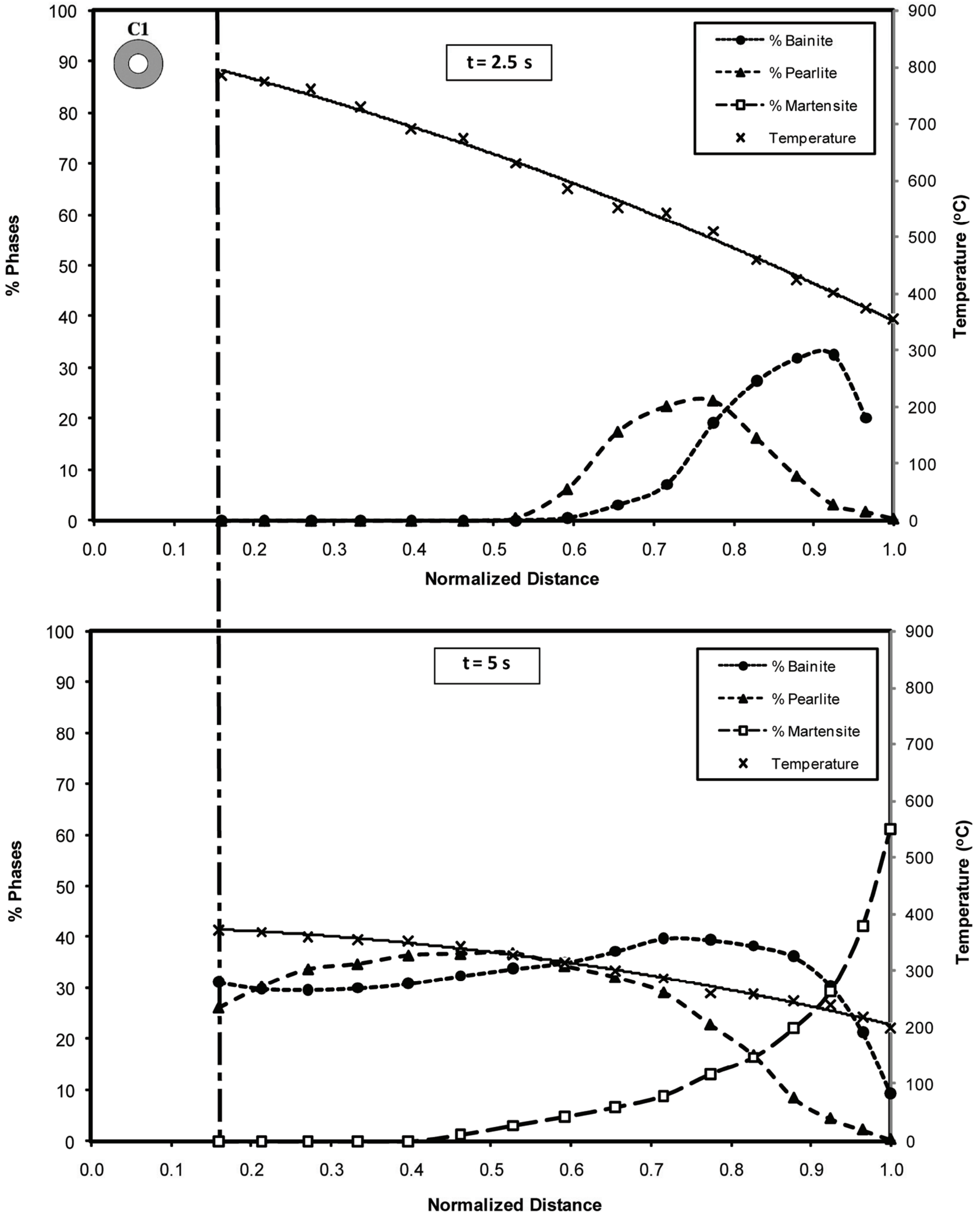

Figure 8.18 Variation of the microstructure and temperature as a function of time during quenching of C60 steel hollow cylinder from 830°C into water at 20°C

Evolution of Stress Field during Quenching with Phase Transformations

Internal stress evolution during quenching with phase transformations is fundamentally different from the one without phase transformation which was discussed in Section 8.2.1. The main reason for this occurrence is the domination of the stress field by phase transformation strains (dilatational and TRIP) over the thermal strains.

Figure 8.16 illustrates the distribution of axial and tangential stress during quenching of C60 steel cylinders with different heights. According to this figure, critical stages in quenching of can be summarized as follows:

Stage 1 : At the beginning of the quenching (t=1s), surface cools faster than the core, then, due to thermal contraction differences, as explained in previous section, tensile stresses are developed on the surface and compressive stresses on the core. This behavior occurs only for a short while during the cooling of austenite. However, thermal stresses developed in this stage are quite high and there might be considerable amount of plastic deformation in soft austenite phase. Figure 8.19 demonstrates this situation for cylinders having different heights. It is clearly seen that for all cylinders, the surface is in tension, the core is on compression. However, the magnitude of the stresses is dependent on the height of the cylinder.

Stage 2: At a slightly later stage (t=5 s), it is observed that the surface gets in compression and the core is responding by getting into tension state. This sharp change in the stress state is due to martensitic phase transformation. Once the surface reaches below M_s temperature, martensitic transformation starts. As mentioned earlier, such a transformation results in a volume increase. The transformed surface starts to expand while the core is still non-transformed and contacting while cooling down. This causes a fast shift on the surface and then the core by changing the sign of the residual stress field.

Stage 3 : At a later stage (t= 30 s) , the surface is almost totally transformed and is cooling down. But the core is still transforming. This causes a decrease in the magnitude of the stresses developed both in the core and the surface. Surface slowly gets in tension and core accordingly gets into compression.

Stage 4: At the end of quenching (t = 100 s), it is observed that the surface is in tension both axially and tangentially, whilst, the core is on compression due to swelling

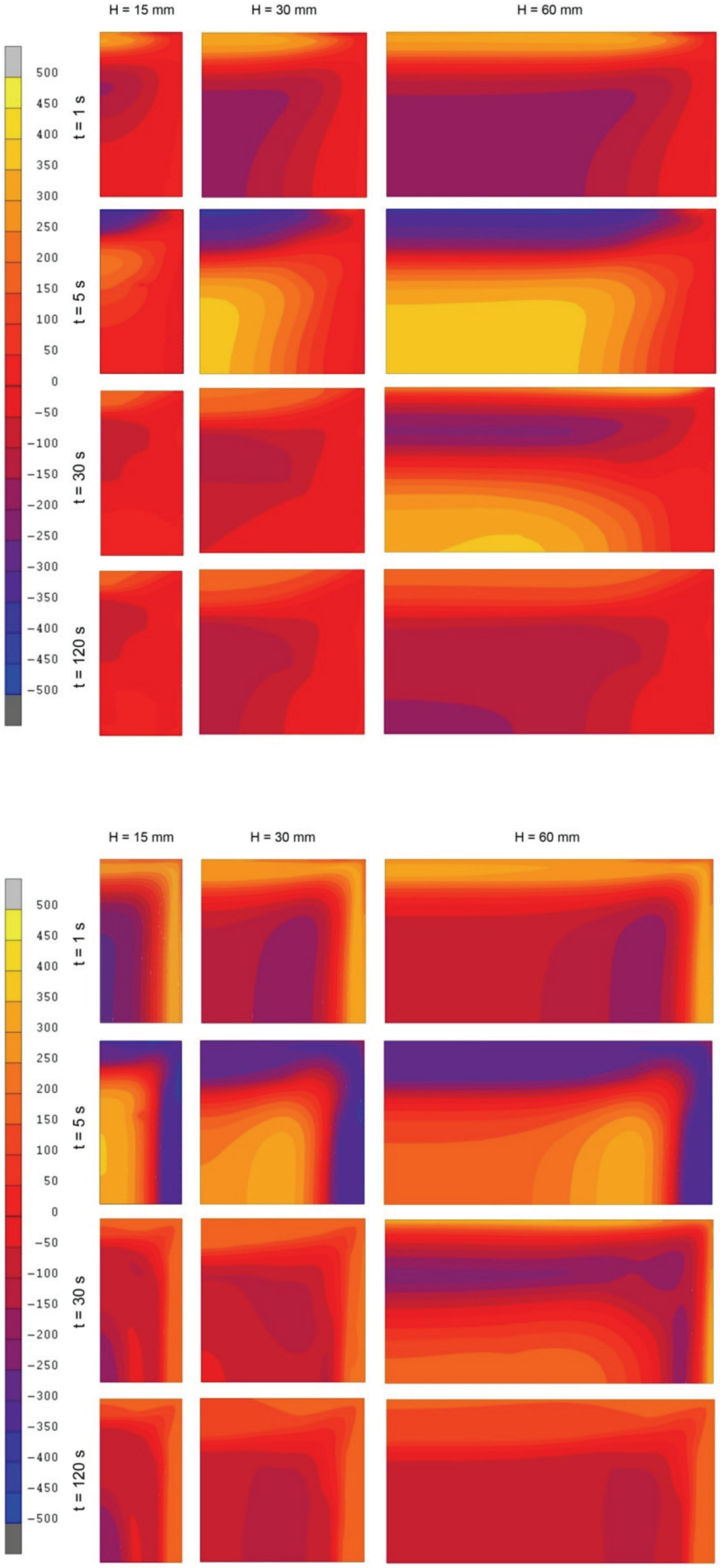

Figure 8.19 Distribution of a) axial., b) tangential component of stress for a C60 steel cylinder (Φ = 30 mm , H = 15mm, 30mm,60mm) quenched from 720°C into water at 20°C

Effect of Quench Bath Temperature

In many cases, the sole parameter that a heat treatment engineer can modify is the selection, agitation and the temperature of the quenchant, from which quench bath temperature is usually the easiest to modify and control. In many cases, it is reported that a higher quench bath temperature leads to more evenly distributed stress distribution with extrema having lower magnitude. This is generally owed to decreasing the difference between the cooling rates of the surface and the core due to lower cooling rates imposed on the surface, which allows the conduction to balance more effective the temperature distribution.

On the other hand, the explanation given in the previous paragraph is not always true, especially in the case of quenching of large specimens with phase transformations. Although milder cooling rates are highly effective in reducing the thermal stresses, they are not always effective against phase transformation stresses. This behavior is usually observed for large specimens for which the time difference between the surface and the core transformations is increased, which increase the effect of the swelling of the core, hence resulting in larger tensile stresses on the surface. For such cases, use of special step quenching techniques with very high cooling rates may decrease the surface residual stresses and may even produce slightly compressive stresses on the surface. Such techniques are usually nominated as “Intensive Quenching” techniques [92, 105, 117, 308, 309].

Another concept that has to be considered for prediction of the distribution of microstructure and residual stresses is the kinetics of wetting process. As stated in Section 2.1, the change from different cooling is not abrupt, it occurs by the motion of the wetting front. Type of the wetting process significantly affects cooling behavior of the quenchant. A Newtonian type of wetting usually promotes uniform heat transfer and minimizes the distortion and residual stress development. In the extreme cases of non-Newtonian wetting, because of large temperature differences, considerable variations in the microstructure, residual stresses are expected resulting in distortion and presence of soft spots.

Another constraint that limits the improvement of residual stresses and distortion even for components of small size is the achievement of required hardness distribution. This constraint becomes more pronounced for steels with low hardenability. Figure 8.20 illustrates such a case. As can be seen from the figure, the specimen quenched in water at 60^{o}C is mainly composed of pearlite and bainite and the maximum fraction of the martensite is almost 10% even at the surface. Although, this type of heat treatment reduces the residual stresses, it is against the principles of hardening since there is almost no hardness gain after the heat treatment.

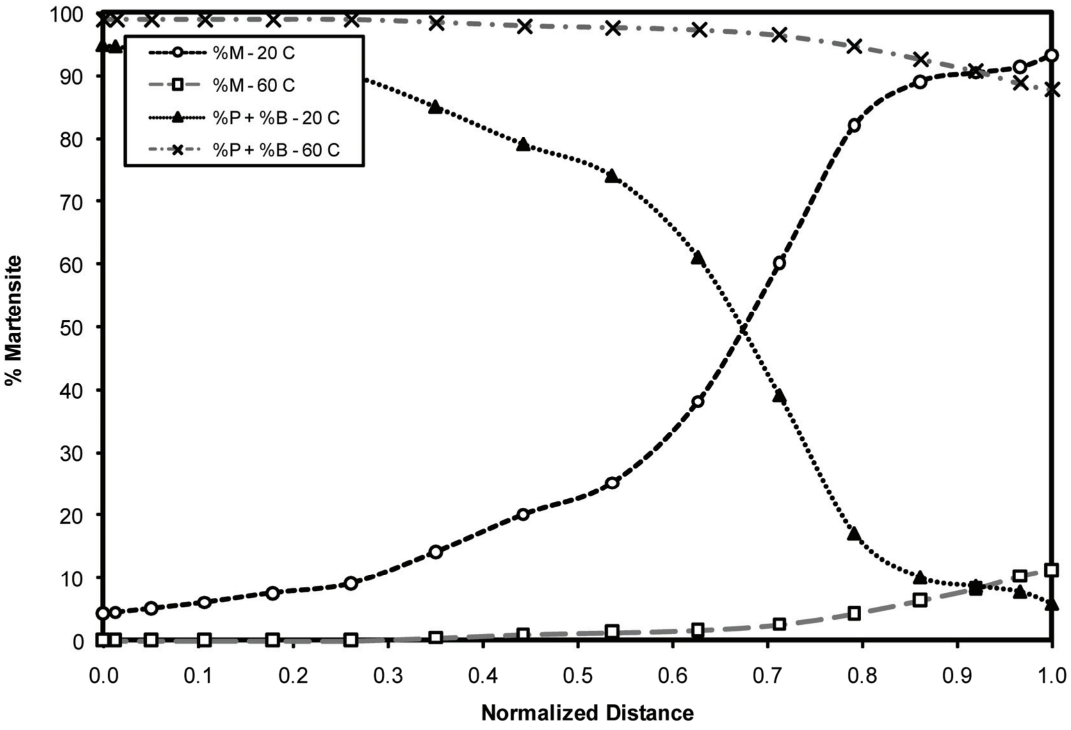

Figure 8.20 Variation of the distribution of the microstructure along the radius for C60 steel specimens (A0) quenched from 830°C into water at 20°C and 60°C.

Effect of Transformation Induced Plasticity on Stress Field Evolution

Figure 8.22 illustrates the variation of the tangential stress state on the surface and the core of a C60 steel cylinder quenched from 830°C in water at 20°C. Although several models for evaluation of TRIP constant (K) (Abrassart [23], Greenwood-Johnson [6], Leblond[24]) as discussed on Section 4.4.2, were used in calculation of TRIP strain, only the results with Leblond`s approach is presented in this section, since they only change the magnitude of the TRIP strain but don`t change the trends substantially. The largest TRIP strains were obtained with Greenwood-Johnson model and the lowest values were achieved with Abrassart`s model. The model of Leblond yields the results in between the extrema and it was observed that it produces the best agreement with experimental results given in Section 8.3.3.

TRIP has a strong influence on the evolution of internal stresses since the stress response of the component with TRIP is fundamentally different than the one without TRIP. In order to understand the underlying mechanism for this occurrence, the evolution of equivalent TRIP strain and classical plastic strain are also presented on the same figure. It is clear that TRIP strain has usually the same order of magnitude with classical plastic strain and in certain cases it is even larger than the classical plasticity strains. It is also observed that TRIP strain has a huge impact on the stress evolution on the surface at the early stages of quenching, whereas it has a considerable impact at core of the specimen at the later stages of quenching As the surface reaches, it unloads and reverse loads faster than the model without TRIP due to large TRIP strains associated with martensitic transformation. A similar behavior is also observed for the core as the core is below the martensite start temperature.

Considering the facts discussed in the previous paragraph, it can easily be predicted that residual stress distribution will be influenced due to the different mechanical histories associated with each case. Figure 8.21, which presents the distribution axial residual stress as a function of the normalized distance from the core, proves this simple prediction. It can be pointed out that the residual stress state on the core and the surface is influenced from TRIP and the effect of latter is more pronounced. The effect of TRIP is usually positive as it usually acts as a relaxation mechanism and reduces the tensile residual stresses on the surface, which have a strong impact on the fatigue and corrosion resistance of the component. However, it is effect is highly case specific and hard to quantify without performing numerical simulations.

The most important conclusion that can be drawn is that it is not possible to accurately determine the residual stress state (sometimes even the sign of the stress) without incorporation of TRIP into constitutive equations. The accuracy of determination is limited to the accuracy of TRIP models and composite deformation behavior. Although most of the current TRIP models are basically implemented by simple addition of TRIP strain rates into constitutive behavior, they are, at least, able to reproduce the trends in natural occurrences in internal stress distribution.

Using the concepts from Section 4.4 and these observations, the consequences of TRIP during quenching of steels can be summarized as follows:

- The effect of TRIP on the mechanical response of the component during quenching is twofold both affecting the stress evolution and the residual stress state. The stress evolution during quenching at a given point can be decomposed into periods of loading, unloading and reverse loading. Particularly, dilatation due to phase transformations initially induces unloading and later a reverse loading. During reverse loading, the stresses are usually sufficient to cause plastic deformation. If the material is in elastic region, TRIP acts as an additional strain and leads to stress relaxation. If the material is in plastic region and the TRIP strain is sufficient to accommodate the deformation then there is no need for additional plastic strain, which leads to a stress relaxation. However, if TRIP strain is not sufficient, and then stress relaxation does not occur since an additional plastic strain is required for further deformation.

- A typical residual stress state for a quench hardened specimen having axisymmetric geometry consists of tensile residual stresses at the surface and compressive ones at the core. These tendencies are highly related to irreversible strain history, which depends both on the material and temperature history (cooling medium, material and geometry). Due to its irreversible nature, TRIP usually enhances the residual stress state described above.
- The contribution of TRIP depends on the proportion of irreversible strains generated by classical plasticity and transformation plasticity. The contribution is expected to be large when the source of irreversible strains is transformation plasticity without the need of classical plasticity. This effect is highly pronounced in the case of surface treatments such as induction, laser hardening and carburizing, in which the transformation plasticity is solely able to accommodate the deformation [26, 43, 310-313].
- The contribution of transformation plasticity in quenching depends on many factors such as the material, size and shape of the specimen, cooling characteristics of the quenching medium. For example, the contribution of TRIP generally increases as the size of the specimen increases. Similarly, an increase in the contribution is expected when the quench capacity of the quenchant increases. Additionally, a reversal in surface residual stresses from tensile to slightly compressive is reported in few cases involving high temperature transformations [210].

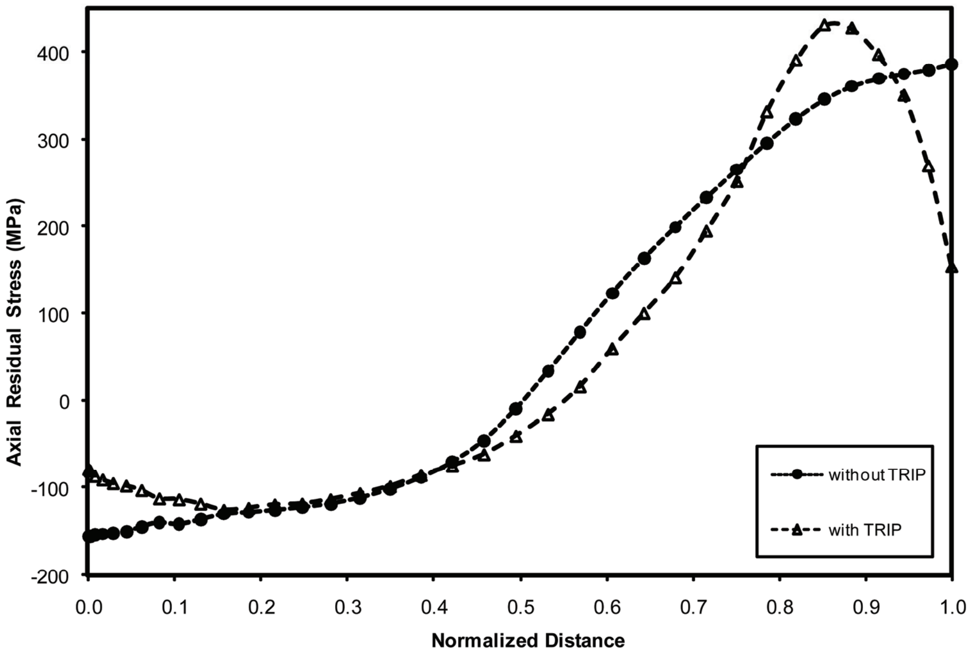

Figure 8.21 The distribution of axial residual stress along the normalized radius for a C60 steel cylinder (ϕ=30 mm,H=60 mm) after being quenched from 830°C into water at 20°C.

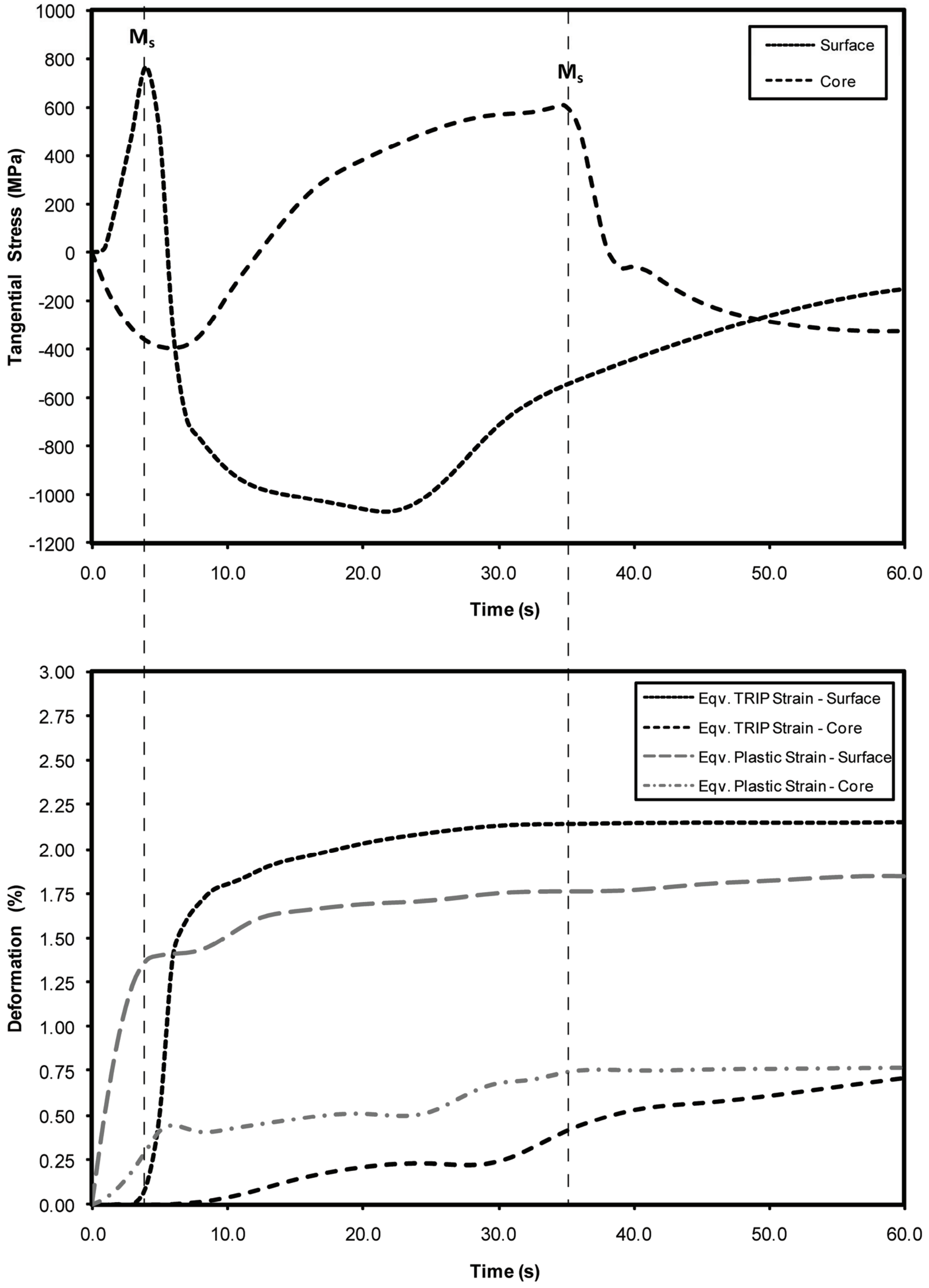

Figure 8.22 Variation of a) tangential stress, b) $\bar{\varepsilon}^{p}$ and $\bar{\varepsilon}^{tr}$ during quenching of a C60 steel cylinder (ϕ=30 mm, H=60 mm) from 830°C into water at 20°C

8.3.3 QUENCHING OF ECCENTRICALLY DRILLED CYLINDERS (3D)

Final stage of the verification of the all the capabilities of the framework was based on the comparison of predicted microstructure and residual stress distribution with SEM investigation and XRD residual stress measurements. All the possible improvements and couplings except the effect of stress and plasticity on phase transformation was enabled to test “real” capabilities of the framework to the full. Some of the important improvements which are tested in this section can be cited as follows:

- Implementation of plastic memory loss due to phase transformations.
- Implementation of TRIP using Leblond model.
- Calculation of dilatational strains using experimental structural dilatation values instead of density changes.
- Use of improved material and process data

The quality of the microstructure prediction is initially investigated for axisymmetric specimens in order to detect and point out the unavoidable experimental errors, then; it is investigated on eccentrically drilled specimens to determine the effect of asymmetry. However, quantitative comparison of predicted and observed microstructures is a challenging task due to inherent limitations of metallographic inspection and image analysis. So, the accuracy of the model is also tested on XRD residual stress measurements, which is a better tool for quantitative evaluation.

Verification of the Prediction of the Microstructure

Figure 8.23 illustrates predicted and observed microstructure for specimen A2. It can be seen that the outer surfaces (point (a) and (f)) are dominated by martensite phase as expected. For (f), some bainite and Widmanstatten ferrite that nucleated on prior austenite grain boundaries are also observed. Simulation reports a similar result with the exception of lower amount of ferrite. Mid section of thin wall (b) is mainly consisted of martensite and pearlite phases with some bainite and a few amount of ferrite. According to the simulation, this point consists of approximately 55% martensite, 35% pearlite, 9% bainite and 1% ferrite, which is in quite good agreement with the observations. On the other hand, simulations report that the mid section of thick wall (d) is made up of approximately 50% pearlite, 35% martensite, 20% bainite and 5% ferrite. For the same point, SEM micrograph reports a higher amount of martensite and less pearlite and similar amounts of bainite and ferrite. For point (c), simulation state equal amounts of pearlite and martensite (45%), some bainite (9%) and a few ferrite (1%), whereas, it states approximately 65% pearlite, 20% martensite, 10% bainite and 5% ferrite. The micrographs are in good agreement with these predictions.

Figure 8.24 illustrates the predicted and observed microstructure for specimen A3. According to the micrograph, (a) is mainly consisted of bainite and martensite. However, simulation reports a significantly lower amount of bainite although it reports almost 10% bainite near the surface. This inconsistency may be due asymmetric immersion or a chemical inhomogenity (such as Si) which may promote bainitic transformation since the other surface (f) consists of mostly martensite as expected. SEM investigation conveys that the points near inner whole ((c) and (d)) contain predominantly pearlite, martensite and some bainite, while point (c) has considerably more martensite whereas; (d) has more pearlite and ferrite. The simulations results illustrate a similar behavior with these observations. In regards to point (b), simulation forecast 70% martensite, 20% bainite, 9% pearlite and 1% ferrite. The micrograph indicates a similar behavior with less martensite but more pearlite. On the other hand, point (e) is mainly consisted of martensite and bainite. However, the predicted results exhibit some discrepancy with the observed ones, since the simulation results indicate considerably larger amount of bainite then the observed one.

Figure 8.25 illustrates the microstructure of the specimen B1 observed in SEM with the one predicted by FE simulation. From the micrographs, it can be observed that point (a) and (f) on the outer surface consist of mostly martensite, a few amount of bainite and pearlite and trace amount of ferrite. Simulation results report approximately 85% martensite, 10% pearlite and 5% bainite for (a) and (f). According to SEM observation, (f) contains more bainite and Widmanstatten ferrite although the geometry is symmetric. The reason for this occurrence will be discussed later in this section. On the other hand, simulation results report that the point (b) and (e) at the mid-section is consisted of roughly, 25% martensite, 50% pearlite and 20% bainite and 5% of ferrite. The microstructural investigation is in acceptable agreement with the prediction. However, (e) seems to contain a larger amount of martensite and ferrite. The inner surface ((c)-(d)) has almost equal amounts of pearlite and martensite; however their fraction has decreased significantly while the bainite and Widmanstatten ferrite content increased. The microstructure still indicates an asymmetry since (d) contains a larger amount of bainite than (c). Nevertheless, the quality of prediction is still in acceptable limits, considering the limitations of the metallographic inspection.

Figure 8.26 illustrates the comparison of the microstructure distribution of the specimen C2 with predicted ones. From the micrographs, it can be seen that the outer surfaces ((a)-(f)) consists of mostly martensite, few pearlite and trace amount of ferrite. Simulation results report 88% martensite, 8% pearlite, 4% bainite and trace amount of ferrite for the region (a), whereas, 88% martensite, 10% pearlite and 2% bainite are reported for region (f). The mid section of the thin side (b) contains equal amounts of pearlite and martensite, some bainite nearby pearlite regions and a little ferrite surrounding martensite or pearlite. 45% martensite, 45% pearlite, 7% bainite and 3% ferrite is predicted for this region by the computer simulation, which is in a good agreement with the observations. On the other hand, the mid section of thick side (d) is made up of mostly pearlite and some martensite. Bainite sheaves and Widmanstatten ferrite nucleated on prior austenite boundaries is also observed.

Widmanstatten ferrite formation rather than grain boundary allotriomorphs may be due to ferritic transformation at lower temperature at which diffusional transformations are sluggish or due to the effect of stress. The inner surface (c) posses equal amounts of pearlite/bainite mixture and martensite, however; their amounts are slightly decreased with respect to (b). The other inner surface (d) is consisted of mainly pearlite, less martensite, similar amount of bainite, considerably increased amount of mixture of idiomorphic and allotriomorphic ferrite, with respect to the other inner surface (c). Predicted results are in good agreement with observations as the simulation report almost 65% pearlite, 18% martensite, 10% bainite and 7% ferrite.

Figure 8.27 illustrates the accuracy of the microstructural prediction for specimen C3. As can be seen from (a) and (f), the prediction of the microstructure on the surfaces is not quite good since the surface is consisted of mostly martensite and some pearlite, the simulation report only a few pearlite on the surface. This may be due to slightly delayed quenching of the specimen. However, the quality of the prediction of microstructure for the rest of the specimen is quite good. For example, simulation foresees that the point (d) consists of approximately 75% pearlite, 15% martensite, 5% bainite ad 5%ferrite. The micrograph is clearly in accordance with this prediction since it consists of mainly pearlite, then some martensite, few bainite and considerable amount of ferrite nucleated on the prior austenite boundaries. Similarly, point (c) is made up of mostly martensite, pearlite and some bainite according to the SEM observation. Simulation reports 60% martensite, 30% pearlite, 9% bainite and 1% ferrite for the same point. In addition, it can also be seen that the predicted microstructure is in good agreement with the observations for points (b) and (d).

Finally, Figure 8.28 illustrates the predicted and observed microstructure for the thinnest walled specimen with large eccentricity (D3).Micrographs indicates that the thin walled side ((a)-(b)-(c)) is mainly consisted of martensite and bainite. The simulation states a decreasing martensite amount from approximately 90% (a) to 77% (b) and increasing bainite amount from 5% (a) to 15% (c). The results are in agreement with the predictions except the prediction of bainitic transformation. As it was seen on some other micrographs, the surface has considerably larger amount of bainite then it is foreseen. Again, this may be owed to the slightly delayed quenching, strong effect of stress, plasticity and chemical inhomogenity to the bainitic transformation. Another important point that should be noted from the micrographs of the thin side ((a)-(b)-(c)) is that martensite plates and bainite sheaves have significant orientation effect, which also supports the stress affected transformation claim. On the other hand, it can be seen that the quality of the prediction is acceptable for the thick walled side ((d)-(e)-(f)) except the surface (f) in which more pearlite is observed than predicted. This may also support the slightly delayed quenching claim. It should also be noted that point (f) also exhibits some orientation effect but it is not as strong as in the case of point (a).

From Figure 8.28 - 8.28, it can be concluded that the distribution of microstructure is highly affected even by minor changes in the geometry. This is due to complex asymmetric heat transfer problem, which produce considerably different cooling rates. Moreover, it may also be noticed that the quality of prediction of the as-quenched microstructure is quite good in terms of the limitations of metallographic investigations and image analyses. The results from Figure 8.23 – 8.25 also reveal that bainitic transformation is the most problematic transformation for simulation purpose since its kinetics and thermodynamics are highly affected from stress, prior plasticity and local chemical inhomogenity as reported in Section 3.8.

The discrepancies, excluding the inherent numerical/experimental errors may be owed to the following facts:

- Specimens may not be immersed in the quenchant exactly in the same way, which may result in asymmetric fluid flow, even though the geometry is symmetric. This maybe one of the reasons for different microstructures observed in Fig. 8 in symmetric points of B1. The asymmetric variation of the convective heat transfer coefficient will induce an asymmetry in the boundary conditions, which eventually will result in asymmetric stress and microstructure distribution. Another reason for this case may be the chemical inhomogenity.
- The material has been considered chemically homogeneous before and during quenching. However, it is known that a real material is not homogeneous at all and it contains certain compositional fluctuations due to segregations before quenching. In addition, chemical inhomogenity may be because of the solute enrichment of the austenite due to prior diffusional phase transformations.
- The computation of microstructure is based on additivity principle. However, there exist several experimental and theoretical researches commenting on the non-additivity of the phase transformations during steel quenching, especially for the bainitic transformation [196, 224, 225, 252].
- Prediction of the thermal field may be weak due to use of same heat transfer coefficient for the surface and the bottom-top of the specimens. In practice, it is expected that both these regions have a different convective heat transfer coefficients.
- The effect of stress on phase transformations has been neglected due to the reasons stated in Section 2.3.3. However, asymmetric stress field in the component may introduce some discrepancies. The effect of stress and plasticity is expected to be more pronounced for martensite, bainite and Widmanstatten ferrite phases, which occur by displacive mechanism.

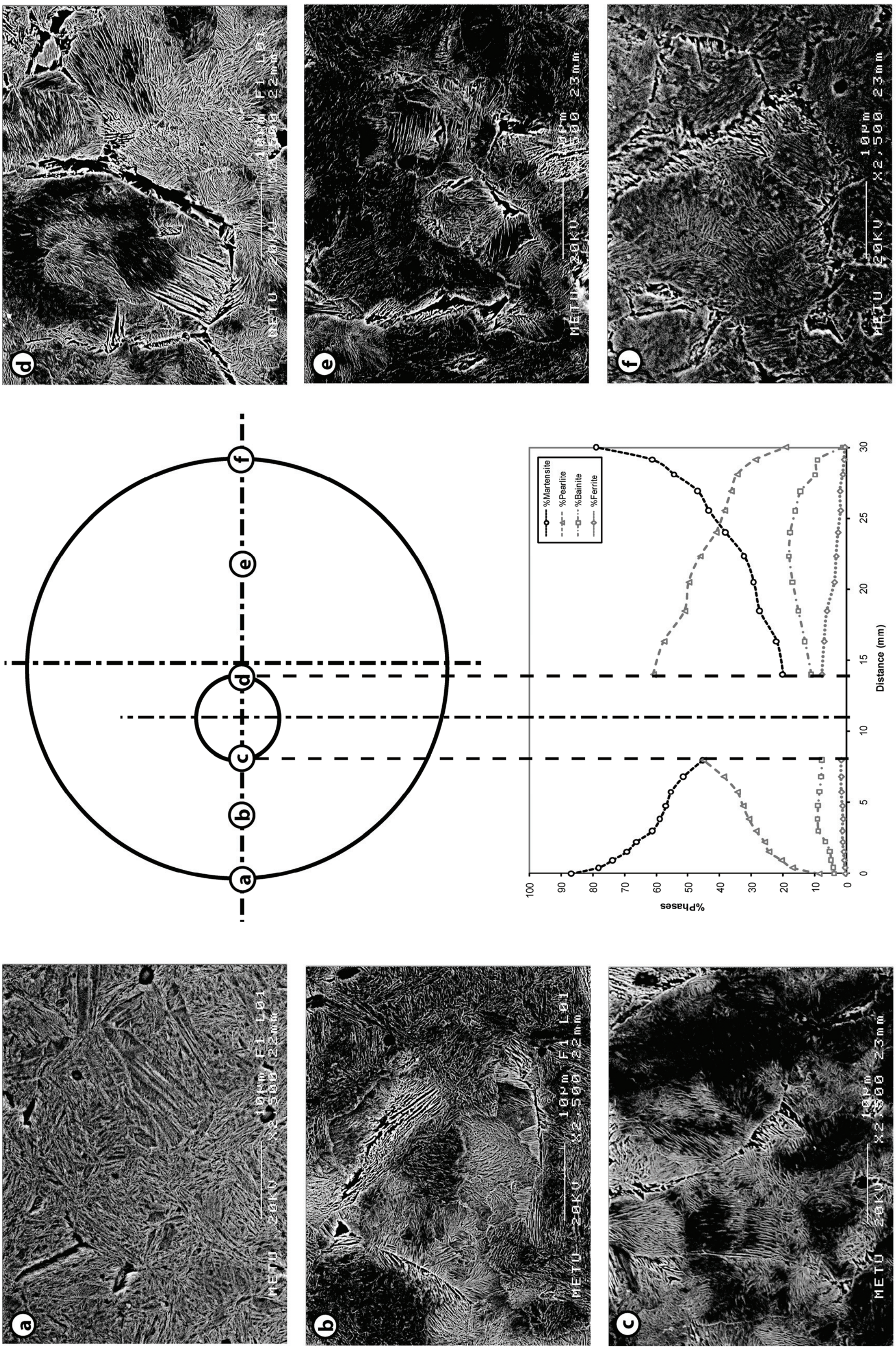

Figure 8.23 Observed and predicted microstructures for specimen A2

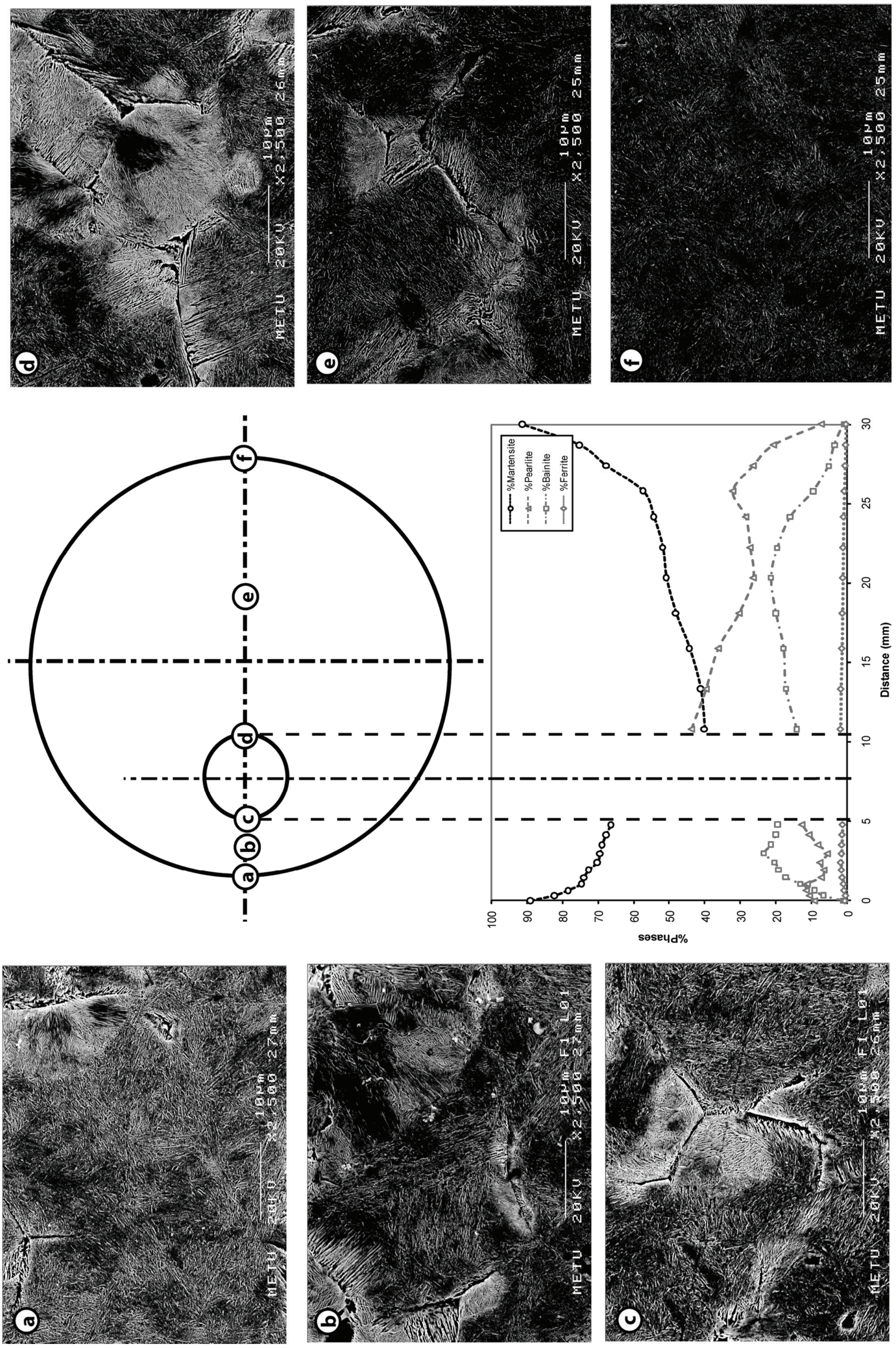

Figure 8.24 Observed and predicted microstructures for specimen A3

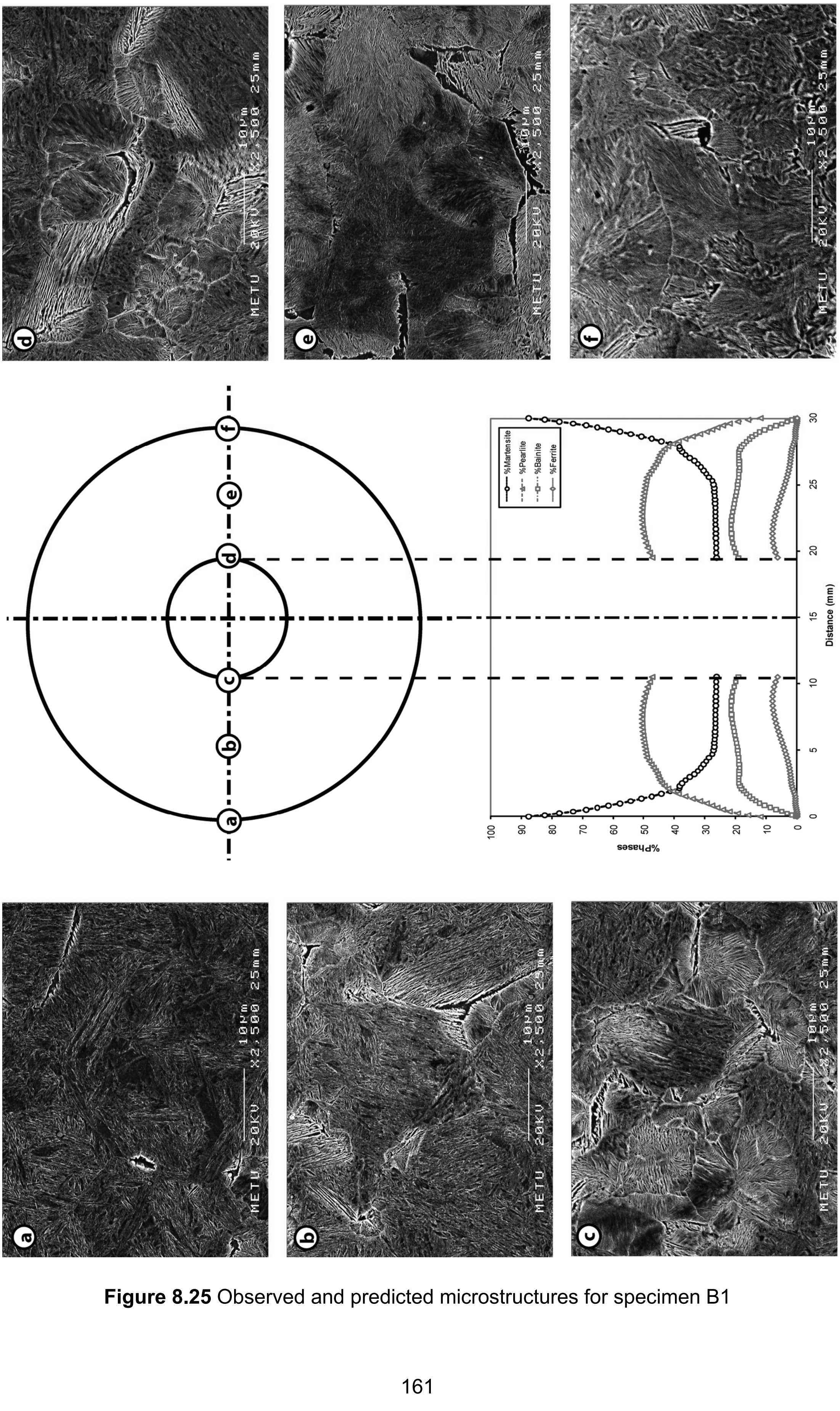

Figure 8.25 Observed and predicted microstructures for specimen B1

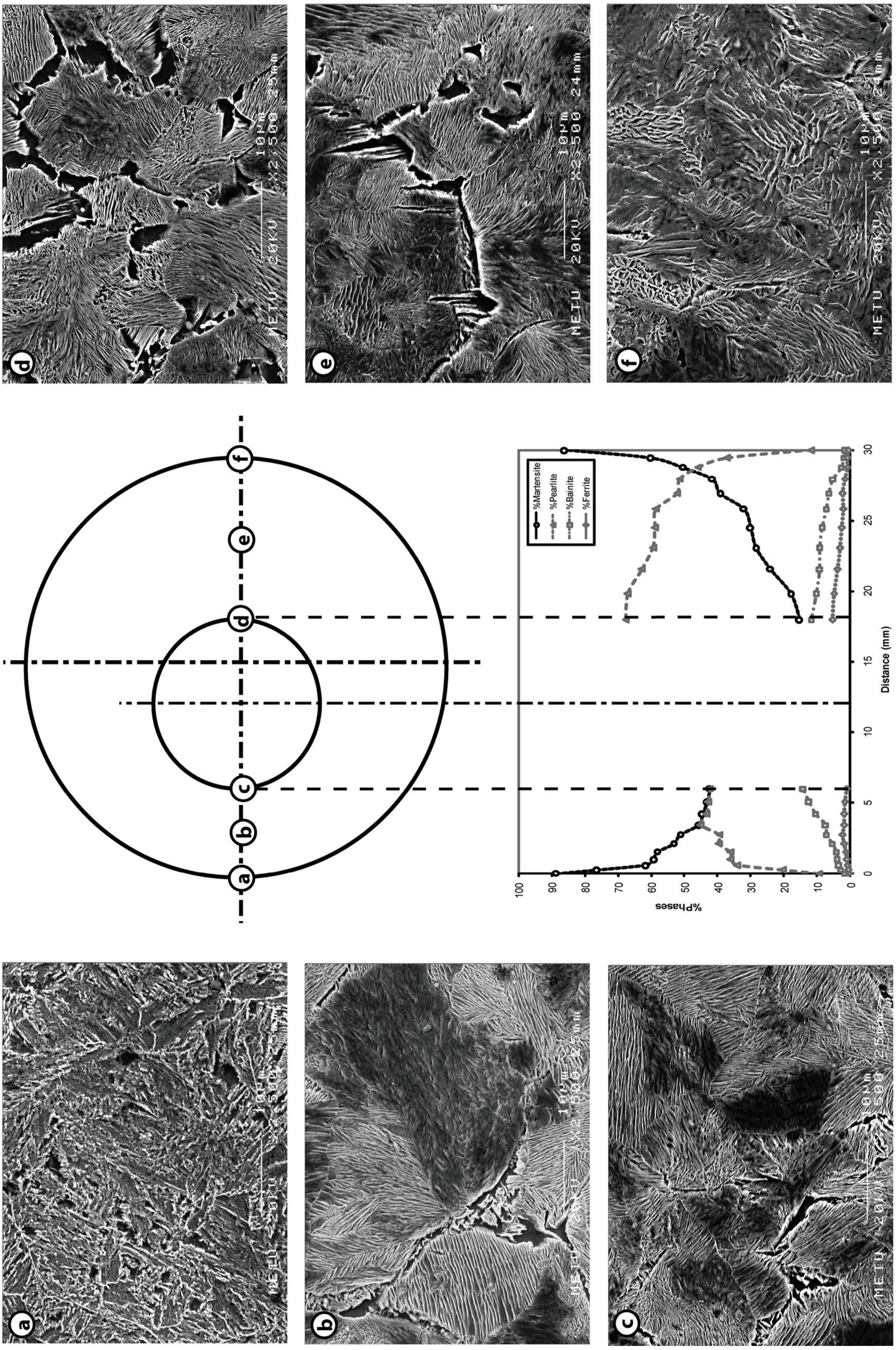

Figure 8.26 Observed and predicted microstructures for specimen C2

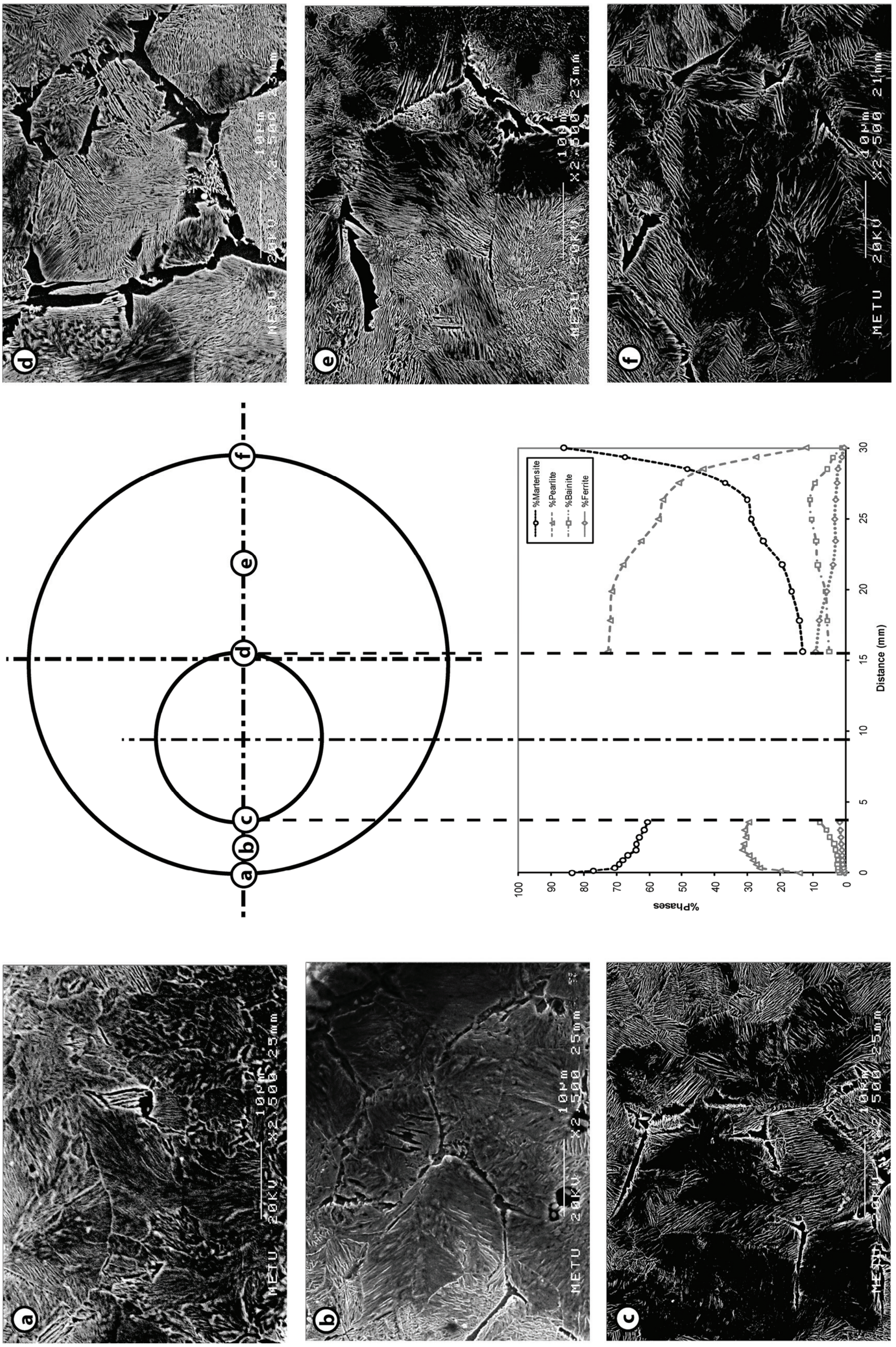

Figure 8.277 Observed and predicted microstructures for specimen C3

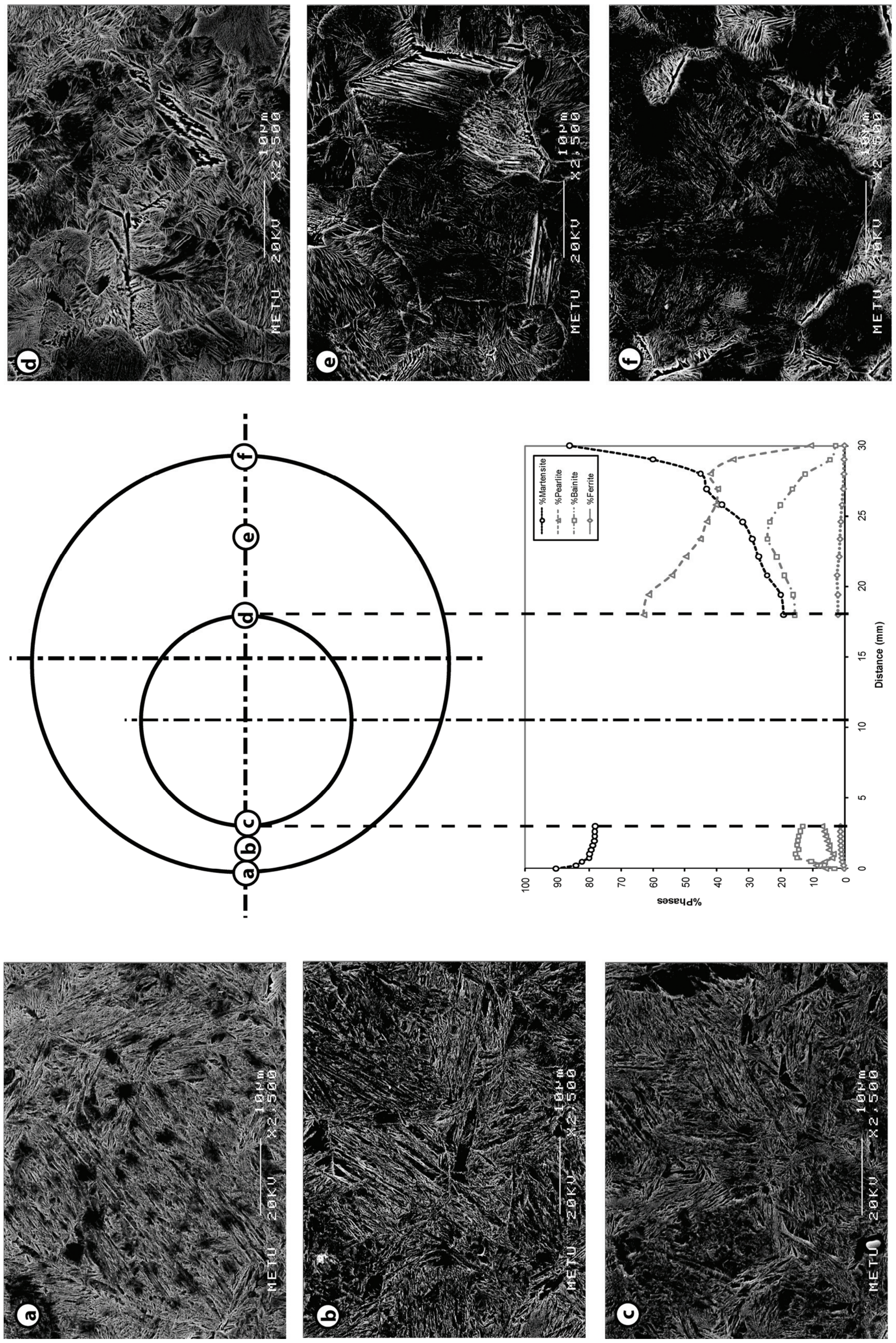

Figure 8.28 Observed and predicted microstructures for specimen D3

Verification of the Prediction of the Residual Stress State

The distribution of tangential component of residual stress is presented on Figure 8.29-8.30. On those figures, the magnitude of the tangential residual stress is plotted versus the angle θ. From these figures, it can be deduced that simulation results show a good agreement with experimental measurements both in terms of the trends and the magnitude of residual stresses.

It is hard to setup an easy relationship correlating the developed stress profile and the geometry (hole diameter, eccentricity ratio). The most obvious observation is that stresses developed on the thinnest cross section are usually larger than the one developed on the thickest side. Another observation that can be made for the cylinders with R=1 is that magnitude of the tangential stress increases as the diameter of the hole increases and there is also a critical diameter for which the stress state exhibit a transition from compression to tension.

On the other hand, it is even more complicated to establish a common rule for cylinders with eccentrically drilled holes It is observed that the stress at (A) is increase with increasing eccentricity for specimen group A-B, whereas, it is decreased for the specimen group C-D. A detailed dimensionless analysis with all the involved dimensionless numbers may result to establish a more general relationship. However, such an analysis was not performed for this study.

In order to establish more common rules, major principle Cauchy stress is also investigated. To determine the predominant stress state without presenting the reference coordinate system and all of the components of Cauchy stress tensor, the magnitude of the major principle stress may be used. Figure 8.31 illustrates the distribution of the major principle Cauchy stress after quenching process. From this figure, a more general rule can be derived:

- Point A and D are always in tension.
- Point C is always in compression.
- Point B may be either in tension or in compression depending on a complex set of parameters. However, S1 has a strong effect on the stress state of B.

To understand the physical origin of residual stresses during quench hardening of asymmetric or 3D components, one must carefully trace heat transfer, phase transformations and mechanical phenomena from the start till the end of process. The discussion of the development of stresses on axisymmetric parts was done in the previous section. Hereby, the principles will be extended to general geometries.

As mentioned previously, residual stress state depends on both the thermal stresses and phase transformation stresses. However, phase transformation stresses are usually larger than the thermal ones. Thus, consideration of cooling rates and sequence of phase transformations at critical stages may provide the engineers to predict the sign and the order of magnitude of the residual stresses without the need of performing numerical simulations. In general, the larger the time difference between phase transformations at two equilibrating regions is, the larger the developed stresses will be.

Using the basic principles discussed in the previous sections, the critical stages for evolution of internal stresses during quenching of an arbitrary shaped component can be generalized as follows:

Stage 1: This stage starts at the beginning of quenching and lasts as the phase transformations start. During this stage, austenite cools down at different rates at different regions. An internal stress state is developed due to the differences in rate of thermal contraction and variation of thermomechanical properties, Fast cooling regions (i.e., regions close to the surfaces in contact with the quenchant), are loaded in tension, whereas slow cooling regions are loaded in compression, which may be considered analogous to the quenching without phase transformations discussed in the previous section. Although this stage is usually quite short, it`s effect on distortion may be significant to considerable amount plastic deformation in soft austenite phase. Internal stress generation and prior plastic deformation of the parent austenite may also affect subsequent phase transformations especially at the deformed surface. For example, this may result in a local variation of Ms temperature on the surface and subsequent diffusion controlled phase transformations may be accelerated significantly on the surface of the component.

Stage 2: This stage starts as the phase transformations start. During this stage, large transformation strains are generated at the transforming regions due structural dilation and transformation plasticity which dominates over thermal contraction. At this stage, TRIP strains have a significant impact on the overall inelastic strains since TRIP strains are of the same order of magnitude or larger during this stage. This leads to a fast unloading and reverse loading on transforming regions while the untransformed regions react to equilibrate those stresses. Transforming regions are loaded in compression whereas the untransformed regions are loaded in tension.

Stage 3: This stage starts with the transformation of untransformed regions from the previous stage. During this stage, already transformed regions experience thermal contraction as they cool down, whereas, the transforming regions expands due to transformations. Similar to previous stage, this causes an unloading and reverse loading. Already transformed regions are loaded in tension while the transforming regions are loaded in compression.

Stage 4: At the final stage, austenite is almost completely transformed into different transformation products and thermal stresses are generated as the specimen cools down. However, those stresses are not so significant because of small temperature gradients. Practically, only minor changes in the stress distribution occur.

By using these concepts, results on Figure 8.1 may be interpreted to setup a general relationship as follows:

- If S1 is greater than a critical thickness ($S1 > S1_C$) both the thin and walled side behaves like a shallow hardening part and at the critical stages, large stresses are generated between A-B and C-D. Those stresses are mostly balanced in the same section. For example, as A is loaded in tension, B is loaded in compression. As a result, at the end of the quenching A and D are in tension, whereas B and C are in compression (A3 and B3 on Figure 8.31).
- If S1 is smaller than a critical thickness ($S1 < S1_C$), the thin side behaves like a through hardening part, whereas the thick section behaves like a shallow hardening part. Since there is only a small time difference between completions of transformations of the thin side, the stresses developed on this section are not large. Stress state at A can have the same sign on B. Those stresses are balanced in C-D section. At the end, A, B, D is in tension whereas large compressive stresses are generated at C (C3, D3 on Figure 8.31).
- The critical thickness $S1_C$ is not easy to determine and it is a complex function of all material and process parameters. The only method to determine $S1_C$ seems to be performing a series of simulations.
- Dimensionless analysis methods may also work to predict $S1_c$ for considerably simple cases such as quenching of steels of high hardenability during which all the component is transformed to only martensite. The predictive capability of such kind of analysis seems to be quite weak for quenching with both martensitic and diffusion controlled transformation. However, the set of dimensionless numbers used in the analysis must surely include parameters related with martensitic transformation besides thermal, mechanical, geometrical and mixed type of dimensionless numbers. If there exist diffusion controlled transformations, this dimensionless numbers should also include dimensionless numbers related to anisothermal transformation kinetics.

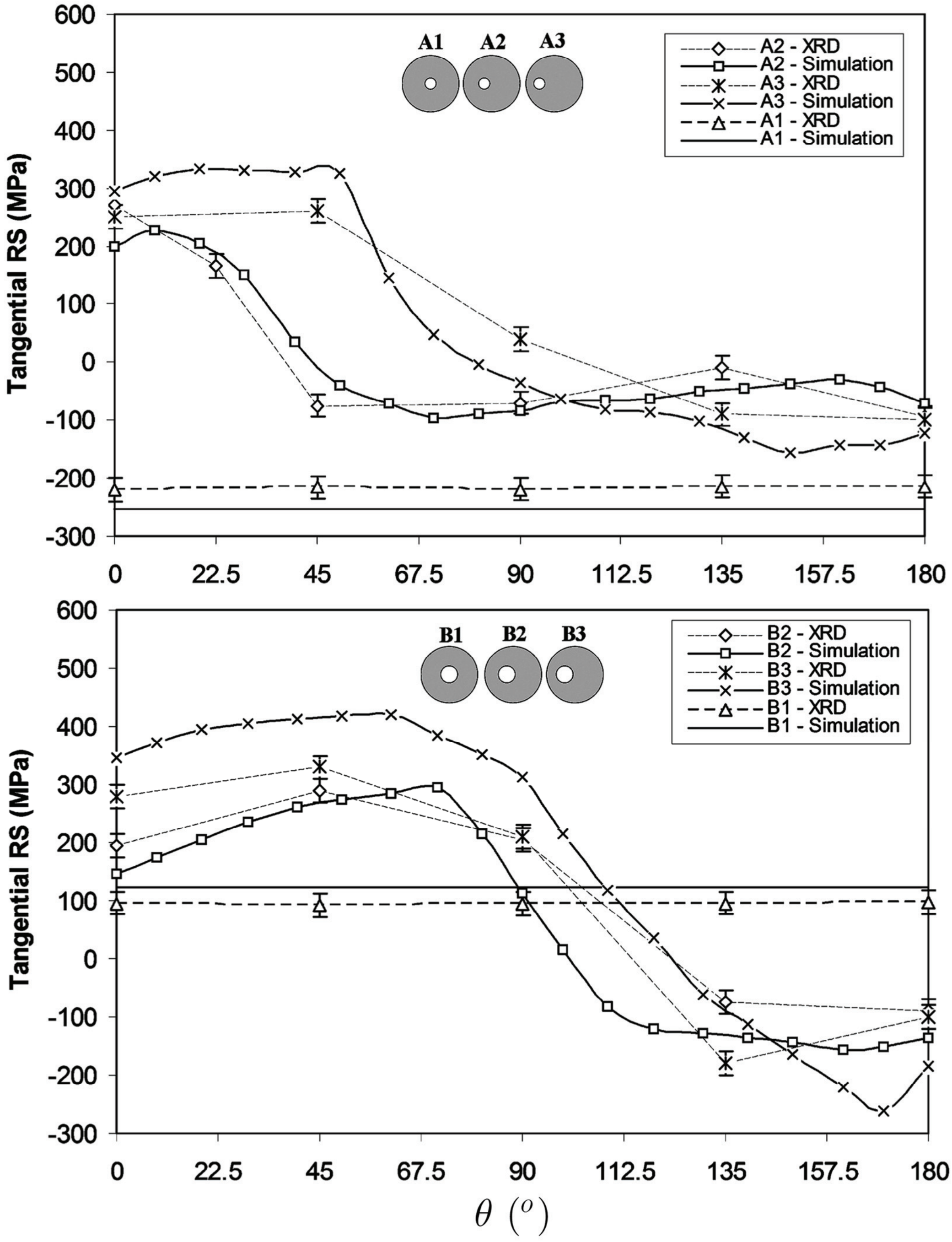

Figure 8.29 Predicted and measured (XRD) tangential residual stress distributions along the circumference of A/B series specimens after quenching from 830°C into water at 20°C

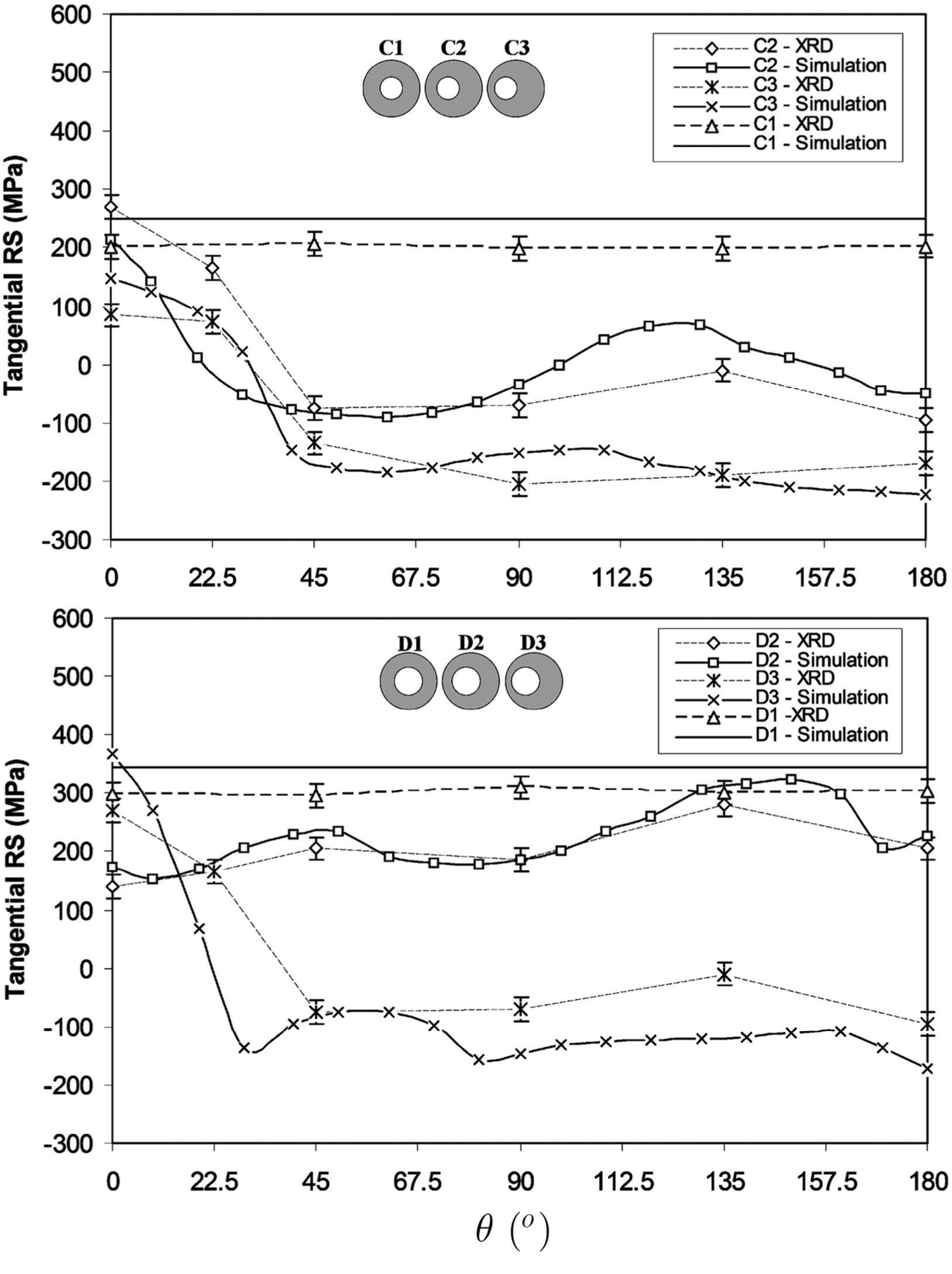

Figure 8.30 Predicted and measured (XRD) tangential residual stress distributions along the circumference of C/D series specimens after quenching from 830°C into water at 20°C

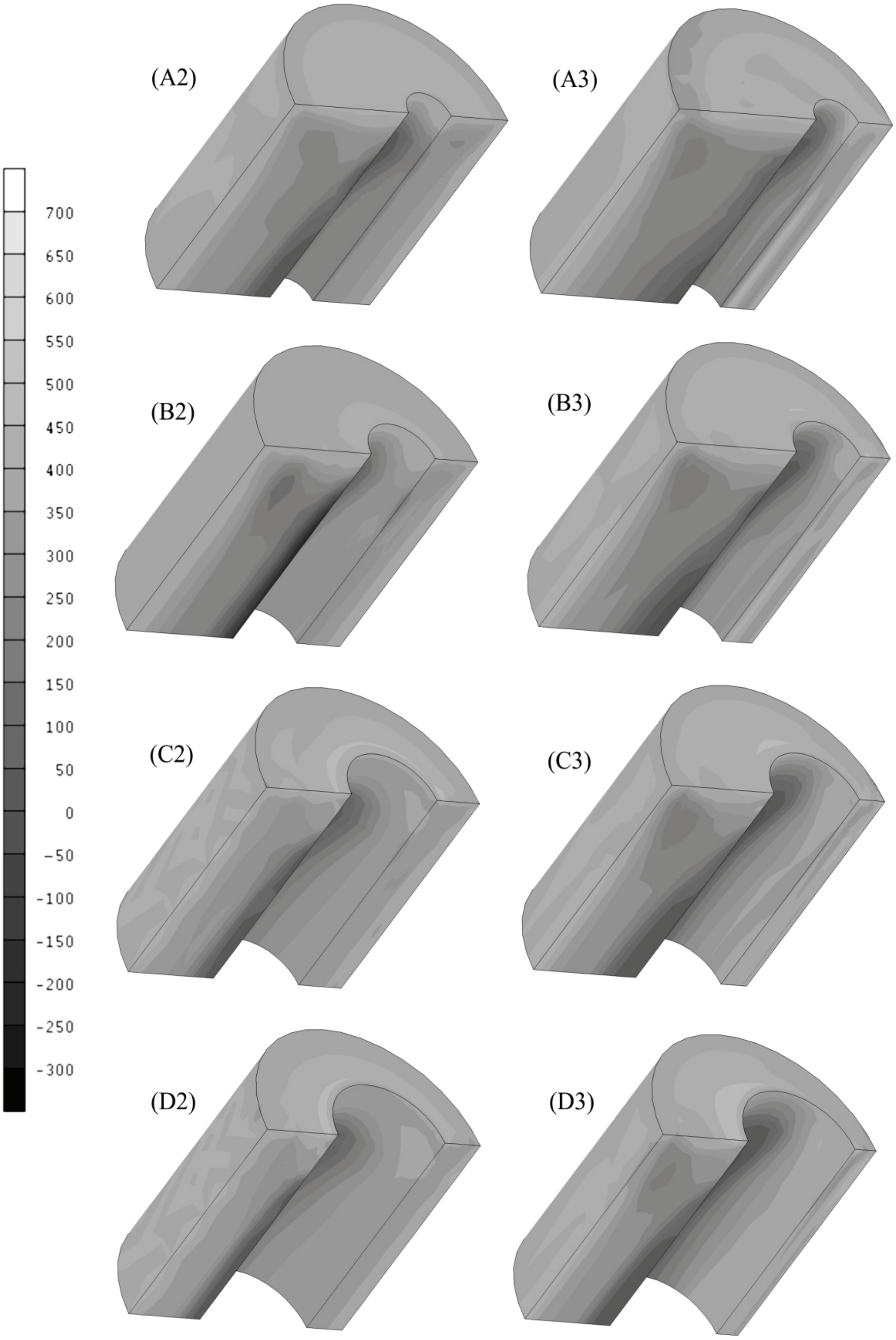

Figure 8.31 Variation of the major principle Cauchy stress for C60 steel specimens after quenching from 830^{0}C into water at 20^{o}C

CHAPTER 9

CONCLUSIONS AND RECOMMENDATIONS

9.1 GENERAL

Quench hardening is a common manufacturing process to produce steel components with reliable service properties. Although quench hardening is a vital part of production based on steel, it is also one of the major causes of rejected components and production losses. Distortion, cracking, achievement of desired distribution of microstructure and residual stresses are the most important problems during quenching of steels. In order to solve this problem, the dependence of the properties of the final product on the physics of the process must be understood clearly, so that analysis or experimentation can be used to design processes to achieve optimum quality at desired production rates. Modeling is one of the most crucial elements in the design and optimization of quenching systems.

During quenching, parts are usually subjected to continuous heating and cooling cycles during which microstructural and mechanical evolutions occur simultaneously at different length scales. Modeling of these processes necessitates dealing with inherent complexities such as large material property variations, complex couplings and domains, combined heat and mass transfer mechanisms, phase transformations and complex boundary conditions. In this chapter, it is intended to present a comprehensive reference for scientist interested in simulation of quenching, including many aspects of quenching process from involved physics to modeling. Some of those aspects can be summarized as: physical events involved, review of modeling approaches, detailed mathematical treatment of the problem, guidelines for implementation of the proposed models in commercial FEA software and state of the in simulation of quenching. This chapter may also be a valuable reference for scientists interested in the simulation of other thermal materials processing methods. The principles and modeling approaches presented in this chapter may be extended to a variety of thermal treatments ranging from conventional heat treatments to state of the art materials processing techniques.

Before concluding this thesis, it should be emphasized that although a great deal of progress has been achieved in simulation of steel quenching, there are still many problems requiring solution which makes the field open to scientist from a wide range of different disciplines such as structural mechanics, material science, physics and mathematics.

Although this thesis was focused primarily on the modeling and simulation of the process, there are other complementary steps in industrial implementation of quenching simulations. A vital step in achieving success in simulations is the acquisition of accurate process and material data. The second important element of the solution is the “control of quenching”. , which requires development of engineering systems to control the heat transfer so that the actual quenching may be optimized with respect to the simulation results. It should be noted that simulation of quenching will only remain as a “scientific curiosity” without the control of quenching.

Simulation and control of thermal processing of materials is a promising research field both in terms of the industrial and the scientific output. A great progress achieved in the field since the early studies from 70`s. However, total success still requires hard work, collaboration and development of new methods. The author hopes that this thesis is a step for progress in the field.

9.2 FUTURE RESEARCH

Current architecture of the framework allows performing parametric studies in the following fields with some revisions (from minor to major):

- Gas and water jet quenching
- Austenization and tempering
- Laser, flame and induction hardening.
- Welding
- Thermochemical heat treatments such as carburizing, boriding etc.
- Any cold/hot processing technique involving microstructural changes
- Simulation and design of integrated heat treatments
- Simulation of state of the art thermal processing techniques such as injection molding, crystal growing, rapid prototyping

Moreover, following improvements can be made on the architecture of the framework for obtaining more realistic results (according to the ease of implementation):

- Implementation of kinematic hardening
- Implementation of TRIP model with kinematic hardening
- Implementation of mass transfer field for simulation of thermal treatments with compositional variations such as carburizing, boriding, nitriding.
- Testing and improvement of large strain capabilities

Finally and maybe most importantly, the framework can be used as a platform for testing physically based multi-scale theories for computation of microstructural evolution and TRIP.

REFERENCES

[1] Ziegler H. An Introduction to Thermomechanics. Amsterdam: North-Holland, 1983.

[2] Denis S, Farias D, Simon A. Mathematical-Model Coupling Phase-Transformations and Temperature Evolutions in Steels. ISIJ Int. 1992;32:316.

[3] Bhadeshia H, Christian JW. Bainite in Steels. Metallurgical Transactions a-Physical Metallurgy and Materials Science 1990;21:767.

[4] Gur CH, Tekkaya AE. Numerical Investigation of Non-Homogeneous Plastic Deformation in Quenching Process. Mater. Sci. Eng. A-Struct. Mater. Prop. Microstruct. Process. 2001;319:164.

[5] Mitter W. Umwandlungsplastizitat Und Ihre Berucksichtigung Bei Der Berechnung Von Eigenspannungen. Materialkundlich-Technische 1987;7.

[6] Greenwood GW, Johnson RH. The Deformation of Metals under Small Stresses During Phase Transformations. Proc. Roy. Soc. 1965;283:403.

[7] Magee CL. Transformation Kinetics, Micro-Plasticity and Ageing of Martensite in Fe-31ni. , vol. PhD. Pittsburgh , USA: Carnegie Inst. of Tech., 1966.

[8] Fischer FD, Oberaigner ER, Tanaka K, Nishimura F. Transformation Induced Plasticity Revised an Updated Formulation. Int. J. Solids Struct. 1998;35:2209.

[9] Fischer FD, Sun QP, Tanaka K. Transformation-Induced Plasticity (Trip). Applied Mechanics Reviews 1996;49:317.

[10] Embury JD, Deschamps A, Brechet Y. The Interaction of Plasticity and Diffusion Controlled Precipitation Reactions. Scr. Mater. 2003;49:927.

[11] Lusk MT, Lee Y-K. A Global Material Model for Simulating the Transformation Kinetics of Low Alloy Steels. Proceedings of the 7th International Seminar of the International IFHT. Budapest, Hungary: IFHT, 1999. p.273.

[12] Reti T, Felde I. A Non-Linear Extension of the Additivity Rule. Comput. Mater. Sci. 1999;15:466.

[13] Denis S, Sjostrom S, Simon A. Coupled Temperature, Stress, Phase-Transformation Calculation Model Numerical Illustration of the Internal-Stresses Evolution During Cooling of a Eutectoid Carbon-Steel Cylinder. Metallurgical Transactions a-Physical Metallurgy and Materials Science 1987;18:1203.

[14] Inoue T, Wang ZG. Coupling between Stress, Temperature, and Metallic Structures During Processes Involving Phase-Transformations. Mater. Sci. Technol. 1985;1:845.

[15] Liu CC, Liu Z, Xu XJ, Chen GX, Wu JZ. Effect of Stress on Transformation and Prediction of Residual Stresses. Mater. Sci. Technol. 1998;14:747.

[16] Lee SJ, Lee YK. Effect of Austenite Grain Size on Martensitic Transformation of Low Alloy Steel. Proceedings of the 5th Pacific Rim International Conference on Advanced Materials and Processing. Beijing, China: The Chinese Society of Metals, 2004. p.3169.

[17] Ju DY, Narazaki M, H. K. Computer Predictions and Experimental Verification of Residual Stresses and Distortion in Carburizing-Quenching of Steel. Journal of Shanghai Jiao Tong University 2000;E:7.

[18] Denis S, Gautier E, Simon A, Beck G. Stress-Phase-Transformation Interactions - Basic Principles, Modelling, and Calculation of Internal Stresses. Mater. Sci. Technol. 1984;1:805.

[19] Inoue T, Wang Z. Coupling Betwen Stress, Temperature, and Metallic Structures During Processes Involving Phase Transformations. Mater. Sci. Technol. 1984;1:845.

[20] Voigt W. Lehrbuch der Kristallphysik 1928.

[21] Geijselaers HJM. Numerical Simulation of Stresses Due to Solid State Transformations. vol. PhD. Twente: University of Twente.

[22] Leblond JB, Mottet G, Devaux JC. A Theoretical and Numerical Approach to the Plastic Behavior of Steels During Phase-Transformations .1. Derivation of General Relations. J. Mech. Phys. Solids 1986;34:395.

[23] Abrassart F. Stress-Induced Gamma-]Alpha' Martensitic Transformation in 2 Carbon Stainless-Steels - Application to Trip Steels. Metallurgical Transactions 1973;4:2205.

[24] Leblond JB. Mathematical-Modeling of Transformation Plasticity in Steels .2. Coupling with Strain-Hardening Phenomena. Int. J. Plast. 1989;5:573.

[25] Leblond JB, Devaux J, Devaux JC. Mathematical-Modeling of Transformation Plasticity in Steels .1. Case of Ideal-Plastic Phases. Int. J. Plast. 1989;5:551.

[26] Sjostrom S. Interactions and Constitutive Models for Calculating Quench Stresses in Steel. Mater. Sci. Technol. 1984;1:823.

[27] Fischer FD, Reisner G, Werner E, Tanaka K, Cailletaud G, Antretter T. A New View on Transformation Induced Plasticity (Trip). Int. J. Plast. 2000;16:723.

[28] Tanaka K, Terasaki T, Goto S, Antretter T, Fischer FD, Cailletaud G. Effect of Back Stress Evolution Due to Martensitic Transformation on Iso-Volume Fraction Lines in a Cr-Ni-Mo-Al-Ti Maraging Steel. Materials Science and Engineering A 2003;341:189.

[29] Inoue T, Tanaka K. Elastic-Plastic Stress Analysis of Quenching When Considering a Transformation. Int. J. Mech. Sci. 1975;17:361.

[30] Kobasko NI. Methods of Overcoming Self-Deformation and Cracking During Quenching of Metal Parts. Met. Sci. Heat Treat. 1975;17:287.

[31] Kobasko NI. Computer-Analysis of Thermal Processes During Quenching of Steel. Met. Sci. Heat Treat. 1976;18:846.

[32] Kobasko NI. Thermal Processes During Quenching of Steel - Reply. Met. Sci. Heat Treat. 1976;18:602.

[33] Liscic B. Influence of Some Cooling Parameters on Depth of Hardening and Possibility of Measuring Quenching Intensity During Steel Hardening. Strojarstvo 1977;19:189.

[34] Inoue T, Haraguchi K, Kimura S. Analysis of Stresses Due to Quenching and Tempering of Steel. Transactions of the Iron and Steel Institute of Japan 1978;18:11.

[35] Inoue T, Raniecki B. Determination of Thermal-Hardening Stress in Steels by Use of Thermoplasticity Theory. J. Mech. Phys. Solids 1978;26:187.

[36] Kobasko NI. Effect of Pressure on Quenching of Steel. Met. Sci. Heat Treat. 1978;20:31.

[37] Denis S, Chevrier JC, Beck G. Study of Residual-Stresses Introduced by Quenching in TA6ZRD(685) Cylinders. Journal of the Less-Common Metals 1980;69:265.

[38] Inoue T, Nagaki S, Kawate T. Successive Deformation of a Viscoelastic-Plastic Tube Subjected to Internal-Pressure under Temperature Cycling. J. Therm. Stresses 1980;3:185.

[39] Giusti J. Contraintes Et Deformations Residuelles D'origine Thermique. Application Au Soudage Et a La Trempe Des Aciers. 1981.

[40] Inoue T, Nagaki S, Kishino T, Monkawa M. Description of Transformation Kinetics, Heat-Conduction and Elastic-Plastic Stress in the Course of Quenching and Tempering of Some Steels. Ingenieur Archiv 1981;50:315.

[41] Sjöström S. Calculation of Quench Stresses in Steel. vol. PhD. Linköping, Sweden: University of Linköping, 1982.

[42] Gergely M, Tardy P, Buza G, Reti T. Prediction of Transformation Characteristics and Microstructure of Case-Hardened Components. Heat Treat. Met. 1984;11:67.

[43] Josefson BL. Effects of Transformation Plasticity on Welding Residual-Stress Fields in Thin-Walled Pipes and Thin Plates. Mater. Sci. Technol. 1984;1:904.

[44] Fernandes FBM, Denis S, Simon A. Mathematical Model Coupling Phase Transformation and Temperature Evolution During Quenching of Steels. Mater. Sci. Technol. 1985;10:838.

[45] Leblond JB, Mottet G, Devaux J, Devaux JC. Mathematical-Models of Anisothermal Phase-Transformations in Steels, and Predicted Plastic Behavior. Mater. Sci. Technol. 1985;1:815.

[46] Denis S, Gautier E, Sjostrom S, Simon A. Influence of Stresses on the Kinetics of Pearlitic Transformation During Continuous Cooling. Acta Metallurgica 1987;35:1621.

[47] Gautier E, Simon A, Beck G. Transformation Plasticity During the Pearlitic Transformation of a Eutectoid Steel. 1987;35:1367.

[48] Liscic B, Filetin T. Computer-Aided Determination of the Process Data for Hardening and Tempering of Structural-Steels. Neue Hutte 1988;33:257.

[49] Miller AK. The Matmod Equations in Unified Constitutive Equations for Creep and Plasticity. Amsterdam: Elsevier Applied Science Publishers Ltd., 1987.

[50] Reti T, Gergely M, Tardy P. Mathematical Treatment of Nonisothermal Transformations. Mater. Sci. Technol. 1987;3:365.

[51] Gautier E, Simon A. Transformation Plasticity Mechanisms for Martensitic Transformation of Ferrous Alloys. Phase Transformation 1988;87:285.

[52] Assaker D, Golinval JC, Hogge M, Geradin M. Thermo-Plasticity Versus Thermo-Viscoplasticity for Residual Stresses. In: Owen DRJ, Hinton E, Onate E, editors. Computational Plasticity. UK: Pineridge Press, 1989. p.501.

[53] Tensi HM, Kunzel T. Importance of the Different Boiling Phases for the Cooling of Parts by Immersion - Numerical-Simulation and Experimental Revision. Neue Hutte 1987;32:354.

[54] Bates CE, Totten GE. Procedure for Quenching Media Selection to Maximize Tensile Properties and Minimize Distortion in Aluminum-Alloy Parts. Heat Treat. Met. 1988;15:89.

[55] Kobasko NI. Increasing the Service Life and Reliability of Components through the Use of New Steel Quenching Technology. Met. Sci. Heat Treat. 1989;31:645.

[56] Reti T, Gergely M. Computerized Process Planning in Heat-Treatment Practice Using Personal Computers. Heat Treat. Met. 1991;18:117.

[57] Stringfellow RG, Parks DM. A Self-Consistent Model of Isotropic Viscoplastic Behavior in Multiphase Materials. Int. J. Plast. 1991;7:529.

[58] Saunders N. Computer Modeling of Phase-Diagrams. Mater. Sci. Technol. 1992;8:112.

[59] Stringfellow RG, Parks DM, Olson GB. A Constitutive Model for Transformation Plasticity Accompanying Strain-Induced Martensitic Transformations in Metastable Austenitic Steels. Acta Metall. Mater. 1992;40:1703.

[60] Umemoto M, Hiramatsu A, Moriya A, Watanabe T, Nanba S, Nakajima N, Anan G, Higo Y. Computer Modelling of Phase Transformation from Work-Hardened Austenite. ISIJ Int. 1992;32:306.

[61] Mujahid SA, Bhadeshia H. Coupled Diffusional Displacive Transformations - Effect of Carbon Concentration. Acta Metall. Mater. 1993;41:967.

[62] Besserdich G, Scholtes B, Muller H, Macherauch E. Consequences of Transformation Plasticity on the Development of Residual-Stresses and Distortions During Martensitic Hardening of Sae-4140 Steel Cylinders. Steel Res. 1994;65:41.

[63] Luiggi NJ, Betancourt AE. Multiphase Precipitation of Carbides in Fe-C Systems .1. Model-Based Upon Simple Kinetic Reactions. Metall. Mater. Trans. B-Proc. Metall. Mater. Proc. Sci. 1994;25:917.

[64] Luiggi NJ, Betancourt AE. Multiphase Precipitation of Carbides in Fe-C System .2. Model-Based on Kinetics of Complex-Reactions. Metall. Mater. Trans. B-Proc. Metall. Mater. Proc. Sci. 1994;25:927.

[65] Sjostrom S, Ganghoffer JF, Denis S, Gautier E, Simon A. Finite-Element Calculation of the Micromechanics of a Diffusional Transformation .2. Influence of Stress Level, Stress History and Stress Multiaxiality. Eur. J. Mech. A-Solids 1994;13:803.

[66] Marketz F, Fischer FD. A Mesoscale Study on the Thermodynamic Effect of Stress on Martensitic-Transformation. Metall. Mater. Trans. A-Phys. Metall. Mater. Sci. 1995;26:267.

[67] Shipway PH, Bhadeshia H. Mechanical Stabilisation of Bainite. Mater. Sci. Technol. 1995;11:1116.

[68] Chang LC, Bhadeshia H. Stress-Affected Transformation to Lower Bainite. J. Mater. Sci. 1996;31:2145.

[69] Marketz F, Fischer FD, Tanaka K. Micromechanics of Transformation-Induced Plasticity and Variant Coalescence. J. Phys. IV 1996;6:445.

[70] Tanaka K, Nishimura F, Fischer FD, Oberaigner ER. Transformation Thermomechanics of Alloy Materials in the Process of Martensitic Transformation: A Unified Theory. J. Phys. IV 1996;6:455.

[71] Todinov MT. A New Approach to the Kinetics of a Phase Transformation with Constant Radial Growth Rate. Acta Mater. 1996;44:4697.

[72] Todinov MT, Knott JF, Strangwood M. An Assessment of the Influence of Complex Stress States on Martensite Start Temperature. Acta Mater. 1996;44:4909.

[73] Bhadeshia H. Martensite and Bainite in Steels: Transformation Mechanism & Mechanical Properties. J. Phys. IV 1997;7:367.

[74] Chen JR, Tao YQ, Wang HG. A Study on Heat Conduction with Variable Phase Transformation Composition During Quench Hardening. J. Mater. Process. Technol. 1997;63:554.

[75] Denis S. Considering Stress-Phase Transformation Interactions in the Calculation of Heat Treatment Residual Stresses. CISM Courses and Lectures - No 368, Mechanics of Solids with Phase Changes 1997.

[76] Jones SJ, Bhadeshia H. Kinetics of the Simultaneous Decomposition of Austenite into Several Transformation Products. Acta Mater. 1997;45:2911.

[77] Lusk M, Jou HJ. On the Rule of Additivity in Phase Transformation Kinetics. Metall. Mater. Trans. A-Phys. Metall. Mater. Sci. 1997;28:287.

[78] Reti T, Horvath L, Felde I. A Comparative Study of Methods Used for the Prediction of Nonisothermal Austenite Decomposition. J. Mater. Eng. Perform. 1997;6:433.

[79] Reisner G, Werner EA, Kerschbaummayr P, Papst I, Fischer FD. The Modeling of Retained Austenite in Low-Alloyed Trip Steels. JOM-J. Miner. Met. Mater. Soc. 1997;49:62.

[80] Starink MJ. Kinetic Equations for Diffusion-Controlled Precipitation Reactions. J. Mater. Sci. 1997;32:4061.

[81] Brachet JC, Gavard L, Boussidan C, Lepoittevin C, Denis S, Servant C. Modelling of Phase Transformations Occurring in Low Activation Martensitic Steels. J. Nucl. Mater. 1998;263:1307.

[82] Cherkaoui M, Berveiller M, Sabar H. Micromechanical Modeling of Martensitic Transformation Induced Plasticity (Trip) in Austenitic Single Crystals. Int. J. Plast. 1998;14:597.

[83] Reisner G, Werner EA, Fischer FD. Micromechanical Modeling of Martensitic Transformation in Random Microstructures. Int. J. Solids Struct. 1998;35:2457.

[84] Todinov MT. Alternative Approach to the Problem of Additivity. Metall. Mater. Trans. B-Proc. Metall. Mater. Proc. Sci. 1998;29:269.

[85] Lee YK, Lusk MT. Thermodynamic Prediction of the Eutectoid Transformation Temperatures of Low-Alloy Steels. Metall. Mater. Trans. A-Phys. Metall. Mater. Sci. 1999;30:2325.

[86] Lusk MT. A Phase-Field Paradigm for Grain Growth and Recrystallization. Proc. R. Soc. London Ser. A-Math. Phys. Eng. Sci. 1999;455:677.

[87] Todinov MT. Influence of Some Parameters on the Residual Stresses from Quenching. Model. Simul. Mater. Sci. Eng. 1999;7:25.

[88] Bates CE, Totten GE. Quantifying Quench-Oil Cooling Characteristics. Adv. Mater. Process. 1991;139:25.

[89] Kobasko NI. Technological Aspects of Quenching (Review). Met. Sci. Heat Treat. 1991;33:253.

[90] Bates CE, Totten GE. Quench Severity Effects on the as-Quenched Hardness of Selected Alloy-Steels. Heat Treat. Met. 1992;19:45.

[91] Han SW, Kang SH, Totten GE, Webster GM. Immersion Time Quenching. Adv. Mater. Process. 1995;148:AA42.

[92] Kobasko NI. Basics of Intensive Quenching. Adv. Mater. Process. 1995;148:W42.

[93] Reti T, Felde I, Horvath L, Kohlheb R, Bell T. Quenchant Performance Analysis Using Computer Simulation. Heat Treat. Met. 1996;23:11.

[94] Sverdlin AV, Blackwood R, Totten GE. Thermal Method for Cleaning Polymer Quenching Media. Met. Sci. Heat Treat. 1996;38:255.

[95] Sverdlin AV, Totten GE, Bates C, Jarvis LM. Use of the Quenching Factor for Predicting the Properties of Polymer Quenching Media. Met. Sci. Heat Treat. 1996;38:248.

[96] Sverdlin AV, Totten GE, Webster GM. Quenching Media Based on Polyalkylene Glycol for Heat Treatment of Aluminum Alloys. Met. Sci. Heat Treat. 1996;38:252.

[97] Sverdlin AV, Totten GE, Webster GM. Analysis of Polymer-Based Quenching Media. Met. Sci. Heat Treat. 1996;38:56.

[98] Totten GE, Webster GM. Quenching Fundamentals: Maintaining Polymer Quenchants. Adv. Mater. Process. 1996;149:AA64.

[99] Totten GE, Webster GM, Blackwood RR, Jarvis LM, Narumi T. Chute Quench Recommendations for Continuous Furnace Applications with Aqueous Polymer Quenchants. Heat Treat. Met. 1996;23:36.

[100] Totten GE, Webster GM, Gopinath N. Quenching Fundamentals: Effect of Agitation. Adv. Mater. Process. 1996;149:73.

[101] Archambault P, Denis S, Azim A. Inverse Resolution of the Heat-Transfer Equation with Internal Heat Source: Application to the Quenching of Steels with Phase Transformations. J. Mater. Eng. Perform. 1997;6:240.

[102] Liscic B, Totten GE. Benefits of Delayed Quenching. Adv. Mater. Process. 1997;152:180.

[103] Totten GE, Webster GM, Tensi HM, Liscic B. Standards for Cooling Curve Analysis. Adv. Mater. Process. 1997;151:68LL.

[104] Totten GE, Clinton NA, Matlock PL. Poly(Ethylene Glycol) and Derivatives as Phase Transfer Catalysts. J. Macromol. Sci.-Rev. Macromol. Chem. Phys. 1998;C38:77.

[105] Kobasko NI. Basics of Intensive Quenching. Adv. Mater. Process. 1999;156:H31.

[106] Tensi HM, Stitzelberger-Jakob P, Totten GE. Surface Rewetting of Aluminum. Adv. Mater. Process. 1999;156:H15.

[107] Totten GE, Tensi HM, Lainer K. Performance of Vegetable Oils as a Cooling Medium in Comparison to a Standard Mineral Oil. J. Mater. Eng. Perform. 1999;8:409.

[108] Totten GE, Webster GM. Stability & Drag-out of Polymers. Adv. Mater. Process. 1999;155:H63.

[109] Totten GE, Mackenzie DS. Aluminum Quenching Technology: A Review. Aluminium Alloys: Their Physical and Mechanical Properties, Pts 1-3, vol. 331-3. Zurich-Uetikon: Trans Tech Publications Ltd, 2000. p.589.

[110] Totten GE, Webster GM, Jarvis LM. Quenching Fundamentals: Cooling Curve Analysis. Adv. Mater. Process. 2000:H44.

[111] Ahrens U, Besserdich G, Maier HJ. Modelling Phase Transformations in Steels - Have Complex Experiments Become Obsolete? Sind aufwaendige experimente zur beschreibung der phasenumwandlung von staehlen noch zeitgemaeß? 2002;57:99.

[112] Denis S, Archambault P, Gautier E, Simon A, Beck G. Prediction of Residual Stress and Distortion of Ferrous and Non-Ferrous Metals: Current Status and Future Developments. J. Mater. Eng. Perform. 2002;11:92.

[113] Rometsch PA, Wang SC, Harriss A, Gregson PJ, Starink MJ. The Effect of Homogenizing on the Quench Sensitivity of 6082. Aluminum Alloys 2002: Their Physical and Mechanical Properties Pts 1-3, vol. 396-4. Zurich-Uetikon: Trans Tech Publications Ltd, 2002. p.655.

[114] Totten GE, Webster GM, Tensi HM. Fluid Flow Sensors for Industrial Quench Baths: A Literature Review. Heat Treat. Met. 2002;29:6.

[115] Funatani K, Canale LCF, Totten GE. Chemistry of Quenching : Part Iii - Energy Conservation by Utilization of the Thermal Content of Steel for Surface Modification. Proceedings of the 22nd Heat Treating Society Conference and the 2nd International Surface Engineering Congress. Indianapolis, Indiana, USA: ASM International, 2003. p.156.

[116] Rometsch PA, Starink MJ, Gregson PJ. Improvements in Quench Factor Modelling. Mater. Sci. Eng. A-Struct. Mater. Prop. Microstruct. Process. 2003;339:255.

[117] Kobasko NI, Aronov MA, Powell JA, Canale LCF, Totten GE. Intensive Quenching Process Classification and Applications. Heat Treat. Met. 2004;31:51.

[118] Canale LD, Totten GE. Overview of Distortion and Residual Stress Due to Quench Processing Part 1: Factors Affecting Quench Distortion. Int. J. Mater. Prod. Technol. 2005;24:4.

[119] Liscic B. Controllable Heat Extraction Technology - What It Is and What It Does. Int. J. Mater. Prod. Technol. 2005;24:170.

[120] Pietzsch R, Brzoza M, Kaymak Y, Specht E, Bertram A. Minimizing the Distortion of Steel Profiles by Controlled Cooling. Steel Res. Int. 2005;76:399.

[121] Stratton PF, Ho D. Individual Component Gas Quenching. Heat Treat. Met. 2000;27:65.

[122] Stratton PF. Modelling Gas Quenching of a Carburised Gear. Heat Treat. Met. 2002;29:29.

[123] Stratton PF, Richardson A. Validation of a Single Component Gas Quenching Model. J. Phys. IV 2004;120:537.

[124] Brzoza M, Specht E, Ohland J, Belkessam O, Lubben T, Fritsching U. Minimizing Stress and Distortion for Shafts and Discs by Controlled Quenching in a Field of Nozzles. Materialwiss. Werkstofftech. 2006;37:97.

[125] Taleb L, Cavallo N, Waeckel F. Experimental Analysis of Transformation Plasticity. Int. J. Plast. 2001;17:1.

[126] Luiggi NJ. Comments on the Analysis of Experimental Data in Nonisothermal Kinetics. Metall. Mater. Trans. A-Phys. Metall. Mater. Sci. 2003;34A:2679.

[127] Serajzadeh S. Modelling of Temperature History and Phase Transformations During Cooling of Steel. J. Mater. Process. Technol. 2004;146:311.

[128] Tszeng TC, Shi G. A Global Optimization Technique to Identify Overall Transformation Kinetics Using Dilatometry Data - Applications to Austenitization of Steels. Mater. Sci. Eng. A-Struct. Mater. Prop. Microstruct. Process. 2004;380:123.

[129] Wolff M, Bohm M, Lowisch G, Schmidt A. Modelling and Testing of Transformation-Induced Plasticity and Stress-Dependent Phase Transformations in Steel Via Simple Experiments. Comput. Mater. Sci. 2005;32:604.

[130] Wolff M, Bohm M, Dalgic M, Lowisch G, Lysenko N, Rath J. Parameter Identification for a Trip Model with Backstress. Comput. Mater. Sci. 2006;37:37.

[131] Wolff M, Bohm M, Dalgic M, Lowisch G. Validation of a Tp Model with Backstress for the Pearlitic Transformation of the Steel 100Cr6 under Step-Wise Loads. Comput. Mater. Sci. 2007;39:49.

[132] Funatani K. Modeling and Simulation Technology for the Advancement of Materials Processing Technology. vol. 120. Nancy, France: EDP Sciences, Les Ulis Cedex A, F-91944, France, 2004. p.737.

[133] Inoue T, Okamura K. Material Database for Simulation of Metallo-Thermo-Mechanical Field. vol. 2. St. Louis, MO, United States: ASM International, 2000. p.753.

[134] Houghton RL. Heat Treating Technology Roadmap Update 2006, Part I: Process and Materials Technology. Heat Treating Progress 2006;6:54.

[135] Cherkaoui M. Transformation Induced Plasticity: Mechanisms and Modeling. J. Eng. Mater. Technol.-Trans. ASME 2002;124:55.

[136] Cherkaoui M, Berveiller M. Micromechanical Modeling of the Martensitic Transformation Induced Plasticity in Steels. Smart Mater. Struct. 2000;9:592.

[137] Cherkaoui M, Berveiller M. Mechanics of Materials Undergoing Martensitic Phase Change: A Micro-Macro Approach for Transformation Induced Plasticity. Z. Angew. Math. Mech. 2000;80:219.

[138] Cherkaoui M, Berveiller M. Moving Inelastic Discontinuities and Applications to Martensitic Phase Transition. Arch. Appl. Mech. 2000;70:159.

[139] Cherkaoui M, Berveiller M, Lemoine X. Couplings between Plasticity and Martensitic Phase Transformation: Overall Behavior of Polycrystalline Trip Steels. Int. J. Plast. 2000;16:1215.

[140] Denis S, Archambault P, Gautier E, Simon A, Beck G. Phase Transformations and Generation of Heat Treatment Residual Stresses in Metallic Alloys. Ecrs 5: Proceedings of the Fifth European Conference on Residual Stresses, vol. 347-3. Zurich-Uetikon: Trans Tech Publications Ltd, 2000. p.184.

[141] Oberste-Brandenburg C, Bruhns OT. Tensorial Description of the Transformation Kinetics During Phase Transitions. Z. Angew. Math. Mech. 2000;80:S197.

[142] Ronda J, Oliver GJ. Consistent Thermo-Mechano-Metallurgical Model of Welded Steel with Unified Approach to Derivation of Phase Evolution Laws and Transformation-Induced Plasticity. Computer Methods in Applied Mechanics and Engineering 2000;189:361.

[143] Grostabussiat S, Taleb L, Jullien JF, Sidoroff F. Transformation Induced Plasticity in Martensitic Transformation of Ferrous Alloys. J. Phys. IV 2001;11:173.

[144] Antretter T, Fischer FD, Tanaka K, Cailletaud G. Theory, Experiments and Numerical Modelling of Phase Transformations with Emphasis on Trip (Vol 73, Pg 225, 2002). Steel Res. 2002;73:366.

[145] Levitas VI, Cherkaoui M. Special Issue On: Micromechanics of Martensitic Phase Transformations. Int. J. Plast. 2002;18:1425.

[146] Taleb L, Sidoroff F. A Micromechanical Modeling of the Greenwood-Johnson Mechanism in Transformation Induced Plasticity. Int. J. Plast. 2003;19:1821.

[147] Antretter T, Fischer FD, Cailletaud G. A Numerical Model for Transformation Induced Plasticity (Trip). J. Phys. IV 2004;115:233.

[148] Oberste-Brandenburg C, Bruhns OT. A Tensorial Description of the Transformation Kinetics of the Martensitic Phase Transformation. Int. J. Plast. 2004;20:2083.

[149] Tszeng TC, Zhou GF. A Dual-Scale Computational Method for Correcting Surface Temperature Measurement Errors. J. Heat Transf.-Trans. ASME 2004;126:535.

[150] Turteltaub S, Suiker ASJ. Transformation-Induced Plasticity in Ferrous Alloys. J. Mech. Phys. Solids 2005;53:1747.

[151] Taleb L, Petit S. New Investigations on Transformation Induced Plasticity and Its Interaction with Classical Plasticity. Int. J. Plast. 2006;22:110.

[152] Tjahjanto DD, Turteltaub S, Suiker ASJ, van der Zwaag S. Modelling of the Effects of Grain Orientation on Transformation-Induced Plasticity in Multiphase Carbon Steels. Model. Simul. Mater. Sci. Eng. 2006;14:617.

[153] Turteltaub S, Suiker ASJ. Grain Size Effects in Multiphase Steels Assisted by Transformation-Induced Plasticity. Int. J. Solids Struct. 2006;43:7322.

[154] Turteltaub S, Suiker ASJ. A Multiscale Thermomechanical Model for Cubic to Tetragonal Martensitic Phase Transformations. Int. J. Solids Struct. 2006;43:4509.

[155] Wolff M, Bohm M, Schmidt A. Modelling of Steel Phenomena and Their Interactions - an Internal Variable Approach. Materialwiss. Werkstofftech. 2006;37:147.

[156] Meftah S, Barbe F, Taleb L, Sidoroff F. Parametric Numerical Simulations of Trip and Its Interaction with Classical Plasticity in Martensitic Transformation. Eur. J. Mech. A-Solids 2007;26:688.

[157] Nedjar B. An Enthalpy-Based Finite Element Method for Nonlinear Heat Problems Involving Phase Change. Comput. Struct. 2002;80:9.

[158] Majorek A, Scholtes B, Muller H, Macherauch E. Influence of Heat-Transfer on the Development of Residual-Stresses in Quenched Steel Cylinders. Steel Res. 1994;65:146.

[159] Totten GE, Tensi HM, Canal LCF. Chemistry of Quenching : Part Ii - Fundamental Thermophysical Processes Involved in Quenching. Proceedings of the 22nd Heat Treating Society Conference and the 2nd International Surface Engineering Congress. Indianapolis, Indiana. USA: ASM International, 2003. p.148.

[160] Totten GE, Tensi HM, Canale LCF. Chemistry of Quenching : Part I - Fundemental Interfacial Chemical Processes Involved in Quenching. Proceedings of the 22nd Heat Treating Society Conference and the 2nd International Surface Engineering Congress. Indianapolis, Indiana, USA: ASM International, 2003. p.141.

[161] Allen FS, Fletcher AJ, Mills A. The Characteristics of Certain Experimental Quenching Oils. Steel Res. 1989;60:522.

[162] Fernandes P, Prabhu KN. Effect of Section Size and Agitation on Heat Transfer During Quenching of Aisi 1040 Steel. J. Mater. Process. Technol. 2007;183:1.

[163] Dakins ME, Bates CE, Totten GE. Calculation of the Grossman Hardenability Factor from Quenchant Cooling Curves. Metallurgia 1989;56:S7.

[164] Felde I, Reti T, Segerberg S, Bodin J, Sarmiento S. Numerical Methods for Safeguarding the Performance of the Quenching Process. Materials Science, Testing and Informatics Ii, vol. 473-474. Zurich-Uetikon: Trans Tech Publications Ltd, 2005. p.335.

[165] Tensi HM, Stitzelbergerjakob P. Evaluation of Apparatus for Assessing Effect of Forced-Convection on Quenching Characteristics. Mater. Sci. Technol. 1989;5:718.

[166] Felde I, Reti T, Segerberg S, Bodin J, Totten GE. Characterization of Quenching Performance by Using Computerized Procedures and Data Base of Heat Treatment Processes. ASM Proceedings: Heat Treating, 2001. p.93.

[167] Segerberg S. Cooling Curve Analysis - Focus on Additives. Metallurgia 2002;69:6.

[168] Bodin J, Segerberg S. Measurement and Evaluation of the Power of Quenching Media for Hardening. Heat Treat. Met. 1993;20:15.

[169] Segerberg S, Bodin J, Felde I. A New Advanced System for Safeguarding the Performance of the Quenching Process. Heat Treat. Met. 2003;30:49.

[170] Felde I, Reti T, Segerberg S, Bodin J, Sarmiente S. Numerical Methods for Safeguarding the Performance of the Quenching Process. Materials Science Forum, vol. 473-474, 2005. p.335.

[171] Felde I, Reti T, Segerberg S, Bodin J, Sarmiento GS, Totten GE, Gu J. Numerical Methods for Safeguarding the Performance of the Quenching Process. Cailiao Rechuli Xuebao/Transactions of Materials and Heat Treatment 2004;25:519.

[172] Troell E, Kristoffersen H, Bodin J, Segerberg S, Felde I. Unique Software Bridges the Gap between Cooling Curves and the Result of Hardening. HTM - Haerterei-Technische Mitteilungen 2007;62:110.

[173] Liscic B. Possibilities for the Calculation, the Measurement and the Control of the Temperature Development During Quenching. Neue Hutte 1983;28:405.

[174] Liscic B. Critical Heat-Flux Densities, Quenching Intensity and Heat-Extraction Dynamics During Quenching in Vapourisable Liquids. Heat Treat. Met. 2004;31:42.

[175] Zienkiewicz OC. Numerical Methods in Heat Transfer Wiley and Sons Ltd., 1981.

[176] Hughes TJR, Liu WK. Implicit-Explicit Finite-Elements in Transient Analysis - Stability Theory. Journal of Applied Mechanics-Transactions of the Asme 1978;45:371.

[177] Hughes TJR, Liu WK. Implicit-Explicit Finite-Elements in Transient Analysis - Implementation and Numerical Examples. Journal of Applied Mechanics-Transactions of the Asme 1978;45:375.

[178] Hughes TJR, Pister KS, Taylor RL. Implicit-Explicit Finite-Elements in Non-Linear Transient Analysis. Computer Methods in Applied Mechanics and Engineering 1979;17-8:159.

[179] Donea J, Giuliani S. Finite-Element Analysis of Steady-State Nonlinear Heat-Transfer Problems. Nuclear Engineering and Design 1974;30:205.

[180] Wood WL, Lewis RW. Int. J. Numer. Methods Eng. 1975:679.

[181] Ready J. Fe-C Phase Diagram.

[182] Christian JW. The Theory of Transformations in Metals and Alloys. Oxford: Pergamon Press, 1975.

[183] Cahn JW. Transformation Kinetics During Continuous Cooling. Acta Metallurgica 1956;4:572.

[184] Scheil E. Arch. Eisenhuettenwes 1935:565.

[185] Hashiguchi K, Kirkaldy JS, Fukuzumi T, Pavaskar V. Prediction of the Equilibrium, Paraequilibrium and No-Partition Local Equilibrium Phase-Diagrams for Multicomponent Fe-C Base Alloys. Calphad-Comput. Coupling Ph. Diagrams Thermochem. 1984;8:173.

[186] Kirkaldy JS, Baganis EA. Thermodynamic Prediction of Ae3 Temperature of Steels with Additions of Mn, Si, Ni, Cr, Mo, Cu. Metallurgical Transactions a-Physical Metallurgy and Materials Science 1978;9:495.

[187] Kirkaldy JS, Venugopalan D. Phase Transformations in Ferrous Alloys. In: Marder AR, Goldstein JI, editors. New York: The Metallurgical Society of AIME, 1984. p.125.

[188] Steven W, G. HA. JISI 1956:349.

[189] Andrews KW. JISI 1965:721.

[190] Avrami M. Kinetics of Phase Change. I. General Theory. J. Chem. Phys. 1939;7:1103.

[191] Avrami M. Kinetics of Phase Change. Ii. Transformation-Time Relations for Random Distribution of Nuclei. J. Chem. Phys. 1940;8:212.

[192] Avrami M. Kinetics of Phase Change Iii. Granulation, Phase Change, and Microstructure. J. Chem. Phys. 1941;9:177.

[193] Johnson WA, Mehl RF. Reaction Kinetics in Processes of Nucleation and Growth. Trans. AIME 1939;135:416.

[194] Kolmogorov AN. On the Statistical Theory of the Crystallization of Metals. Izv. Akad. Nauk SSSR, Ser. Mat. 1937:355.

[195] Mittemeijer EJ. Analysis of the Kinetics of Phase-Transformations. J. Mater. Sci. 1992;27:3977.

[196] Hsu TY. Additivity Hypothesis and Effects of Stress on Phase Transformations in Steel. Curr. Opin. Solid State Mat. Sci. 2005;9:256.

[197] Jahanian S, Mosleh M. The Mathematical Modeling of Phase Transformation of Steel During Quenching. J. Mater. Eng. Perform. 1999;8:75.

[198] Kamat RG, Hawbolt EB, Brimacombe JK. Diffusion Modeling of Pro-Eutectoid Ferrite Growth to Examine the Principle of Additivity. Journal of Metals 1988;40:A52.

[199] Kang SH, Im YT. Three-Dimensional Finite-Element Analysis of the Quenching Process of Plain-Carbon Steel with Phase Transformation. Metall. Mater. Trans. A-Phys. Metall. Mater. Sci. 2005;36A:2315.

[200] Kuban MB, Jayaraman R, Hawbolt EB, Brimacombe JK. An Assessment of the Additivity Principle in Predicting Continuous-Cooling Austenite-to-Pearlite Transformation Kinetics Using Isothermal Transformation Data. Metallurgical Transactions a-Physical Metallurgy and Materials Science 1986;17:1493.

[201] Nordbakke MW, Ryum N, Hunderi O. Non-Isothermal Precipitate Growth and the Principle of Additivity. Philos. Mag. A-Phys. Condens. Matter Struct. Defect Mech. Prop. 2002;82:2695.

[202] Reti T. On the Physical and Mathematical Interpretation of the Isokinetic Hypothesis. J. Phys. IV 2004;120:85.

[203] Serajzadeh S. A Mathematical Model for Prediction of Austenite Phase Transformation. Mater. Lett. 2004;58:1597.

[204] Scheil E. Anlaufzeit Der Austenitumwandlung. Arch. Eisenhuttenwes 1935;8:565.

[205] Koistinen DP, Marburger RE. A General Equation Prescribing the Extent of the Austenite-Martensite Transformation in Pure Iron-Carbon Alloys and Plain Carbon Steels. Acta Metallurgica 1959;7:59.

[206] Tzitzelk.I, Hougardy HP, Rose A. Mathematical-Description of Ttt Diagram for Isothermal Transformation and Continuous Cooling. Archiv Fur Das Eisenhuttenwesen 1974;45:525.

[207] Watt DF, Coon L, Bibby M, Goldak J, Henwood C. An Algorithm for Modeling Microstructural Development in Weld Heat-Affected Zones .A. Reaction-Kinetics. Acta Metallurgica 1988;36:3029.

[208] Heckel RW, Balasubr.M. Effects of Heat Treatment and Deformation on Homogenization of Compacts of Blended Powders. Metallurgical Transactions 1971;2:379.

[209] Stouvenot F, Denis S, Simon A, Denis JP, Ducamp C. Experimental-Study and Prediction of Structural Transformations and Cracking in a Solidified Thin-Walled Low-Carbon Steel. Memoires Et Etudes Scientifiques De La Revue De Metallurgie 1988;85:508.

[210] Denis S, Sjostrom S, Simon A. Coupled Temperature, Stress, Phase Transformation Calculation; Model Numerical Illustration of the Internal Stresses Evolution During Cooling of a Eutectoid Carbon Steel Cylinder. Metallurgical transactions. A, Physical metallurgy and materials science 1987;18 A:1203.

[211] Ahrens U, Maier HJ, Maksoud AEM. Stress Affected Transformation in Low Alloy Steels - Factors Limiting Prediction of Plastic Strains. J. Phys. IV 2004;120:615.

[212] Antretter T, Fischer FD, Cailletaud G, Ortner B. On the Algorithmic Implementation of a Material Model Accounting for the Effects of Martensitic Transformation. Steel Res. Int. 2006;77:733.

[213] Denis S. Prediction of the Residual Stresses Induced by Heat Treatments and Thermochemical Surface Treatments. Rev. Metall.-Cah. Inf. Techn. 1997;94:157.

[214] Liu CC, Ju DY, Inoue T. A Numerical Modeling of Metallo-Thermo-Mechanical Behavior in Both Carburized and Carbonitrided Quenching Processes. ISIJ Int. 2002;42:1125.

[215] Liu CC, Yao KF, Lu Z, Gao GF. Study of the Effects of Stress and Strain on Martensite Transformation: Kinetics and Transformation Plasticity. J. Comput-Aided Mater. Des. 2000;7:63.

[216] Liu CC, Yao KF, Xu XJ, Liu Z. Models for Transformation Plasticity in Loaded Steels Subjected to Bainitic and Martensitic Transformation. Mater. Sci. Technol. 2001;17:983.

[217] Maalekian M, Kozeschnik E, Chatterjee S, Bhadeshia H. Mechanical Stabilisation of Eutectoid Steel. Mater. Sci. Technol. 2007;23:610.

[218] Todinov MT. Mechanism for Formation of the Residual Stresses from Quenching. Model. Simul. Mater. Sci. Eng. 1998;6:273.

[219] Bhadeshia H. Thermodynamic Analysis of Isothermal Transformation Diagrams. Metal Science 1982;16:159.

[220] Babu SS, Bhadeshia H. Mechanism of the Transition from Bainite to Acicular Ferrite. Mater. Trans. JIM 1991;32:679.

[221] Babu SS, Bhadeshia H. Stress and the Acicular Ferrite Transformation. Mater. Sci. Eng. A-Struct. Mater. Prop. Microstruct. Process. 1992;156:1.

[222] Bhadeshia H, David SA, Vitek JM, Reed RW. Stress-Induced Transformation to Bainite in Fe-Cr-Mo-C Pressure-Vessel Steel. Mater. Sci. Technol. 1991;7:686.

[223] Matsuzaki A, Bhadeshia H, Harada H. Stress Affected Bainitic Transformation in a Fe-C-Si-Mn Alloy. Acta Metall. Mater. 1994;42:1081.

[224] Liu CC, Ju DY, Yao KF, Liu Z, Xu XJ. Bainitic Transformation Kinetics and Stress Assisted Transformation. Mater. Sci. Technol. 2001;17:1229.

[225] Maier HJ, Ahrens U. Isothermal Bainitic Transformation in Low Alloy Steels: Factors Limiting Prediction of the Resulting Material's Properties. Z. Metallk. 2002;93:712.

[226] Meng QP, Rong YH, Hsu TY. Effect of Internal Stress on Autocatalytic Nucleation of Martensitic Transformation. Metall. Mater. Trans. A-Phys. Metall. Mater. Sci. 2006;37A:1405.

[227] Veaux M, Denis S, Archambault P. Modelling and Experimental Study of the Bainitic Transformation, Residual Stresses and Deformations in the Quenching Process of Middle Alloyed Steel Parts. J. Phys. IV 2004;120:719.

[228] Veaux M, Louin JC, Houin JP, Denis S, Archambault P, Aeby-Gautier E. Bainitic Transformation under Stress in Medium Alloyed Steels. J. Phys. IV 2001;11:181.

[229] Tszeng TC. Autocatalysis in Bainite Transformations. Mater. Sci. Eng. A-Struct. Mater. Prop. Microstruct. Process. 2000;293:185.

[230] Inoue T, Wang ZG. Finite Element Analysis of Coupled Thermoinelastic Problem with Phase Transformation. Int. Conf. Num. Meth. in Industrial Forming Processes 1982.

[231] Loshkarev VE. Mathematical Modeling of the Hardening Process with Allowance for the Effect of Stresses on Structural Transformations in Steel. Met. Sci. Heat Treat. 1986;28:3.

[232] Fujita M, Suzuki M. Effect of High-Pressure on Isothermal Transformation in High-Purity Fe-C Alloys and Commercial Steels. Transactions of the Iron and Steel Institute of Japan 1974;14:44.

[233] Fujita T, Yamaoka S, Fukunaga O. Pressure-Induced Phase-Transformation in Bawo4. Mater. Res. Bull. 1974;9:141.

[234] Jepson MD, Thompson FC. The Acceleration of the Rate of Isothermal Transformation of Austenite. Journal of the Iron and Steel Institute 1949;162:49.

[235] Nilan TG. Morphology and Kinetics of Austenite Decomposition at High Pressure. Transactions of the Metallurgical Society of Aime 1967;239:898.

[236] Radcliffe SV, Warlimont H. Dislocation Generation in Iron-Carbon Alloys by Hydrostatic Pressure. Physica Status Solidi 1964;7:K67.

[237] Schmidtmann E, Grave H. Effect of Different Chromium Contents and an All-Round Pressure of 25-Kbar on Transformation Behavior of Steels with 0.45 Percent C. Archiv Fur Das Eisenhuttenwesen 1977;48:431.

[238] Chen GA, Yang WY, Guo SZ, Sun ZQ. Strain-Induced Precipitation of Nb(Cn) During Deformation of Undercooled Austenite in Nb-Microalloyed Hsla Steels. Pricm 5: The Fifth Pacific Rim International Conference on Advanced Materials and Processing, Pts 1-5, vol. 475-479. Zurich-Uetikon: Trans Tech Publications Ltd, 2005. p.105.

[239] Gao M, Gu HX, Xiao FR, Liao B, Qiao GY, Yang K, Shan YY. Effect of Hot Deformation on Pearlite Transformation of 86crmov7 Steel. J. Mater. Sci. Technol. 2004;20:89.

[240] Goodenow RH, Hehemann RF. Transformations in Iron and Fe-9 Pct Ni Alloys. Transactions of the Metallurgical Society of Aime 1965;233:1777.

[241] Hanlon DN, Sietsma J, van der Zwaag S. The Effect of Plastic Deformation of Austenite on the Kinetics of Subsequent Ferrite Formation. ISIJ Int. 2001;41:1028.

[242] Khlestov VM, Konopleva EV, McQueen HJ. Effects of Deformation and Heating Temperature on the Austenite Transformation to Pearlite in High Alloy Tool Steels. Mater. Sci. Technol. 2002;18:54.

[243] Lee JW, Liu TF. Phase Transformations in an Fe-8al-30mn-1.5si-1.5c Alloy. Mater. Chem. Phys. 2001;69:192.

[244] Qi JJ, Yang WY, Sun ZQ, Zhang XZ, Dong ZF. Kinetics of Structure Evolution During Deformation Enhanced Transformation in a Low Carbon Steel Ss400. Acta Metall. Sin. 2005;41:605.

[245] Saito Y, Shiga C. Computer-Simulation of Microstructural Evolution in Thermomechanical Processing of Steel Plates. ISIJ Int. 1992;32:414.

[246] Sim HS, Lee KB, Yang HR, Kwon H. Influence of Severe Accumulative Rolling in a Low Carbon Microalloyed Steel. Microalloying for New Steel Processes and Applications, vol. 500-501. Zurich-Uetikon: Trans Tech Publications Ltd, 2005. p.581.

[247] Sim HS, Lee KS, Lee KB, Yang HR, Kwon H. Influences of Severe Deformation and Alloy Modification on Secondary Hardening and Fracture Behavior. Pricm 5: The Fifth Pacific Rim International Conference on Advanced Materials and Processing, Pts 1-5, vol. 475-479. Zurich-Uetikon: Trans Tech Publications Ltd, 2005. p.183.

[248] Sun ZP, Yang WY, Qi JJ. Characteristics of Deformation-Enhanced Transformation in Plain Low Carbon Steel. Pricm 5: The Fifth Pacific Rim International Conference on Advanced Materials and Processing, Pts 1-5, vol. 475-479. Zurich-Uetikon: Trans Tech Publications Ltd, 2005. p.49.

[249] Umemoto M, Hiramatsu A, Moriya A, Watanabe T, Nanba S, Nakajima N, Anan G, Higo Y. Computer Modeling of Phase-Transformation from Work-Hardened Austenite. ISIJ Int. 1992;32:306.

[250] Yoshie A, Fujioka M, Watanabe Y, Nishioka K, Morikawa H. Modeling of Microstructural Evolution and Mechanical-Properties of Steel Plates Produced by Thermomechanical Control Process. ISIJ Int. 1992;32:395.

[251] Zhou RF, Yang WY, Zhou R, Sun ZQ. Effects of C and Mn Elements on Deformation-Enhanced Ferrite Transformation in Low Carbon (Mn) Steels. J. Univ. Sci. Technol. Beijing 2005;12:507.

[252] Bhadeshia HKDH. The Bainite Transformation: Unresolved Issues. Materials Science and Engineering A 1999;273-275:58.

[253] Hase K, Garcia-Mateo C, Bhadeshia HKDH. Bainite Formation Influenced by Large Stress. Mater. Sci. Technol. 2004;20:1499.

[254] Jin XJ, Min N, Zheng KY, Hsu TY. The Effect of Austenite Deformation on Bainite Formation in an Alloyed Eutectoid Steel. Mater. Sci. Eng. A-Struct. Mater. Prop. Microstruct. Process. 2006;438:170.

[255] Lee CH, Bhadeshia H, Lee HC. Effect of Plastic Deformation on the Formation of Acicular Ferrite. Mater. Sci. Eng. A-Struct. Mater. Prop. Microstruct. Process. 2003;360:249.

[256] Liu CC, Yao KF, Liu Z. Quantitative Research on Effects of Stresses and Strains on Bainitic Transformation Kinetics and Transformation Plasticity. Mater. Sci. Technol. 2000;16:643.

[257] Singh SB, Bhadeshia H. Quantitative Evidence for Mechanical Stabilisation of Bainite. Mater. Sci. Technol. 1996;12:610.

[258] Su TJ, Veaux M, Aeby-Gautier E, Denis S, Brien V, Archambault P. Effect of Tensile Stresses on Bainitic Isothermal Transformation. J. Phys. IV 2003;112:293.

[259] Abbasi F, Fletcher AJ. Mater. Sci. Technol. 1985;1:10.

[260] Donghui X, Zhonghua L, Jingxie L. Modelling Simulation Mater. Sci. Eng. 1996:111.

[261] Fletcher AJ, Soomro AB. Effect of Transformation Temperature Range on Generation of Thermal Stress and Strain During Quenching. Mater. Sci. Technol. 1986;2:714.

[262] Gur CH, Tekkaya AE. Finite Element Simulation of Quench Hardening. Steel Res. 1996;67:298.

[263] Gur CH, Tekkaya AE, Schuler W. Effect of Boundary Conditions and Workpiece Geometry on Residual Stresses and Microstructure in Quenching Process. Steel Res. 1996;67:501.

[264] Inoue T, Yamaguchi T, Wang ZG. Stresses and Phase-Transformations Occurring in Quenching of Carburized Steel Gear Wheel. Mater. Sci. Technol. 1985;1:872.

[265] Iyer J, Brimacombe JK, Hawbolt EB. Development of a Mathematical-Model to Predict the Structure and Mechanical-Properties of Control-Cooled Eutectoid Steel Rods. Journal of Metals 1983;35:87.

[266] Reed-Hill RE, Abbaschian R. Physical Metallurgy Principles.

[267] Belytscko T, Liu WK, Moran B. Nonlinear Finite Elements for Continua and Structures. Chicester: John Wiley & Sons, 2000.

[268] Simo JC, Hughes TJR. Computational Inelasticity. New York: Springer-Verlag, 1997.

[269] Denis S. Mode?lisation des Interactions Contrainte-transformation de Phases et Calcul par E?le?ments Finis de la Gene?se des Contraintes Internes au Cours de la Trempe des Aciers 1987.

[270] Denis S, Boufoussi M, Chevrier JC, Simon A. Analysis of the Development of Residual Stresses for Surface Hardening of Steels by Numerical Simulation : Effect of Process Parameters. Intern, Conf. on « Residual Stresses » (ICRS4) 1994:513.

[271] Fortunier R. Simulation Numerique Du Procedee De Cementation-Induction. 1993.

[272] Rammerstorfer FG, Fischer DF, Mitter W, Bathe KJ, Snyder MD. On Thermo-Elastic-Plastic Analysis of Heat-Treatment Processes Including Creep and Phase Changes. Computers and Structures 1981;13:771.

[273] Zandona M, Mey A, Boufoussi M, Denis S, Simon A. Calculation of Internal Stresses during Surface Heat Treatment of Steels. Residual Stresses 1993:1011.

[274] Magnee A. Le De?fi de Contraintes Internes Ge?ne?re?es Par Le Traitement Thermique 1993:37.

[275] Massicart L. Contraintes Residuelles Et Transformation Perlitique : Prevision Par Calcul Et Approche Experimentale. 1991.

[276] Rammerstorfer FG, Fischer FD, Till ET, Mitter W, Grundler O. The Influence of Creep and Transformation Plasticity in the Analysis of Stresses Due to Heat Treatment. Numerical Methods in Heat Transfer 1983:447.

[277] Colonna F, Massoni E, Denis S, Chenot JL, Wendenbaum J, Gauthier E. On Thermo-Elastic-Viscoplastic Analysis of Cooling Processes Including Phases Changes. J. Mater. Process. Technol. 1992;34:525.

[278] Chaboche J-L. Viscoplastic Constitutive Equation for the Description of Cyclic and Anisotropic Behavior of Metals. 17th Polish Conference on Mechanics of Solids, vol. 25. Szczyrk, 1975. p.33.

[279] Reuss A. Berechnung Der Fliessgrenze Von Mischkristallen Auf Grund Der Plastizitatsbeding Fur Einkristalle. Z. Angew. Math. Mech. 1929;2:49.

[280] Matthies HG. A Decomposition Method for the Integration of the Elastic Plastic Rate Problem. Int. J. Numer. Methods Eng. 1989;28:1.

[281] Simo JC, Taylor RL. Consistent Tangent Operators for Rate-Independent Elastoplasticity. Computer Methods in Applied Mechanics and Engineering 1985;48:101.

[282] Ortiz M, Simo JC. An Analysis of a New Class of Integration Algorithms for Elastoplastic Constitutive Relations. Int. J. Numer. Methods Eng. 1986;23:353.

[283] Ortiz M, Popov EP. Accuracy and Stability of Integration Algorithms for Elastoplastic Constitutive Relations. Int. J. Numer. Methods Eng. 1985;21:1561.

[284] Owen DRJ, Hinton E. Finite Elements in Plasticity: Redwood Burn Ltd., 1980.

[285] Patel JR, Cohen M. Criterion for the Action of Applied Stress in the Martensitic Transformation. Acta Metallurgica 1953;1:531.

[286] Cherkaoui M, Berveiller M. Special Issue: Mechanics of Martensitic Phase Transformation in Sma and Trip Steels. Int. J. Plast. 2000;16:1133.

[287] Fischer FD, Schlogl SM. The Influence of Material Anisotropy on Transformation-Induced Plasticity in Steel Subject to Martensitic-Transformation. Mech. Mater. 1995;21:1.

[288] Jacques P, Furnemont Q, Mertens A, Delannay F. On the Sources of Work Hardening in Multiphase Steels Assisted by Transformation-Induced Plasticity. Philos. Mag. A-Phys. Condens. Matter Struct. Defect Mech. Prop. 2001;81:1789.

[289] Jacques P, Furnemont Q, Pardoen T, Delannay F. On the Role of Martensitic Transformation on Damage and Cracking Resistance in Trip-Assisted Multiphase Steels. Acta Mater. 2001;49:139.

[290] Suiker ASJ, Turteltaub S. Computational Modelling of Plasticity Induced by Martensitic Phase Transformations. Int. J. Numer. Methods Eng. 2005;63:1655.

[291] Taleb L, Cavallo N, Waeckel F. Experimental Analysis of Transformation Plasticity (Vol 17, Pg 1, 2001). Int. J. Plast. 2001;17:1029.

[292] Taleb L, Petit-Grostabussiat S. Elastoplasticity and Phase Transformations in Ferrous Alloys: Some Discrepencies between Experiments and Modeling. J. Phys. IV 2002;12:187.

[293] De Jong M, Rathenau GW. Mechanical Properties of Iron and Some Iron Alloys While Undergoing Allotropic Transformation. Acta Met. 1959;7:246.

[294] Franitza S. Zur Berechnung Der Waerme- Und Umwandlungsspannungen in Langen Kreiszylindern. 1972.

[295] Marketz F, Fischer FD. Micromechanical Modeling of Stress-Assisted Martensitic-Transformation. Model. Simul. Mater. Sci. Eng. 1994;2:1017.

[296] Marketz F, Fischer FD. Simulation of Stress-Assisted Martensitic-Transformation in Elastoplastic Materials. Z. Angew. Math. Mech. 1994;74:T16.

[297] Johnson RH, Greenwood GW. Nature 1962;195:138.

[298] Dasalos Y. Comportement Dilatometrique Et Mecanique De L´Austenite Metastable D´Un Acier a 533. IRSID, 1981.

[299] Leblond JB, Devaux J, Devaux JC. Mathematical Modelling of Transformation Plasticity in Steels: I. Case of Ideal-Plastic Phases. Int. J. Plast. 1989;5:551.

[300] Ahrens U. Beanspruchungsabhaengiges Umwandlungsverhalten und Umwandlungsplastizitaet Niedrig Legierter Sta?hle mit Unterschiedlich Hohen Kohlenstoffgehalten 2003.

[301] Dalgic M, Lowisch G. Einfluss Einer Aufgepraegten Spannung Auf Die Isotherme, Perlitische Und Bainitische Umwandlung Des Waelzlagerstahls 100cr6. HTM 2004;59:28.

[302] Lemaitre J. Handbook of Materials Behavior Models 2001.

[303] Schroeder R. Untersuchungen Zur Spannungs- Und Eigenspannungs-Ausbildung Beim Abschrecken Von Stahlzylindern. vol. Ph.D.: University of Karlsruhe, 1985.

[304] Yu HJ, Wolfstieg U, Macherauch E. Arch. Eisenhuettenwes 1978;49.

[305] Yu HJ, Wolfstieg U, Macherauch E. Arch. Eisenhuettenwes 1980;51.

[306] Wever F, Rose A. Atlas Fur Waermbehandlung Der Staehle, 1954.

[307] Schröder R. Untersuchungen Zur Spannungs- Und Eigenspannungs-Ausbildung Beim Abschrecken Von Stahlzylindern. vol. Ph.D.: University of Karlsruhe, 1985.

[308] Aronov MA, Kobasko NI, Wallace JF, Schwam D, Powell JA. Practical Application of Intensive Quenching Technology for Steel Parts. Heat Treat. Met. 2000;27:13.

[309] Kobasko NI. Basics of Intensive Quenching .2. Adv. Mater. Process. 1996;150:CC40.

[310] Besserdich G, Scholtes B, Muller H, Macherauch E. Development of Residual Stresses and Distortion During Hardening of Sae 4140 Cylinders Taking into Account Transformation Plasticity. Residual Stresses 1993:975.

[311] Pont D, Bergheau JM, Leblond JB. Three-Dimensional Simulation of a Laser Surface Treatment through Steady State Computation in the Heat Source's Comoving Frame. Proceedings of IUTAM Symposium Mechanical Effects of Welding 1992:85.

[312] Yang YS, Na SJ. Effect of Transformation Plasticity on Residual Stress Fields in Laser Surface Hardening Treatment. Journal of heat treating 1991;9:49.

VITA

Caner Şimşir was born in Ankara, on 8th September 1977. He completed his high school education in Ankara Anadolu Lisesi. He started his undergraduate studies at the Department of Metallurgical and Materials Engineering at Middle East Technical University in 1995 and took his BSc. degree in 2000 ranking as the top graduate. He became a research assistant at the department in the same year, and started his graduate studies. He had his MSc. degree in September 2002, with a thesis entitled as "Low Velocity Ballistic Characterization of Steel Armor Plates by Drop-Weight Test". After having the MSc. degree, he started to work on his PhD. thesis on simulation of thermal processing of materials. During the last year of his PhD, he also worked as a research fellow on "Continuous Production of Nano-structured Aluminum Sheets by Severe Plastic Deformation" project (105M174) supported by TÜBİTAK. He is currently writing two book chapters on simulation of thermal processing, which will be published by CRC Press. He will soon start working at IWT in University of Bremen (Stiftung Institut für Werkstofftechnik – Materials Engineering Institute) as a research fellow. His current research interests include numerical methods, applied mathematics, multi-scale modeling, physics and mechanics of materials.

List of Published Papers:

1. Simsir C, Gur CH. 3-D FEM Simulation of Steel Quenching and Investigation of the Effect of Asymmetric Geometry on Residual Stress Distribution. J. Mater. Process. Tech., 2008 (In Press)
2. Şimşir C., Karpuz P., Gür C.H., "Investigation of the Effect of Hardening Behavior on ECAP Performance", Materials Science and Engineering A, 2008 (In Press)
3. Şimşir C., Karpuz P., Gür C.H., "Simulation of Equal Channel Angular Pressing Applied to Produce Structures with Ultrafine-Sized Grains", International Journal of Microstructure and Materials Properties , 2008 (In Press)
4. Şimşir C., Gür C.H., "Determination of the Microstructure and Residual Stress State in the Quenched Steel Components by Computer Simulation", Proceedings of International Metallurgy and Materials Engineering Conference (IMMC), İstanbul, Turkey, 2006
5. Şimşir C., Karpuz P., Gür C.H., "Finite Element Simulation of Equal Channel Angular Pressing (ECAP) Applied to Produce Nano-size Grains", Proceedings of International Metallurgy and Materials Engineering Conference (IMMC), İstanbul, Turkey, 2006
6. Şimşir C., Gür C.H., "Finite Element Simulation of Steel Quenching with Phase Transformations", Proceedings of IHTSE, Hungary, 2006
7. Şimşir C., Gür C.H., "Finite Element Simulation of Steel Quenching in Order to Investigate Residual Stresses and Distortion", Proceedings of International Distortion Engineering (IDE) Conference, Bremen, Germany ,2005

8. Şimşir C., Gür C.H., “Finite Element Simulation of Steel Quenching in order to Determine the Microstructure and Residual Stresses”, EUROMAT, Prag, Czech Republic
9. Şimşir C, Gür C.H., “Finite Element Simulation of Steel Quenching without Phase Transformations to Predict the Residual Stresses and Distortion”, International Metallurgy and Materials Engineering Conference (IMMC), İstanbul, 2005
10. Şimşir C., Ögel B., “Ballistic Characterization of Steel Armour Plates by Drop Weight Test”, Proceedings of 1st Defence Technologies Conference (SAVTEK), Ankara, Turkey, 2002

Submitted papers (currently at referee):

1. Şimşir C., Gür C.H., “A FEM Based Framework for Simulation of Thermal Processing of Materials”, Journal of Computational Physics
2. Şimşir C., Gür C.H., “A Mathematical Framework for Simulation of Thermal Processing of Materials: Application to Steel Quenching”, Turkish Journal of Environmental and Engineering Sciences

Papers in Preparation:

1. Şimşir C., Gür C.H., “A Review on Simulation on Modeling and Simulation of Quenching ” for Journal of ASTM International, Special Issue on Quenching Technologies and Control of Quenching
2. Şimşir C., Karpuz P., Kim Y.S., Gür C.H., “Investigation of the Effect of Kinematic Hardening on ECAP performance” for Scripta Materialia.
3. Şimşir C., Gür C.H., “Modeling of the Effect of Stress and Prior Plasticity on the as-quenched Microstructure and Experimental Verification” for Acta Materialia
4. Şimşir C., Soyarslan C., Karpuz P., Gür C.H., Tekkaya A.E., “A Continuum Damage Mechanical Investigation of ECAP process” for Acta Materialia

Book Chapters:

1. Şimşir C., Gür C.H., “Simulation of Quenching” Chapter in “Handbook of Thermal Process Modelling of Steels”, to be published in 2009 by CRC Press – Francis & Taylor Group, supported by IFHTSE, Editors : Gür C.H. and Pan L.
2. Şimşir C., Gür C.H., “Quenching Theory and Technology, 2nd Edition” Chapter in “Quenching Technology and Control (2nd Edition)”, to be published in 2008 by CRC Press - Taylor & Francis Group, Editor: B. Liscic